CALIFORNIA INSTITUTE OF TECHNOLOGY

EARTHQUAKE ENGINEERING RESEARCH LABORATORY

STEEL MOMENT-RESISTING FRAME RESPONSES IN SIMULATED STRONG GROUND MOTIONS: OR HOW I LEARNED TO STOP WORRYING AND LOVE THE BIG ONE

BY

ANNA H. OLSEN

REPORT NO. EERL 2008-02

PASADENA, CALIFORNIA

MAY 2008

A Report on Research Supported by the California Institute of Technology Under the Supervision of Thomas H. Heaton

Steel Moment-Resisting Frame Responses in Simulated Strong Ground Motions: or How I Learned to Stop Worrying and Love the Big One

Thesis by

Anna H. Olsen

In Partial Fulfillment of the Requirements

for the Degree of

Doctor of Philosophy

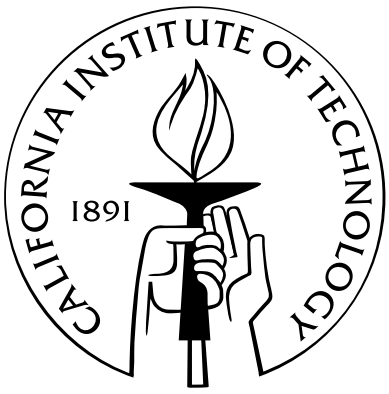

California Institute of Technology

Pasadena, California

2008

(Defended April 24, 2008)

Acknowledgements

This thesis exists because of the vision and guidance of my advisor, Professor Tom Heaton. Tom was always available to provide explanations when I was (frequently) confused, discuss the directions and implications of my research, and encourage me through the difficult times. I truly appreciate his ready advice and support.

Members of my committee also challenged me and provided guidance for this thesis. Professor Jim Beck helped me to learn and apply the Bayesian model class selection method. Professor John Hall provided the building designs and models, and he helped me interpret the results. Dr Tom Jordan gave me excellent feedback on this thesis and provided additional information on current ground motion simulation studies. Professor Zee Durón introduced me to research as an undergraduate and encouraged me to continue my studies at Caltech. He has continued to provide invaluable guidance and support.

This research was funded, in part, by the Southern California Earthquake Center. I used their allotment on the University of Southern California High Performance Computing Center cluster to calculate the building responses in this thesis. This thesis would not have been completed in a timely manner if not for this funding and access to a reliable computing cluster. This research also received support from a Hartley Fellowship and from a Housner Fellowship.

My fellow graduate students in the Civil and Mechanical Engineering Departments helped me to complete the coursework and this thesis. I learned as much from other graduate students as I did from the faculty. Alex Taflanidis, Julie Wolf, and Matt Muto reviewed early drafts of this thesis, and I appreciate their feedback. In many conversations about this thesis, Matt especially helped me to understand and

communicate this work better.

This thesis also would not exist but for the love and support of my parents. They reluctantly sent me to California for my higher eduction, and I hope this thesis shows that that was the right decision.

Abstract

This thesis studies the response of steel moment-resisting frame buildings in simulated strong ground motions. I collect 37 simulations of crustal earthquakes in California. These ground motions are applied to nonlinear finite element models of four types of steel moment frame buildings: six- or twenty-stories with either a stiffer, higher-strength design or a more flexible, lower-strength design. I also consider the presence of fracture-prone welds in each design. Since these buildings experience large deformations in strong ground motions, the building states considered in this thesis are collapse, total structural loss (must be demolished), and if repairable, the peak inter-story drift. This thesis maps these building responses on the simulation domains which cover many sites in the San Francisco and Los Angeles regions. The building responses can also be understood as functions of ground motion intensity measures, such as pseudo-spectral acceleration (PSA), peak ground displacement (PGD), and peak ground velocity (PGV). This thesis develops building response prediction equations to describe probabilistically the state of a steel moment frame given a ground motion. The presence of fracture-prone welds increases the probability of collapse by a factor of 2–8. The probability of collapse of the more flexible design is 1–4 times that of the stiffer design. The six-story buildings are slightly less likely to collapse than the twenty-story buildings assuming sound welds, but the twenty-story buildings are 2–4 times more likely to collapse than the six-story buildings if both have fracture-prone welds. A vector intensity measure of PGD and PGV predicts collapse better than PSA. Models based on the vector of PGD and PGV predict total structural loss equally well as models using PSA. PSA alone best predicts the peak inter-story drift, assuming that the building is repairable. As "rules of thumb," the twenty-story

steel moment frames with sound welds collapse in ground motions with long-period PGD greater than 1 m and long-period PGV greater than 2 m/s, and they are a total structural loss for long-period PGD greater than 0.6 m and long-period PGV greater than 1 m/s.

Contents

List of Figures

List of Tables

Chapter 1

Introduction

Engineered structures can fail. Structures have design flaws and construction flaws. They deteriorate. Myriad sets of circumstances can conspire to destroy a structure. These circumstances could be natural or man-made, intentional or accidental, common or unusual, predictable or unforeseen. No matter the particular circumstances, every structure has its limits. A hurricane breaches levees; an inadequate design leads to a bridge collapse; unanticipated wind gusts topple a construction crane.

By anticipating some of these circumstances, engineers try to avoid catastrophic failure of structures. Academic structural engineering programs teach future engineers the principles of sound design. Practicing engineers specify designs intended to avoid flaws and, if unavoidable, expose unknown flaws before they cause failure. Professional engineering societies develop standards for design, construction, and maintenance based on scientific research and lessons learned through experience. Engineers believe that their designs and constructions are robust against catastrophic failure. If they believe anything different, they develop better structures.

The beliefs that an original structure is unsound, and that the original can be sufficiently improved, predicate pursuing a revised structure. An engineer must anticipate a problem before seeking a solution, and that solution must exist. But how do engineers come to believe a structure is sound or unsound? Engineers can know there is cause for concern, but knowledge of the future behavior of structures is no more than educated speculation; no one can predict the future with certainty. Yet an engineer must anticipate reasonable sets of circumstances that may happen and

believe—not know—that the proposed or existing structure is robust in those circumstances. Separating knowledge from belief is a vital part of anticipating the behavior of structures.

The amount of control over catastrophic events, as well as knowledge and belief about the future, inform the proposed solutions to problematic structures. An engineer must first identify a problem, and then she must believe that the problem should be addressed. A solution to the problem assumes there is control over the circumstances that cause the problem. This hypothetical engineer cannot prevent hurricanes or earthquakes or floods, but she can control the structures located near the seashore or in seismically active areas or in flood plains. Belief about the severity and frequency of the circumstances that lead to failure affect how engineers perceive their amount of control over those circumstances. A second hypothetical engineer may believe that a great earthquake is so unlikely that he may neglect considering its effects. He knows that great earthquakes happen, but he believes that they are so infrequent that their consequences can be safely neglected. This belief implies a lack of control as well: a great earthquake may be inevitable, but it is so devastating that nothing can be done. Yet leveraging the control over the design and construction of structures may mitigate the worst consequences of an otherwise completely devastating event.

Thus it behooves the engineering community to identify, study, and resolve the circumstances that cause catastrophic failure. By making potential failures widely known, engineers may be able to develop robust solutions and integrate them into routine practice.

1.1 Motivation

Steel moment-resisting frame buildings are engineered structures, and like all structures, there are circumstances that can cause their failure. Steel moment frames exist in seismically active areas, and engineers employ this lateral force-resisting system in new designs. Depending on the seismicity of a particular region, this class of buildings

may be subject to earthquakes that release small to moderate to enormous amounts of energy. The behavior of a steel moment frame depends on this original release of energy, on site characteristics, and on the design, construction, and modification of the building itself. In order to judge the adequacy of steel moment frame systems, an engineer must know how these systems behave in all plausible ground motions. Specifically, the most significant response of any structure is failure, and thus the types of ground motions that cause collapse or a total structural loss of steel moment frames should be identified. The purpose of this thesis is to characterize the responses of steel moment frame buildings to a variety of ground motions that cause elastic, inelastic, and collapse behaviors.

Unfortunately the most compelling evidence of structural response is experience. Engineers tend to be a conservative group, seeking solid evidence to inform their decisions. Since their judgment is critical, engineers should avoid speculation and incomplete evidence. Certainly the results of careful research and experimentation have transferred to engineering practice, but only disasters provide stark evidence and sufficient motivation to make important and swift changes to engineering practice. Waiting for real-life evidence of steel moment frame behavior in moderate (magnitudes between 6.5 and 7.0), large (magnitudes between 7.0 and 7.5), and great (magnitudes greater than 7.5) earthquakes is impractical given the uncertain recurrence of such events. Instead, this thesis relies on the results of simulations to provide evidence of steel moment frame responses in earthquakes over a range of magnitudes.

This work characterizes the response of steel moment frames by applying simulated ground motions to nonlinear finite element models of the buildings. This study could have simulated the building responses with other methods, some of which are discussed in the next section on previous work. Nonlinear finite element models, however, rely on the fewest simplifications and assumptions. Although the finite element models lack some important known behaviors, using these nonlinear models is necessary to adequately characterize the response of steel moment frames. The results of this and similar studies may justify the use of simpler models in the future.

Recorded strong ground motions are limited to a relatively few, but growing,

number of instrumented sites. In a sufficiently large earthquake, every point on the surface of the earth moves, but scientists cannot record all the movements. Seismologists first deployed modern instrumentation in the 1920s, and thus there are historic earthquakes for which there are no adequate ground motion records. Simulated ground motions can fill in these spatial and temporal gaps in recorded ground motions, albeit in a speculative and potentially contentious way. Seismologists are developing sophisticated models of the earth's crust to simulate the rupture mechanics of, and wave propagation in, an earthquake. The products of these simulations represent plausible descriptions of how the earth's surface could have moved in a historic earthquake or could potentially move in a future earthquake. Simulated ground motions provide a wealth of information about possible but as yet unrecorded ground movements. More to the point of this thesis, simulated ground motions can be applied to building models to predict how structures may behave in future earthquakes.

Information about the full range of steel moment frame responses can be used to characterize the seismic risk of this lateral force-resisting system. A complete seismic hazard analysis must consider all possible earthquakes and evaluate their likelihoods, and similarly a complete seismic risk analysis of structures must predict the response of the structure in all possible earthquakes. One way to discuss the seismic risk of steel moment frame buildings is to compare different designs. Given the same seismic hazard, does a shorter or taller design assume less risk? Does a stiffer, higher-strength design perform better than a more flexible, lower-strength design? What effect does a design flaw such as fracture-prone welds have on the seismic risk? This thesis simulates the responses of models with these characteristics, compares their performances, and comments on the adequacy of the structural system. The conclusions about the relative performances of the different designs can inform the choice of one proposed design over another.

A second way to understand the seismic risk of steel moment frames is to follow the methodology of Performance-Based Earthquake Engineering. This method attempts to quantify the probabilistic cost of structures in terms of monetary losses, lost operational time, and casualties. This thesis develops relationships between characteristics

of ground motion (also known as intensity measures) and steel moment frame responses (termed engineering demand parameters). These relationships characterize the best prediction of the building response given a value of the ground motion characteristic, as well as an estimate of the uncertainty of the predicted building response. Used in conjunction with a probabilistic seismic hazard analysis, the steel moment frame response relationships developed in Chapter 6 can quantify the probabilistic response of a similar building in its lifetime. These responses can then be used to predict economic losses in a building's lifetime (for example, Mitrani-Reiser (2007)). However, the relationships between intensity measure and steel moment frame response developed in this thesis should be used with caution since they have not been validated with evidence from historic earthquakes.

1.2 Previous Work

1.2.1 Studies of Historic Earthquakes

The experiences of past earthquakes significantly influence the understanding of seismic building response. Certain classes of building may perform better or worse than others, and thus they are deemed superior or inferior designs. These impressions of relative performance are not always supported by a careful examination of the specific circumstances of building construction or local ground motions. Although experiences of building responses in earthquakes provide invaluable information, the interpretation of that information must be supported by often fragmentary evidence and should be as free of personal bias as possible. Reconnaissance reports of structural response in earthquakes can influence the general understanding of seismic building performance.

Engineering reports following the 1906 San Francisco earthquake generally praised the performance of steel frame buildings. In a survey of fire proofing systems, Himmelwright (1906) noted:

> The successful manner in which tall [steel] buildings withstood the effects

> of the earthquake was most gratifying to those who designed them. These buildings had never before been subjected to violent earthquake shocks, and many architects and engineers doubted their ability to withstand such surface movements without injury. Their very satisfactory behavior under the recent severe test furnishes also abundant and conclusive proof that the principles involved in their design are correct. (pp. 242–243)

Failures of engineered buildings were attributed to poor construction or soft soils:

> Any one who has carefully studied earthquake destruction can not fail to appreciate that great structural losses are due primarily, except in the immediate region of a fault line or upon loose deposits, to faulty design, poor workmanship, and bad materials; let us hope through ignorance and a blind disregard for earthquake possibilities; yet I regret to add that I feel convinced that much of the bad work is due to a combination of criminal carelessness, viscous and cheap construction. (Derleth, 1907, pp. 21–22)

These reports imply that proper attention to design and construction inevitably results in sound buildings; there is no acknowledgment of the limitations of current knowledge or honest mistakes.

Not all reports from the 1906 San Francisco earthquake provided such untempered praise of steel frame buildings. Soulé (1907) made several prescient observations about the response of steel frames, including: the largest bending moments occurred in the middle stories; the frames developed shear stresses particularly above and near the basement; most failures were a shearing of rivets and connections, especially in the lower stories and ground floors; and "the frames in these high buildings seemed to be the most severely wrenched" (p. 144). He recommended stiffening the joints and connections, providing bracing near the ground floor, and adding more columns on the first and second floors.

In the intervening sixty-five years until the 1971 San Fernando earthquake, the field of earthquake engineering developed, including a science of seismic building response. Seismic design provisions codified earthquake engineering practice and began

to define the accepted understanding of seismic building response. Now building response would be compared to the expectations defined in the building code. Albert C. Martin & Associates (1972) performed an elastic analysis of the seventeen-story, steel moment-resisting frame, Department of Water and Power Headquarters in Los Angeles following the San Fernando earthquake. They found that the simulated building response matched the recorded data, and the induced member forces "greatly exceed the code forces, although this was not considered to be a really severe earthquake, much less a maximum credible earthquake" (pp. 51–52). Bertero et al. (1978) identified large-amplitude, long-duration acceleration pulses as the cause of severe structural damage to the Olive View Medical Center. The authors recommended that the design of future structures at sites near known faults should account for the large ground velocities resulting from these near-source, acceleration pulses. Since this was a new finding, sixteen years and the 1994 Northridge earthquake transpired before this recommendation found its way into the 1997 Uniform Building Code in the form of near-source amplification factors.

The 1971 San Fernando earthquake provided information about the general seismic response of new steel frame designs. From post-earthquake observations, flexible frames, both steel and concrete, sustained primarily nonstructural damage, whereas the stiffer cores for stairs, elevators, and utilities, experienced large inter-story drifts (Steinbrugge et al., 1975). Tall steel frame buildings consistently performed better than reinforced concrete frames (Steinbrugge et al., 1971; Whitman et al., 1973). Reports differ, however, on the relative performance of shorter and taller buildings. Steinbrugge et al. (1971) observed that "there was almost always negligible or minor damage to numerous earthquake resistive multistory structures located 20 to 25 miles from the earthquake and was in sharp contrast to the comparatively rare damage to adjacent one-story non-reinforced (and non-earthquake resistive) brick structures" (p. 35). In contrast, Whitman et al. (1973) found that buildings taller than five stories sustained less damage than shorter buildings. They concluded that there was sufficient evidence from the San Fernando earthquake "to document these trends in probabilistic terms" (pp. 96–97). In a case study of twin fifty-two-story office towers

in downtown Los Angeles at the end stages of construction, Steinbrugge et al. (1971) documented a 25% increase in the number of weld cracks after the earthquake. The authors cautioned: "it is premature to speculate very far into this particular case due to the lack of time and detailed information, but the potential problem of earthquake induced weld stress cracks in modern steel frame buildings is disquieting" (p. 39). These observations of building response in the San Fernando earthquake provide evidence for currently debated issues of steel frame design and construction.

The amount and type of damage to buildings in the 1994 Northridge earthquake surprised the engineering community. Engineers believed that welded steel moment-resisting frames were one of the best lateral force-resisting systems for seismically active regions. The discovery of fracture-prone welds caused engineers to reevaluate their beliefs. The engineering community wanted to understand how such a potentially devastating flaw could go seemingly unnoticed for two decades. The SAC Steel Project formed to study all aspects of steel moment-resisting frames. The reports resulting from this project document all aspects of welded steel moment frames. Reis and Bonowitz (2000) authored a report on the past performance of steel frames, and they described the evolution of welded steel moment-resisting frame design:

> With each earthquake, building codes progress. The observed performance of real buildings—especially poor performance—can have a profound impact on provisions for structural materials and systems. Though changes are sometimes written and adopted slowly even after earthquakes, they frequently take effect before thorough investigations are complete. For steel moment frames, it was more the *lack* of earthquake damage data that propelled the standards for their design. Until Northridge, [welded steel moment frame] buildings simply did not produce the multiple and repeated failures that force building codes to change. ... That was as much due to their absence as anything else. But without notable failures, seismic code provisions for steel frames developed incrementally, and almost always in ways that would encourage and broaden their use. As a result, [welded steel moment frame] design practice was shaped more by

design and construction feasibility than by code limitations. (p. 4-1)

The 1989 Loma Prieta and 1994 Northridge earthquakes caused an unexpectedly large amount of economic loss for such relatively moderate earthquakes. In response to these two events, the engineering community began development of a new philosophy of structural design (Poland et al., 1995). Existing building codes require only the preservation of life safety; if the occupants of a building survive the earthquake, the building performance is acceptable by current standards. The new approach to building design, Performance-Based Earthquake Engineering, acknowledges that standards other than life safety can apply to building performance and strives to reliably predict building performance (Applied Technology Council, 2007). The recognition of other performance levels is a direct consequence of the economic losses in the 1989 Loma Prieta and 1994 Northridge earthquakes.

The 1995 Kobe earthquake significantly damaged steel frame buildings and caused many collapses. The majority (70%) of steel buildings damaged in this earthquake were older construction. Of the damaged modern steel buildings: 300 had minor damage; 266 had moderate damage; 332 had severe damage; and 90 collapsed. Most collapsed buildings were two to five stories, and no building over seven stories collapsed (Nakashima, 2000). Engineers observed a similar weld fracture problem in 1995 Kobe buildings as in 1994 Northridge buildings. Mahin et al. (2003) compared the building performance in both earthquakes: "While Japanese construction practices differ from those used in the United States in several basic ways, [welded steel moment frame] buildings in Kobe suffered even more severe damage than observed in California; in fact, more than 10% of these structures collapsed. ... No loss of life resulted from this damage to [welded steel moment frame] structures in the United States and none of these structures collapsed." However, the largest documented dynamic ground displacements near a steel frame building in Northridge is less than 0.3 m (Somerville et al., 1995) compared to 0.5 m in Kobe (Building Research Institute, 1996). The experiences of buildings in historic earthquakes provide documentation of what happened, but that evidence is incomplete and open to several interpretations.

Following major earthquakes there is often a recognition that the damage and

loss of life could have been worse. The particular fault location and orientation may have induced the largest ground motions in areas without engineered buildings (for example, Northridge) or the particular rupture induced unusually small ground motions (for example, Aagaard et al. (2004)). Engineers recognize that the experience of a moderate earthquake cannot be easily extrapolated to that of a great earthquake (for example, Frazier et al. (1971)). Satisfactory building performance in a moderate earthquake does not imply satisfactory performance in a great earthquake. After major earthquakes, interpretations of the experiences differ. Some engineers point to successfully, or unsuccessfully, designed and constructed buildings as exemplary of the general performance of that class of buildings in earthquakes. Other engineers take a more cautious tone by emphasizing the often uncertain evidence of building performance in specific historic earthquakes.

1.2.2 Computational Modeling

In addition to the experiences of building response in historic earthquakes, computational modeling provides insight into understanding seismic building response. Engineers use mathematical models of buildings which range in the level of detail from simple to quite sophisticated. Lumped element modeling with simple stiffness models characterizes the building response with one or several discrete degrees of freedom. A building can also be modeled as a continuum. This approach formulates building response as either propagating waves or as a modal superposition. A third modeling technique is finite elements which can have sophisticated material models and detailed descriptions of element behavior. Each method of modeling building response contributes to the general understanding of building behavior.

Lumped element models form the basis of the conceptual understanding of building response. Basic engineering training uses single-degree-of-freedom oscillators to explain the fundamental behavior of a variety of systems. In practice, the initial design of buildings is based on the response of a series of single-degree-of-freedom oscillators (that is, the response spectra). Thus, using single- or multiple-degree-of-

freedom oscillators to model building response is natural and instructive for engineers. Since the oscillator model is general, it can be used to describe the response of many building types in different kinds of ground motion. I limit this discussion, however, to a brief overview of studies that employ oscillators to describe general structural response in pulse-like, near-source ground motions.

Mylonakis and Reinhorn (2001) derive a closed-form description of the response of a single-degree-of-freedom oscillator to acceleration pulses. The authors find that severe structural damage may occur if the pulse duration is long compared to the structural period and if there is not sufficient ductility. Chopra and Chintanapakdee (2001) compared the acceleration-, velocity-, and displacement-sensitive regions of the response spectra for near- and far-source ground motions in order to reconcile the different structural behaviors in each type of ground motion. MacRae et al. (2001) compared the responses of short-, medium-, and long-period inelastic oscillators to determine the structural demand as a function of distance to the fault. Mavroeidis et al. (2004) performed a parametric study of elastic and inelastic oscillators to determine what ground motion characteristics affect structural response. They found that pulse duration most significantly affected structural performance. These studies use simple oscillators to inform the general understanding of seismic building response and to provide evidence for recommended changes to the building code.

Continuous models of building response are more complex than lumped element models, but they provide additional insight into the physics of seismic building response. Todorovska and Trifunac (1989) modeled buildings as continua in two dimensions and derived closed-form solutions for harmonic, horizontal shear wave excitation. The authors describe the contributions of symmetric and antisymmetric (with respect to the vertical centerline) modes of vibration to the building response. They also show that the phase velocities of incident seismic waves affect the transfer of energy from the ground to the building. Safak (1999) developed a layered media building model that treats each building story as a distinct layer. The wave propagation through the building is described by each layer's wave speed and by transmission and reflection coefficients at the layer interfaces. Huang (2003) used a continuous shear beam to

model tall building response in near-source ground motions. The author found that higher modes affect building response when the fundamental structural period is long compared to the pulse duration. The author also proposed an "effective response spectrum" to incorporate this phenomenon in design calculations.

A third way to model building behavior, specifically framed buildings, is with finite elements. The framing members are modeled with one or more elements, and the physical behavior of these pieces are defined with simple or complex models. Hall et al. (1995) used finite element models of steel moment frame buildings to study their behavior in near-source ground motions. The authors described the dynamic deformed shape of the buildings as well as the collapse mechanism in pulse-like ground motions. Gupta and Krawinkler (2000a) studied the responses of frame models of three-, nine-, and twenty-story buildings in ground motions representing various seismic hazard levels. Employing finite element models allowed the authors to consider the performance of important structural members, such as panel zones, columns, and column splices.

One important advantage of finite element modeling is the ability to model collapse of buildings. In strong ground motions, large inter-story drifts can develop, inducing a second-order moment due to the eccentric load (that is, the P-Δ effect). Simple oscillators do not explicitly account for this effect. Challa and Hall (1994) studied the severity of ground motions required to collapse a regular plan, twenty-story, steel moment frame building. The authors concluded that the ground motions that caused collapse were "quite severe," and it was unclear at the time whether such strong ground motions were plausible. Gupta and Krawinkler (2000b) studied the P-Δ conditions that indicate collapse of tall steel buildings. The authors found that the buildings became sensitive to P-Δ effects consistent "with the attainment of a drift at which the global pushover curve shows a clear negative slope." They proposed a design procedure to check for designs sensitive to P-Δ effects in the assumed seismic hazard. Villaverde (2007) summarized the current literature on building collapse experiences and modeling.

Another advantage of finite element modeling techniques is the ability to model

building response in three spatial dimensions. Carlson (1999) developed a nonlinear finite element program to model severe deformations in steel buildings. The author verified the program with case studies and then studied the three-dimensional effects on an irregular-plan building. The author found that peak-to-peak ground displacement predicted damage to tall buildings better than peak-to-peak ground acceleration. MacRae and Mattheis (2000) compared the response of a three-dimensional, three-story building model to the response of the equivalent two-dimensional model. The authors found that the two-dimensional model neither overestimated nor underestimated the three-dimensional drifts. However, the methods to measure drift in ground motions with two horizontal components depended on the assumed axes. The authors also found that excitations in the orthogonal direction increase drift in the principal direction. In companion papers, Liao et al. (2007a,b) studied the responses of three-dimensional models of steel moment frame buildings. The first paper developed the finite element model and found that torsional effects are important because structural members failed asymmetrically. The second paper quantified the reliability and redundancy of these buildings.

1.2.3 End-to-End Simulations

With the advancement of ground motion simulation and improved computational power, end-to-end simulations are feasible. These simulations begin with an earthquake source model, propagate the seismic waves on a regional scale, apply the resulting surface ground motions to building models, and record the building responses. These studies presently assume the same building model at all locations in the simulation domain, but future studies may consider a mix of buildings more consistent with existing or proposed building inventories. The results of these studies map the building responses on the simulation domain, thereby identifying sites where the buildings perform well or poorly.

Currently there are a limited number of end-to-end studies of building response. Hall et al. (1995) used simulated ground motions from a scenario magnitude 7.0

earthquake on a blind thrust fault in the Los Angeles basin. They applied the ground motions to two types of flexible buildings: a twenty-story steel moment frame which satisfies the seismic provisions of the 1991 and 1994 Uniform Building Codes; and a three-story base-isolated building. The authors found that the ground motions induced steel frame responses larger than those anticipated in the building code and identified the possibility of collapse. This early study emphasized the preliminary nature of the findings, but subsequent studies have supported and elaborated these initial results.

Krishnan et al. (2006) studied the responses of tall steel moment frame buildings in scenario magnitude 7.9 earthquakes on the southern San Andreas fault. This work used three-dimensional, nonlinear finite element models of an existing eighteen-story moment frame building as is, and redesigned to satisfy the 1997 Uniform Building Code. The authors found that the simulated responses of the original building indicate the potential for significant damage throughout the San Fernando and Los Angeles basins. The redesigned building fared better, but still showed significant deformation in some areas. The rupture on the southern San Andreas that propagated north-to-south induced much larger building responses than the rupture that propagated south-to-north.

Krishnan and Muto (2008) used the same building models as the previous study, as well as a building with an L-shaped plan, to simulate the response of steel moment frames in a magnitude 7.8 scenario earthquake on the southern San Andreas, also known as "ShakeOut". The authors recommended using the following estimates to characterize the damage in ten- to thirty-story, steel moment frame buildings: 5% (of an estimated 150 existing buildings of this type) collapse; 10% are red-tagged, or deemed unsafe to enter; 15% with enough damage to cause loss of life; and 20% with visible damage requiring building closure.

Olsen et al. (2008) simulated the responses of twenty-story steel moment frames in earthquakes on the northern San Andreas fault. The authors studied the building responses to ground motions based on the 1989 Loma Prieta and 1906 San Francisco earthquakes. This thesis presents some of the results used in this paper and also

considers the steel moment frame responses as functions of intensity measures.

1.2.4 Building Design and Weld State

Several studies considered different designs of tall steel buildings, arguing that one type of design performs better than another in seismic areas. In seismic design provisions for ductile buildings, the strength can be reduced by a factor R, since it is assumed that the post-yield strength of ductile buildings provides sufficient lateral force resistance to preserve life safety. Designs with lower-strength tend to be more flexible as well. Lee and Foutch (2006) considered several designs of three-, nine-, and twenty-story steel moment frames using different R factors. They used an incremental dynamic analysis to determine the inter-story drift ratio capacity of the moment frames. For the twenty-story buildings, this capacity was reduced from 7.7% for designs with an R factor of 8 (the stiffest considered) to 5.6% for designs with an R factor of 12 (the most flexible considered); twenty-story, more flexible designs tended to collapse at lower inter-story drift ratios compared to stiffer designs. The authors concluded, however, that maintaining the lower bound on the reduced design response spectrum, C_s, safely allows the design of more flexible buildings without compromising life safety. Hall (1998) studied the relative performance of four steel moment frame designs: short versus tall; and stiffer, higher-strength versus more flexible, lower-strength. The author employed nonlinear finite element models of the designs in time history analyses with simulated strong ground motions. He found that, of the four considered designs, the shorter, stiffer building performed best in the moderate (magnitude 6.7) and large (magnitude 7.0) earthquakes considered. Naeim and Graves (2006) used strong ground motions from a magnitude 7.15 scenario earthquake on the Puente Hills fault at eighteen sites to generate response spectra with an elastic-perfectly plastic material model. The authors concluded that taller, more flexible buildings are "substantially safer" than shorter, stiffer buildings, assuming both classes of buildings are properly designed and constructed. These studies draw different conclusions about the relative performance of different steel moment frame

designs.

The problem of fracture-prone welds in welded steel moment frame buildings has been well documented. In addition to comparing the relative performance of four steel moment frame designs, Hall (1998) considered the effect of brittle welds on building response. He found that the presence of brittle welds increases the story drifts and increases the likelihood that the buildings lose lateral force-resisting capacity (that is, collapse). The SAC Steel Project generated several reports documenting fractured welds in existing buildings, testing welded connections in laboratories, and modeling the response of buildings with fracture-prone welds. Luco and Cornell (2000) compared the response of steel moment frames with brittle welds to those with sound welds and studied the effect of changing the parameter values of the assumed weld fracture model. The authors found that the presence of brittle welds is significant in the strongest ground motions that induce severely nonlinear behavior. The assumed weld fracture material model only affected the results in moderate ground motions; in smaller ground motions there were not enough weld fractures, and in larger ground motions significant damage accumulated for all fracture models. Rodgers and Mahin (2006) performed scaled laboratory testing on, and computational modeling of, two-story steel moment frames with brittle welds. The authors concluded that the ground motion amplitude and character most significantly affected the response of the moment frames with brittle welds. The problem of brittle welds in older, welded steel moment frames is well known.

1.2.5 Building Response Prediction

Several intensity measures have been proposed to predict the response of buildings in seismic ground motions. Anderson and Bertero (1987) described the inherent uncertainties of predicting building response from ground motion records of the same earthquake. They showed that peak ground acceleration is not a good intensity measure to predict building response. They recommended considering incremental velocity (the area under an acceleration pulse) and peak ground displacement as

better intensity measures. Makris and Black (2004) argued that peak ground velocity is not an adequate intensity measure because it does not distinguish between long-duration acceleration pulses and a series of large spikes in acceleration. The authors used a dimensional analysis to conclude that acceleration pulses better predict the response of buildings than do velocity pulses.

Spectral values are commonly used to predict seismic building response. Gupta and Krawinkler (2000c) studied the use of spectral displacement to predict the total roof drift and peak inter-story drift of frame structures. The authors developed modification factors for the spectral displacement at the fundamental structural mode to account for "[multiple-degree-of-freedom] effects, inelasticity effects, and P-Δ effects." Then they found a relationship to predict total roof drift from the peak inter-story drift. Baker and Cornell (2005) studied a vector of intensity measures consisting of spectral acceleration and a parameter, ϵ, that measures the difference between the observed spectral acceleration and that predicted by a ground motion prediction equation. The authors argued that using both parameters to scale ground motions resulted in more accurate predictions of building response than using spectral acceleration alone. The literature is not clear on what intensity measure best predicts steel moment frame building response.

1.3 Outline of Chapters

Chapter 2 describes the steel moment frame buildings used in this thesis. The buildings have four distinct designs: six or twenty stories designed to the 1992 Japanese Building Code or the 1994 Uniform Building Code seismic provisions. With these four building designs, shorter versus taller buildings and stiffer, higher-strength versus more flexible, lower-strength buildings can be compared. Chapter 2 also describes the nonlinear finite element models of these designs. The buildings are characterized in terms of their elastic modal periods and pushover curves. Different modeling assumptions, such as how to apply the ground motions and how to model brittle welds, are studied to understand their effect on the simulated building responses.

The next three chapters present the results of applying simulated ground motions to steel moment frame building models. Chapter 3 considers two sets of earthquakes in the San Francisco Bay area: one set simulates the ground motions in the 1989 Loma Prieta earthquake and a second set models three magnitude 7.8 earthquakes on the northern San Andreas fault, based on a scenario of the 1906 San Francisco earthquake. Chapter 3 compares the responses of the stiffer, higher-strength versus the more flexible, lower-strength designs and compares the responses of models with fracture-prone (brittle) welds versus sound (perfect) welds.

Chapter 4 considers studies of fault ruptures in the Los Angeles basin. One study generated ground motions on ten faults and a second study generated broadband ground motions from ruptures on the Puente Hills fault system. (This second study is the only study I consider that produced broadband (periods greater than 0.1 s) ground motions; all other studies produced long period (periods greater than 2 s) ground motions.) Chapter 4 uses the broadband ground motions to compare the responses of the shorter and taller buildings. This chapter also compares the building responses in the Los Angeles basin for simulations on the Puente Hills fault system from the two studies and for multiple realizations of the same earthquake (that is, the same magnitude and same fault).

Chapter 5 shows the building responses to simulations on the southern San Andreas fault. These simulations generate building responses to distant earthquakes with ground motions amplified by sedimentary basins, as well as building responses to near-source ground motions from great earthquakes. This chapter also presents the building responses as measured by the permanent total drift ratio in addition to collapse and peak inter-story drift ratio.

Chapter 6 brings the building responses of Chapters 3–5 together and develops probabilistic building response prediction equations based on intensity measures. This chapter compares several proposed relationships based on pseudo-spectral acceleration, peak ground displacement, and peak ground velocity.

Chapter 7 concludes this thesis with a discussion of the significant findings from this study. This chapter identifies the significant conclusions and suggests how to

expand on this work.

Chapter 2

Building Models

This chapter describes the steel moment-resisting frame (MRF) building designs and the nonlinear finite element models of the buildings used in this thesis. The models represent buildings of shorter and taller height, and they represent stiffer, higher-strength and more flexible, lower-strength designs. I do not discuss the responses of these four buildings as individual designs. Rather, I consider the responses in comparison: how do shorter buildings behave compared to taller buildings; how do stiffer, higher-strength designs compare to more flexible, lower-strength designs; and how do buildings with fracture-prone welds compare to those with sound welds?

The second half of this chapter characterizes the building models and how they are used in this thesis. I report the first and second elastic modal periods and show pushover curves of the models. I also discuss the deformed shape of steel MRF buildings under an idealized pulse excitation because this type of ground motion induces an important collapse mechanism in these buildings. There are several decisions about how to model the seismic response of steel MRFs that may affect the conclusions. I identify some of these initial decisions, or modeling assumptions, and study the sensitivity of the building responses to these assumptions.

2.1 Building Designs

Hall (1997) designed four steel MRF buildings. Each building has either six or twenty above-ground stories, and the design of the lateral force-resisting system conforms

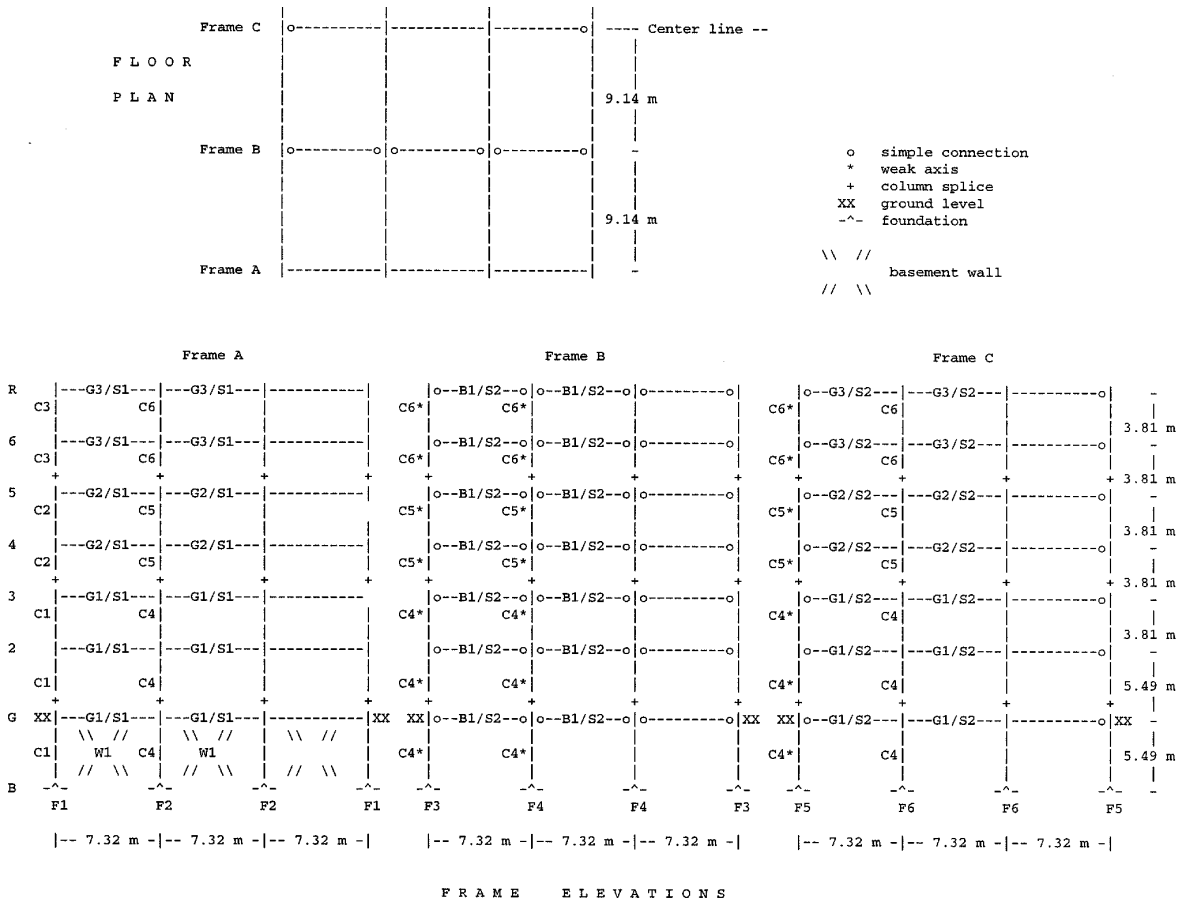

Figure 2.1: This six-story building (J6), designed to the 1992 JBC seismic provisions, is stiffer and stronger than the equivalent building designed to the 1994 UBC (U6). Reproduced from Hall (1997).

to either the 1992 Japanese Building Code (JBC) or 1994 Uniform Building Code (UBC) seismic provisions. This section describes the properties of the building designs as distinct from the finite element models of the buildings. All buildings have a rectangular floor plan and are regular in plan and elevation (Figures 2.1–2.4). Appendix A lists the beam and column schedules. The buildings consist of several frames. The perimeter frames have moment-resisting joints. The interior frames mostly have simply-supported joints.

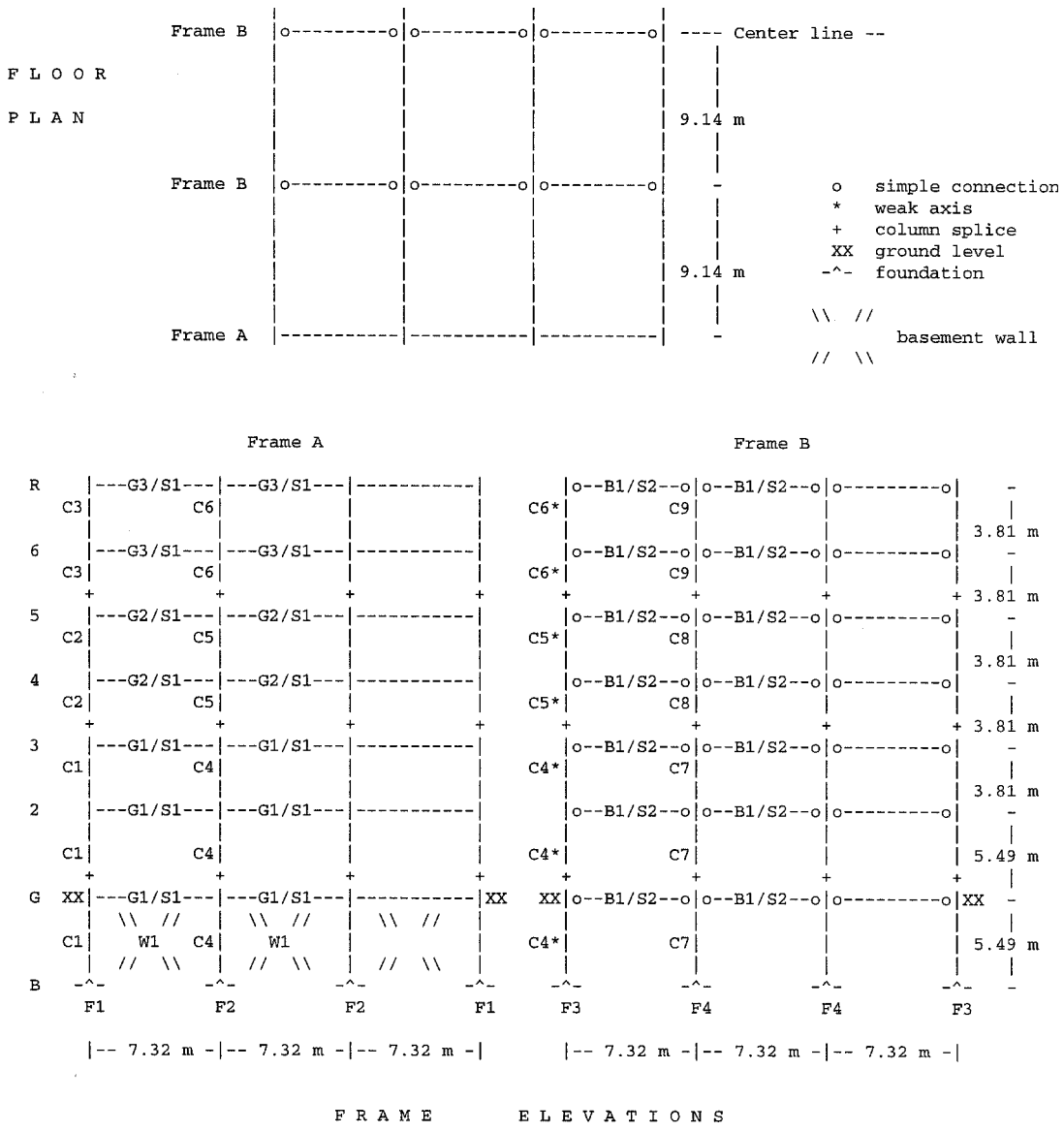

Figure 2.2: This six-story building (U6), designed to the 1994 UBC seismic provisions, is more flexible and has a lower-strength than the equivalent building designed to the 1992 JBC. Reproduced from Hall (1997).

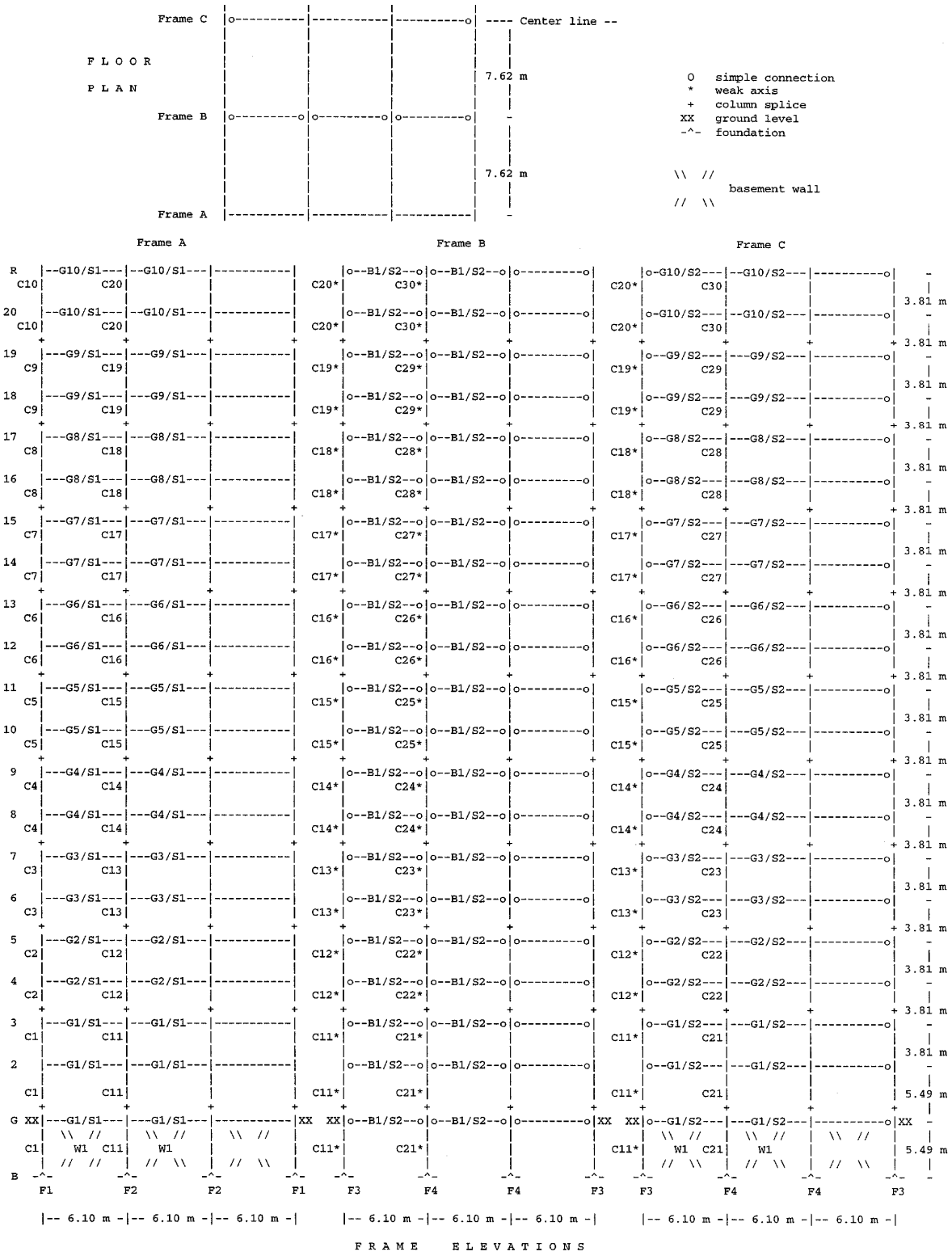

Figure 2.3: This twenty-story building (J20), designed to the 1992 JBC seismic provisions, is stiffer and stronger than the equivalent building designed to the 1994 UBC. Reproduced from Hall (1997).

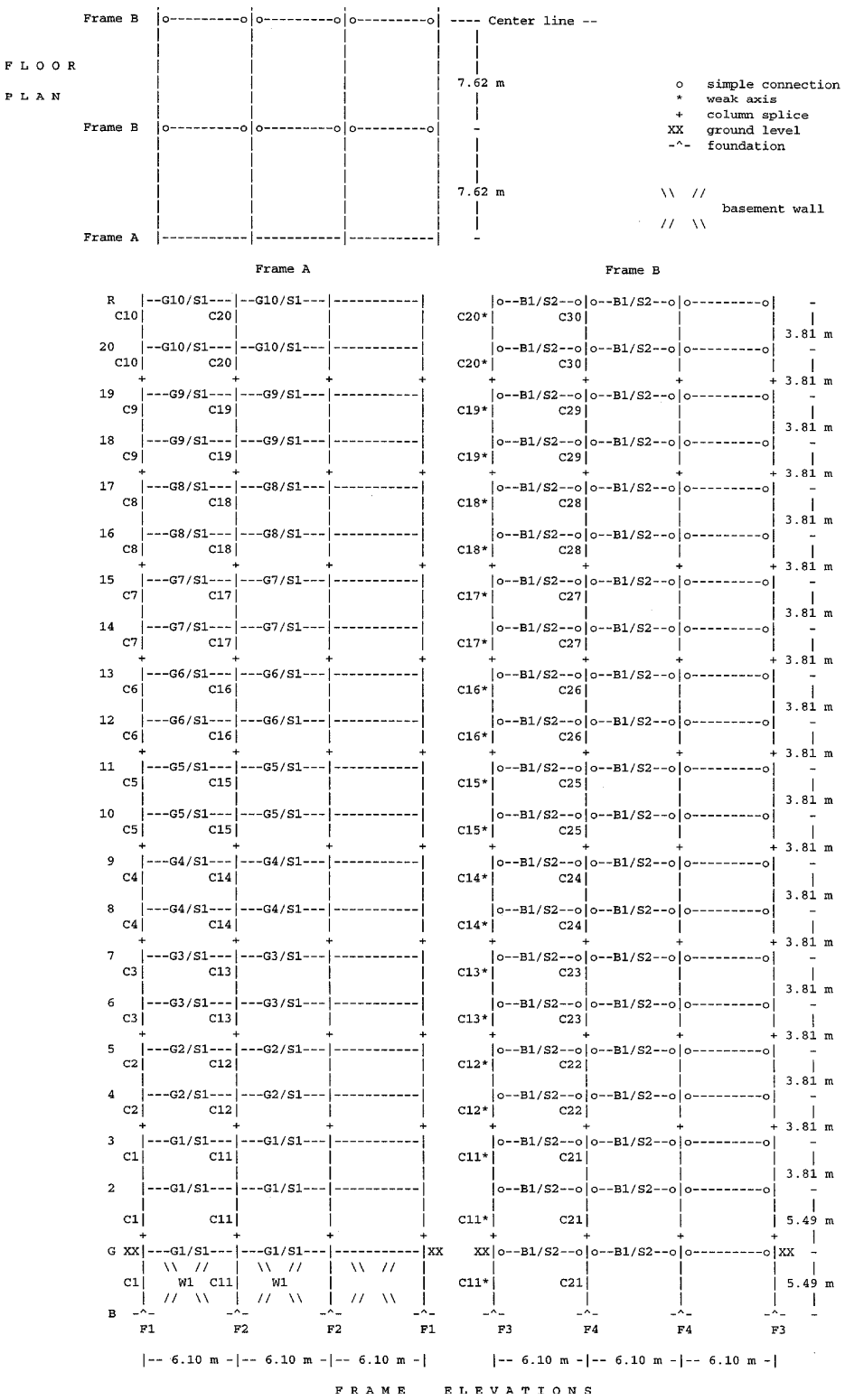

Figure 2.4: This twenty-story building (U20), designed to the 1994 UBC seismic provisions, is more flexible and has a lower-strength than the equivalent building designed to the 1992 JBC. Reproduced from Hall (1997).

Model	*Z*	*I*	R_W	*S*	*T*	*C*	*V/W*	*Drift limit*
U6	0.4	1	12	1.2	1.22 s	1.312	0.0437	0.25%
U20	0.4	1	12	1.2	2.91 s	0.736	0.0300	0.25%

Table 2.1: This table reports the values of 1994 UBC design parameters for the six- and twenty-story building designs. Reproduced from Hall (1997).

Model	*Z*	*Soil*	R_t	*T*	C_o	*Q/W*	*Drift limit*
J6	1	Type 2	0.990	0.73 s	0.2	0.1980	-
J20	1	Type 2	0.410	2.24 s	0.2	0.0820	0.50%

Table 2.2: This table reports the values of 1992 JBC design parameters for the six- and twenty-story building designs. Reproduced from Hall (1997).

2.1.1 Building Height

Building height affects the seismic response of steel MRFs. Existing steel MRF buildings can be generally categorized as short or tall, and the seismic responses of buildings at each height are different. In this thesis I simulate the responses of short and tall buildings with models that have six or twenty stories. For all buildings, the first floor height is 5.49 m, and the height of each upper story is 3.81 m. The basement height is 5.49 m. Thus the ground-to-roof height of the six-story buildings is 24.54 m and the height of the twenty-story buildings is 77.88 m.

2.1.2 Seismic Design Provisions

Hall (1997) designed the buildings to satisfy the seismic provisions of the 1992 JBC or the 1994 UBC. Tables 2.1 and 2.2 report the values of important design parameters.

The 1997 UBC adopted near-source factors to account for larger ground motions within 15 km of a fault due to directivity. The near-source factors at a site depend on the potential magnitudes and slip rates of local faults, as well as the distance between the fault and the site. The fault is categorized as type A, B, or C: type A faults have the potential to generate earthquakes of magnitudes greater than 7.0 and have a slip rate greater than 5 mm/year; type C faults have a magnitude potential less than 6.5 and have a slip rate less than 2 mm/year; and type B faults are those not characterized as type A or B. Most segments on the San Andreas fault are type

A, and most other faults in California are type B. Depending on the fault type and distance between the site and fault, the velocity-based near-source factor, N_v, ranges from 2.0 (sites within 2 km of the fault) to 1.0 (sites greater than 10 km to the fault). For example, in order to satisfy the 1997 UBC, a building designed in San Francisco within 10 km of the San Andreas would have a N_v of 1.2.

Hall (1998) compared the four building designs used in this thesis to the 1997 UBC seismic provisions. Lateral loads were applied to each design, according to the static lateral force procedure, until the stresses or drifts reached their allowed limits. The base shear at this limiting load was compared to the design base shear for each design. The six-story JBC design satisfies the 1997 UBC seismic provisions for all velocity-based near-source factors. The twenty-story JBC design satisfies only the least stringent near-source factor ($N_v = 1.2$). Neither the six-story or twenty-story UBC designs satisfies the 1997 UBC seismic provisions. Thus, the building responses of the JBC designs may be consistent with those of 1997 UBC designs for shorter buildings at all near-source sites and for taller buildings at sites with N_v less than or equal to 1.2.

Although the buildings were designed to the provisions of two specific building codes, I do not compare the two building codes themselves. The philosophy of the JBC is to promote stronger buildings that remain elastic in moderate earthquakes. The UBC philosophy promotes longer-period buildings which are less vulnerable in moderate, more frequent earthquakes. I compare the building designs as realizations of these philosophies instead of comparing the specific rules that generate specific buildings.

2.2 Finite Element Models

Since this thesis applies strong ground motions to steel MRFs, the building models must account for the deformation of such frames in large lateral loads. The finite element models are multi-degree-of-freedom frames with nonlinear, hysteretic material models and panel zone yielding. The finite element models account for the second-

order moments induced in columns that support eccentric vertical loads, or P-Δ effects. The following sections describe aspects of the finite element models that are pertinent to this thesis. Hall (1997) provides further details of the models, which are used in this thesis without modification.

2.2.1 Planar Frame Models

The building models are planar, and thus only produce planar responses. The buildings are rectangular in plan and have uniform mass and stiffness in plan as well. Since the centers of mass and rigidity are the same, a uniform ground motion at the base of the model cannot excite a torsional component in elastic response. Further, it is assumed that out-of-plane loading does not contribute to in-plane response. Since seismic ground motions have two horizontal components, a building deforms in the two horizontal directions by bending about the strong and weak axes of the columns simultaneously. The models in this thesis do not include torsional or out-of-plane responses.

The models explicitly define the beams, columns, joints, and basement walls of several frames to represent the buildings. Every model has an exterior frame with moment-resisting joints. The JBC models have an interior frame with simply-supported joints and a half interior frame with moment-resisting joints. (The half frame is due to explicitly modeling only half the building.) The UBC models have a single interior frame that represents one and a half frames with simply-supported joints. (The half is the contribution of the frame with simply-supported joints on the transverse centerline.) Rigid springs that represent the floor systems connect the frames.

Although the building models used in this thesis are planar, the building responses of three-dimensional models should be similar to those of planar models. Carlson (1999) compared the responses of two- and three-dimensional models of a seventeen-story steel moment resisting frame with a masonry service core. The author included the strength and stiffness contributions of the interior gravity frames in

both models. The author showed that the two- and three-dimensional building model responses did not differ significantly for most of the considered, recorded ground motions. For some simulations, however, the peak inter-story drift ratio (IDR, discussed in Section 2.4) of the three-dimensional building model was less than the peak IDR of the two-dimensional building model. Chi et al. (1998) modeled the same seventeen-story building with two- and three-dimensional building models as well. Their two-dimensional model, however, only included one exterior moment-resisting frame. A three-dimensional model connected the moment and gravity frames with a rigid floor system, and a second three-dimensional model used beam elements with rotational springs at the ends to model bolted shear plate connections. The authors applied strong ground motions recorded near the building in the 1994 Northridge earthquake to compare the recorded and simulated building responses. The peak IDRs in the two-dimensional models were approximately 2.5%, whereas the peak IDRs in the three-dimensional models were 1.2–1.3% (rigid floor and no core), 1.8–2.3% (rigid floor with core), and 1.3–1.6% (flexible floor with core). The present thesis considers only the responses of two-dimensional models of steel moment frame buildings. These studies suggest that the planar models capture most of the building response in strong ground motions. I expect a three-dimensional model of these building would predict similar, or slightly smaller, peak inter-story drifts compared to the planar model.

2.2.2 Fiber Method

The finite element models use the fiber method to discretize the buildings. This procedure subdivides the lengths of beams and columns into segments and further subdivides each segment cross section into fibers (Figure 2.5). Thus each beam or column has sixty-eight or eighty individual elements or fibers (eight segments times eight or ten fibers).

This method is distinct from the plastic hinge formulation. According to that discretization, a beam or column behaves as a single element with the capacity to form plastic hinges (or kinks) at the ends. Hall and Challa (1995) compared the responses

of twenty-story MRFs modeled with the plastic hinge or fiber element method. They applied a ramped, harmonic base excitation to the frames and found that the two models predict the rate of collapse onset and ductility demands consistently. However, the detailed responses of the two models before collapse differ. The plastic hinge model predicts somewhat larger lateral displacements of floors 2–5. The fiber element model develops an obvious, unrecovered lateral displacement before the plastic hinge model does. Consequently the fiber element model collapses before the plastic hinge model does.

For the purposes of this thesis, the advantage of the fiber method is the ability to model brittle welds. The behavior of each fiber can be specified independently, and fibers representing welded segments can thus have a fracture model. I describe specific weld fracture models in Section 2.2.7.

2.2.3 Beam and Column Elements

The beam and column elements have distinct material models for axial and shear deformations (Hall, 1997). Each fiber has a nonlinear, hysteretic, axial stress-strain model. Figure 2.6 shows the backbone curve of this model. The five user-defined parameters shown in this figure completely define the curve, which in turn defines the axial deformation behavior of the beam or column fibers. Table 2.3 lists the material model parameters and the values I use in this thesis. Each beam or column segment has linear shear stiffness in the plane of the frame. Tensile and compressive behaviors are the same.

The finite element models also account for residual stresses in the steel. The user defines a residual stress, and the model distributes that stress, as tensile or compressive, over the cross section of each segment. I use a residual stress of 6 ksi in the building models.

Two fibers of each beam segment model a deck-slab floor system. The concrete slab axial stress-strain material model is linearly elastic-perfectly plastic in compression and linear to a tensile crack stress. After cracking, the slab fiber no longer resists

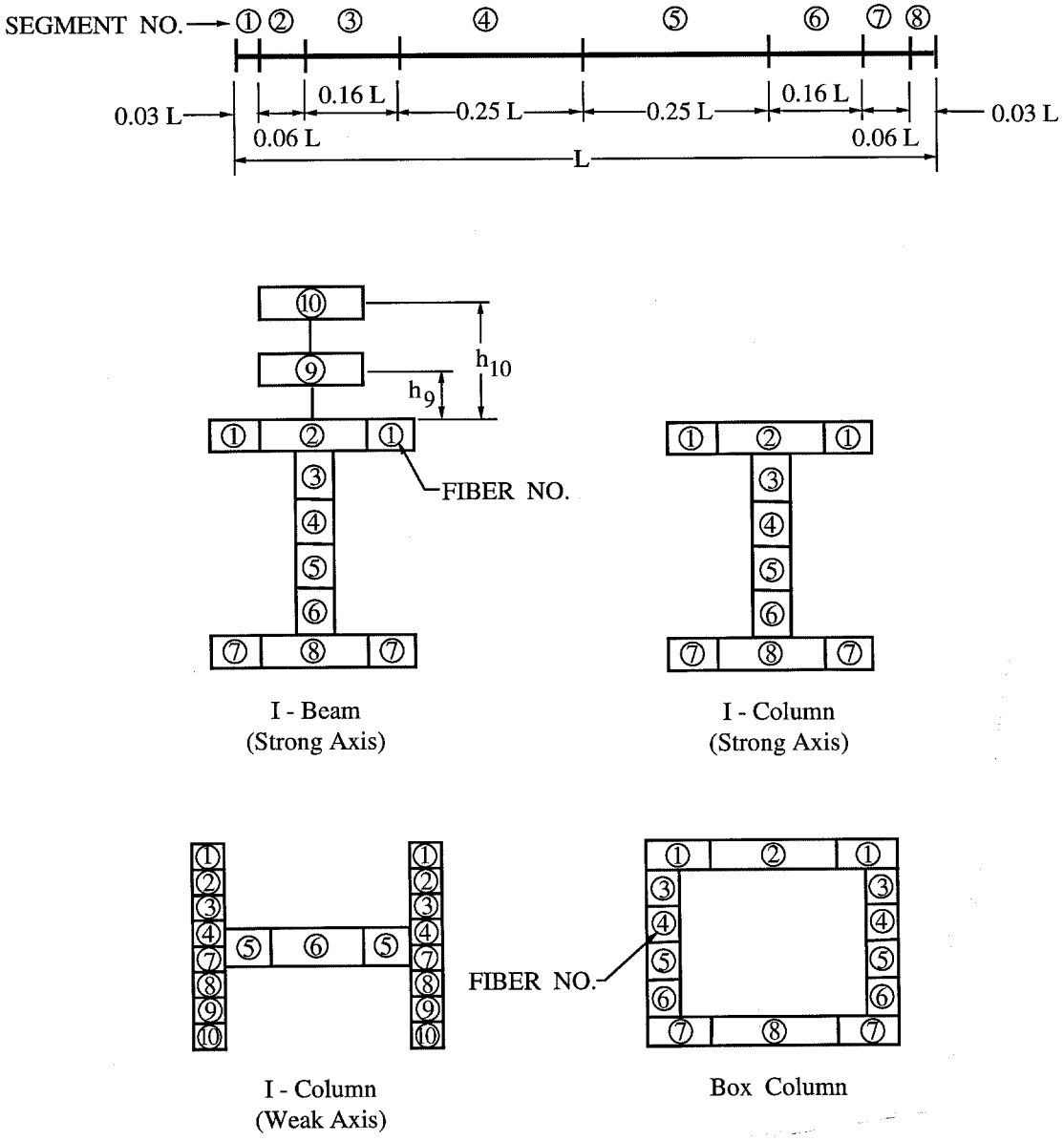

Figure 2.5: The finite element models of the four building designs use the fiber method. Each beam and column element is subdivided into eight segments on the length and into eight or ten fibers on the cross section. Fibers 1–8 represent the steel beam or column. Fibers 9 and 10 represent a deck-slab floor system. Reproduced from Hall (1997).

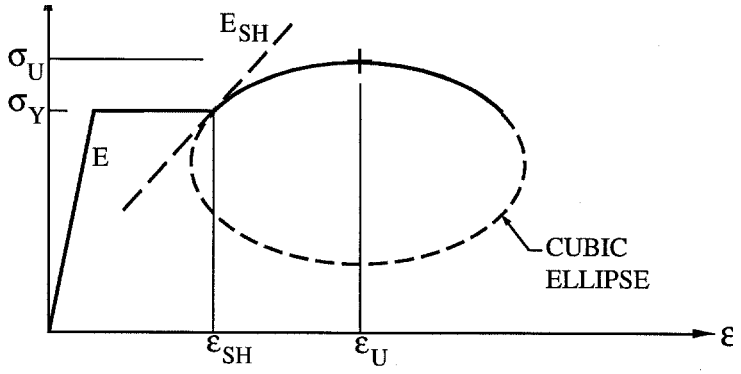

Figure 2.6: The axial stress-strain material model for each fiber is nonlinear and hysteretic. This curve defines the backbone shape for both tensile and compressive loading. Table 2.3 defines the parameters and their values. Reproduced from Hall (1997).

Parameter	*Symbol*	*Value*
Young's modulus	E	29,000 ksi
Initial strain hardening modulus	E_{SH}	580 ksi
Yield stress	σ_Y	42 ksi
Ultimate stress	σ_U	50 ksi
Strain at onset of strain hardening	ϵ_{SH}	0.012
Strain at ultimate stress	ϵ_U	0.16
Poisson's ratio	-	0.3

Table 2.3: These parameter values define the nonlinear, axial stress-strain behavior of the element fibers. This thesis does not consider alternate material models.

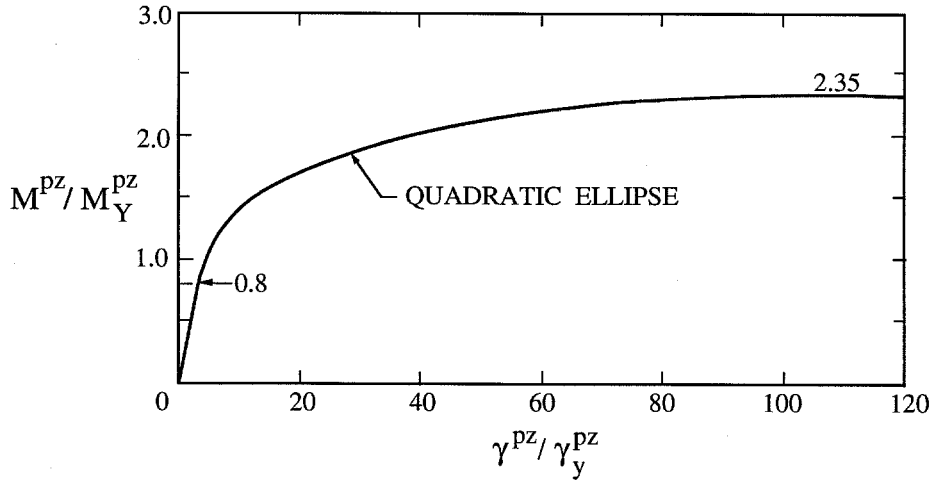

Figure 2.7: This backbone curve defines the nonlinear, hysteretic moment-shear strain relation of the panel zone element. M^{pz} is the magnitude of the double couple in the panel zone due to the moment and shear forces in the adjacent beams and columns, and γ^{pz} is the shear strain in the panel zone. Reproduced from Hall (1997).

tensile loading, but it can resist compressive loads if the crack closes.

2.2.4 Panel Zones

The finite element models include an element to explicitly model the deformation at beam-to-column joints, also known as panel zone behavior. This element models the moment versus shear strain behavior with a nonlinear, hysteretic relationship. Figure 2.7 defines this relation. In the finite element models the shear stress at yield, τ_Y, is 24 ksi, and the panel zone shear modulus, G^{pz}, is 11,6000 ksi. The panel zone yield moment, M_Y^{pz} in Figure 2.7, is 0.8 times the product of the panel zone volume and the shear stress at yield. The panel zone shear strain at yield, γ_Y^{pz}, is the shear stress at yield divided by the panel zone shear modulus.

In small ground motions, the beam-to-column joints remain rigid to ensure that the beams and columns deform in double curvature, as intended in a moment-resisting frame. In strong ground motions, however, panel zone yielding significantly and advantageously contributes to the steel MRF response. Challa and Hall (1994) identify two positive contributions of panel zone yielding in large ground motions: "First,

such panel zones reduce the ductility demands on the other structural elements by dissipating energy themselves. Second, being relatively weak, such panel zones act as fuses and limit the column moments, making it more difficult to form a collapse mechanism involving column hinges." Panel zone yielding is an important mechanism to include in MRF models that sustain large deformations.

2.2.5 Basement Walls and Soil-Structure Interaction

The finite element models of the four building designs include basement walls and soil-structure interaction. The wall elements have linear shear stiffness, but they do not resist rigid rotations. The wall elements also provide some linear, axial stiffness to the adjacent columns and beams. Soil-structure interaction is modeled with horizontal and vertical axial springs at the base of each column. The stress-strain relationship of the springs is bilinear and hysteretic.

This thesis uses a simple model of soil-structure interaction because it is adequate for the purposes of this thesis. Wong (1975), for example, studied several phenomena induced by the coupling of soils and structural foundations. The author developed sophisticated models to understand the physical behavior. Jennings and Bielak (1973) considered a simplification of the soil-structure interaction problem: they modeled the soil with an elastic half-space and the structure with an n-degree-of-freedom oscillator. The authors reformulated the problem as (n + 2) single-degree-of-freedom, viscously damped, elastic oscillators with rigid-base excitation and showed that all natural periods of the structure lengthen with soil interaction. The authors concluded that, for tall buildings, soil-structure interaction significantly affected only the fundamental period, and the effect was due to rocking of the structure rather than translation of the base. Stewart et al. (2003) compared the soil-structure interaction design procedures in the pre-2000 and 2000 *National Earthquake Hazards Reduction Program Recommended Provisions for Seismic Regulations for New Buildings and Other Structures*. The authors concluded that the effects of soil-structure interaction on long-period structures are negligible since the structure itself is so flexible. Thus,

this thesis uses a simple model to incorporate the main effect of soil-structure interaction (that is, a lengthening of the fundamental period of the building). However, I do not expect that including this interaction significantly affects the building responses.

2.2.6 Damping

The finite element models have light, viscous damping. One source is stiffness-proportional damping. This damping is 0.005 of the stiffness at the fundamental mode of the building model. This amount corresponds to the following fractions of critical damping for the four designs: 1.3% (J6), 0.98% (U6), 0.49% (J20), and 0.41% (U20). The second source of damping is inter-story shear damping. In addition to the stiffness of each column, there is a capped, viscous shear damper as well. The damping force is linear until the relative lateral velocities in adjacent floors reaches 0.1 m/s. For this and larger velocities, the damping force is a constant. This constant is found by applying the seismic design forces as a fraction of the design weight scaled by 0.02 (six-story designs) or 0.01 (twenty-story designs). The capped damping force constant is the resulting inter-story shear force.

2.2.7 Brittle Welds

In this study, the steel MRF finite element models may have fracture-prone or sound welds. Recall from Section 2.2.3 that each beam and column element is subdivided into eight segments along the length, and the cross section of each segment is subdivided into eight or ten fibers (Figure 2.5). Certain segments of beam and column elements represent welds. For all beams at a moment-resisting joint, the beam end segment represents a weld. The middle segment of some columns represents a welded column splice (see Figures 2.1–2.4 for locations), and the end segment of column elements at the foundation represents a column base plate weld. The fibers of the segments that represent welded connections each have a fracture strain. If the axial strain in a fiber exceeds the fracture strain, then that fiber no longer resists tensile loads. The fiber can continue to resist compressive loads as usual if it re-establishes

contact.

The fracture strain may not be the same for all fibers in a segment that represents a weld. For beams, the top fibers (fibers 1–4 in Figure 2.5) represent the weld between the beam top flange and the column flange, and the bottom fibers (fibers 5–8 in Figure 2.5) represent the weld between the beam bottom flange and the column flange. The finite element model allows different definitions of the fiber fracture strains for the two welds, or groups of fibers. All fibers of the column splice and base plate segments represent a single weld, and thus all fibers in those segments have the same fracture strain.

The finite element model randomly assigns a fracture strain to a weld from a user-defined distribution of fracture strains. Figure 2.8 shows two such distributions, called "B" and "F" welds from Hall (1997) and Hall (1998), respectively. The finite element model samples the fracture strain for each beam top flange, column splice, and column base plate weld from one distribution at the top of Figure 2.8. Similarly, the model samples the fracture strain of each beam bottom flange weld from one distribution at the bottom of Figure 2.8. For example, the finite element model randomly chooses a fracture strain for a column splice weld from the B weld distribution of possible column splice fracture strains (top of Figure 2.8). This sampling repeats for all welds. After this assignment completes, the distribution of all assigned fracture strains should resemble the user-defined distribution. In statistical jargon, the sampled distribution should resemble the population distribution.

The B and F weld fracture strain distributions are two models of brittle weld failure. The B distributions are bimodal: there are either relatively low or high fracture strains, but no moderate fracture strains. The F weld distribution is more uniform at the moderate fracture strains. There is no empirical evidence to recommend one distribution is better than the other. In Section 2.7.3 I compare the simulated responses of models with B or F weld distributions. For all other sections of this thesis, I use the B weld distribution to model buildings with brittle welds. I denote buildings with sound, or perfect, welds with P.

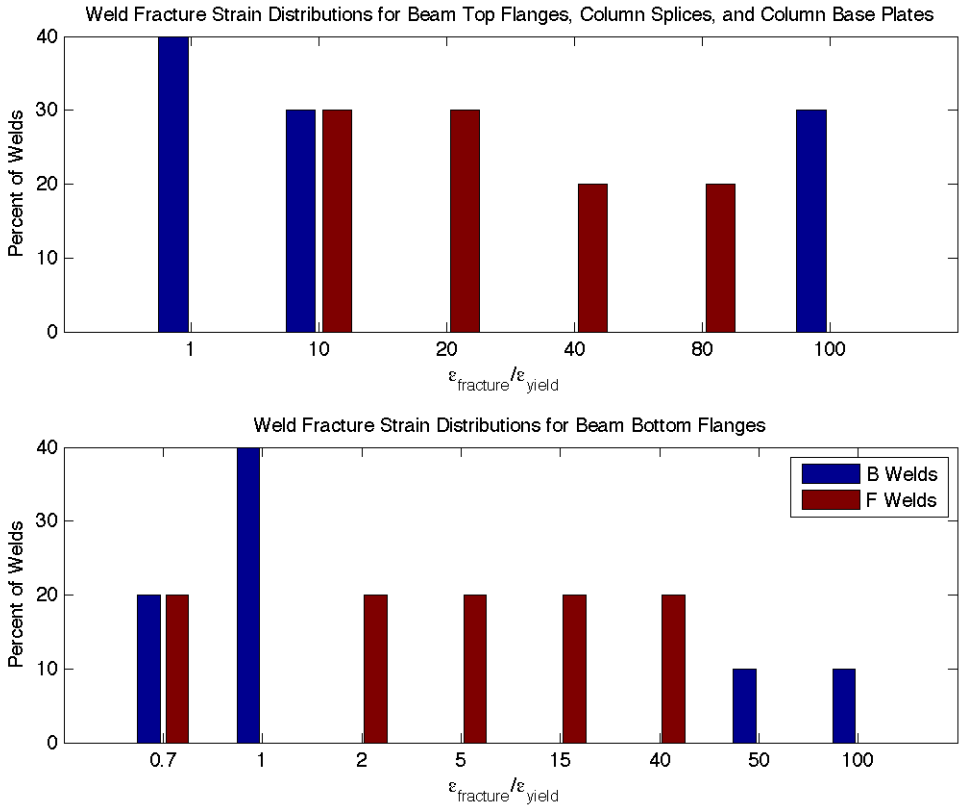

Figure 2.8: For models with brittle welds, the finite element model randomly samples a weld fracture strain from a user-defined fracture strain distribution. This thesis considers two such distributions: B and F welds.

	Modal Periods [s]	
Model	*First*	*Second*
J6P	1.2	0.4
J20P	3.2	0.9
U6P	1.6	0.5
U20P	3.8	1.0

Table 2.4: The modal periods indicate what energy content in ground motions amplify the building response through resonance. Thus, ground motions should have energy content for periods at least equal to and greater than the first mode period.

2.3 Characterization of Building Models

The preceding sections describe the components of the nonlinear finite element models, and the following sections describe the building models as systems of those components. I report the undamped, first and second modal periods and characterize the flexibility and strength of the building models by performing pseudo-static pushover analyses. The simulated ground motions used in this thesis are primarily near-source, and so I discuss the deformed shape and collapse mechanism of steel MRFs in strong ground motions.

2.3.1 Elastic Periods

One characterization of a building is its modal periods. Figure 2.9 shows the frequency response of the four, undamped building models. There is significant amplification of the harmonic building response near the first modal period. Table 2.4 reports the elastic first and second mode periods without the viscous damping described in Section 2.2.6. The second mode periods are approximately one-third of the first mode periods, which is predicted by the shear beam model of a building. The building response at the first modal period dominates the resonance behavior. Ground motions with significant energy at the first modal period amplify the building response compared to ground motions with energy at other periods.

There are two characteristic types of ground motions in the set assembled for this thesis. The first type is dominated by a near-source directivity pulse in displacement

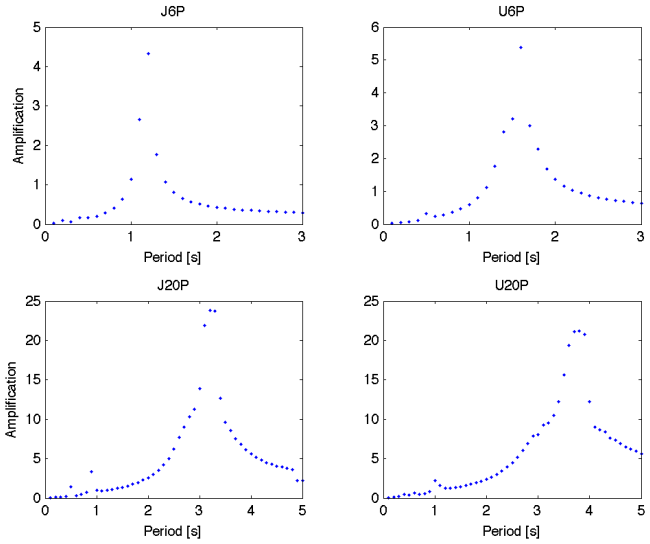

Figure 2.9: The frequency response of the building models provide one characterization of the models. Amplification refers to the amplitude of steady state roof displacement divided by the amplitude of the excitation.

and velocity. If the period of this pulse is approximately the fundamental period of a building, then the pulse induces a large, transient resonance amplification. Hall et al. (1995) describe the building response in such a pulse: as the ground moves forward, the base of the building follows the ground while the top lags. When the pulse reverses direction, the top has forward momentum while the base begins to move in the backward direction. The top moving forward as the base moves backward causes shear deformations, especially in the lower stories.

The second type of ground motions in this set are characterized by amplification of surface waves in sedimentary basins. This trapping of long-period energy in basins results in long-duration, primarily harmonic ground motions. If the dominant period of these ground motions is approximately the fundamental period of a building, the building will experience steady-state resonance, and the amplified, long-duration excitation leads to large building responses as well.

Figures 2.10 and 2.11 report the peak IDRs of twenty- and six-story buildings by story. For twenty-story buildings, primarily stories 2–4 collapse (that is, peak IDR exceeds 10%), and for six-story buildings, the collapses (peak IDR exceeds 16%)

happen mostly in stories 1–3. For buildings that do not collapse, the peak IDR can happen in the upper stories, but it is much more likely that the peak IDR is in the lowest stories.

The energy content of simulated ground motions affects how they can be used. Deterministic ground motion models provide accurate predictions of long-period content. The short-period content is not well understood, but stochastic ground motion models exist to include energy at short periods (for example, Graves and Pitarka (2004)). Thus not all simulated ground motions can be used in all applications. Long-period ground motions are not adequate to predict the response of buildings sensitive to short-period energy. However, it is appropriate to apply long-period ground motions to a building with a long fundamental period. In this thesis I apply long-period ground motions (energy content greater than 2 s) to buildings with a fundamental period longer than 2 s, and I apply broadband ground motions (energy content greater than 0.1 s) to all building models.

2.3.2 Pushover Curves

Another way to characterize building response is with a pushover curve. A pushover curve relates the shear in the ground floor columns (base shear) to the lateral roof displacement for increasing lateral loads. To generate the curves I apply a slowly increasing, pseudo-static, lateral load to each model. The load must increase slowly enough so inertial and damping forces do not contribute to the base shear. The lateral load is distributed vertically in proportion to the lateral design loads. Figures 2.12 and 2.13 show the pushover curves for the eight building models in this thesis.

The curves show three important characteristics of the buildings: stiffness, base shear at yield, and ductility. The stiffness is the initial slope of the pushover curves. I use this characteristic to compare the models, rather than as an absolute value. That is, a model is "stiffer" or "more flexible." The base shear at yield is one measure of the building's strength. Similar to stiffness, I use building strength to compare designs

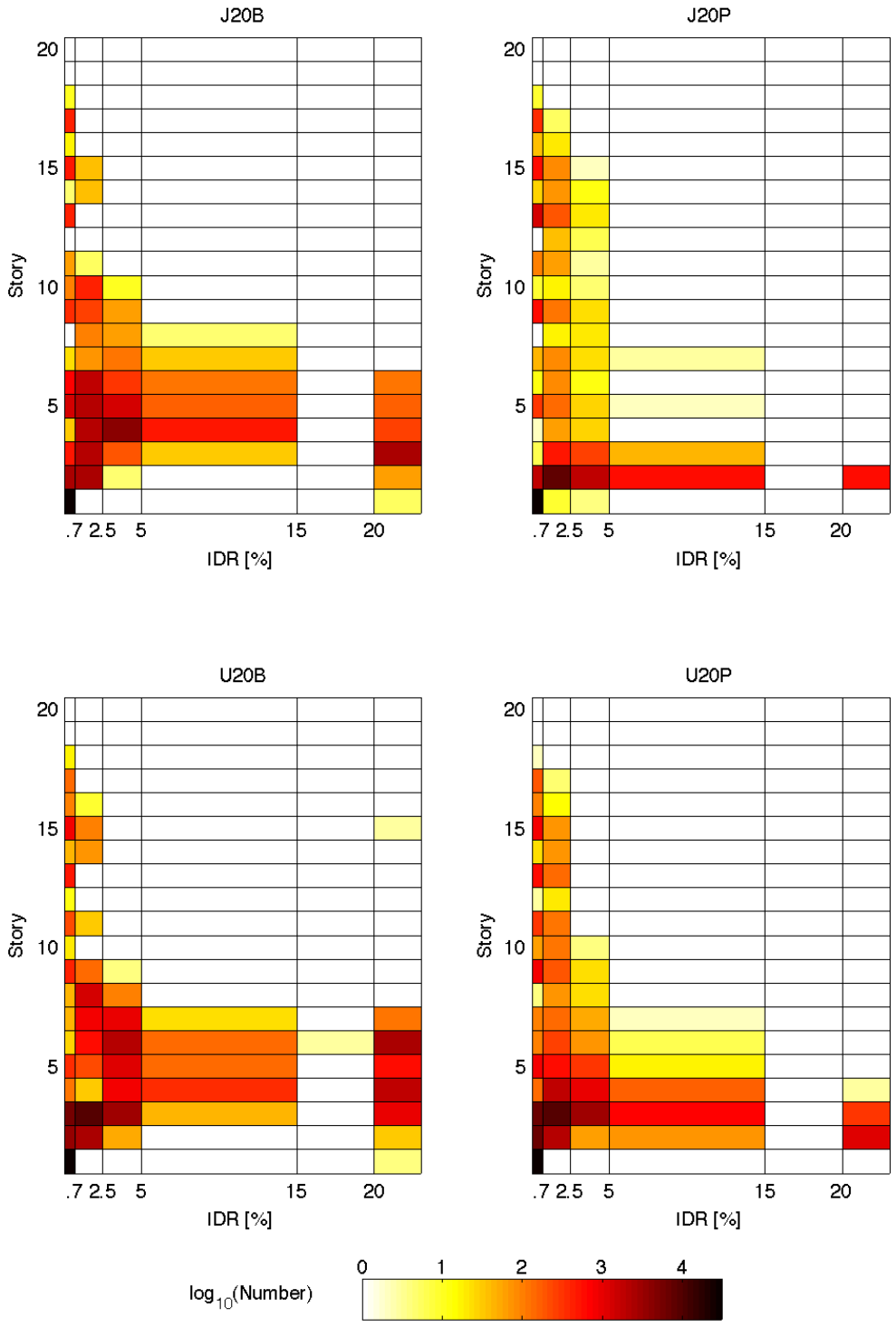

Figure 2.10: For twenty-story buildings, this figure disaggregates the peak IDR by story, or in other words, shows in what story the peak IDR occurred. Models that collapse in the simulations (peak IDR greater than 10%) develop peak drifts in the first six or seven stories. The building models can develop small peak IDRs in the first eighteen stories.

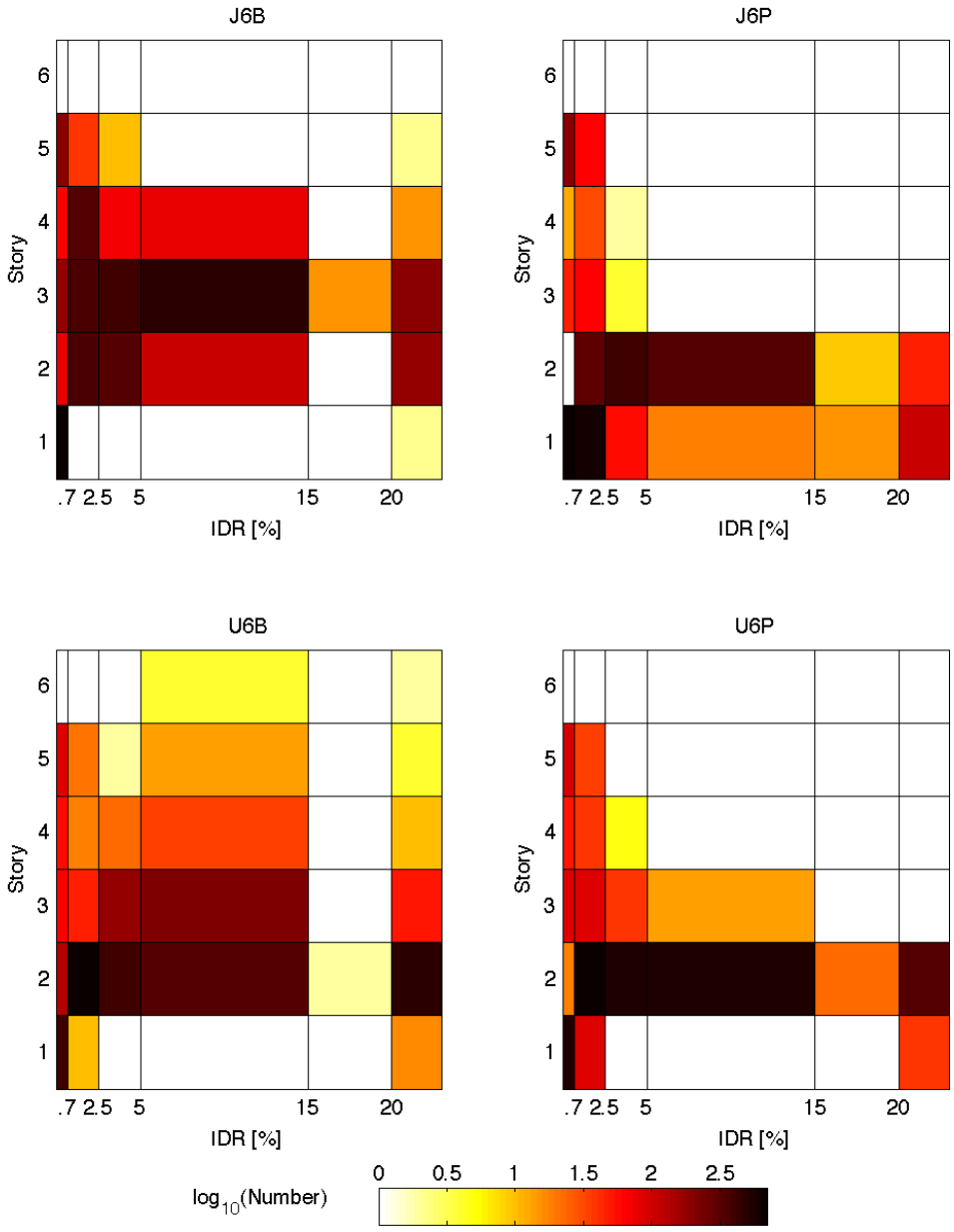

Figure 2.11: For the six-story buildings, this figure disaggregates the peak IDR by story. Models that collapse (that is, with a peak IDR greater than 16%) tend to do so in the first four stories. Small peak IDRs develop in any of the first five stories.

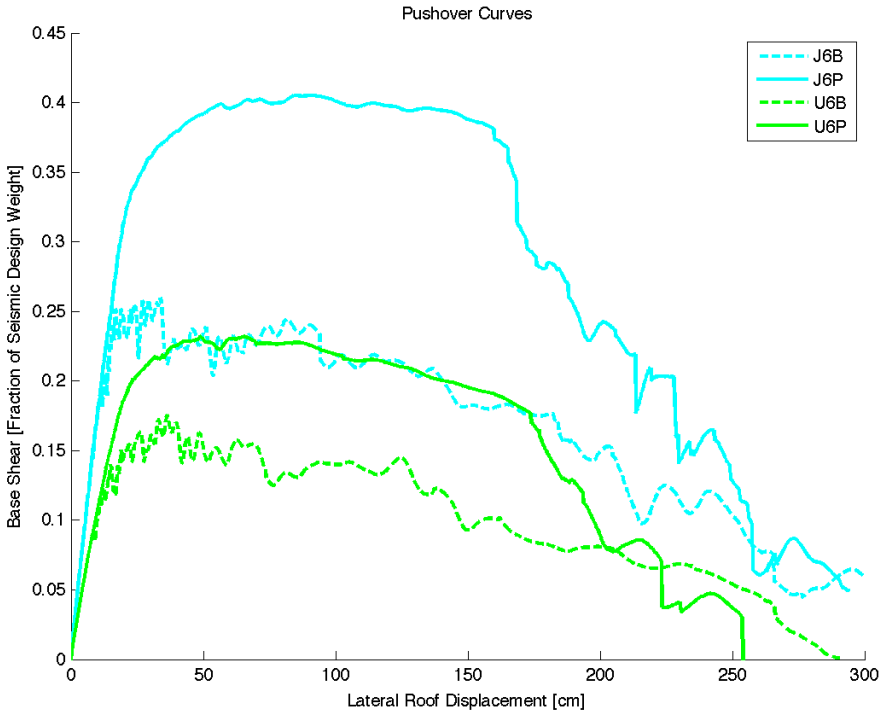

Figure 2.12: This figure shows the pushover curves for the six-story building models.

as higher- or lower-strength. A building's ductility is the ratio of the displacement after which the base shear drops precipitously to the displacement at yield. Ductility indicates the relative amount of deformation that a building can sustain after it has yielded. Note that the ductilities of the building models are similar for the JBC and UBC designs.

2.4 Measurement of Building Responses

Researchers and practitioners use various measurements of building response, depending on the response they want to characterize. One engineer may be interested in the behavior of individual beams, columns, or joints. Another may study a few critical members for the onset and progress of yielding or for the physics of collapse. On a larger scale an engineer may want to characterize the response of entire floors or the building as a whole. Each of these studies requires a different measure of building

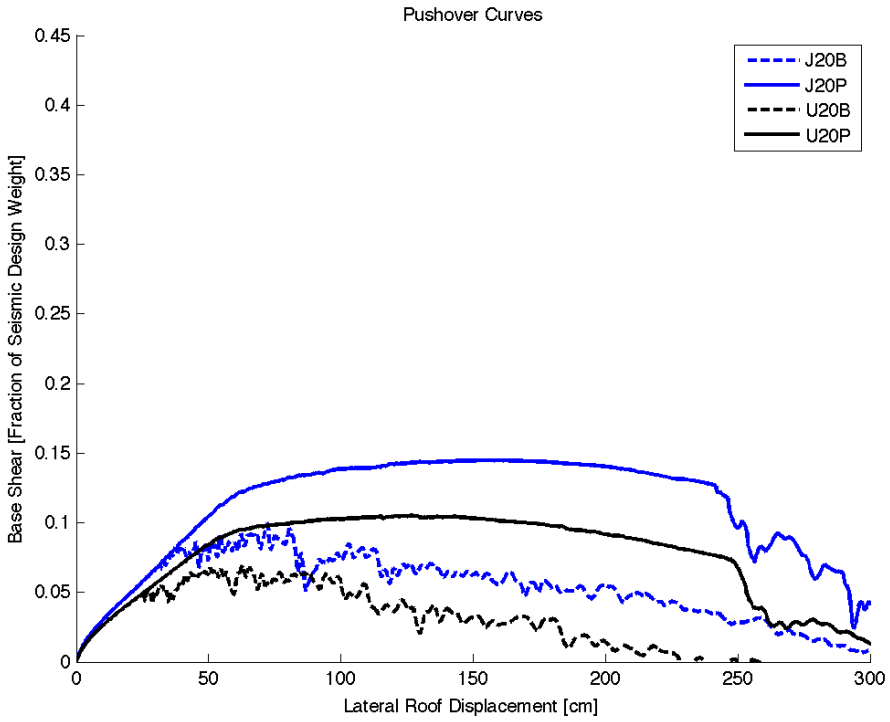

Figure 2.13: This figure shows the pushover curves for the twenty-story steel moment frame building models.

response, appropriate to the level of detail under consideration.

Due to the large number of building responses, I measure overall building performance. One measure is peak dynamic inter-story drift ratio. The inter-story drift ratio quantifies the amount of shear deformation within a story by expressing the relative lateral displacement of two floors as a ratio of the story height. The largest such ratio for all stories and for all time steps in the ground motion time history is the peak IDR.

The peak IDR is a common measure of building response. For example, FEMA 356 uses peak IDR to categorize building response: if the peak IDR is less than 0.007, the building is safe for "immediate occupancy" (American Society of Civil Engineers, 2000). If the peak IDR exceeds 0.025, the building state threatens "life safety." For peak IDRs greater than 0.05, FEMA 356 considers the response a "collapse." These numbers are guidelines to characterize states of building damage based on a quantifiable parameter; they represent a judgement of what the peak IDR would have been during the earthquake in order to produce the post-earthquake damage.

The second response measure is collapse, a categorical description. For the models I consider, collapse refers to the loss of all lateral load-resisting capacity. The finite element program I use does not model the physical collapse of the building; it does not account for some important deterioration mechanisms known to cause collapse in real buildings. Rather, I assume the loss of lateral resistance when the simulation shows unrealistically large deformations. No six-story building model shows reasonable deformations for peak IDRs greater than 0.16, whereas no twenty-story model has reasonable deformations with peak IDRs greater than 0.10 (Figure 4.5). Thus, as a practical matter, I terminate the simulation when the peak IDR reaches 0.2 (for computational efficiency) and deem the model response a collapse. Note that defining collapse as implausibly large deformations in the simulation differs from the definition in FEMA 356.

The third building response measure describes whether the building is a total structural loss, another categorical description. If a building does not collapse in a given ground motion, it may still develop a permanent lateral deformation that

cannot be repaired. In this case, the building is deemed a total structural loss and demolished. I measure this state by calculating the permanent drift over the ground-to-roof building height. If the ratio of the permanent total drift to the building height exceeds 0.0091, then the building is a total structural loss (Iwata et al., 2006). In this way, the three measures of building response (collapse, total structural loss, and peak IDR) characterize three important, permanent or transient, building states.

2.5 Broadband versus Long-Period Peak Ground Measures

This thesis collects and employs both broadband and long-period ground motions. The broadband ground motions have energy content for periods longer than 0.1 s, and the long-period ground motions have energy content for periods longer than 2 s. The peak ground displacement and velocity of a broadband ground motion are different for the same ground motion filtered for long-periods. For most ground motions, the peak ground displacement and velocity of the broadband ground motion are larger than those of the equivalent long-period ground motion.

This thesis measures the peak ground displacement and velocity for both broadband and long-period ground motions. I denote the peak ground displacement and velocity of a broadband ground motion as $\mathrm{PGD_{bb}}$ and $\mathrm{PGV_{bb}}$, respectively. Similarly, I abbreviate the peak ground displacement and velocity of a long-period ground motion with $\mathrm{PGD_{lp}}$ and $\mathrm{PGV_{lp}}$. If there is no distinction between the broadband and long-period peak ground measures, then I use peak ground displacement and peak ground velocity in a general sense.

2.6 Forms of Building Response Figures

This thesis presents maps of peak IDR. The maps report the response of a single building model at all sites in the simulation domain. No city is uniformly built

with steel MRFs, and thus the maps do not predict patterns of responses for the metropolitan areas as built. Rather, presenting the data in this manner highlights areas of large responses for each building model and indicates the areal extent of large building responses.

In addition to the maps, I graph the simulation results as functions of a ground motion intensity measure. The purpose of these graphs is to understand the building deformation as a response to the ground motion. Many intensity measures could characterize the ground motion time histories. I consider peak ground displacement (PGD), peak ground velocity (PGV), and pseudo spectral velocity ($PSV = \omega SD$, where ω is the fundamental circular frequency and SD is spectral displacement) as possible characterizations of the ground motions. Figure 2.14 graphs the peak IDR as a function of each intensity measure. There is more scatter in peak IDR as a function of PGD than as a function of PGV. The scatter in peak IDR varies with PSV: as PSV increases so does the scatter in peak IDR. For elastic building responses, PSV predicts peak IDR well because PSV filters the ground motion at the fundamental period of the building. For inelastic building responses, however, PSV no longer predicts peak IDR well because inelastic building behavior is not well characterized by the elastic response. The scatter in peak IDR for larger PSV is as large as—if not larger than—the scatter in peak IDR as a function of PGV. PGV is a more broadband measure of ground motion than PSV. Since this thesis studies building response in strong ground motions, PGV is a better intensity measure than PGD or PSV.

In all graphs of building response, I show the building state (that is, collapse or total structural loss) and peak IDR on two plots, one above the other. For some figures, the top plot reports the proportion of sites on which the model collapses or is a total structural loss for a given PGV value. The bottom plot reports the normalized peak IDR if the building stands. I normalize the peak IDR by removing the linear trend, which can be seen in Figure 2.14. For example, Figure 2.16 compares building responses in different orientations with respect to the horizontal ground motions. For a $\mathrm{PGV_{bb}}$ of approximately 3 m/s, buildings oriented at an angle, θ, equal to 60 deg collapse on 40% of the sites in the simulation domain. If the building stands or is

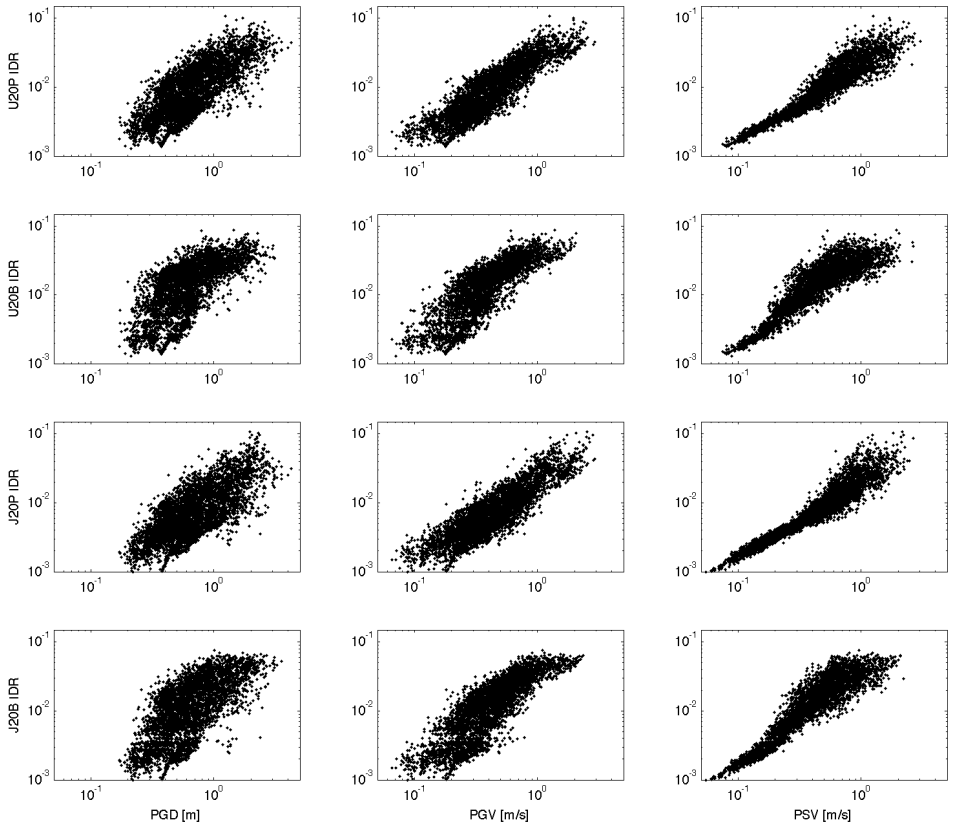

Figure 2.14: The remainder of this chapter, as well as Chapters 3–5, compare building responses as functions of a ground motion intensity measure. This figure motivates the choice of PGV as the intensity measure in these chapters. (Collapsed buildings are not represented in these plots.) PGD, PGV, and pseudo-spectral velocity (PSV; or similarly, spectral displacement or spectral acceleration) have an approximately linear relationship with peak inter-story drift ratio. The variance in peak IDR is smaller as a function of PGV compared to that from PGD. For PSV less than 0.2 m/s, the variance is quite small, however for larger PSV, the variance is larger. For large ground motions, the variance is larger for peak IDR as a function of PSV than for peak IDR as a function of PGV. Chapter 6 compares quantitatively building response prediction models based on PGD, PGV, and pseudo-spectral acceleration.

repairable at this PGV, then the range of peak IDR could be 0.3–3 times the median peak IDR.

Other figures compare two building responses at each site in the simulation domain. That is, the same ground motion is applied to two building models, and the building responses are compared directly. In these figures, the top plot has two lines, representing the proportion of sites where either of the two buildings collapses or is a total structural loss. The bottom plot reports the ratio of the peak IDR in one building to the peak IDR in the second, assuming both buildings stand or are repairable at the site.

2.7 Modeling Assumptions

To generate the responses of steel MRF buildings at so many sites for so many simulated earthquakes, I make several initial decisions about the modeling procedure. These choices include: how to combine the horizontal ground motions into a single resultant; whether to include the vertical component of ground motion; the distribution of weld fracture strain; and the seed number that generates the random assignment of fracture strain to individual welds. The following sections describe these choices and evaluate the effect of each choice on the results. Only the choices of how to resolve the two horizontal components of ground motion and of weld fracture strain distribution noticeably affect the building responses. The chosen horizontal resultant produces larger building responses for the same ground motion than other possible resultants. The chosen weld fracture strain distribution produces smaller building responses for the same ground motion, compared to an alternate distribution.

2.7.1 Horizontal Ground Motions

There is no standard way to apply two-component horizontal ground motions to buildings. The orientation of an existing building site is known with respect to a specific fault, so the horizontal components of ground motion can be properly applied in this case. This thesis, however, considers buildings at all sites in two broad geographic

regions (that is, the San Francisco and Los Angeles metropolitan areas). The orientation of a rectangular-plan building with respect to predicted ground motions is unknown at all sites. The streets in west Los Angeles, for example, run predominantly north-south (NS) and east-west (EW), but the longitudinal axis of a rectangular-plan building may be NS or EW. A building set at an angle with respect to the regular street grid, maybe for aesthetic reasons, would further complicate this issue. As a second example, the streets in Santa Monica are rotated approximately 45 deg from North. It is impractical to assign the most likely orientation of a rectangular-plan building at all 13,754 sites in the four simulation domains I consider.

I choose a particular orientation of the building models with respect to the ground motions based on the building response. I want to characterize the most damaging building response for a given ground motion. Further, the planar building models require a single horizontal component of ground motion and a single vertical component. I combine the two horizontal components to produce a single horizontal resultant that represents the most damaging orientation of a building with respect to the given ground motion.

Peak-to-peak velocity (V_{pp}) is a good measure of ground motion for predicting the response of steel MRF buildings, since a large forward-and-back pulse in displacement induces large drifts in the lowest stories. I orient the short dimension of the building models in the direction of the largest peak-to-peak velocity. I find this direction by combining the orthogonal NS and EW components at angles of 0 to 179 deg in increments of 1 deg (equation 2.1), producing 180 resultant horizontal ground motions. I select the resultant with the largest peak-to-peak velocity and apply that ground motion to building models at the site associated with the original NS and EW components. This angle is not the same for all sites in the simulation domain nor for all simulations on the same domain, so the buildings are not uniformly oriented with respect to North.

$$\text{Resultant}(t) = [\text{EW component}(t)] \cos\theta + [\text{NS component}(t)] \sin\theta \qquad (2.1)$$

The building response in the short dimension should be smaller than that in the long dimension. The design for wind loads requires more lateral force resistance in the short dimension due to the larger building surface area in the long dimension. Thus the building design is stiffer in the short dimension, resulting in smaller responses. By aligning the short dimension of the building with the largest peak-to-peak velocity, the resulting building responses should be relatively large for the given three-component ground motion but not the largest possible. If the long dimension of the building aligned with the largest peak-to-peak velocity, then the building response would be larger than the responses predicted in this thesis.

I evaluate the effect of choosing the resultant with the largest peak-to-peak velocity by comparing the building responses in several alternate horizontal resultants. The ground motions are from a magnitude 7.15 simulation on the Puente Hills fault in the Los Angeles basin. I combine the two horizontal components at angles of 0 to 150 deg in increments of 30 deg at all sites. This exercise produces six distinct ground motions at each site, including the pure EW ($\theta = 0$ deg) and NS ($\theta = 90$ deg) components. I compare the building responses to these six resultants and to the resultant with the largest peak-to-peak velocity.

Figure 2.15 maps the peak IDRs of the twenty-story, more flexible model with perfect welds (U20P) for six of the seven combinations. The resultants from angles of 0 (EW) and 150 deg induce large peak IDRs on small areal extents, compared to the other resultants. The pure NS component and the resultant with the largest peak-to-peak velocity induce large peak IDRs on the largest areal extents. Figure 2.16 graphs the simulated responses as a function of PGV_{bb}, which is independent of the combination of the two horizontal components. Resultants from angles of 30, 60, and 90 deg, and the largest peak-to-peak resultant cause collapse of the building on a larger proportion of sites for a given PGV_{bb} than do the other resultants. The largest peak-to-peak velocity resultant consistently produces the highest proportions of collapse. If the building remains standing, the peak IDRs are larger for resultant ground motions at these angles compared to the other angles. As desired, applying the horizontal resultant with the largest peak-to-peak velocity induces building responses

larger than those from other resultants.

I also find the resultant that maximizes peak-to-peak velocity by three algorithms. The three algorithms first combine the horizontal components at every angle from 0 to 179 deg in increments of 1 deg, generating 180 resultants. After this, the algorithms are distinct. The first algorithm finds the extrema in each resultant, determines the largest difference between consecutive extrema, and then finds the maximum difference over all resultants. This algorithm is not robust: for example, it cannot distinguish between consecutive maxima in the resultant. However, by inspection of dozens of the resultants, this algorithm consistently chooses the obviously large peak-to-peak velocity. The second algorithm measures the long period pulse, characteristic of near-source ground motions. This algorithm filters each resultant with a low-pass, Butterworth filter with a corner period of 2.5 s. Since the filter removes short-period content, the long-period pulse remains, albeit slightly attenuated. Since the purpose of the algorithm is not to find the value of the largest peak-to-peak velocity, but rather which resultant has the largest value, the amount of attenuation is not important. This method is robust because the filtered resultants have consecutive extrema that are peak positive and peak negative. The third method is the simplest: it calculates the distance between the most positive velocity and the most negative velocity over the entire unfiltered ground motion time history.

Figures 2.17 and 2.18 compare the peak IDRs for the twenty-story, more flexible building models with prefect welds (U20P) subject to the ground motions from each peak-to-peak velocity algorithm. The algorithm does not significantly affect the building response to the ground motion at the sites in the simulation domain. This study uses the first algorithm to select the combination of the two horizontal components that maximizes the peak-to-peak velocity. For computational efficiency, however, the difference between the peak positive and peak negative velocities (algorithm 3) can be used in place of the true peak-to-peak velocity (algorithm 1).

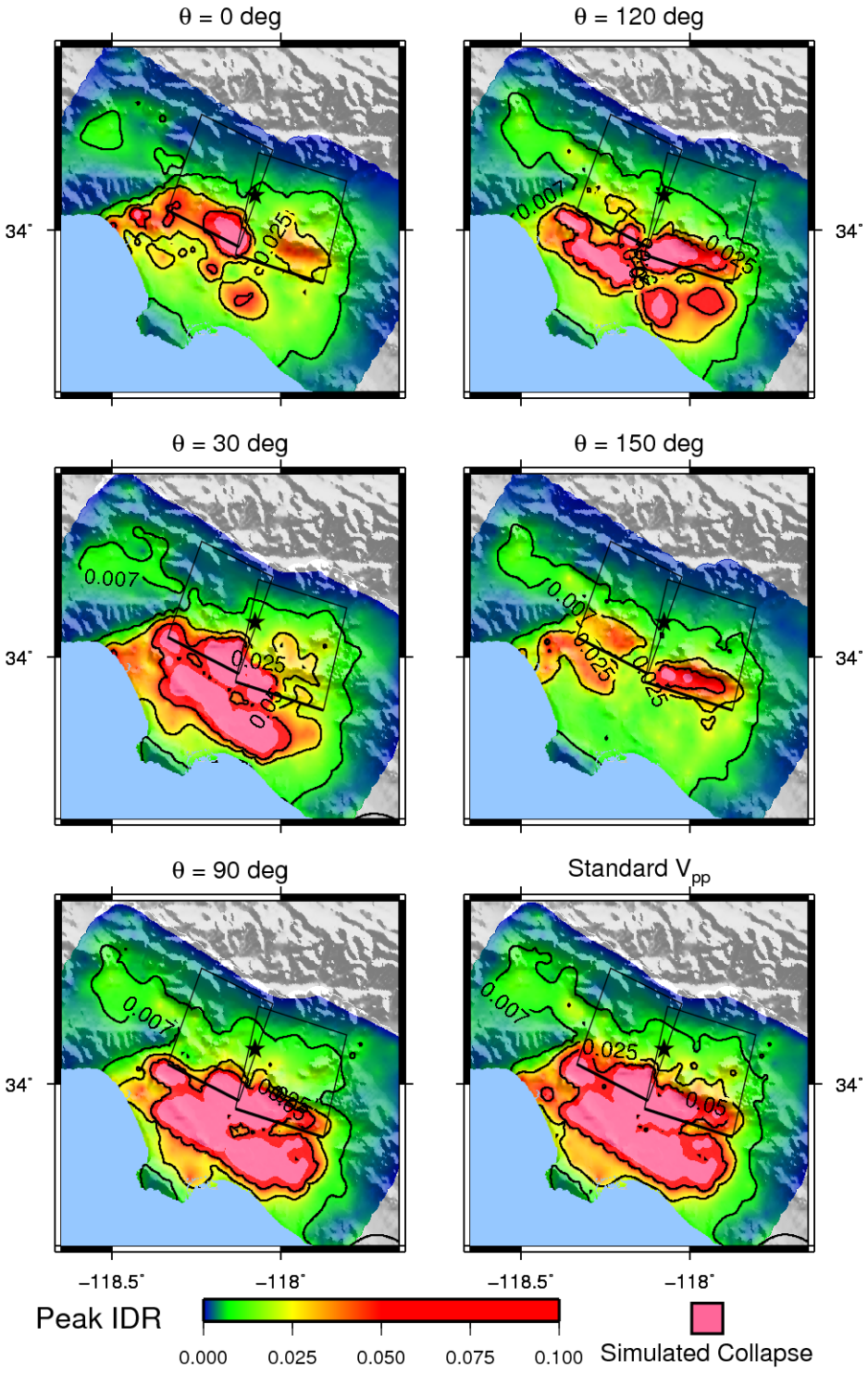

Figure 2.15: This figure maps U20P building responses to ground motions with various combinations of the horizontal components. For this simulation on the Puente Hills fault, the EW component (0 deg) induces smaller U20P building responses at a given site than does the NS component (90 deg). As desired, the resultant with the largest peak-to-peak velocity causes the largest building responses for each site on the simulation domain.

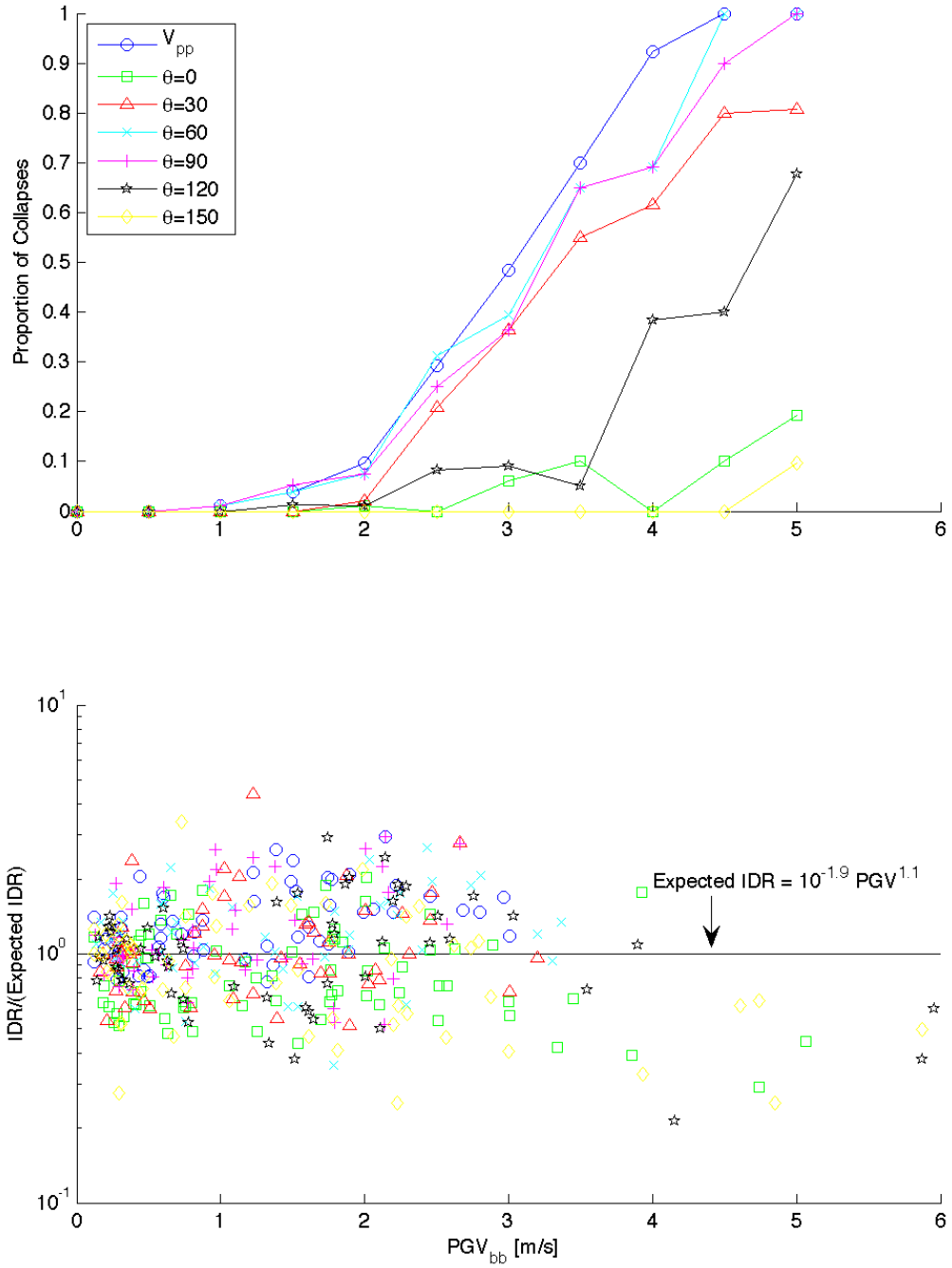

Figure 2.16: This figure compares the U20P building responses to several combinations of the horizontal component of ground motion. The resultant with the largest peak-to-peak velocity induces more collapses for a given PGV_{bb}. If the models do not collapse, the resultant with the largest peak-to-peak velocity also tends to induce larger peak IDRs than do the resultants from a single angle at all sites.

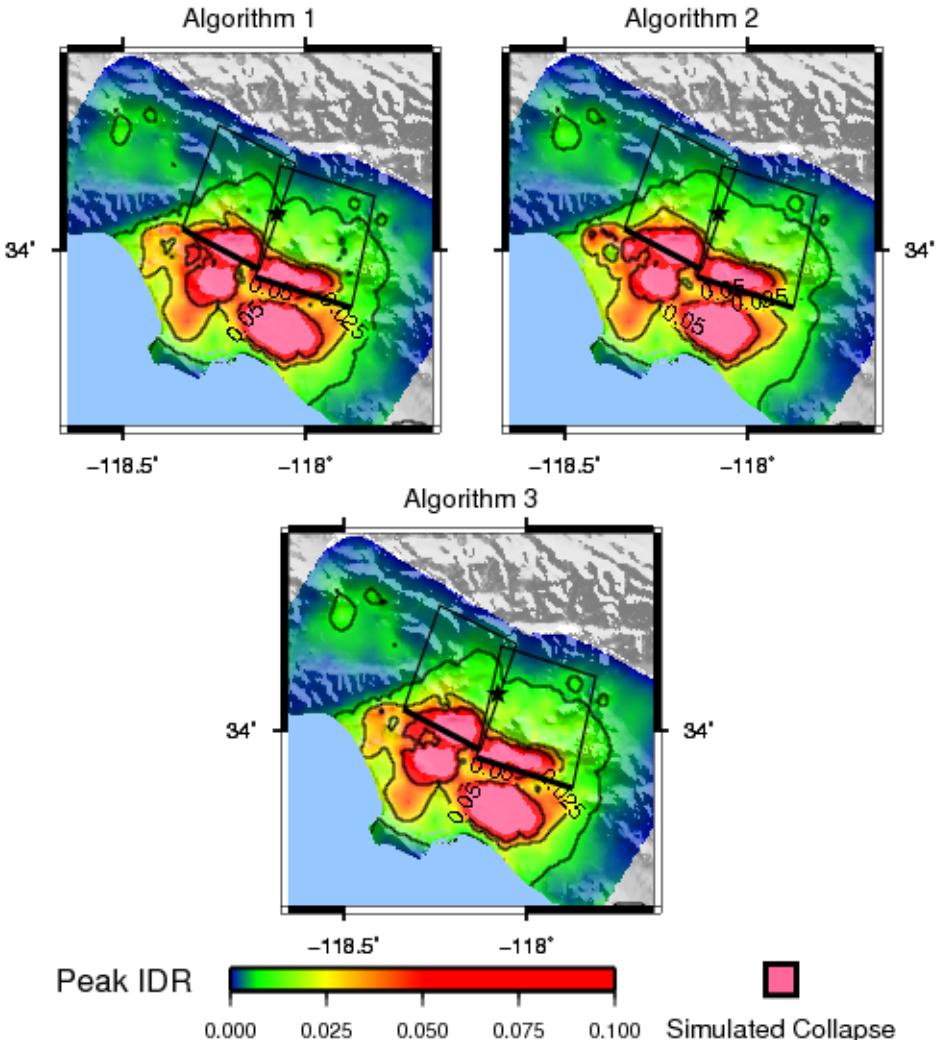

Figure 2.17: This figure compares U20P responses to resultant horizontal ground motions chosen by 3 peak-to-peak velocity algorithms. There are no apparent differences due to the peak-to-peak velocity algorithm.

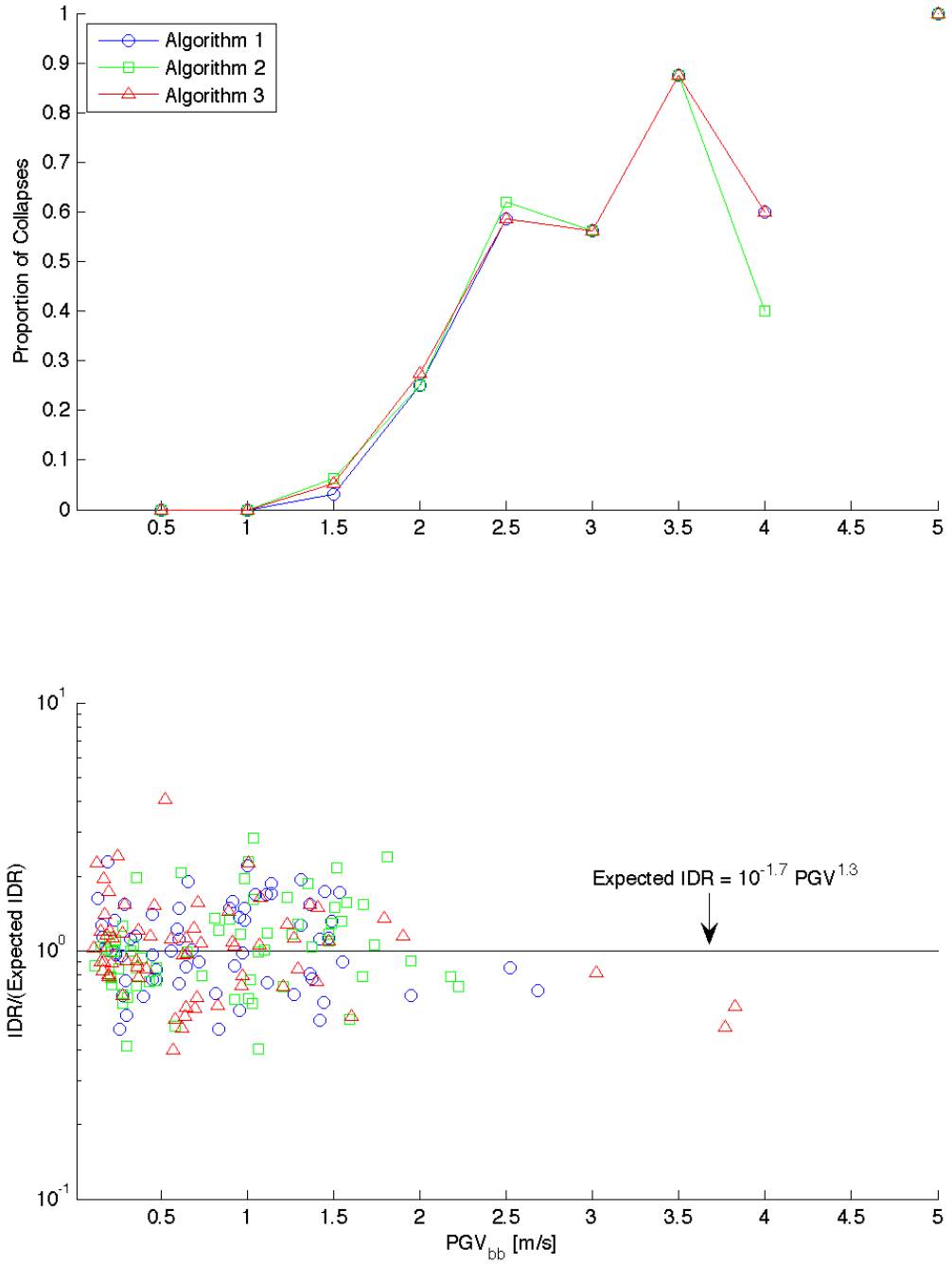

Figure 2.18: This figure compares the U20P model responses to ground motions with the resultant horizontal component determined by three algorithms. There is no systematic difference in the building response due to the algorithm that measures the peak-to-peak velocity.

2.7.2 Vertical Ground Motions

Seismic ground motions induce primarily lateral loads in buildings. In an earthquake the ground motions are three-dimensional, and thus an earthquake induces both lateral and vertical forces in buildings, along with moments. As a rule of thumb (codified in the building code), the vertical ground motion is approximately two-thirds of the horizontal motion. Also, buildings must withstand a constant downward acceleration of 1 g, which induces constant vertical loads. Thus buildings are inherently stronger vertically than laterally. For these reasons, engineers sometimes neglect vertical ground motions to simplify the model.

For the four building models, I simulate the building response with and without the vertical component of ground motion. Figure 2.19 maps the peak IDR. Based on this figure, there are no obvious differences in building response due to the presence of vertical ground motion. Figure 2.20 compares the building responses directly. The buildings collapse on similar proportions of sites with or without the vertical component. For $\mathrm{PGV_{bb}}$ at which there are differences, buildings subject to only the resultant horizontal component collapse on a slightly greater proportion of sites than do buildings subject to the vertical component as well. If both buildings at a site remain standing, the peak IDR is approximately the same if the vertical component is included or not. For large ground motions ($\mathrm{PGV_{bb}}$ greater than 2 m/s) neglecting the vertical component slightly over-predicts the probability of building collapse.

2.7.3 Brittle Weld Distribution

For models with brittle welds, each weld location has an assigned propensity to fracture. (Refer to Section 2.2.7 for a complete description of the weld model.) The finite element algorithm assigns each weld a fracture strain as a fraction of the yield strain ($\epsilon_{\mathrm{fracture}}/\epsilon_{\mathrm{yield}}$). If the strain in an individual weld fiber exceeds the fracture strain, the fiber does not carry tensile loads for the remainder of the simulation; it may carry compressive loads, though, if re-engaged. The random assignment of fracture strain to a weld samples from a user-specified distribution of fracture strains. Figure 2.8

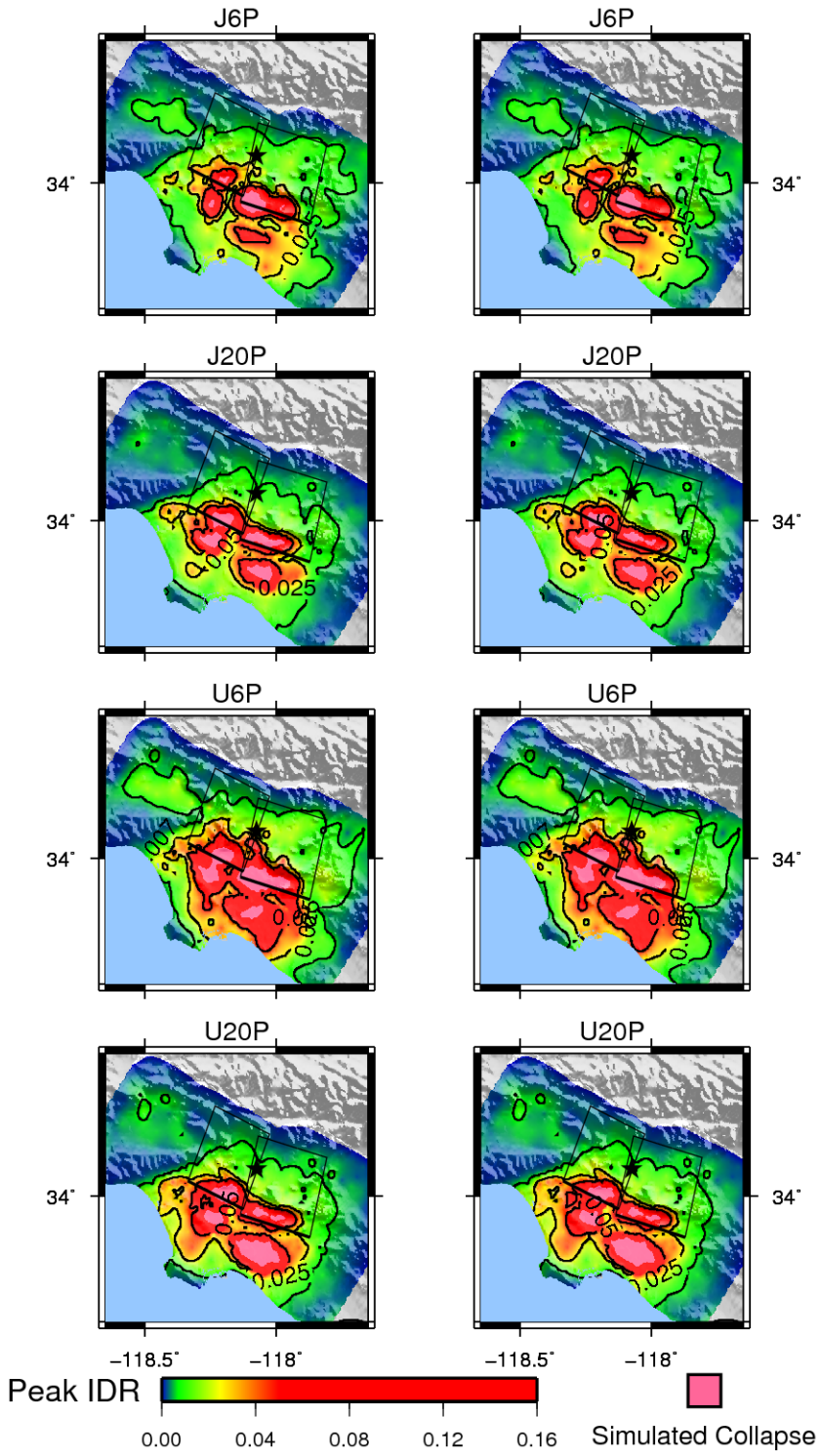

Figure 2.19: This figure compares building responses to ground motions with only the resultant horizontal component (maps on the left) and with both vertical and resultant horizontal components (maps on the right). There appears to be no difference in regional extent of building responses with or without the vertical component.

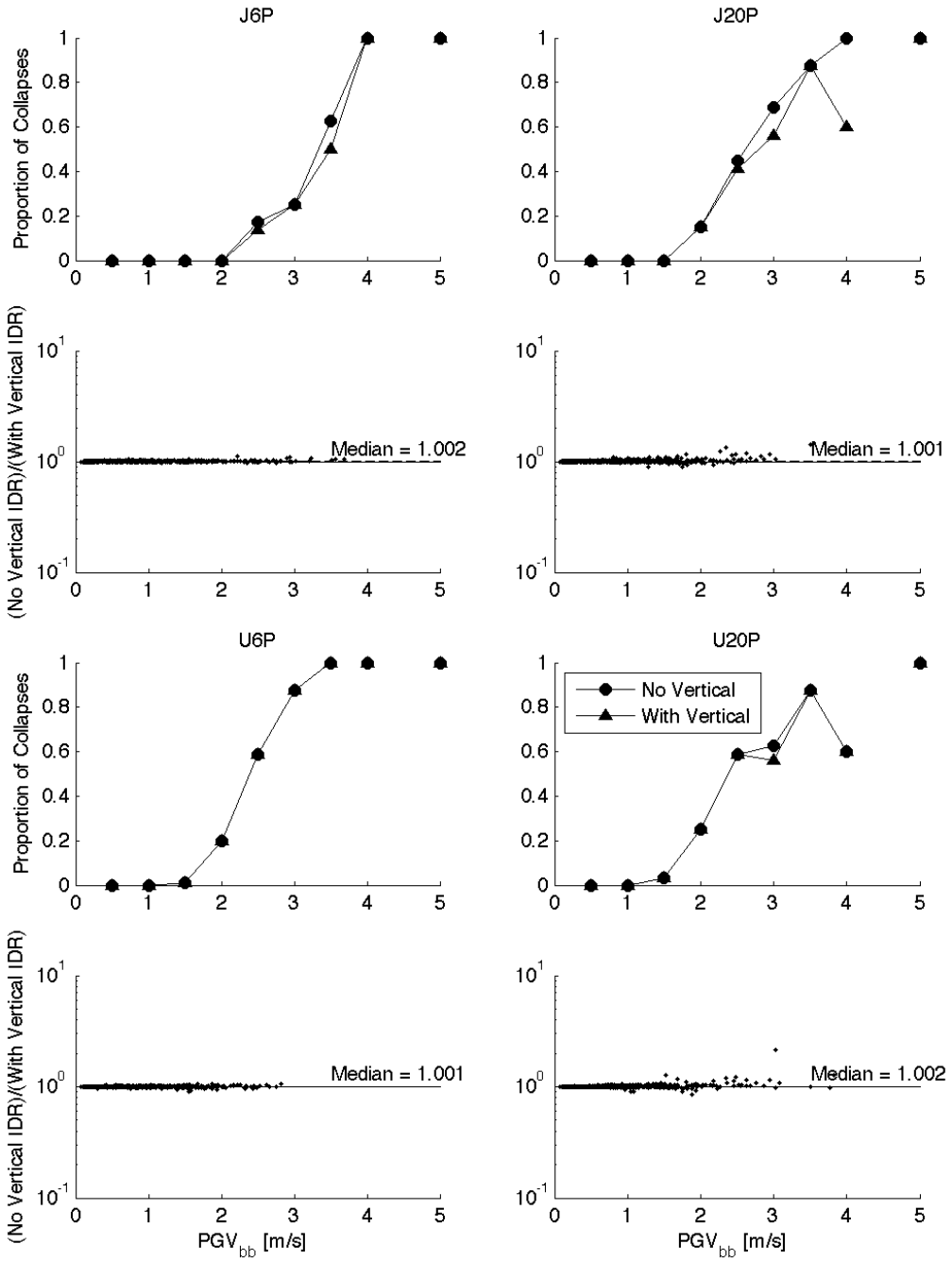

Figure 2.20: This figure compares the building responses to ground motions with and without the vertical component. For ground motions with a PGV_{bb} greater than 2 m/s, neglecting the vertical component may over-predict the number of collapses. However, this effect is insignificantly small.

shows two such weld fracture strain distributions.

I compare the simulated building responses for models with the B and F weld distributions. Figure 2.21 maps the peak IDRs for building models with each fracture strain distribution. The areal extent of large building responses (peak IDR greater than 0.025) is similar for the fracture strain models. Figure 2.22 directly compares the building responses at each site for the two fracture strain distributions. Models with F welds collapse on a consistently greater proportion of sites at a given PGV_{bb} than do models with B welds. If both models remain standing at a site, the peak IDR in the F weld building model tends to be larger than the peak IDR in the B weld model. For the smallest ground motions, there is no difference in peak IDR between the two models because no welds fracture. The weld model can cause different building responses only after the building yields and accumulates fractured welds. For larger ground motions, the peak IDR in F weld models is often 1.1–1.2 times larger then the peak IDR in B weld models and may be up to 4 times for some sites, depending on the building design.

There is no penultimate fracture strain distribution for this problem. The fracture strain distribution is necessary to model a random assignment of weld fracture strain to individual welds. The distribution can only be validated by experience, but there is little evidence from moment-resisting frames in ground motions as large as these. This thesis uses the B weld distribution in the following chapters. The choice of the F weld distribution would have resulted in larger building responses for building models with brittle welds.

2.7.4 Random Seed Number

The assignment of fracture strain to welds in the building model requires a seed number to generate the random sample of the fracture strain distribution. By chance, a seed number may cause an unusually large number of weak welds to be assigned to a localized area. In this case, the model may be inconsistent with an existing building, and certainly this is inconsistent with the purpose of randomly distributing the weld

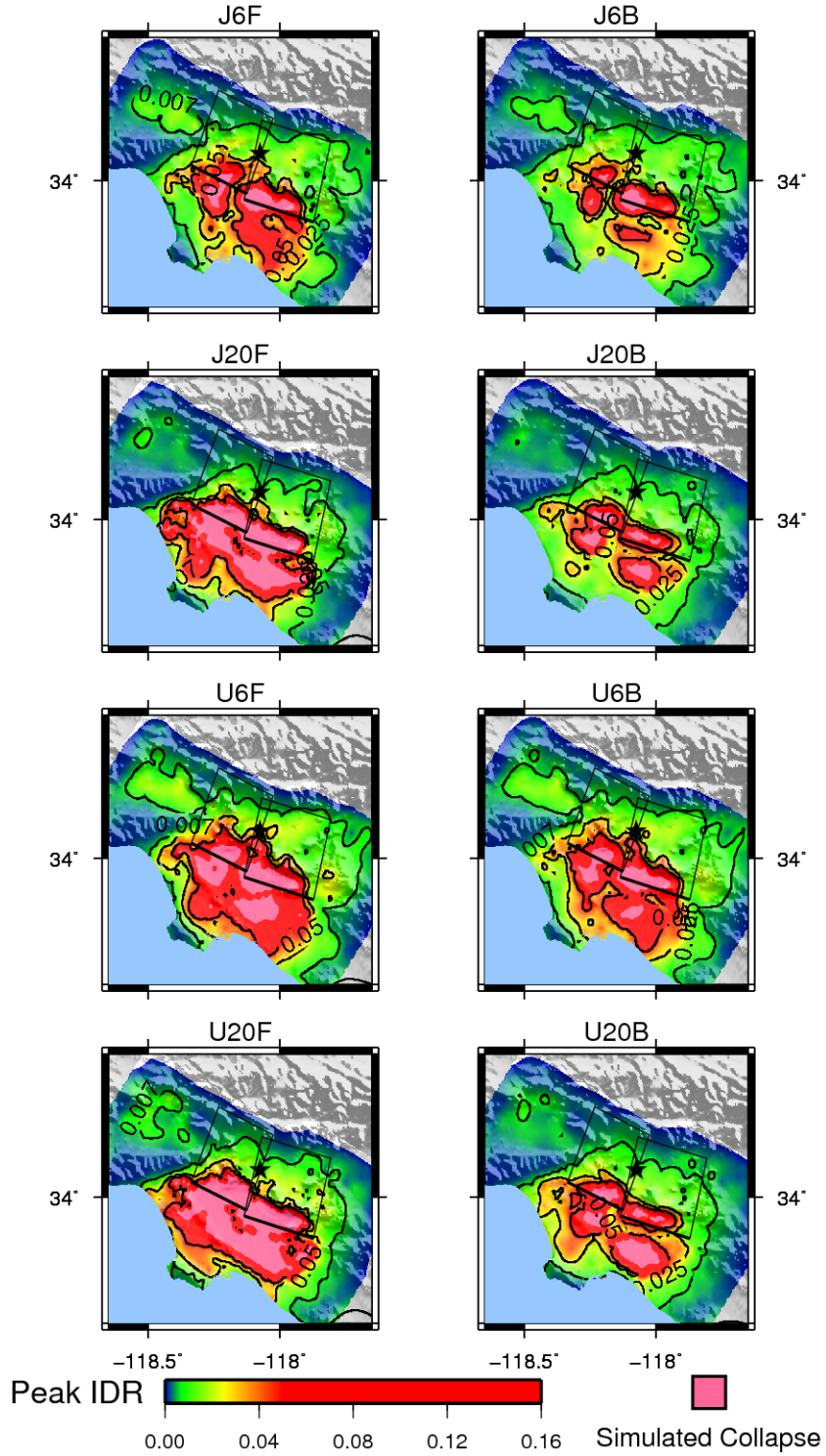

Figure 2.21: This figure compares building responses for models with brittle welds defined by the F weld (maps on left) and B weld (maps on right) distributions. There are differences in the responses at single sites, but the overall areal extent of large building response is consistent for the two weld fracture strain distributions.

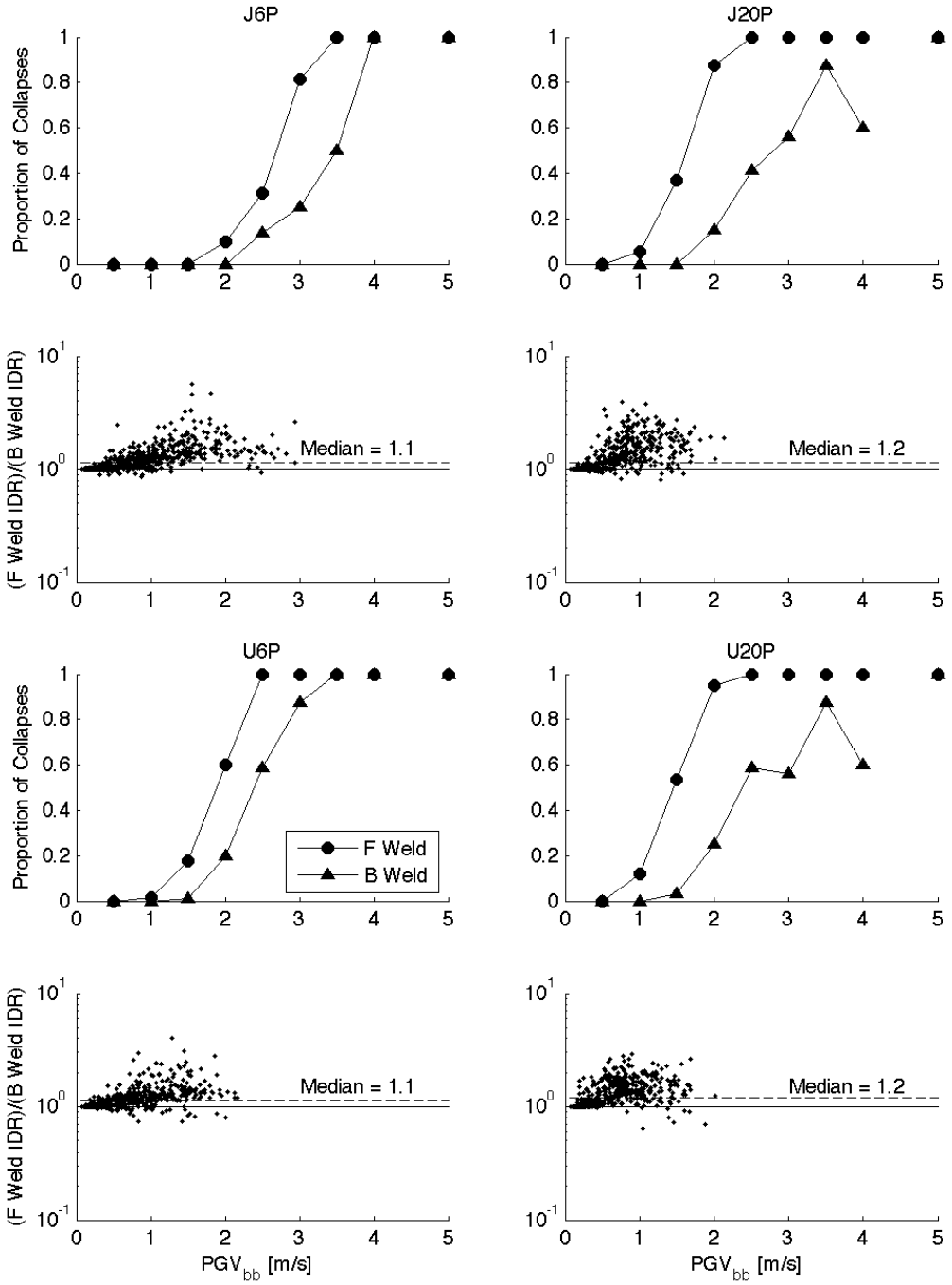

Figure 2.22: The assumed fracture strain distribution for brittle welds affects the building response. Models with F welds collapse on a greater proportion of sites than do models with B welds. If the models do not collapse, those with F welds have a peak IDR most likely 1.1–1.2 times the peak IDR for models with B welds.

fractures throughout the building. In this study, every brittle weld fracture strain assignment begins with the same seed number; models with the same weld fracture strain assignments sit at every site in the simulation domains.

To evaluate the effect of the random seed number on the building response, I compare the responses of four models, each with a different seed number. Figure 2.23 maps the peak IDRs for the twenty-story, more flexible building model with brittle welds (U20B). The areal extent of inelastic building response is similar for all four seeds, and the extent of the largest building responses (peak IDR greater than 0.05) is also similar. Figure 2.24 plots the building responses as functions of PGV_{bb}. There seems to be no consistent difference in building response due to the choice of seed number. The choice of one seed number over another does not contribute significantly to the uncertainty of the building response. The choice of weld fracture strain distribution (for example, B or F welds) affects the response of models with brittle welds more significantly than does the assignment of a sampled fracture strain to a particular weld.

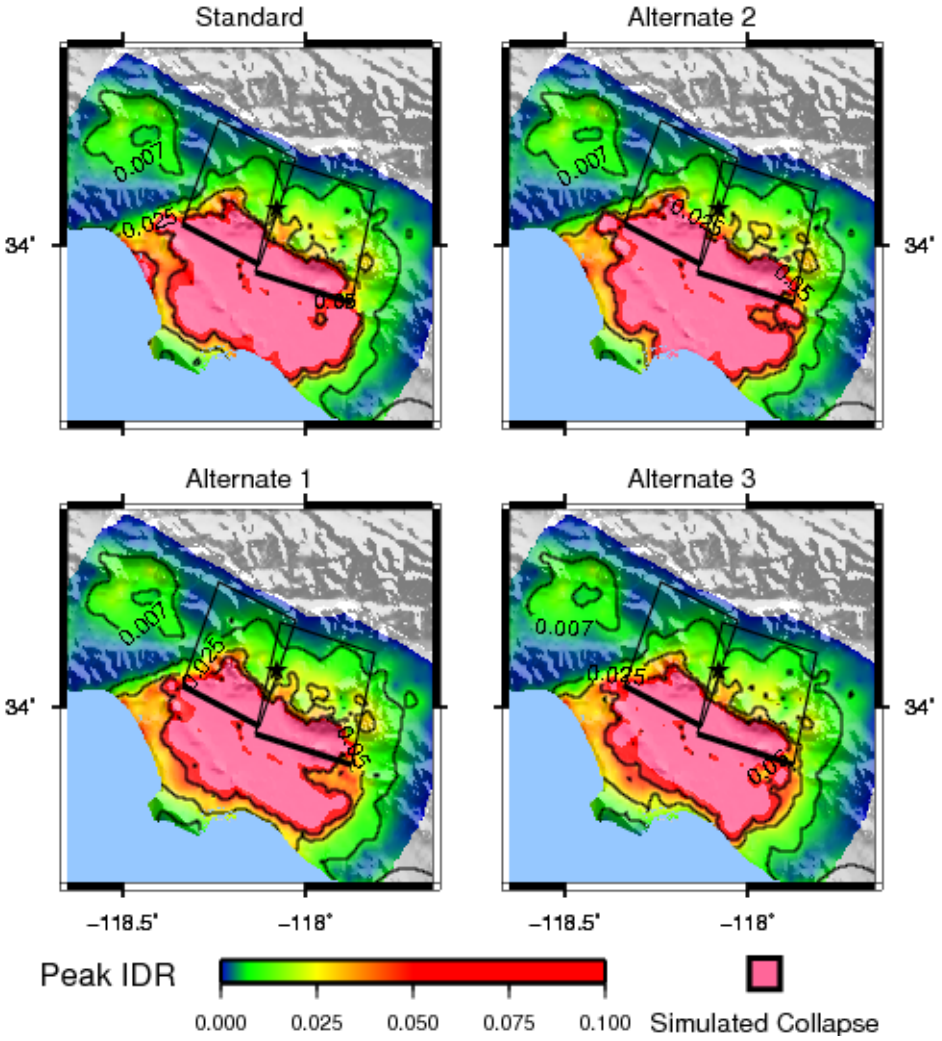

Figure 2.23: This figure compares the response of the U20B model with weld fractures assigned from four initial seed numbers. In each of the four simulations, the model at every site has the same weld fracture strain pattern within the building. While there are slight differences in the extent of building collapses, the models with welds assigned from different seed numbers appear to have similar responses at a given site.

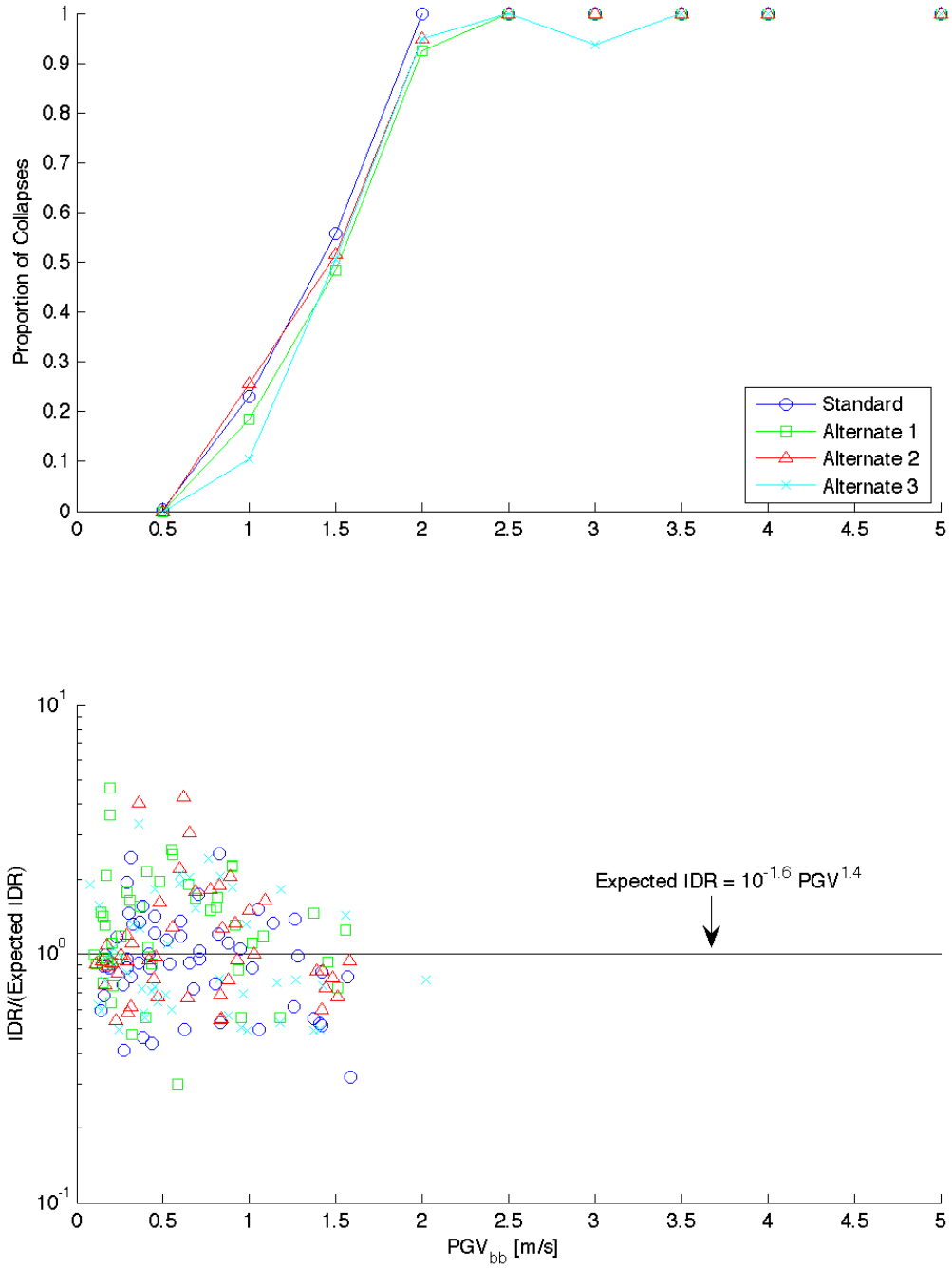

Figure 2.24: This figure compares the responses of brittle weld models with different assignments of fracture strains. Models with brittle weld fracture strains assigned from the four seed numbers considered here respond similarly to the same ground motions. This thesis uses the standard assignment for all brittle welds.

Chapter 3

Simulations in the San Francisco Area

This chapter presents the responses of twenty-story, steel moment-resisting frame (MRF) buildings to simulated earthquakes in the San Francisco Bay area. Aagaard et al. (2008a,b) generated scenario ground motions for the 1989 Loma Prieta and 1906 San Francisco earthquakes, as well as two magnitude 7.8 ruptures on the northern San Andreas fault. I apply these long-period ground motions to two models of twenty-story buildings, and I compare the response of the stiffer, higher-strength building to that of the more flexible, lower-strength building. I also compare the responses of buildings modeled with fracture-prone welds to the responses of buildings with sound welds.

The 1989 magnitude 6.9 Loma Prieta and 1906 magnitude 7.9 San Francisco scenario earthquakes also demonstrate how much more damaging a great earthquake can be compared to a moderate or large earthquake. The seismic response of steel MRF buildings would be significantly different in repeats of each historic earthquake. The areal extent of inelastic building responses in the 1989 Loma Prieta scenario is tiny compared to that in the 1906 San Francisco scenario. Steel MRF buildings in the entire San Francisco Bay region would be affected by a magnitude 7.8 earthquake on the northern San Andreas fault segment near San Francisco. A magnitude 6.9 earthquake would affect a more limited region.

3.1 Ground Motion Study

Several researchers generated ground motions of the 1906 San Francisco earthquake on the occasion of its centennial anniversary (Aagaard et al., 2008a,b). The researchers employed new models of the geologic structure and seismic wave speeds in the San Francisco region. To validate their methods and models, the researchers simulated scenario ground motions for the 1989 Loma Prieta earthquake, based on the Beroza (1991) and Wald et al. (1991) source models. For magnitude 7.8 ruptures on the northern San Andreas fault, they used a series of source models: first they used a source model by Song et al. (2008) inferred from the 1906 earthquake; then they modified the Song source model "to overcome limitations of the data available"; and finally they generated a random slip distribution for comparison.

The ground motions in this thesis are from the modified Song source model, generated by Brad Aagaard. For the same source model, there are three hypocenter locations: the inferred 1906 location, due west of San Francisco (bilateral rupture); a hypothetical location north of San Francisco, near Bodega Bay (unilateral rupture to the south); and a second hypothetical location south of San Francisco, near San Juan Bautista (unilateral rupture to the north). Aagaard et al. (2008b) considered several slip distributions and hypocenter locations to "assess the variability in the ground motions and distributions of shaking" in the various scenario earthquakes.

Table 3.1 lists the simulated earthquakes from the Aagaard et al. (2008a,b) studies that are used in this thesis, and Figure 3.1 maps the faults. Note that the 1906-like simulations are magnitude 7.8 whereas the 1906 earthquake was magnitude 7.9. Figures 3.2 and 3.3 show the long-period peak ground displacements (PGD_{lp}s) and peak ground velocities (PGV_{lp}s) for the five simulations. In this thesis, I measure the PGD_{lp} and PGV_{lp} as the largest vector amplitude of the two horizontal, north-south and east-west, components.

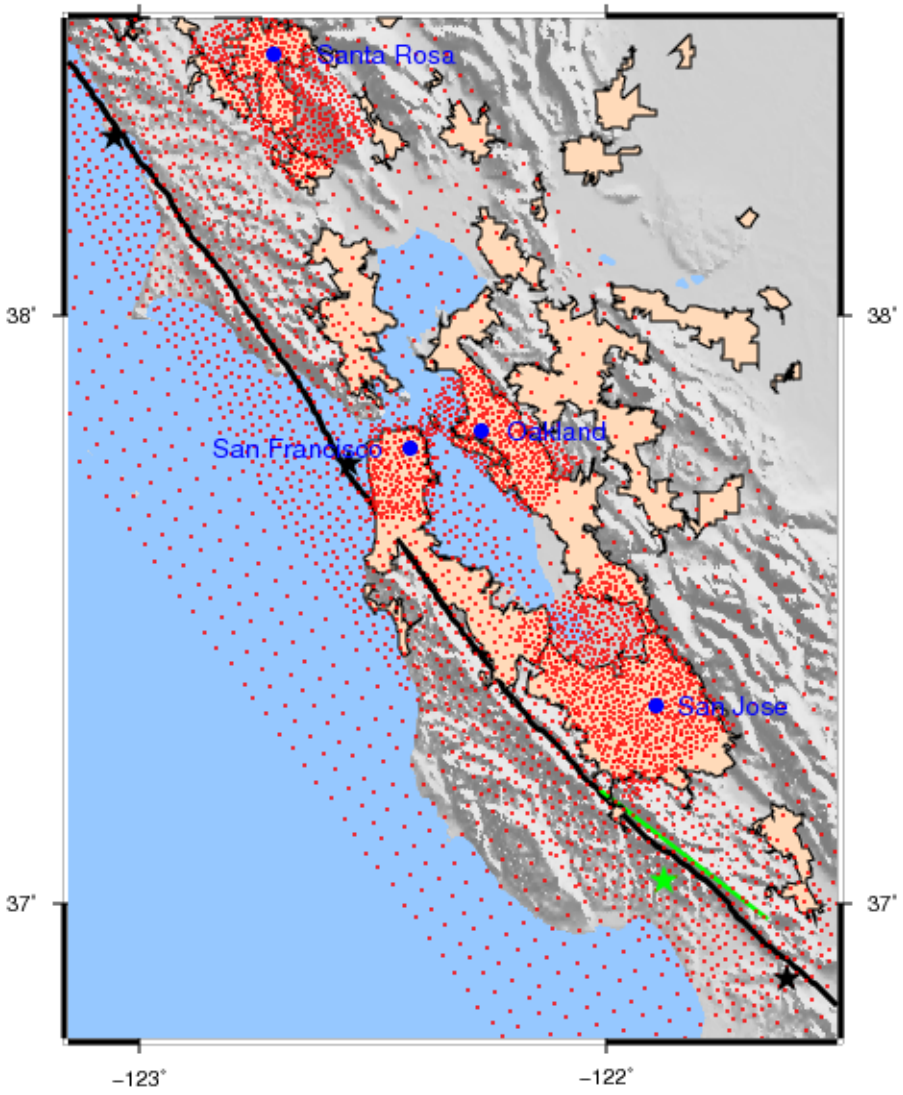

Figure 3.1: The simulation domain in Aagaard et al. (2008a,b) covers the San Francisco Bay area. Red dots locate the 4945 sites in the domain. Beige areas are the urban areas (as defined by the 2000 census). Blue dots locate major cities in the area that have simulation sites on a finer grid. The black line locates the San Andreas fault, and black stars locate the three hypocenters considered in the Aagaard et al. simulations. The green line represents the fault segment on which the Loma Prieta earthquake ruptured, and the green star locates its hypocenter.

Fault name	*Magnitude*	*Source model*	*Hypocenter location*
Loma Prieta	6.9	Beroza	1989 Loma Prieta
Loma Prieta	6.9	Wald et al.	1989 Loma Prieta
Northern San Andreas	7.8	modified Song	north of San Francisco
Northern San Andreas	7.8	modified Song	south of San Francisco
Northern San Andreas	7.8	modified Song	1906 San Francisco

Table 3.1: This table lists the five simulations used in this thesis generated by Aagaard et al. (2008a,b).

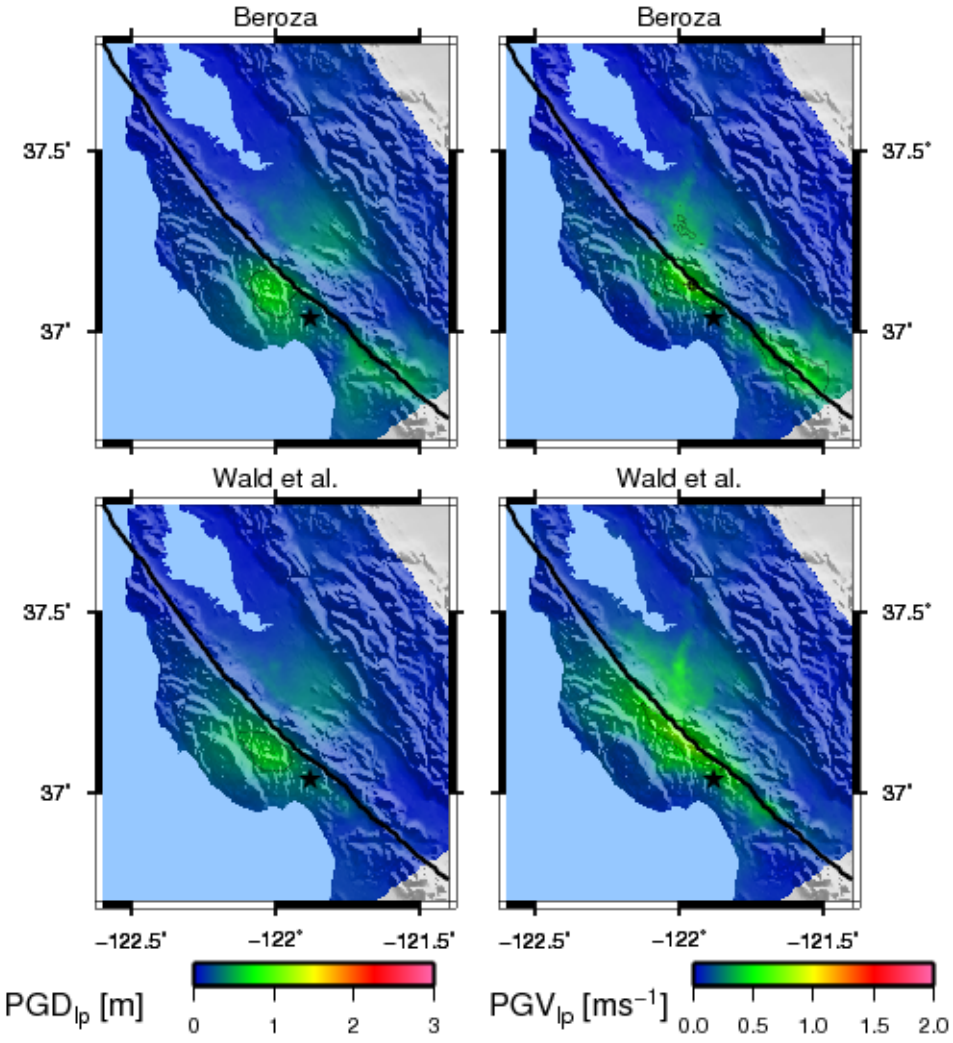

Figure 3.2: Aagaard et al. (2008a) generated ground motions from two source models of the Loma Prieta earthquake: Beroza (top maps) and Wald and others (bottom maps). The largest PGD_{lp} are approximately 0.7 m, and the largest PGV_{lp} are approximately 1.0 m/s. Compared to the magnitude 7.8 simulations, the Loma Prieta earthquake is a small event.

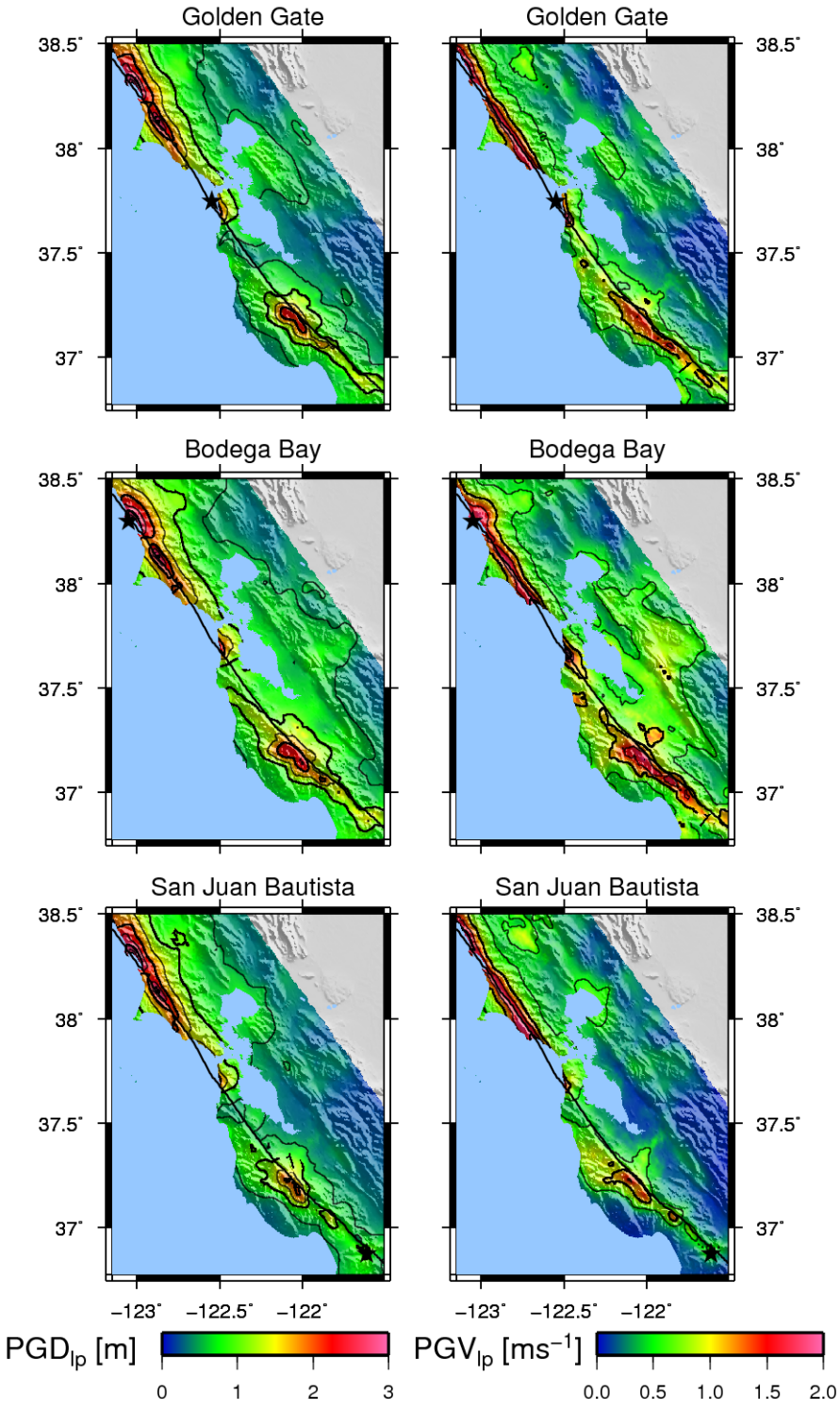

Figure 3.3: Aagaard et al. (2008b) used the same slip distribution (inferred from the 1906 event) and three hypocenter locations to simulate three magnitude 7.8 earthquakes on the northern San Andreas fault. All three simulations have large near-source directivity pulses.

3.2 Building Responses in Loma Prieta versus 1906-Like Simulations

The simulated building responses to the Loma Prieta ground motions are consistent with the experience of that earthquake. Figure 3.4 maps the peak inter-story drift ratios (IDRs) developed in the twenty-story building models and compares them to the urban areas south and east of San Francisco. The areas of largest building response are in the Santa Cruz mountains, and there are some mildly inelastic responses (colored green) in the urban areas near San Jose. These simulations predict no significant peak IDR from twenty-story steel MRF buildings in urban areas. The Beroza model causes a larger area of inelastic building responses than does the Wald et al. model, and the Beroza model induces large responses immediately northwest of the hypocenter. Figure 3.5 graphs the twenty-story building responses as a function of PGV_{lp}. There seems to be no systematic difference between the responses to ground motions from the two source models, even though the models predict different geographic patterns of response.

The 1989 magnitude 6.9 Loma Prieta earthquake is literally and figuratively on a different order of magnitude than the 1906 magnitude 7.9 San Francisco earthquake. Comparing the damage experienced in each earthquake is not a straightforward exercise: the building stocks in the San Francisco urban areas were significantly different in those years. Nonetheless, comparing the extent of damage in the two earthquakes is instructive. Most earthquake engineers today are familiar with the aftermath of the Loma Prieta earthquake, so that experience serves as a point of reference. If a 1906-like earthquake struck the San Francisco Bay area today, steel MRF buildings would be significantly damaged and possibly collapse. Compare the building responses in Figure 3.4 (Loma Prieta scenario) and Figure 3.8 (1906-like simulations). Tall steel MRF buildings in existing urban areas have significantly larger peak IDR in the 1906-like simulations than in the Loma Prieta scenario.

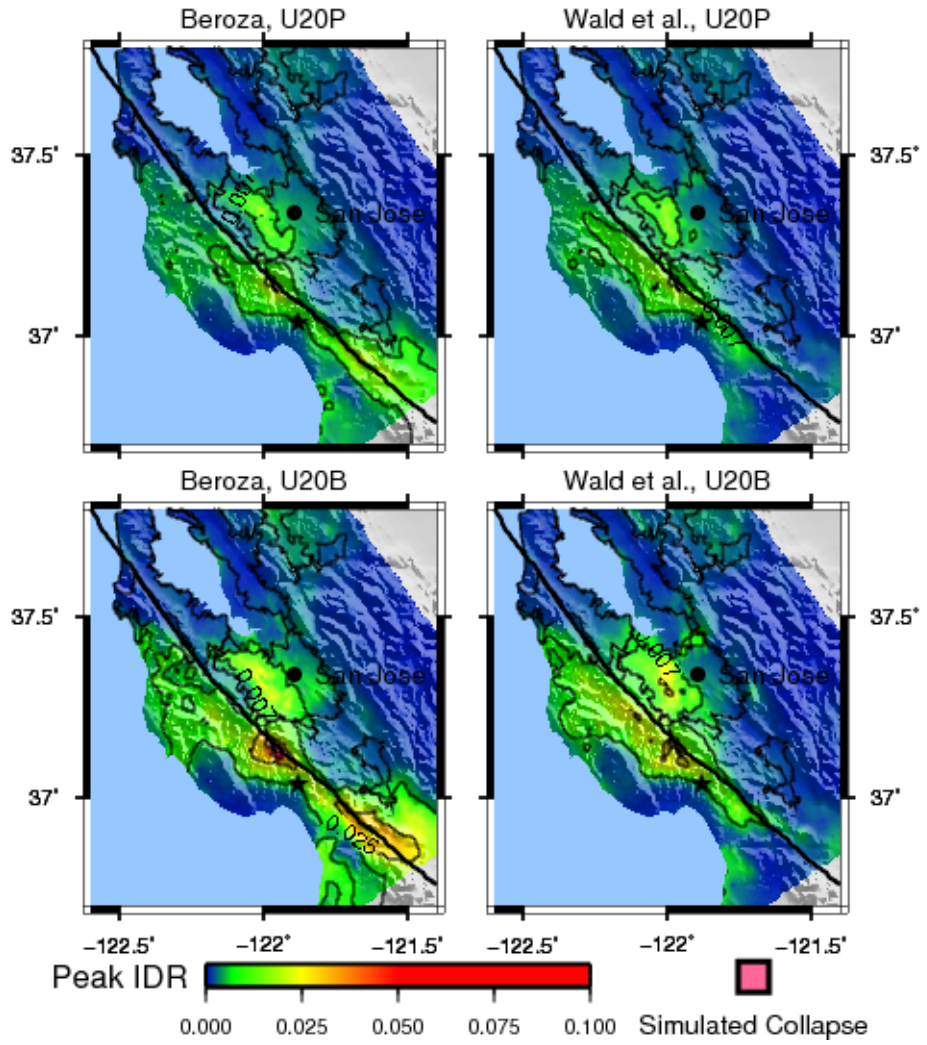

Figure 3.4: The twenty-story, more flexible building responses are similar for ground motions from the Beroza (maps on left) and Wald et al. (maps on right) source models. Urban areas and the city of San Jose are located. Existing steel MRF buildings in the San Jose area may have experienced inelastic building response and specifically some fractured welds, according to this simulation.

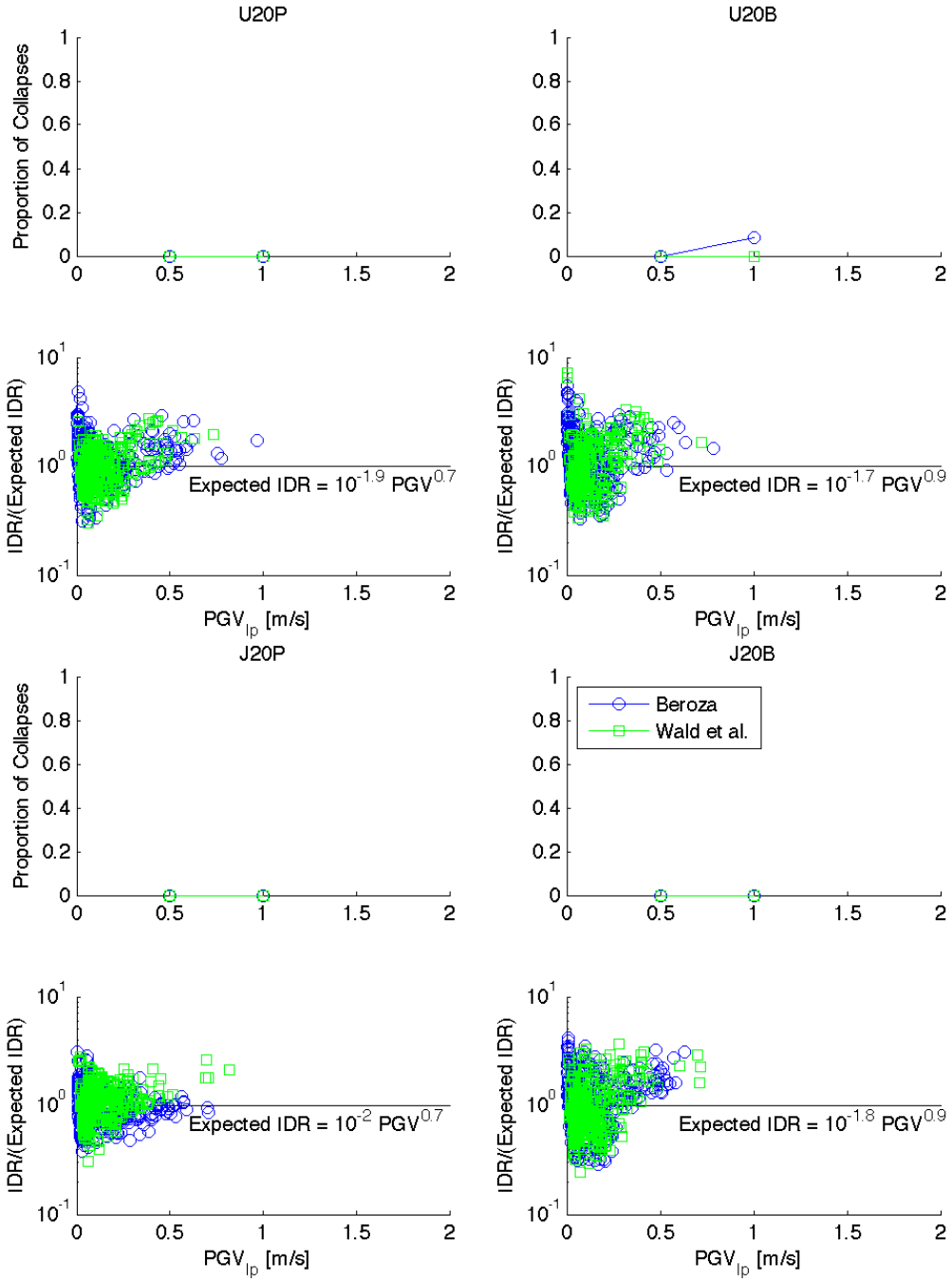

Figure 3.5: The twenty-story steel MRF building responses are not noticeably different for ground motions generated by the Beroza (1991) and Wald et al. (1991) source models of the 1989 Loma Prieta earthquake. In terms of building response as a function of PGV_{lp}, there is no reason to prefer one source model over the other.

3.3 Stiffer versus More Flexible Building Responses

The three magnitude 7.8 earthquakes provide sufficient data to compare the responses of the stiffer, higher-strength models (J20P) to the more flexible, lower-strength models (U20P). Figure 3.6 maps the peak IDRs of these two types of twenty-story buildings for the three simulations. The models show similar patterns of inelastic and collapse responses. The areal extent of inelastic responses appears larger, and the severity of the responses appears greater, for the more flexible, lower-strength model (U20P) compared to the stiffer, higher-strength model (J20P). Tables 3.2 and 3.3 verify these observations. For the urban area as a whole, and for almost all major cities individually, the more flexible, lower-strength model (U20P) collapses on greater percentages of urbanized areas compared to the stiffer, higher-strength model (J20P), for all three magnitude 7.8 simulations. The same statement could be made using exceedance of life safety (peak IDR greater than 0.025) as the response in place of collapse, with one exception: in the Bodega Bay simulation the stiffer, higher-strength model (J20P) response exceeds life safety on 1.6% of the Oakland sub-domain compared to 0.20% for the more flexible, lower-strength model (U20P).

Figure 3.7 directly compares the responses of the stiffer, higher-strength (J20P) and more flexible, lower-strength (U20P) buildings for each site in the three magnitude 7.8 simulations. The top graph reports the proportion of sites with a simulated building collapse. For all PGV_{lp}s, the more flexible, lower-strength (U20P) building collapses on a greater proportion of sites than does the stiffer, higher-strength (J20P) building. The bottom graph compares the ratio of the stiffer, higher-strength (J20P) building peak IDR to the more flexible, lower-strength (U20P) building peak IDR, assuming both models remain standing. For sites with PGV_{lp}s less than 1.5 m/s, this ratio is approximately 0.3–1.5. For sites with PGV_{lp}s greater than 1.5 m/s, it is approximately 0.7. For all PGV_{lp}s, the median ratio of J20P peak IDR to U20P peak IDR is 0.75. Thus, the more flexible, lower-strength building is more likely to collapse than the stiffer, higher-strength building, and the peak IDR of the more flexible, lower-strength building is approximately 1.3 times that of the stiffer, higher-

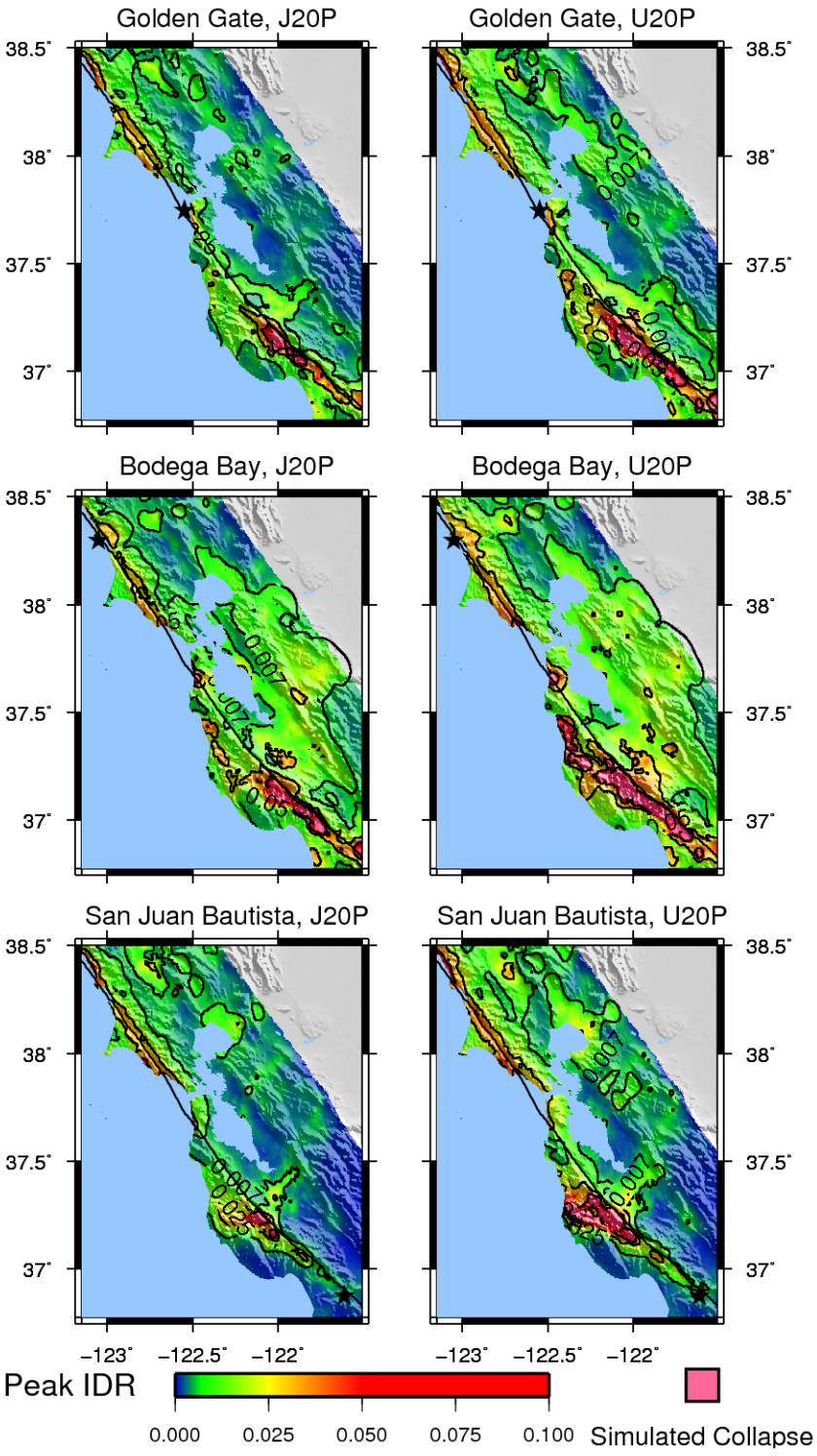

Figure 3.6: In terms of areal extent, there is some difference between the responses of the J20 models (maps on left) and the U20 models (maps on right). Compare the building responses at sites east of San Francisco Bay, for example: the U20 responses tend to be larger than the corresponding J20 responses.

Areas within the Entire Urban Outline [%] that Exceed a Peak IDR of 0.025				
	J20B	*J20P*	*U20B*	*U20P*
1989 Loma Prieta	0.079	0	0.40	0
M 7.8 Bodega Bay	36	4.6	54	10.
1906 San Francisco	9.3	0.99	15	3.1
M 7.8 San Juan Bautista	11	0.95	17	2.4
Areas within Oakland Sub-Domain [%] that Exceed a Peak IDR of 0.025				
1989 Loma Prieta	0	0	0	0
M 7.8 Bodega Bay	18	1.6	48	0.20
1906 San Francisco	0	0	0	0
M 7.8 San Juan Bautista	0	0	0	0
Areas within San Francisco Sub-Domain [%] that Exceed a Peak IDR of 0.025				
1989 Loma Prieta	0	0	0	0
M 7.8 Bodega Bay	48	18	69	35
1906 San Francisco	39	12	49	18
M 7.8 San Juan Bautista	63	6.8	92	13
Areas within San Jose Sub-Domain [%] that Exceed a Peak IDR of 0.025				
1989 Loma Prieta	0.20	0	1.7	0
M 7.8 Bodega Bay	64	11	83	26
1906 San Francisco	14	0.018	18	3.8
M 7.8 San Juan Bautista	11	0.51	14	1.6
Areas within Santa Rosa Sub-Domain [%] that Exceed a Peak IDR of 0.025				
1989 Loma Prieta	0	0	0	0
M 7.8 Bodega Bay	18	0	38	3.1
1906 San Francisco	25	0	25	8.6
M 7.8 San Juan Bautista	38	5.7	27	11

Table 3.2: Depending on the earthquake and building type, the simulated building responses may exceed the FEMA 356 life safety level on a limited or broad portion of the urban area. The Bodega Bay scenario earthquake especially causes damage in large parts of the San Francisco Bay urban area. The entire urban area in the simulation domain is 3266 km^2. Reproduced from Olsen et al. (2008) with authors' permission.

Areas within the Entire Urban Outline [%] with Simulated Collapse				
	J20B	*J20P*	*U20B*	*U20P*
1989 Loma Prieta	0	0	0	0
M 7.8 Bodega Bay	1.7	0.049	6.6	0.24
1906 San Francisco	0.29	0	0.67	0.00092
M 7.8 San Juan Bautista	0.092	0	0.42	0
Areas within Oakland Sub-Domain [%] with Simulated Collapse				
1989 Loma Prieta	0	0	0	0
M 7.8 Bodega Bay	0	0	0	0
1906 San Francisco	0	0	0	0
M 7.8 San Juan Bautista	0	0	0	0
Areas within San Francisco Sub-Domain [%] with Simulated Collapse				
1989 Loma Prieta	0	0	0	0
M 7.8 Bodega Bay	8.8	0.89	24	4.1
1906 San Francisco	0.11	0	1.7	0
M 7.8 San Juan Bautista	1.3	0	1.6	0
Areas within San Jose Sub-Domain [%] with Simulated Collapse				
1989 Loma Prieta	0	0	0	0
M 7.8 Bodega Bay	3.2	0	15	0.033
1906 San Francisco	0.031	0	0.97	0
M 7.8 San Juan Bautista	0	0	0.59	0
Areas within Santa Rosa Sub-Domain [%] with Simulated Collapse				
1989 Loma Prieta	0	0	0	0
M 7.8 Bodega Bay	0	0	4.0	0
1906 San Francisco	0	0	0	0
M 7.8 San Juan Bautista	0.069	0	0.069	0

Table 3.3: Steel MRF building models with brittle welds show simulated collapses on a greater area than models with perfect welds. The stiffer, higher-strength models collapse on a greater area than do the more flexible, lower-strength models. The entire urban area in the simulation domain is 3266 km^2. Reproduced from Olsen et al. (2008) with authors' permission.

strength building if both buildings remain standing.

These simulations also suggest that the near-source factors adopted in the 1997 Uniform Building Code (UBC) reduce the response of twenty-story steel moment frames in strong ground motions. Section 2.1.2 describes the near-source factors and the extent to which the building model designed to the 1992 Japanese Building Code (J20P) satisfies the 1997 UBC. The J20P model does not satisfy the 1997 UBC for all sites in the Aagaard et al. (2008a,b) simulation domain; specifically, the J20P model would not satisfy the 1997 UBC at sites within 5 km of the northern San Andreas. These sites would roughly correspond to the largest peak ground velocities in Figure 3.7. Disregarding the building responses in ground motions with long-period peak ground velocities greater than 1.5 m/s, the response of the J20P model is generally smaller than that of the U20P model. I infer that steel moment frame designs that satisfy the 1997 UBC at all sites would also have smaller responses than an equivalent design satisfying only the 1994 UBC, although the simulations in this thesis do not directly support this claim. The next section shows, however, that fixing brittle welds reduces building response more than designing a stiffer and stronger building.

3.4 Responses of Buildings with Non-Fracturing versus Fracture-Prone Welds

The magnitude 7.8 simulations also provide data to compare the responses of models with sound (or perfect, P) welds to those with fracture-prone (or brittle, B) welds. Figure 3.8 maps the responses of models with perfect and brittle welds in the three magnitude 7.8 simulations. The area of inelastic response (colored green to pink) appears similar for the models with perfect and brittle welds. However, within the areas with inelastic response, the response is much larger for the models with brittle welds, and there are more collapses of models with brittle welds. Tables 3.2 and 3.3 confirm that the models with brittle welds have larger responses than those with

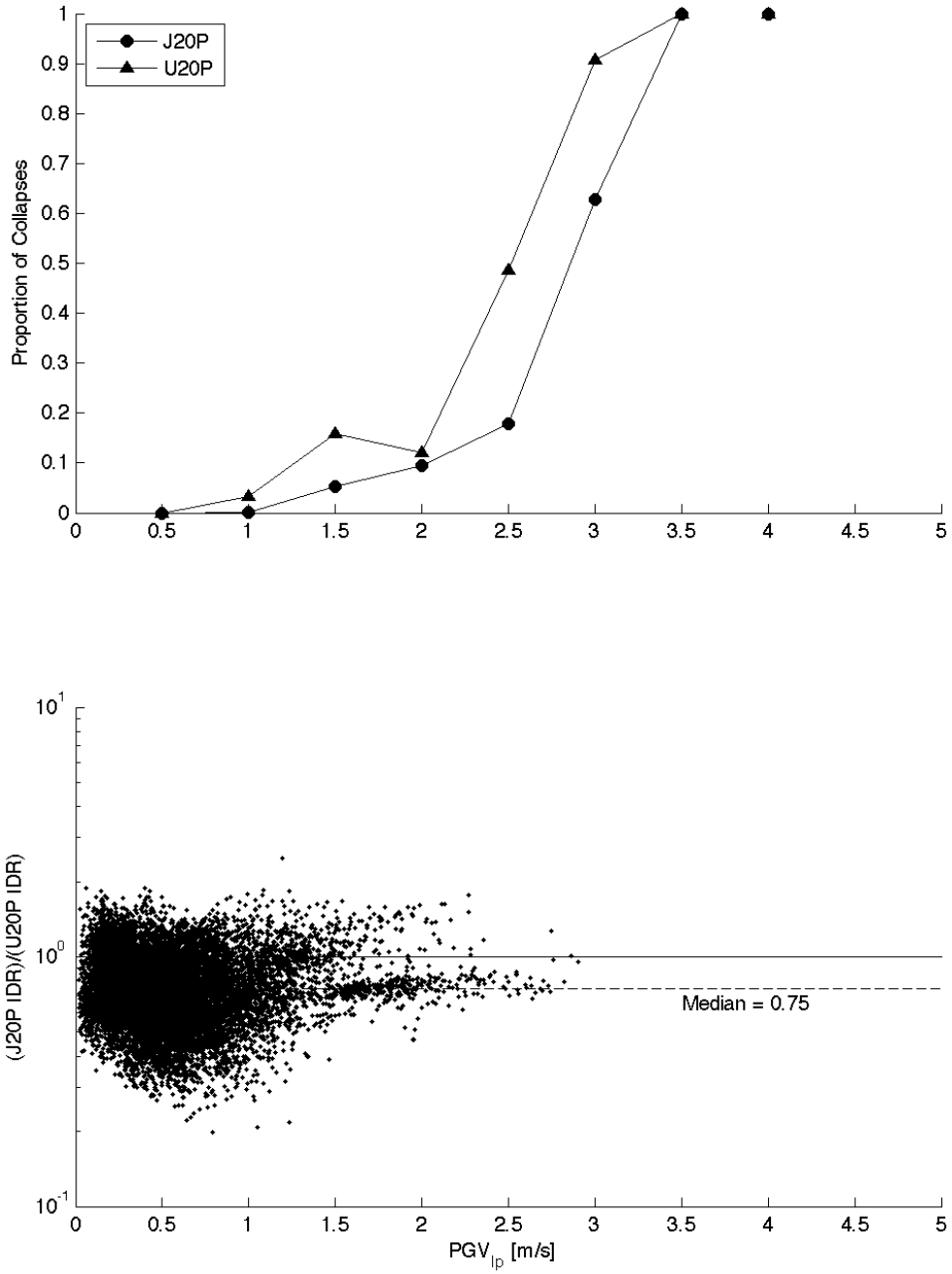

Figure 3.7: This figure compares the responses of J20P and U20P models at each site in the three magnitude 7.8 simulations. For the same PGV_{lp}, the U20 model is more likely to collapse while the J20 model stands. If both buildings remain standing at a site, the peak IDR in the J20 model is most likely to be 0.75 times the peak IDR in the U20 model.

perfect welds in the same simulations. For both the more flexible, lower-strength and stiffer, higher-strength models, the response of the brittle weld models exceeds life safety on an area 2–20 times that of perfect weld models. Similarly, the model with brittle welds collapses on an area 6–30 times that of the models with perfect welds.

Figure 3.9 directly compares the responses of the models with each weld state at each site in the magnitude 7.8 simulations. Similar to Figure 3.7, the top graph of Figure 3.9 reports the proportion of sites with a simulated building collapse. For all PGV_{lp}s, the brittle weld model collapses on a notably greater proportion of sites than does the perfect weld model. The bottom graph of Figure 3.9 compares the ratio of the brittle weld model peak IDR to the perfect weld model peak IDR, assuming both models remain standing at the site. Most of these ratios are 0.5 to 5, with a median of 1.7. For the smallest PGV_{lp}s, this ratio is 1, implying that the building response remains elastic. In the elastic region, the responses of the two models are the same because the brittle welds remain sound. In the inelastic region, however, the brittle welds significantly degrade the lateral load-resisting capacity of the models.

3.5 Effect of Rupture Propagation Direction

Rupture propagation on the northern San Andreas fault significantly affects the geographic pattern of building responses. Both Figures 3.6 and 3.8 demonstrate this effect. In the north-to-south rupture (Bodega Bay), the San Francisco peninsula and areas east of the Bay experience larger building responses than in the other two simulations. The 1906 bilateral rupture (Golden Gate) generally induces lower building responses than does the north-to-south rupture, and the largest responses are limited to areas near the fault. The largest building responses to the south-to-north rupture (San Juan Bautista) are also close to the fault, with a large area of elastic response southeast of San Jose. Tables 3.2 and 3.3 show that the Bodega Bay scenario earthquake is the most damaging of the three simulations for the urban area as a whole. However, the cities of San Francisco and Santa Rosa experience large areas of life threatening responses in the San Juan Bautista scenario earthquake. On its

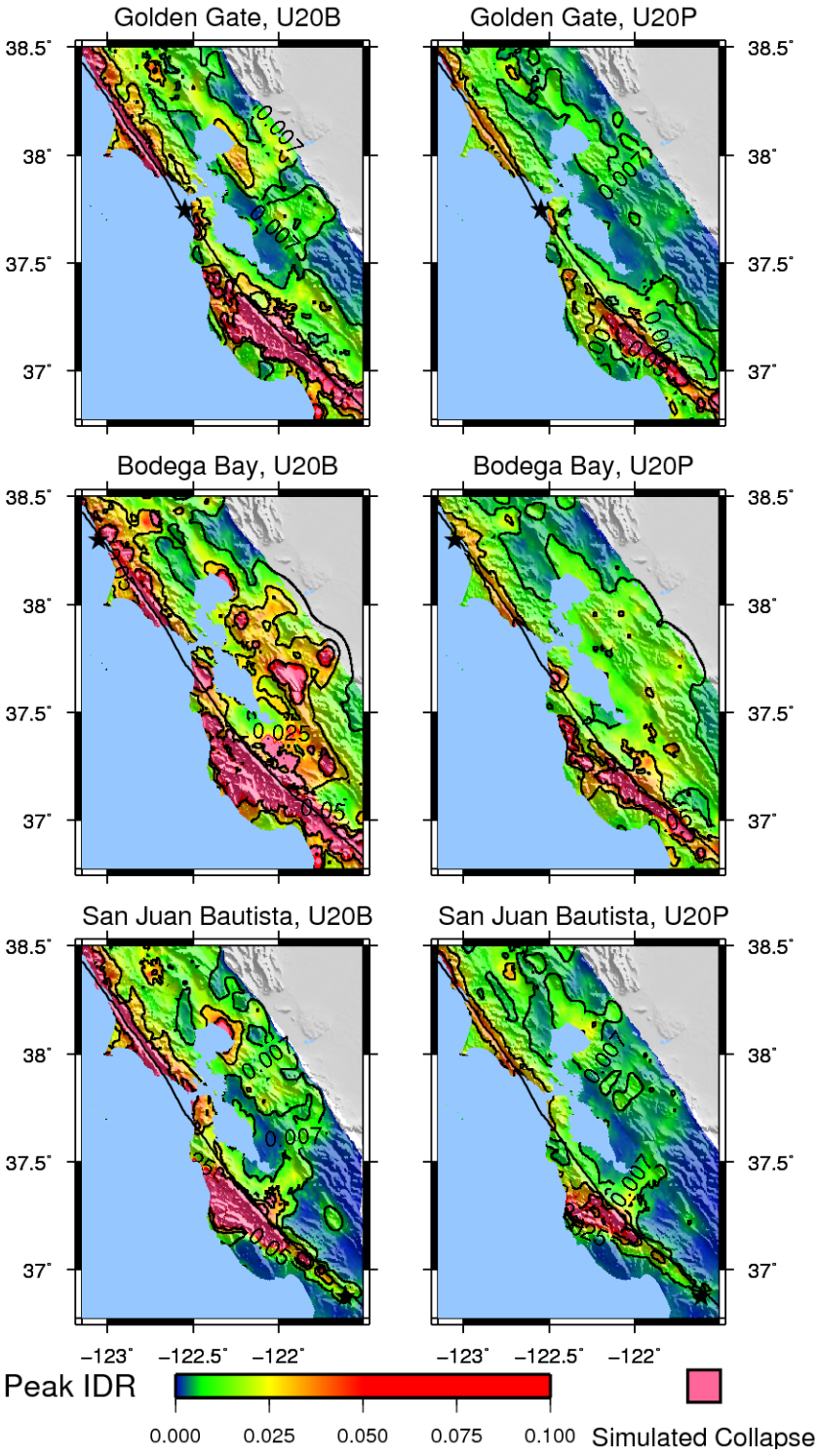

Figure 3.8: The weld state (that is, perfect or brittle) significantly affects building responses. Compare the extent of large peak IDR (peak IDR greater than 0.025, colored yellow to pink) for models with brittle welds (maps on left) and models with perfect welds (maps on right). In the city of San Francisco, for example, the perfect weld peak IDR is generally 0.007–0.025 while the brittle weld peak IDR is generally 0.007–collapse.

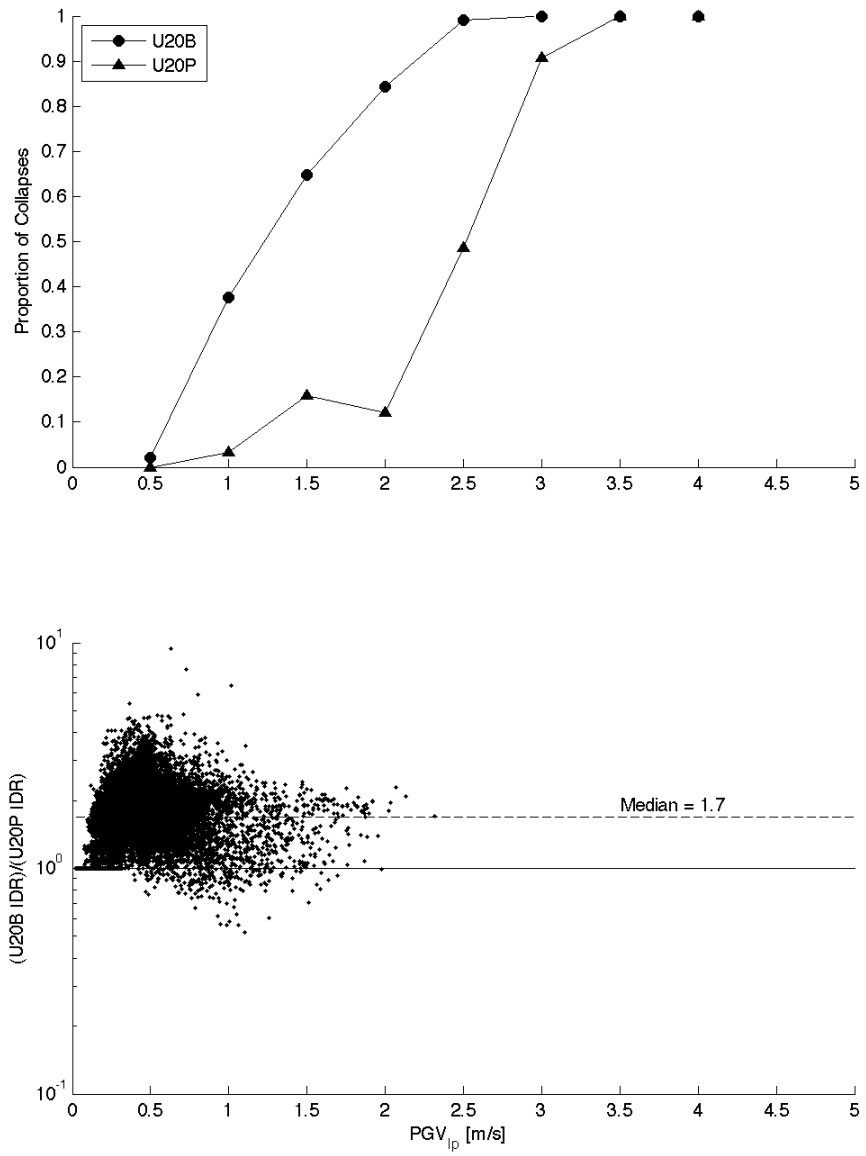

Figure 3.9: This figure compares the response of models with brittle and perfect welds directly at each site of the three magnitude 7.8 earthquakes. The brittle weld model is much more likely to collapse than the perfect weld model. Consider PGV_{lp} of approximately 2 m/s: on 80% of those sites the brittle weld model collapses compared to 10% for the perfect weld model. If both models stand at a site, the peak IDR in the brittle weld model is likely 1.7 times the peak IDR in the perfect weld model.

own, the 1906 scenario causes significantly large steel MRF responses in the urban areas around the San Francisco Bay, even though the responses tend to be smaller in comparison to the two earthquakes with hypothetical hypocenters.

Chapter 4

Simulations in the Los Angeles Basin

This chapter reports the responses of steel moment-resisting frame (MRF) buildings to simulated earthquakes in the Los Angeles basin. I use broadband ground motions from simulations on the Puente Hills fault to compare the responses of shorter and taller steel MRF buildings. The taller buildings are more likely to collapse because they cannot sustain the large inter-story drifts induced in the lower stories. That is, the P-Δ effect affects taller buildings more than shorter buildings.

I also compare the building responses in several simulations of a large earthquake on the Puente Hills fault from two groups of researchers. The predicted building response at a single site can be sensitive to the particular assumed earthquake. However the regional response is similar for Puente Hills earthquakes of similar magnitude. There is general agreement on the effect of an earthquake of approximately magnitude 6.7 or 7.1 in the Los Angeles basin as a whole, despite local uncertainties in building response due to the specifics of the simulation.

The last section of this chapter discusses the utility of multiple simulations of the same magnitude earthquake on the same fault. The resulting building responses from repetitions of the "same earthquake" are quite similar, in terms of both regional extent of large building deformation and response as a function of peak ground velocity (PGV). Multiple simulations characterize the uncertainty in building response due to different rupture models of the same magnitude and fault configuration.

4.1 Ground Motion Studies

Porter et al. (2007) generated ground motions from scenario ruptures on the Puente Hills fault for the California Earthquake Authority. They used deterministic and stochastic models to generate broadband ground motions for periods greater than 0.1 s (Graves and Pitarka, 2004). In the study, the authors simulated a magnitude 7.15 earthquake with five distinct rupture models, varying the rupture speed, rise time, and slip distribution. Figure 4.1 maps the assumed fault and locates the hypocenter. For consistency, I follow the simulation numbering scheme in Porter et al. (2007). Figure 4.2 shows the broadband peak ground displacements (PGD_{bb}s) and peak ground velocities (PGV_{bb}s) for two of the simulations. Again, I measure the PGD and PGV as the largest vector amplitude from the two horizontal, north-south and east-west components of ground motion.

As part of the Pacific Earthquake Engineering Research Center Lifelines program, several groups of Southern California Earthquake Center researchers developed models to generate ground motions in the Los Angeles basin (Day et al., 2001, 2003, 2005). The stated purposes of the studies were to: validate wave propagation models and algorithms with simple and complex earthquake sources and earth structures; characterize the amplification of long-period waves due to sedimentary basins; and archive the ground motions for future engineering studies. They generated long-period ground motions for sixty scenario earthquakes on ten known faults or fault systems in the Los Angeles basin. For each fault in the study, the researchers generated three slip distributions and assumed two hypocenter locations for each slip distribution. The hypocenter locations are relatively deep on the fault (at a distance 0.7 of the fault width as measured from the top of the fault along the dip), and the ruptures propagate up-dip. If the authors had assumed shallow hypocenters and down-dip ruptures instead, the peak ground displacements and velocities would have been smaller (Aagaard et al., 2004).

Table 4.1 lists the scenario earthquakes used in this thesis, and Figure 4.3 locates the faults. Figure 4.4 shows the long-period peak ground displacements and velocities

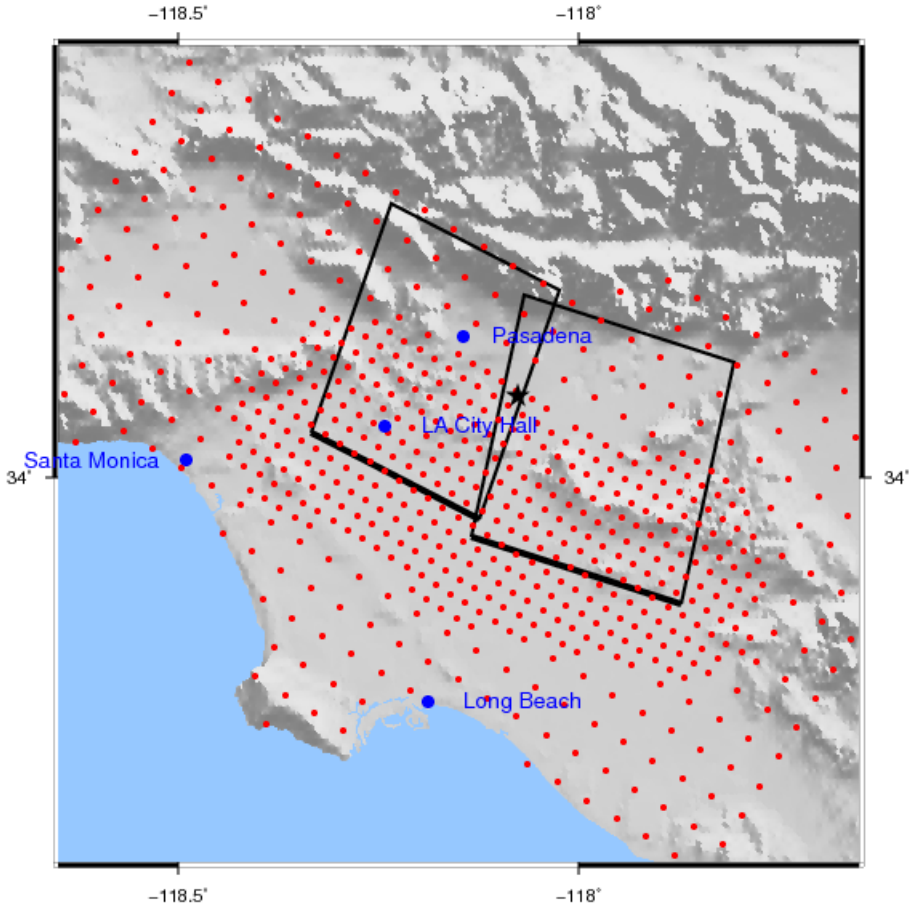

Figure 4.1: The Porter et al. (2007) simulation domain covers the Los Angeles, San Fernando, and San Gabriel basins in the Los Angeles area. Red dots locate the 648 sites in the domain, and blue dots locate major cities in the area. The black lines outline the assumed fault segments, and the black star locates the hypocenter.

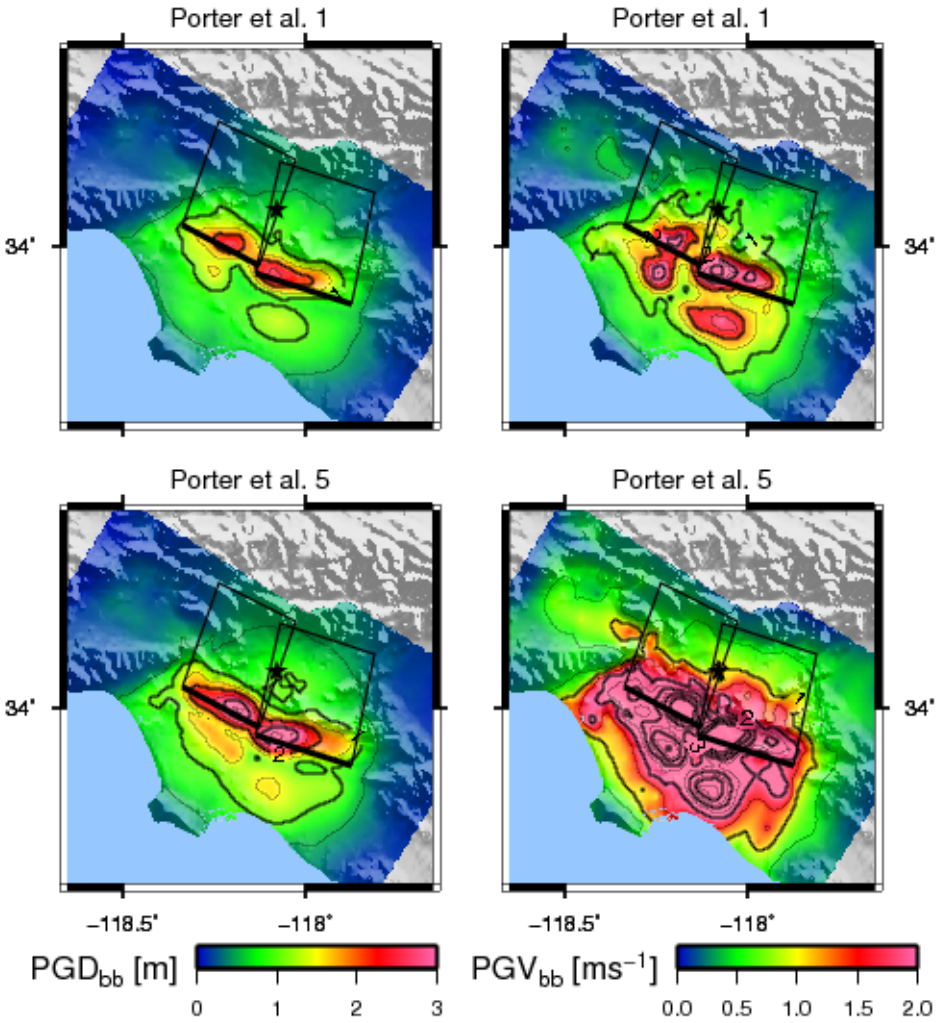

Figure 4.2: Porter et al. (2007) generated five magnitude 7.15 simulated earthquakes on the Puente Hills fault. This figure shows the broadband PGD and PGV for two of these simulations. Simulation 1 (top maps) is representative of the ground motion for all five simulations, whereas simulation 5 (bottom maps) has the largest ground motions of all five simulations.

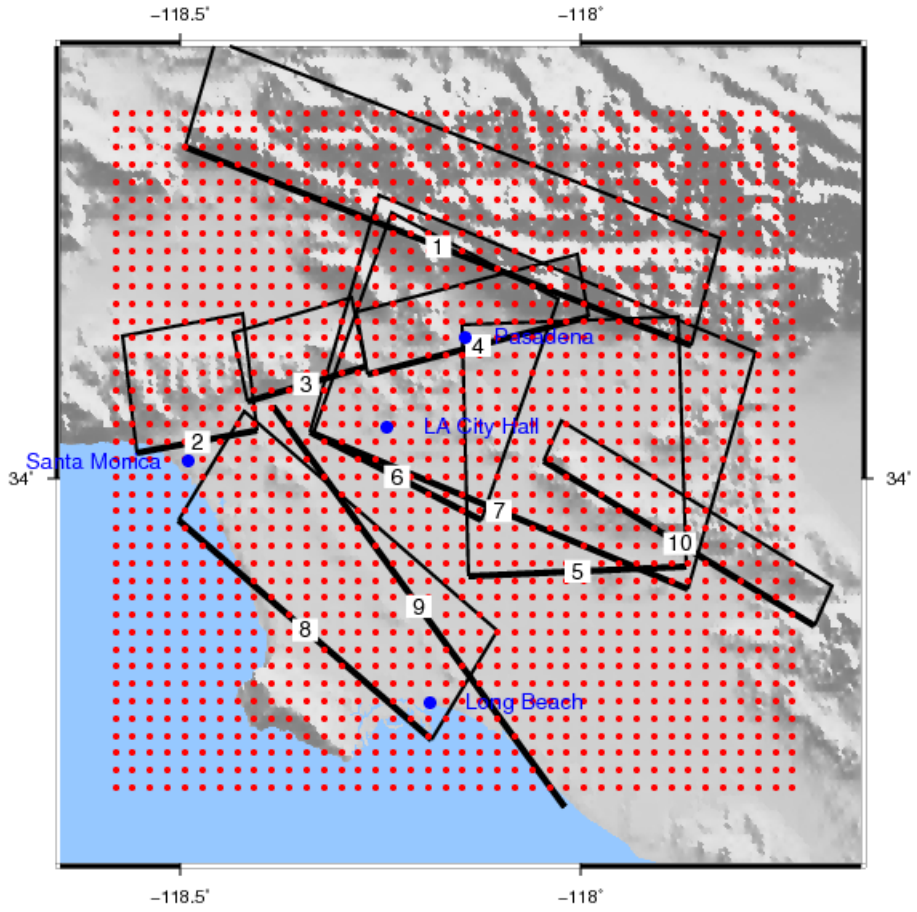

Figure 4.3: Day et al. (2005) simulated long-period ground motions in the Los Angeles basin. Red dots locate the 1600 simulation sites, and blue dots locate major cities in the area. There are simulated ruptures on the ten faults labeled here.

for two simulations.

4.2 Six- versus Twenty-Story Building Responses

Since the Porter et al. (2007) broadband ground motions have energy content in the range of the fundamental periods of both the six- and twenty-story building models, I can compare the responses of the two building heights. Figure 4.5 graphs the peak IDRs for the six- and twenty-story models. Generally, the twenty-story models do not sustain a peak IDR more than 10%, whereas the six-story models sustain up to 16%, without collapsing. Figure 4.6 directly compares the responses of six- and twenty-

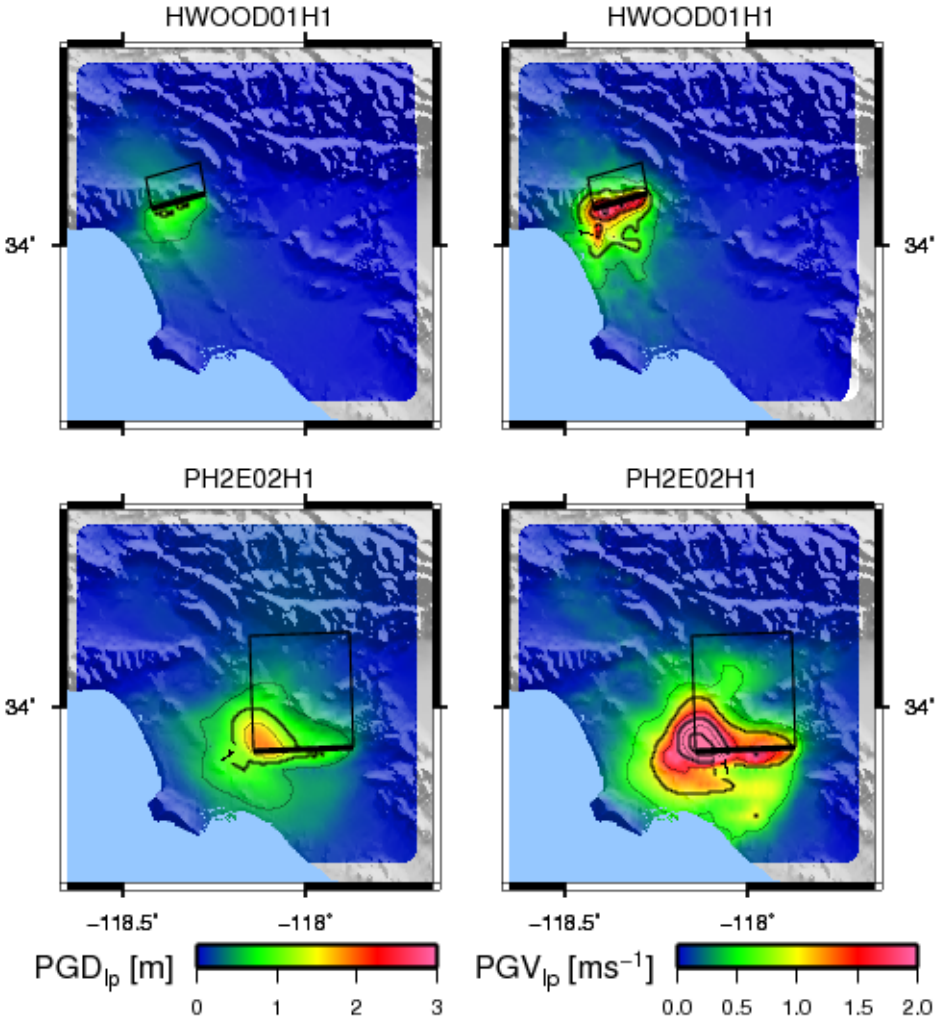

Figure 4.4: This figure shows the long-period PGD and PGV for two simulations in the Los Angeles Basin. The simulation on the Puente Hills fault (bottom maps) generates large ground motions in much of the Los Angeles Basin, whereas the simulation on the Hollywood fault (top maps) has large ground motions in the area above the top edge of the fault.

Fault name	*M*	*No.*	*Fault abbrev.*	*Slip code*	*Hypocenter code*
Compton	6.9	8	COMP	02	H1
Hollywood	6.4	3	HWOOD	02, 04, 06	H1, H2
Puente Hills (2 seg.)	6.8	5	PH2E	02, 05, 09	H1, H2
Puente Hills (3 seg.)	7.1	7	PHALL	02	H1
Puente Hills (1 seg.)	6.7	6	PHLA	01	H1
Newport-Inglewood	6.9	9	NIN	01	H1
Raymond	6.6	4	RAYM2	07	H1
Sierra Madre	7.0	1	SMAD	03	H1
Santa Monica	6.3	2	SMON	03	H1
Whittier	6.7	10	WHIT	01	H1

Table 4.1: This table lists the simulations of long-period ground motions in the Los Angeles basin used in this thesis. Consistent with Day et al. (2005), each scenario earthquake has a name concatenated from a code name, slip code, and hypocenter code. For example, a scenario rupture on the three segments of the Puente Hills fault system with slip distribution two and hypocenter one is coded PHALL02H1.

story models at the same site for all ground motions in the five simulated earthquakes. For three of the building models (the stiffer, higher-strength with perfect and brittle welds (JP and JB) and the more flexible, lower-strength with brittle welds (UB)) the twenty-story building collapses on a greater proportion of sites than does the six-story building. The six-story, more flexible, lower-strength building with perfect welds (U6P) collapses on a greater proportion of sites than does the equivalent twenty-story building (U20P). Assuming both the six- and twenty-story buildings stand at a site, the peak IDR in the six-story building is approximately 1.2–1.6 times that of the twenty-story building, depending on the design and weld state. Thus, in general, the twenty-story building is more likely to collapse than the six-story building (due to P-Δ effects), but if buildings of both heights remain standing at a site, then the peak IDR in the six-story building is larger than the peak IDR in the twenty-story building.

Building height seems not to affect the propensity of a *properly designed and constructed* steel MRF to collapse. For the stiffer, higher-strength building with perfect welds (JP), the twenty-story building is somewhat more likely to collapse than the equivalent six-story building. However, for the more flexible, lower-strength building with perfect welds (UP), the six-story building is somewhat more likely to collapse

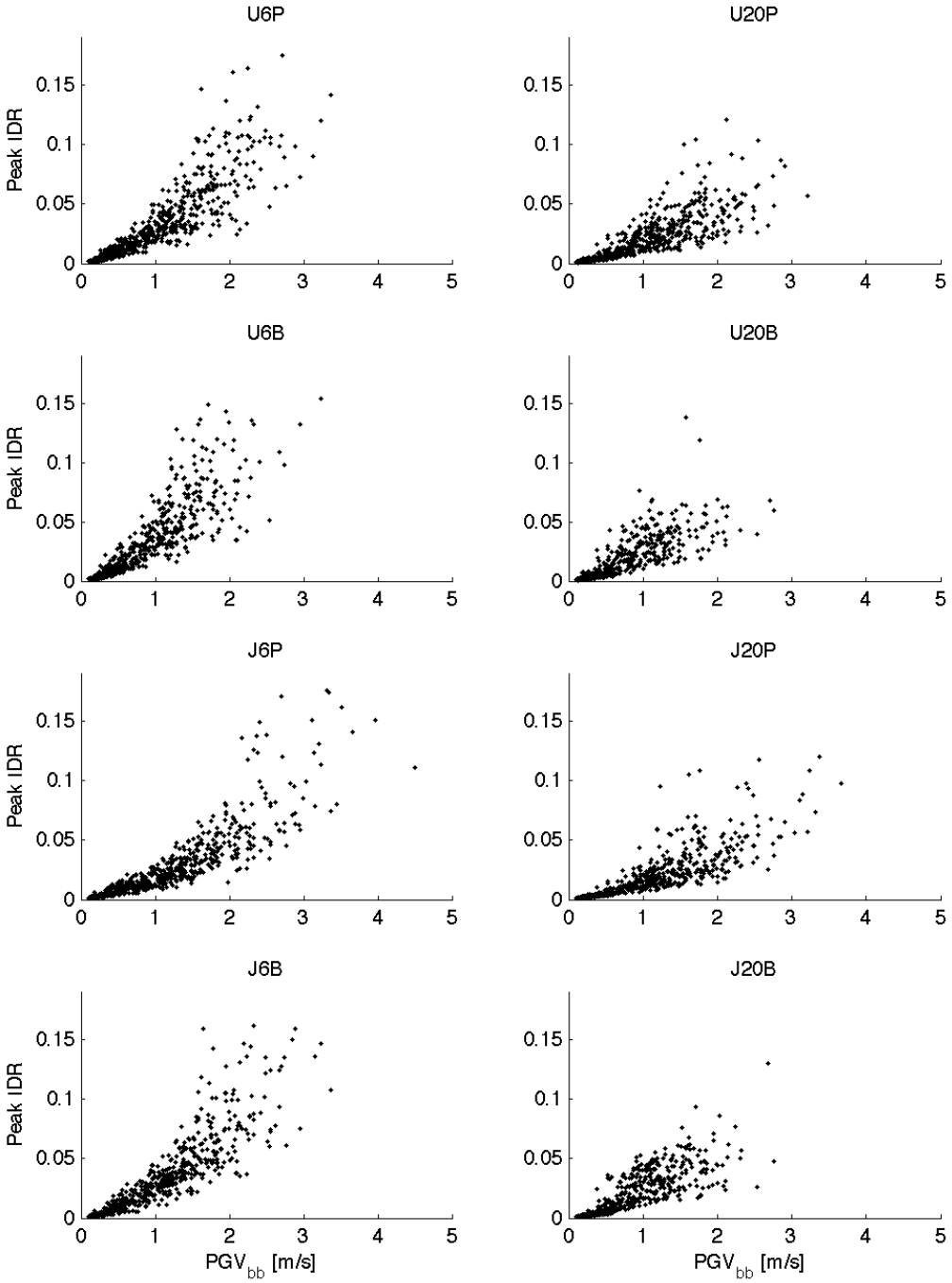

Figure 4.5: In the simulations, six-story building models remain standing with up to 16% peak IDR whereas twenty-story models sustain peak IDRs up to 10%. Since the largest peak IDRs tend to localize in the first few stories, the eccentric gravity load of a twenty-story building is more likely to overcome the moment-resisting capacity of the columns in the lowest stories. Thus, the twenty-story building is more likely to collapse at lower peak IDRs. The data in this figure are from building responses in the Porter et al. 2 simulation.

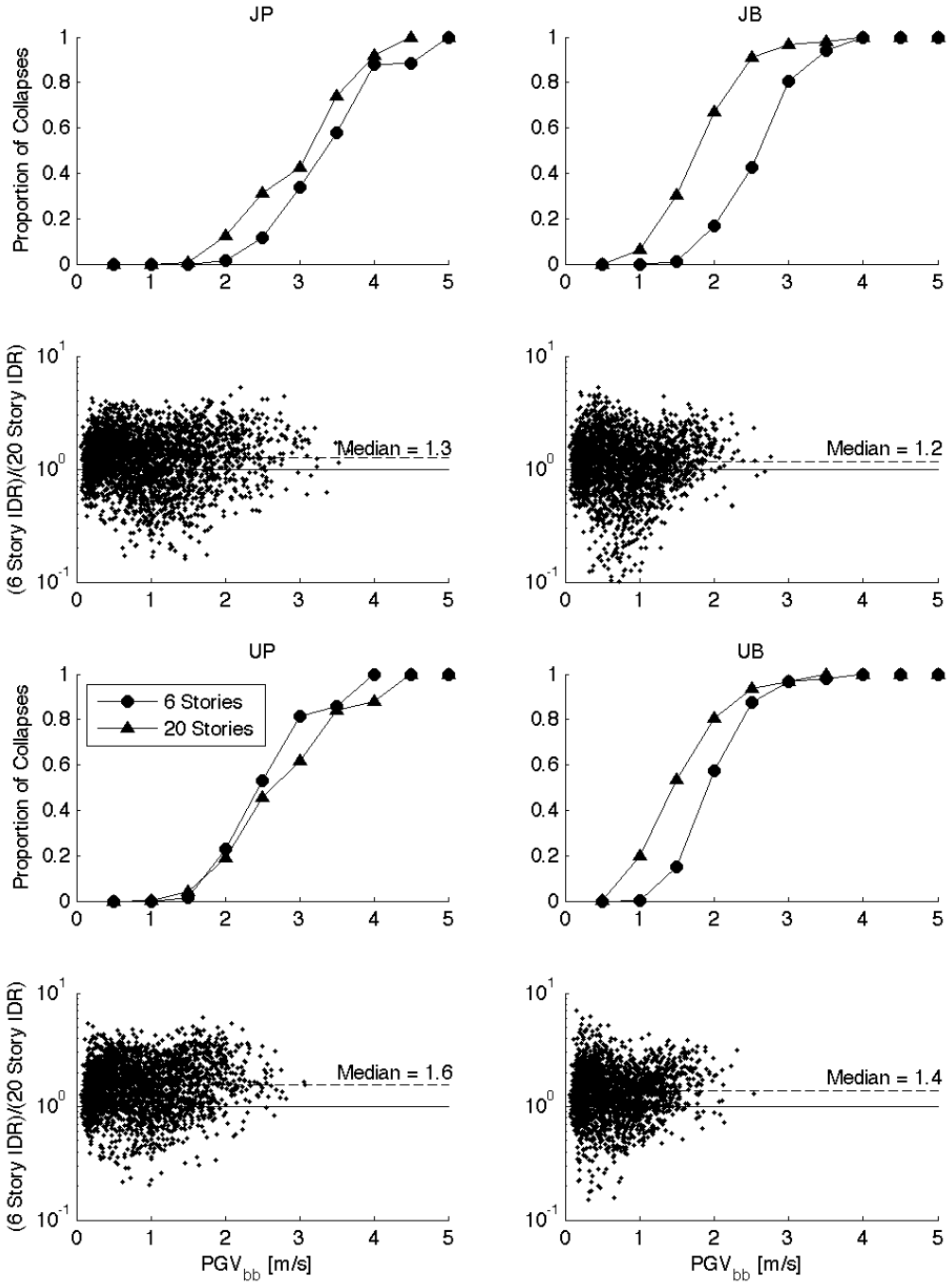

Figure 4.6: For models with perfect welds (graphs on left), the six- and twenty-story buildings have a similar number of collapses. However, if the models have brittle welds (graphs on right), the twenty-story building is much more likely to collapse while the six-story stands. If both buildings remain standing at a site, then the peak IDR of the six-story building is likely 1.2–1.6 times the peak IDR of the twenty-story building, depending on the design and weld state. The data in this figure are from building responses in the five magnitude 7.15 simulations on the Puente Hills fault in Porter et al. (2007).

than the equivalent twenty-story. This result makes sense because engineers assume a seismic hazard and accordingly design buildings to remain standing in ground motions consistent with that hazard. The additional moment induced in the columns of the lowest stories from an eccentric vertical load (that is, the P-Δ effect) is well known. Designs of taller buildings account for this effect.

The presence of brittle welds makes the taller designs more vulnerable to collapse than the six-story buildings. For both the stiffer and more flexible designs, the twenty-story building is much more likely to collapse in a ground motion with a given peak ground velocity than the equivalent six-story building. Obviously the presence of brittle welds significantly degrades the lateral force-resisting capacity of both story heights, but the consequence is much more severe for the twenty-story buildings.

The problem of brittle welds could also be considered as an example of an unknown design or construction flaw. Taller buildings tend to be inherently more unstable than equivalent shorter buildings. An unanticipated flaw makes buildings of both heights even more unstable, especially if buildings of both heights are vulnerable at their bases. Using brittle welds as an example, design and construction flaws make taller buildings more vulnerable to collapse than shorter buildings.

4.3 Puente Hills Fault Simulations

This thesis includes several simulated earthquakes on the Puente Hills fault system. Day et al. (2005) hypothesized three earthquakes that rupture one (magnitude 6.7, PHLA), two (magnitude 6.8, PH2E), or three segments (magnitude 7.1, PHALL) of the fault system. Figure 4.7 maps the twenty-story, more flexible, lower-strength (U20P) building responses to these simulations as well as the responses to one of the Porter et al. (2007) simulations. The areal extent of inelastic building responses (colored green to pink) is similar between the magnitude 6.7 and 6.8 ruptures and between the magnitude 7.1 and 7.15 ruptures. Also the total area of the largest building responses (peak IDR greater than 0.05, colored red to pink) is similar within the two sets of magnitude. However the particular locations of these areas are different

among the two sets.

The magnitude 6.7 and 6.8 simulations (top subfigures) show similar results in the Los Angeles basin: there is a limited area of large peak IDRs in the vicinity of the projected top edge of the fault plane, and the building response over much of the Los Angeles basin is inelastic. The rupture on the Los Angeles segment (top-left subfigure) causes inelastic building responses mostly in the central and western parts of the Los Angeles basin, whereas the rupture on the Santa Fe and Coyote Hills segments (top-right subfigure) causes inelastic responses in the central and eastern portions. This difference is due to the orientation of the fault plane and particular combination of slip distribution and rupture propagation. It is independent of the particular rupture and building model.

Likewise the magnitude 7.1 and 7.15 simulations (bottom subfigures) show similar results: the areas of large peak IDRs cover most of the Los Angeles basin, and the building responses in the entire Los Angeles basin are inelastic. The magnitude 7.1 rupture (bottom-left subfigure) has two distinct areas of large peak IDRs: one area is due south of the southeast fault corner, in the easternmost portion of the basin; and the second area is west and south of the southwest fault corner, in the northwest part of the basin. The magnitude 7.15 rupture (bottom-right subfigure) induces large peak IDRs in the areas above and just south of the projected top edge of the fault plane. This difference in the location of the largest peak IDRs is due to the relative locations of the hypocenter and large patches of slip on the fault plane. The location of the largest peak IDRs is coincident with the location of the largest peak ground displacements and velocities.

Figure 4.8 graphs the building responses in these four Puente Hills earthquakes. Again, the data are consistent within the smaller and larger magnitudes. Buildings in the smaller simulations (magnitude 6.7 and 6.8) collapse on similar proportions of sites with a given PGV_{lp}. If the buildings do not collapse, then buildings in the magnitude 6.7 simulation tend to have smaller peak IDRs compared to the other Puente Hills simulations. Buildings in the larger simulations (magnitude 7.1 and 7.15) collapse on similar proportions of sites for PGV_{lp}s less than 1.5 m/s, but they differ for larger

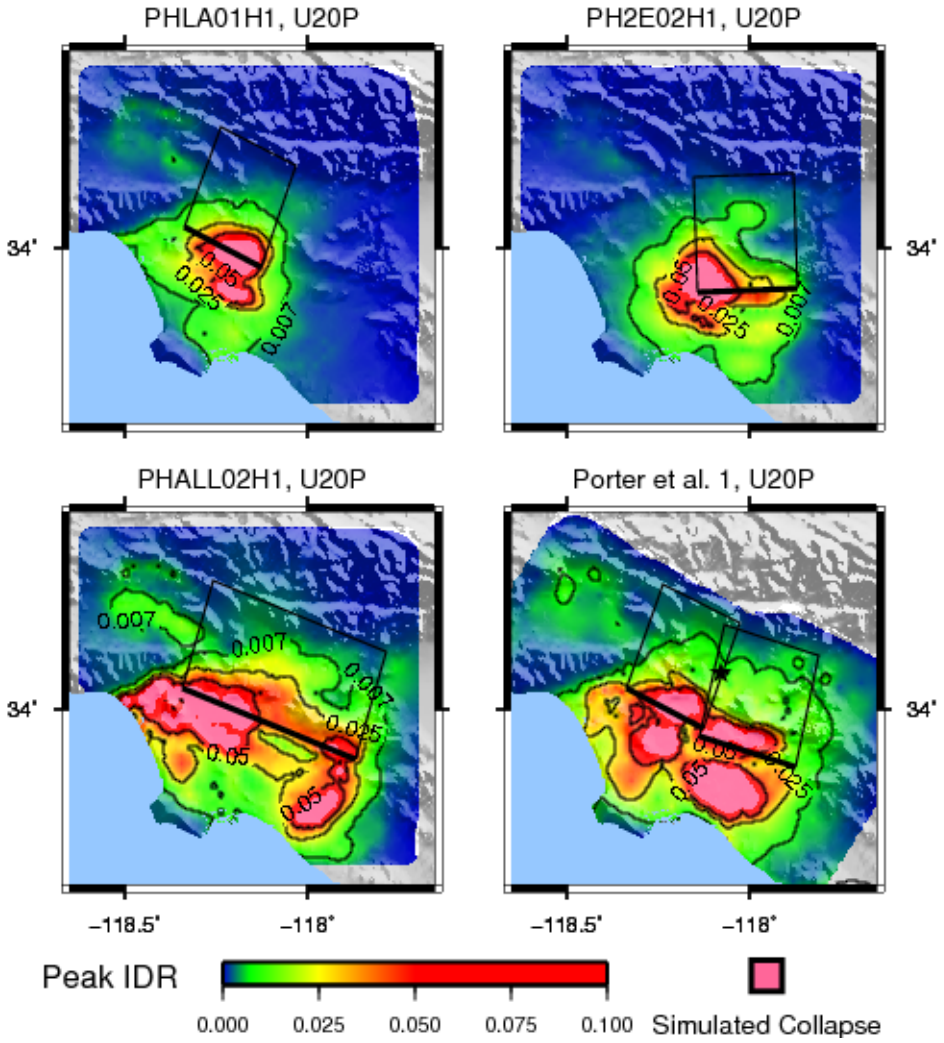

Figure 4.7: This figure compares the U20P building model responses in four simulations on the Puente Hills fault in the Los Angeles area. A magnitude 6.7 or 6.8 earthquake (top left and right maps, respectively) causes inelastic building response on most of the Los Angeles basin with the largest peak IDR (greater than 0.05) in the vicinity of the top edge of the fault. A magnitude 7.1 or 7.15 earthquake (bottom left and right maps, respectively), however, induces inelastic building responses on the entire Los Angeles, San Fernando, and San Gabriel basins, with extensive areas of large peak IDRs in the Los Angeles basin. Note the general similarity in the magnitude 7.1 simulations even though they were provided by two separate research groups.

PGV_{lp}s. The proportion of collapses continues to rise with increasing PGV_{lp} for the magnitude 7.15 simulation (Porter et al. 1), but it levels off, and somewhat declines, for the magnitude 7.1 simulation (PHALL02H1). The PHALL02H1 curve has insufficient data to properly characterize the proportion of collapse (Section 4.4). The symbol at $PGV_{lp} \approx 2$ m/s represents 24 data points, $PGV_{lp} \approx 2.5$ m/s represents 6 data points, and $PGV_{lp} \approx 3$ m/s represents 1 data point. Nonetheless, both large magnitude simulations generate larger peak IDR compared to the smaller magnitude simulations, suggesting there may be a magnitude dependence not considered in this thesis.

4.4 Multiple Simulations of the Same Earthquake

I simulated the responses of the building models for multiple simulations of the same earthquake. Day et al. (2005) and Porter et al. (2007) generated several source models for the same magnitude earthquake on the same fault. These multiple simulations explore the uncertainty inherent in modeling an earthquake. Defining an earthquake simply by magnitude and fault is an ill-posed problem. Many combinations of slip pattern on the fault and rupture characteristics produce the "same earthquake." Multiple simulations give an idea of the sensitivity of the building responses to the simulation. One simulation may not be sufficient to probabilistically model building response in a simulation.

Figures 4.9–4.11 map the twenty-story, more flexible building (U20P) responses to five or six multiple simulations on the same fault. Within each set of building responses, the areal exents of inelastic and collapsed building responses are similar, but there are differences at individual sites. For the ruptures on the Hollywood fault (Figure 4.9), the patterns of building response in the Los Angeles basin are quite similar. For the magnitude 6.8 ruptures on the Puente Hills fault (Figure 4.10), the locations of building collapses differ: there are consistently many collapses above the

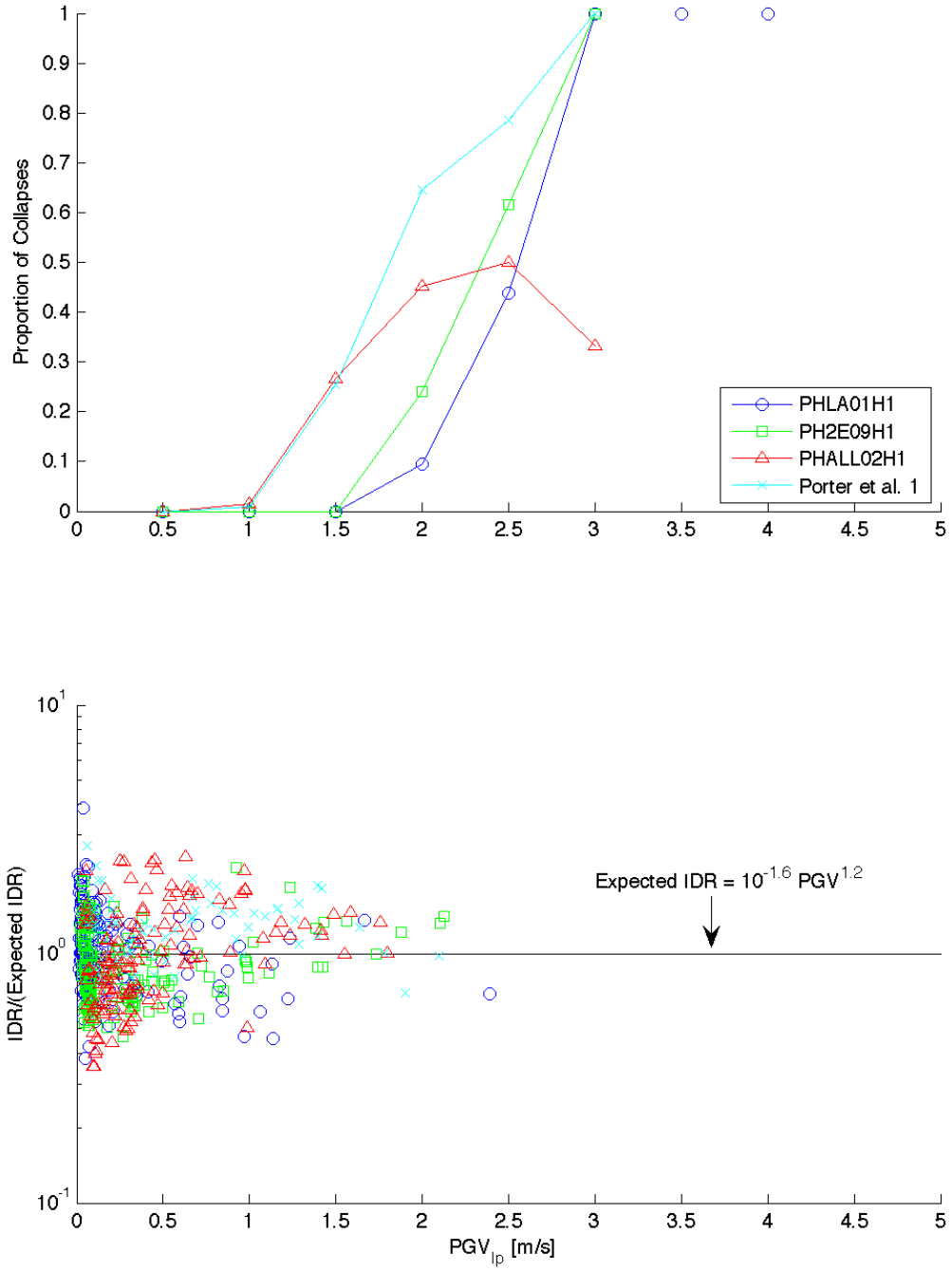

Figure 4.8: This figure compares the collapse and peak IDR responses of the U20P model in four Puente Hills fault simulated earthquakes. The smaller earthquakes (magnitude 6.7 PHLA01H1 and magnitude 6.8 PH2E09H1) have consistent proportions of collapse as functions of long-period peak ground velocity. The proportions of collapse of the larger earthquakes (magnitude 7.1 PHALL02H1 and magnitude 7.15 Porter et al. 1) are consistent for PGV_{lp} less than 2 m/s. The PHALL02H1 curve levels off and declines for PGV_{lp} greater than 2 m/s due to insufficient data at these large intensities to properly characterize the curve.

top edge of the fault, but south of that area, there may or may not be a second area of collapses, depending on the simulation. For the magnitude 7.15 ruptures on the Puente Hills fault (Figure 4.11), the first three simulations show stable patterns of building response, whereas simulation 4 causes collapses on a smaller area and simulation 5 induces collapses on a larger area. These three figures show that a single simulation of an earthquake may be appropriate to get a sense of the regional extent of building responses, but multiple simulations may be necessary to adequately characterize, in a probabilistic manner, the expected ground motion at a specific site.

Figures 4.12–4.14 graph the building responses as functions of peak ground velocity. The relationship between collapse and peak ground velocity is not well defined if there is not sufficient data. The simulations on the Hollywood fault (Figure 4.12) do not generate enough large ground motions to accurately characterize what proportion of buildings collapse at a given PGV_{lp}. For PGV_{lp} greater than 2.5 m/s, there are fewer than four data points for each PGV_{lp} level in each simulation. The suspicious results in Figure 4.12 are due to this lack of data. The simulations on the Puente Hills fault have enough strong ground motions to produce consistent relationships between collapse and peak ground velocity (Figures 4.13 and 4.14). For the two sets of simulations on the Puente Hills fault, there is much more agreement within each set compared to the set on the Hollywood fault. However, within the two Puente Hills sets, there is still uncertainty in the proportion of collapse at a given peak ground velocity. For example, the PH2E02H1 simulation shows 100% collapse of the U20P model for PGV_{lp} approximately 2.5 m/s, compared to 30% in the PH2E09H2 simulation. The building responses in a single simulation are not adequate to characterize the uncertainty in building response as a function of peak ground velocity.

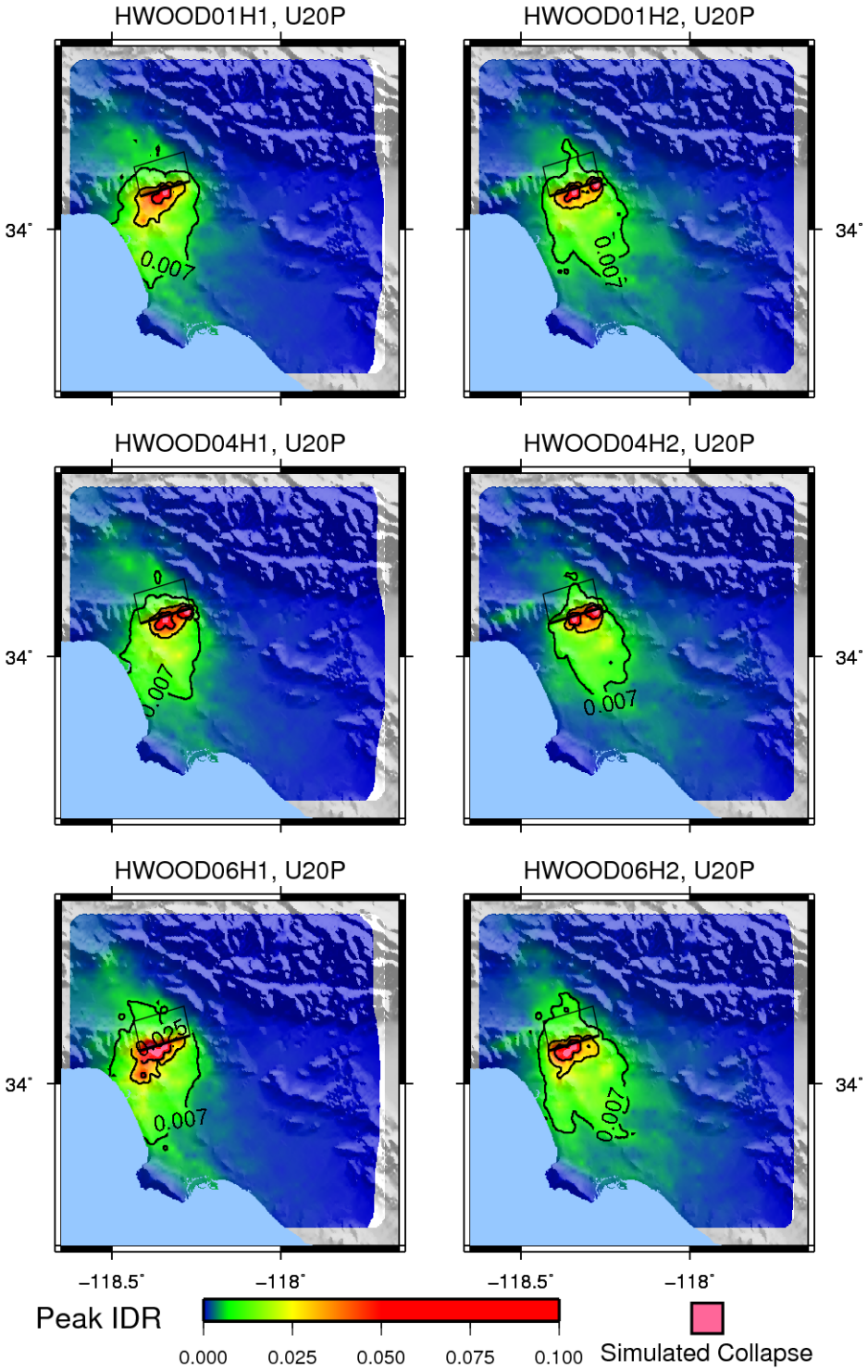

Figure 4.9: This figure maps the responses of the U20P model in multiple realizations of a magnitude 6.4 earthquake on the Hollywood fault.

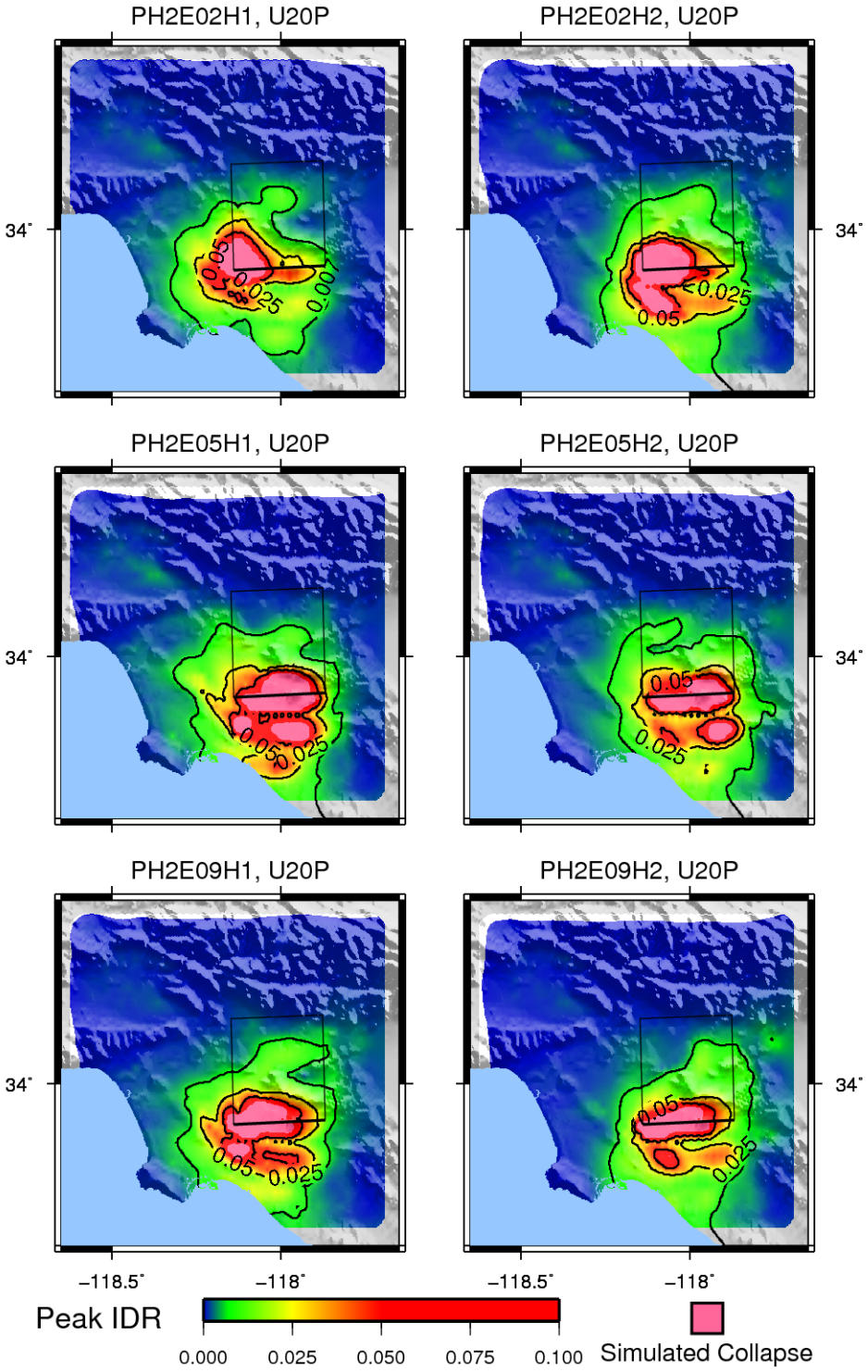

Figure 4.10: This figure maps the responses of the U20P model in multiple realizations of a magnitude 6.8 earthquake on the Puente Hills fault.

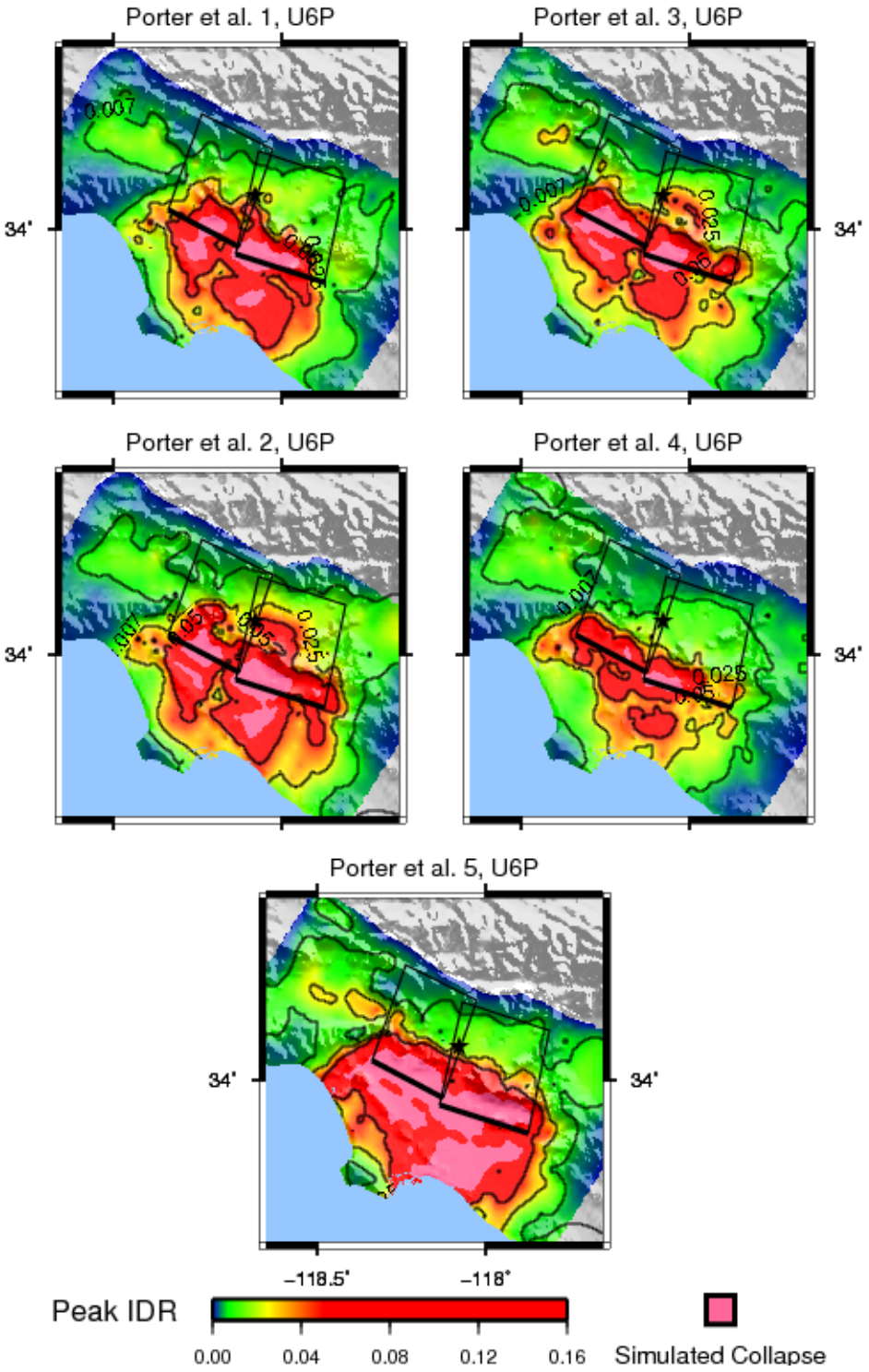

Figure 4.11: This figure shows the U6 building responses to the five Porter et al. (2007) simulations. Simulations 1–3 show similar extents of inelastic and large peak IDR (greater than 0.05) responses. Simulation 4 induces these two types of responses on smaller geographic extents than those of simulations 1–3. Simulation 5 induces these responses on larger extents than those of simulations 1–4. Thus at a single site, there can be large variability in the possible building responses for the same magnitude earthquake on a given fault.

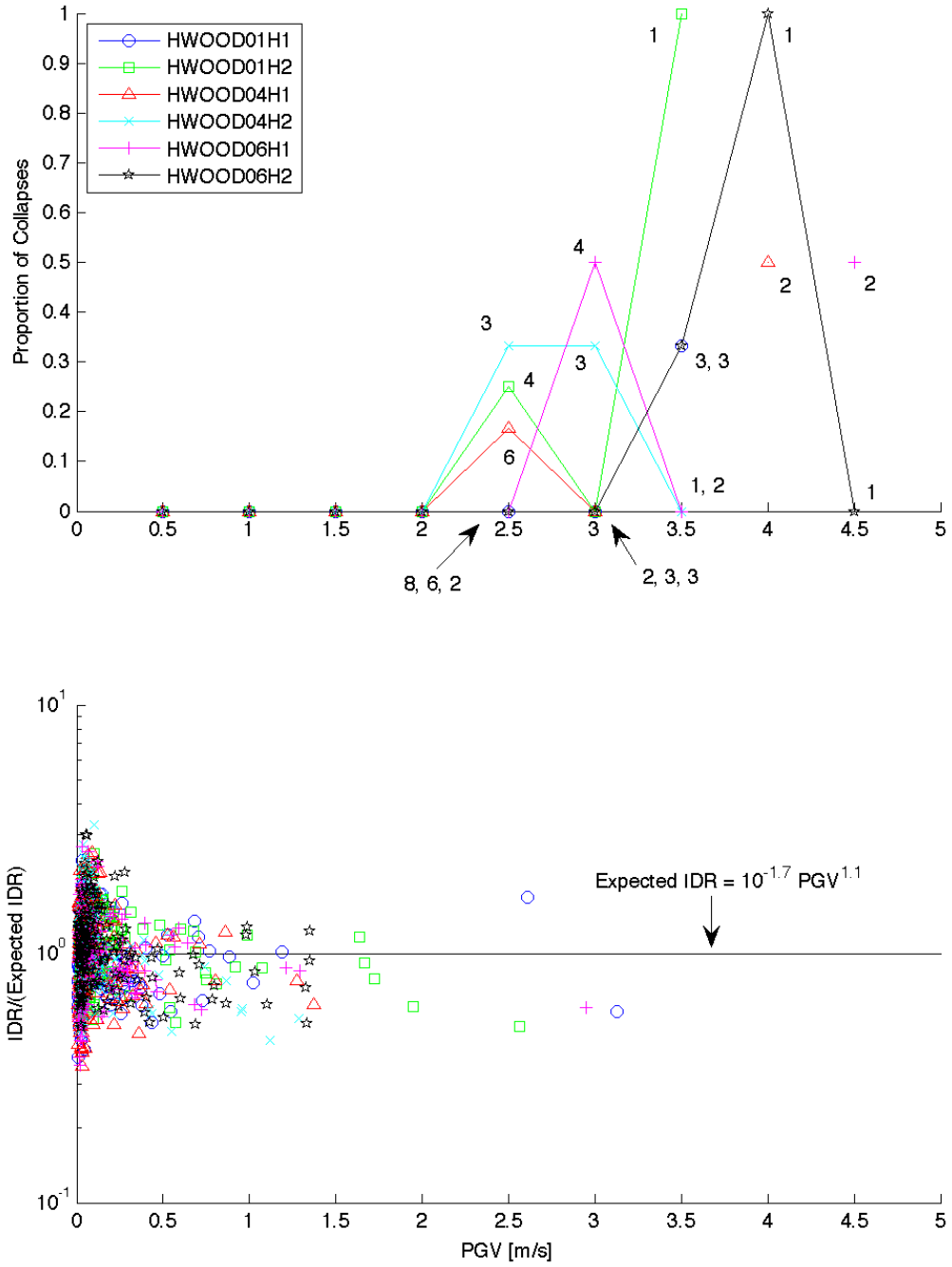

Figure 4.12: This figure compares the responses of the U20P model in multiple realizations of a magnitude 6.4 earthquake on the Hollywood fault. The numbers beside the symbols indicate the amount of data represented by that point. Note the scarcity of data for PGV_{lp} greater than 2.5 m/s.

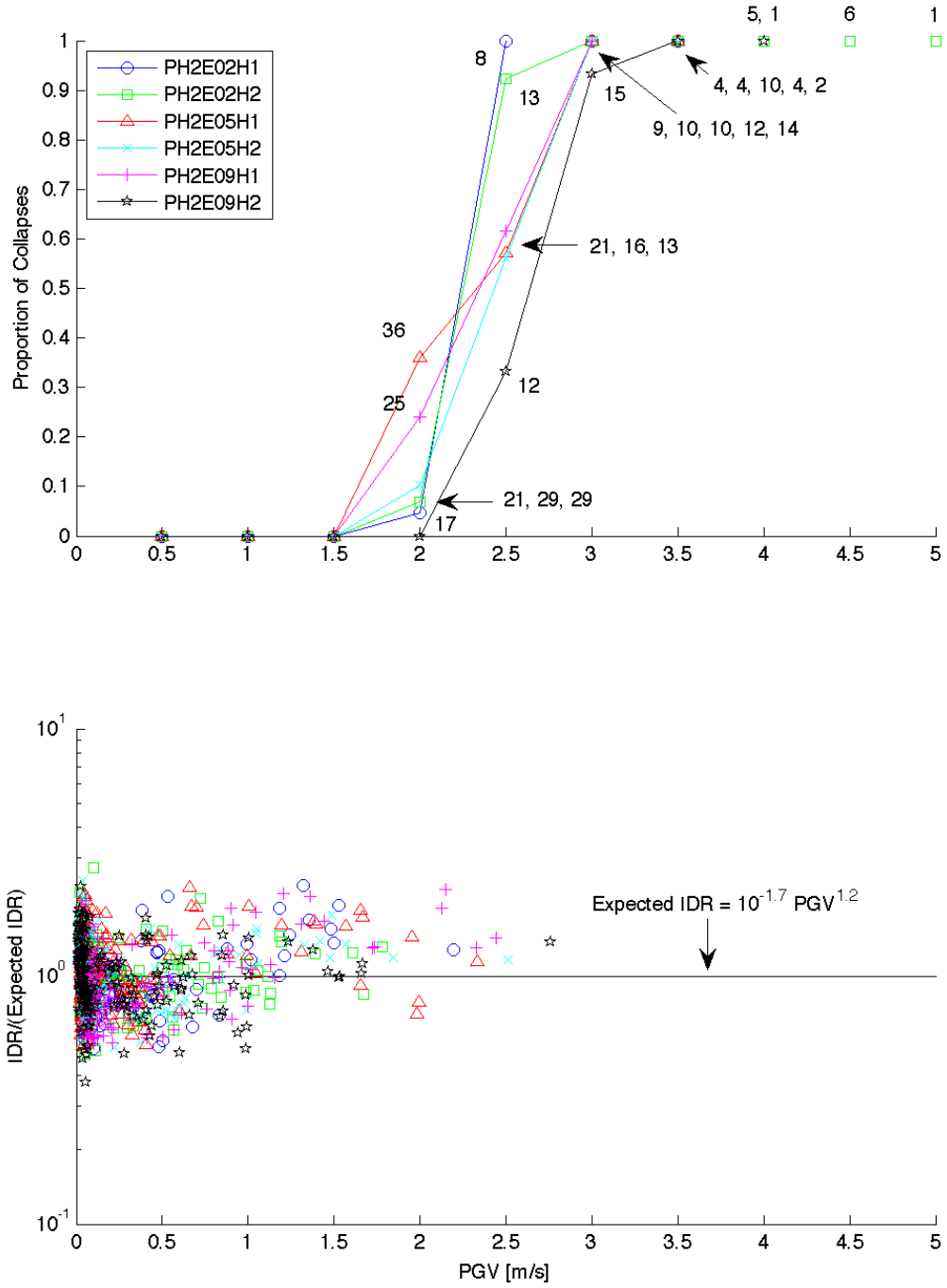

Figure 4.13: This figure compares the responses of the U20P model in multiple realizations of a magnitude 6.8 earthquake on the Puente Hills fault. The numbers beside the symbols indicate the amount of data represented by that point. There is more available data for PGV_{lp} greater than 2.5 m/s, compared to the data from the Hollywood fault. Thus, the probability of collapse is well defined and consistent for all six realizations.

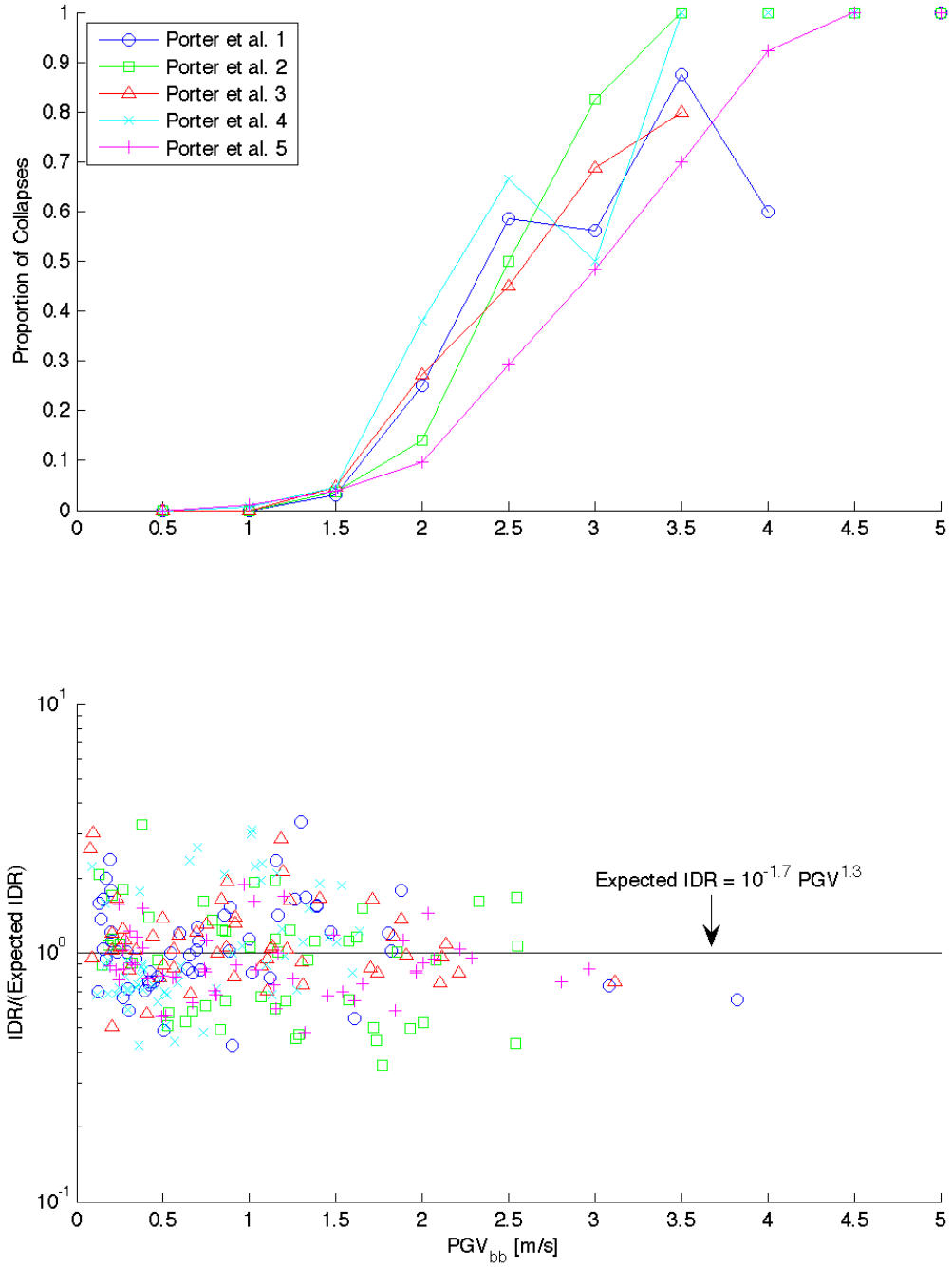

Figure 4.14: This figure compares the responses of the U20P model in multiple realizations of a magnitude 7.15 earthquake on the Puente Hills fault. The building responses are consistent for these five realizations.

Chapter 5

Simulations of Distant Earthquakes

This chapter studies the responses of twenty-story steel moment-resisting frames to simulated magnitude 7.7 and 7.8 ruptures on the southern San Andreas fault. The simulated earthquakes include the ShakeOut scenario earthquake and the two sets of TeraShake scenario earthquakes. The ground motions used in the previous chapters are primarily near-source; in this chapter, the ground motions are mostly characterized by long-period amplification in sedimentary basins. Despite the different character of the ground motions, the building responses as functions of peak ground velocity are consistent with results in previous chapters. This chapter also considers the permanent total drift response of the steel moment frames.

5.1 Ground Motion Studies

To prepare residents of southern California for the next great earthquake, the United States Geological Survey developed a year-long program to study and improve earthquake preparedness and response. Hudnut et al. (2007) defined a source model for a magnitude 7.8 scenario earthquake on the southern San Andreas fault. This earthquake ruptures the fault segments that last broke in 1680, 1812, and 1857, which are east and north of Los Angeles. Several groups simulated ground motions from this source model to provide plausible descriptions of the shaking in the Los Angeles area (for example, Graves et al. (2008)). Chen Ji used the Harvard version of the Southern California Earthquake Center Community Velocity Model (Süss and Shaw,

Version	*Rupture*	*Slip distribution*
1.2	NW to SE, sub-shear	Denali, original slip
1.3	SE to NW, sub-shear	Denali, original slip
1.4	SE to NW, sub-shear	Denali, mirrored slip
2.1	SE to NW, super-shear	from low initial stress
2.2	SE to NW, sub-shear	from medium initial stress
2.3	NW to SE, sub-shear	from high initial stress

Table 5.1: Olsen et al. (2006, 2007) generated three scenario earthquakes each for TeraShake 1 and 2. The TeraShake 1 scenarios differ in the orientation of the assumed slip distribution and the direction of rupture propagation. The TeraShake 2 scenarios differ in the assumed three-dimensional state of stress at the fault plane as well as the direction of rupture propagation.

2003) to generate long-period ground motions for this scenario. Figure 5.1 maps the long-period peak ground displacements and velocities for the entire simulation domain and for a sub-domain centered on the Los Angeles metropolitan area. Near the fault, the long-period peak ground displacements are approximately 3 m, and some long-period peak ground velocities exceed 3 m/s.

In a separate research effort, Olsen et al. (2006, 2007) generated two series of earthquakes on the southern San Andreas fault, called TeraShake 1 and 2. These scenario earthquakes rupture the southern San Andreas segments that produced the 1680 and 1812 earthquakes. TeraShake 1 used a kinematic source model with a final slip distribution based on the Denali earthquake, whereas TeraShake 2 used a dynamic source model. Each set of TeraShake simulations had three distinct ruptures: one rupture propagates from the northwest to the southeast; and two ruptures propagate from the southeast to the northwest. For TeraShake 1 the assumed slip distribution is mirrored for one of the southeast-to-northwest ruptures. The seismic wave speed model for both sets of TeraShake simulations is Version 3.0 of the Southern California Earthquake Center Community Velocity Model, and the period content of the ground motions is periods greater than 2 s. Table 5.1 summarizes the TeraShake ruptures. Figures 5.2 and 5.3 map the long-period peak ground displacements and velocities for TeraShake 1 and 2, respectively.

The predicted ground motions in the TeraShake 2 simulations are notably different

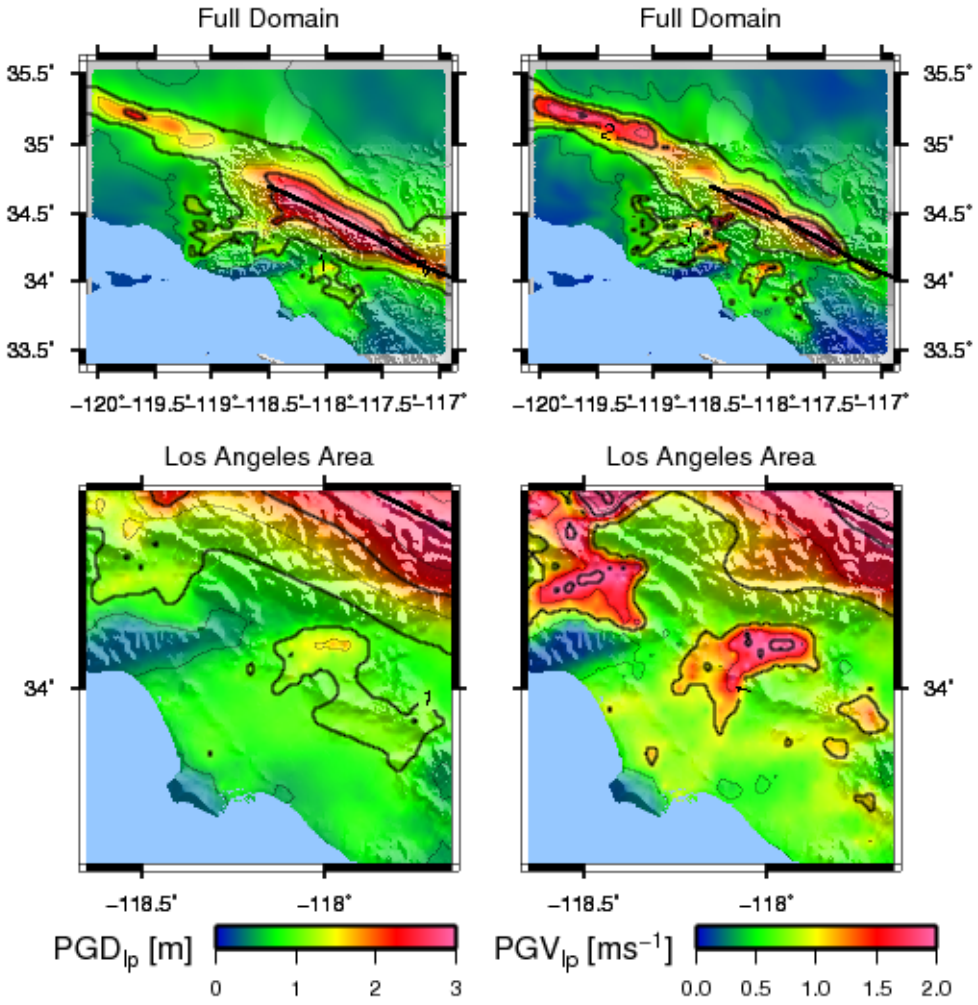

Figure 5.1: The ShakeOut simulation on the southern San Andreas fault ruptures from the southeast to the northwest. The top maps show the peak ground measures for the entire simulation domain, and the bottom maps show them for the Los Angeles metropolitan area.

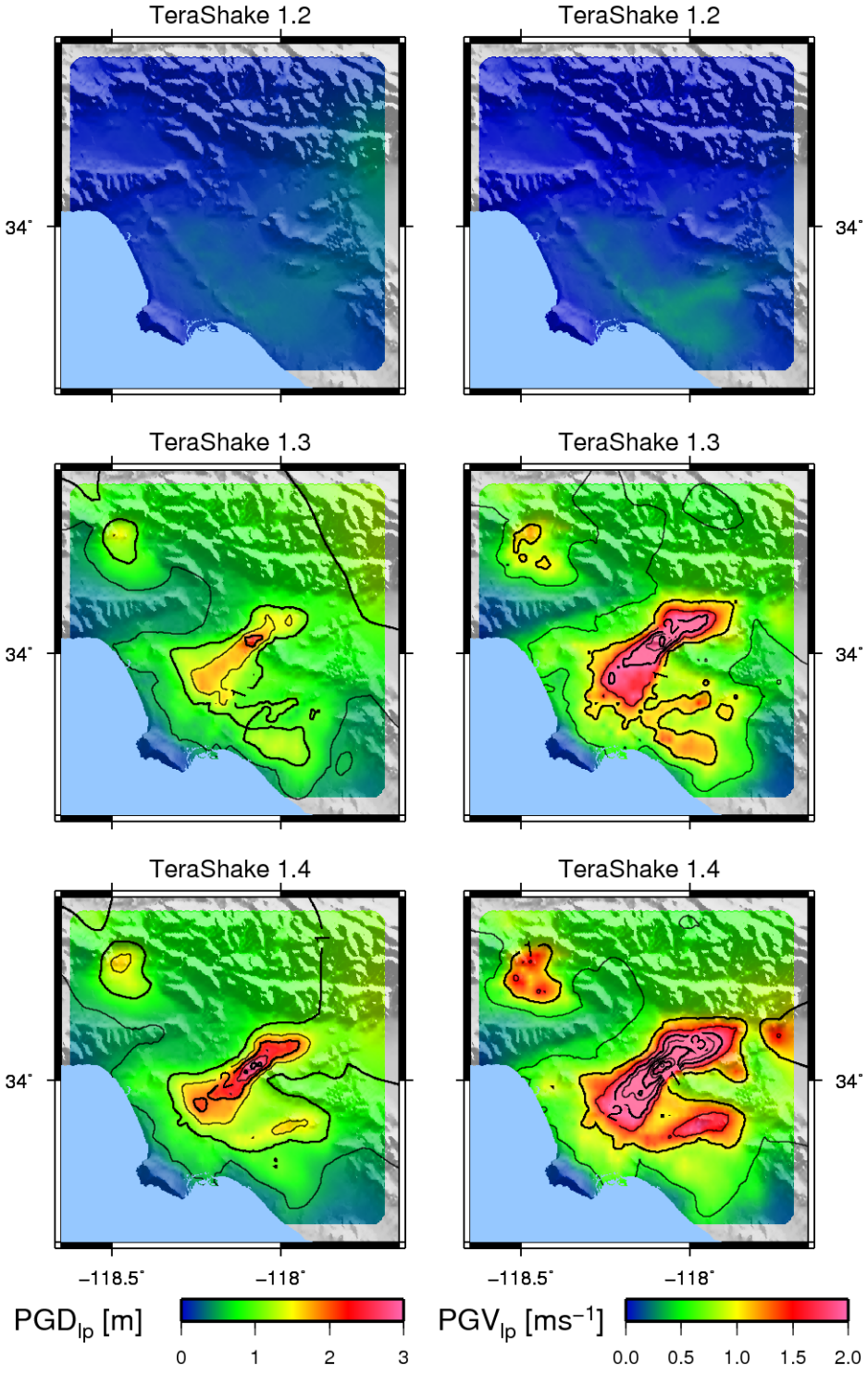

Figure 5.2: The TeraShake scenario earthquakes simulate the ground motions in a magnitude 7.7 rupture of the southern San Andreas fault. TeraShake 1 uses a kinematic source model of rupture propagation on the fault. The resulting ground motions in the Los Angeles basin are large.

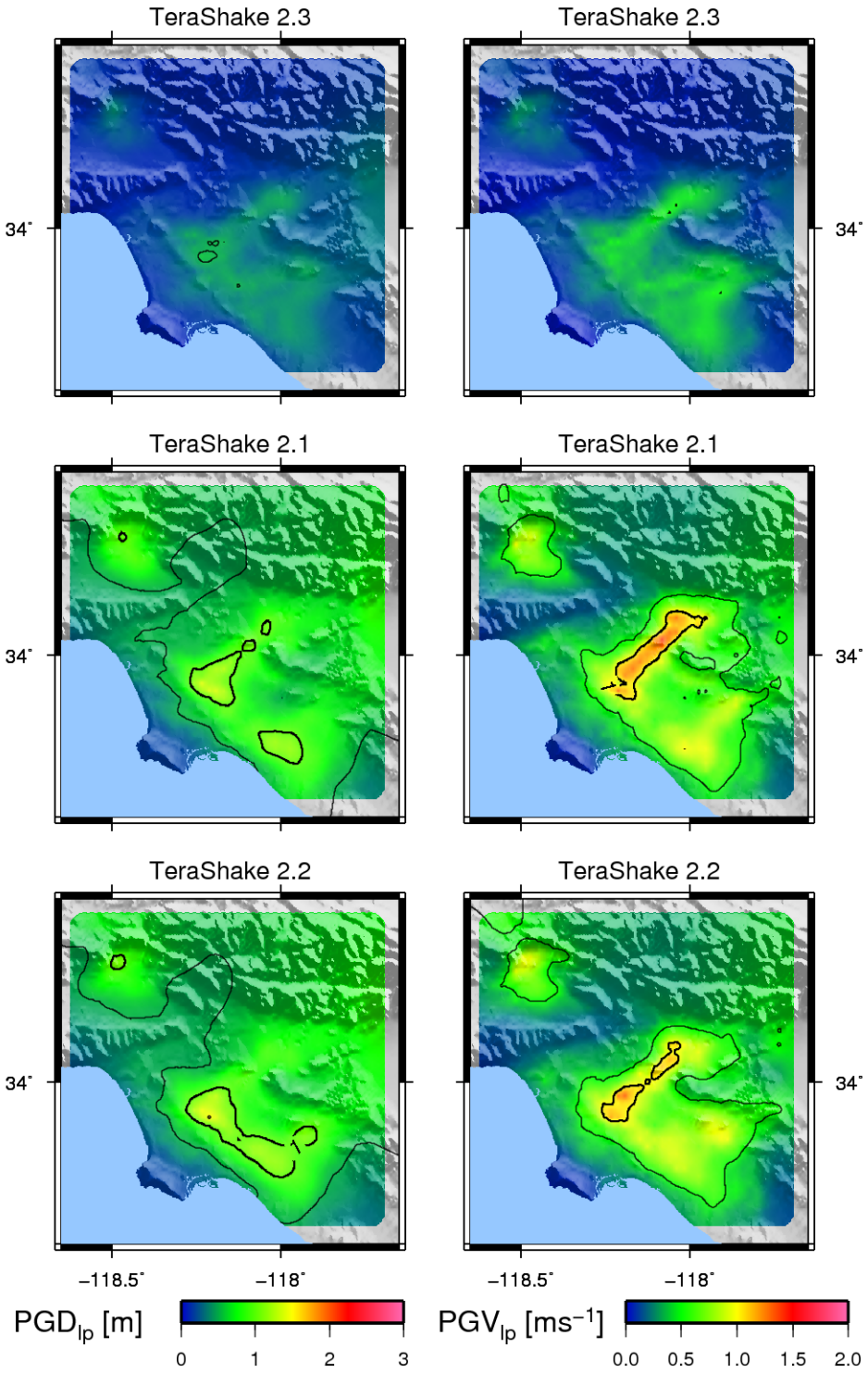

Figure 5.3: TeraShake 2 uses a dynamic source model of rupture propagation on the fault. Compared to the peak ground displacements and velocities in TeraShake 1, the ground motions predicted by TeraShake 2 are smaller. Nonetheless the long-period peak ground displacement is greater than 0.5 m in most of the Los Angeles area, and the long-period peak ground velocity exceeds 1 m/s throughout the Los Angeles basin.

than those in TeraShake 1 due to the type of source model (that is, dynamic or kinematic, respectively). A kinematic source model assumes a final slip distribution, a rupture velocity description, and a slip velocity function. Thus the evolution in time of slip at every location on the fault is modeled directly and explicitly. A dynamic source model defines the state of stress and the friction law in the media near the fault plane. Then the rupture is artificially initiated at the hypocenter. Olsen et al. (2007) sought initial stress distribution and friction law parameter values that resulted in primarily sub-shear rupture propagation. The initial shear stress distribution was based on a previous study of the magnitude 7.3 1992 Landers earthquake and scaled to be consistent with a magnitude 7.7 event. The peak ground displacements and velocities in TeraShake 1 are larger than those in TeraShake 2; the peak ground velocities in TeraShake 2.1 and 2.2 are generally twice as large as those in TeraShake 1.3 and 1.4, respectively.

TeraShake 2 represents the current state of the art for simulation of ground motion time histories. Since TeraShake 2 has a complex source model, the resulting seismic waves are less coherent than those generated by the simpler, TeraShake 1 source model (Olsen et al., 2007). A less coherent wavefront produces lower peak ground displacements and velocities. Furthermore, the ShakeOut simulation used a kinematic source model; peak ground displacements and velocities from a ShakeOut simulation with a dynamic source model would be smaller. Unfortunately, there is little data available to validate earthquake simulations with such large fault slips.

This thesis simulates building responses in the TeraShake 1, TeraShake 2, and ShakeOut (with kinematic source model) simulations. Although the ground motions from the kinematic source models of these magnitude 7.7 and 7.8 earthquakes may be implausibly large, they are available for study. Chapter 6 develops building response prediction models from intensity measures, and these unusually large ground motions contribute to the definition of the prediction models by providing data at large intensities.

5.2 Permanent Total Drift

This section presents the building responses as measured by the permanent total drift ratio (PTDR). In the two previous chapters, the peak inter-story drift ratio measures the building response, which characterizes the dynamic building response and demonstrates collapse. As discussed in Section 2.4, the permanent total drift ratio measures the static offset of the building following the dynamic earthquake excitation. Figure 5.4 maps the permanent total drift ratio for the twenty-story building models in the TeraShake 1.3, TeraShake 2.1, and ShakeOut simulations. The relative building performance of the twenty-story buildings is the same when measured by peak inter-story drift or by permanent total drift: the stiffer, higher-strength design has smaller building responses compared to the more flexible, lower-strength design; and the presence of brittle welds significantly increases the building response compared to buildings with perfect welds.

The areal extent of large permanent total drifts depends on the type of source model (that is, kinematic or dynamic) used to generate the simulated ground motions. Figure 5.4 maps the permanent total drift ratios of the twenty-story models in the TeraShake 1.3, TeraShake 2.1, and ShakeOut simulations. The simulations with kinematic source models (TeraShake 1.3 and ShakeOut) show large permanent drifts throughout the Los Angeles basin; the simulation with a dynamic source model (TeraShake 2.1) induces large permanent drifts on more limited parts of the Los Angeles basin. Nonetheless the TeraShake 2.1 simulation shows that a distant earthquake on the southern San Andreas fault induces large permanent drifts in twenty-story buildings located in the Los Angeles area.

Figure 5.5 compares the three measures of building response for the simulations on the southern San Andreas fault. The curves that show the proportions of collapse and total structural loss as functions of peak ground velocity are quite close for the twenty-story building models. For a small increase in peak ground velocity, the expected building response is collapse instead of total structural loss. Peak ground velocity must increase by 0.3–1 m/s to change the expected building response from

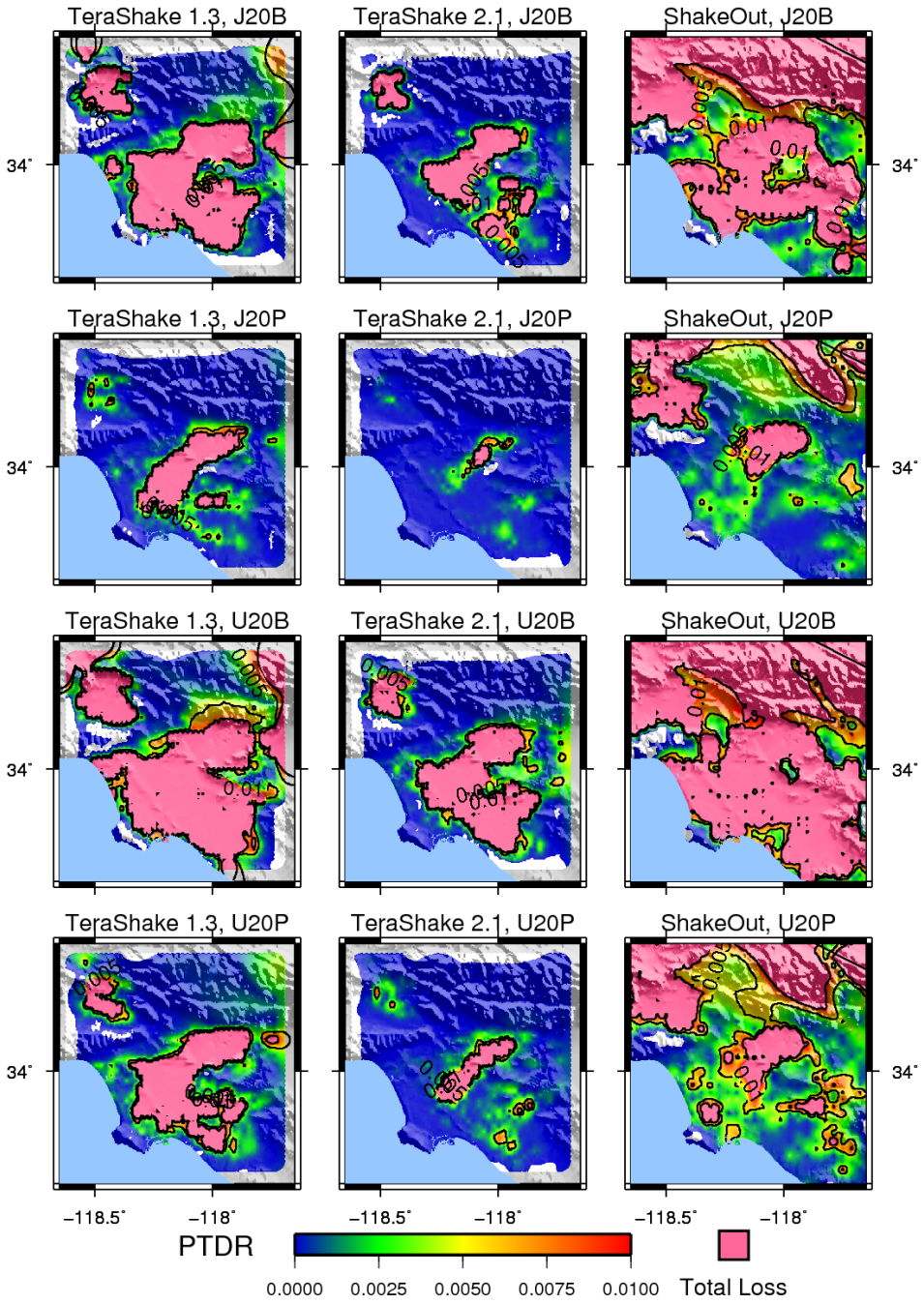

Figure 5.4: This figure shows the permanent total drift ratios for twenty-story buildings in the TeraShake 1.3 (maps on left, kinematic source model), TeraShake 2.1 (maps in middle, dynamic source model), and ShakeOut (maps on right, kinematic source model) simulations. Note the reduction in building response from TeraShake 1.3 to 2.1 due to smaller ground motions from a less coherent source model. Presumably, a dynamic source model of the ShakeOut earthquake would produce smaller ground motions and thus smaller building responses. Nonetheless buildings with brittle welds throughout the Los Angeles and San Fernando basins do not fare well in these great, distant earthquakes.

total structural loss to collapse for buildings with perfect welds. For buildings with brittle welds, an increase in peak ground velocity of less than 0.3 m/s will effect this change in expected building response.

A small margin between total structural loss and collapse is problematic for predicting such important states of building response. As seen in Section 4.4, multiple realizations of the same magnitude earthquake on the same fault result in different predicted peak ground velocities. There is uncertainty in predicting the largest peak ground velocity for a single earthquake, and the uncertainty only increases when trying to establish the seismic risk at a site. If the increment of peak ground velocity from total structural loss to collapse is similar to the uncertainty of predicting the peak ground velocity itself, then distinguishing between total structural loss and collapse is difficult.

5.3 Distant versus Basin Simulations

Although ruptures on the southern San Andreas fault are distant to urban areas, building responses to ground motions from these great earthquakes are comparable to those from large earthquakes in the Los Angeles basin. Figure 5.6 maps the responses of a twenty-story building in three distant, magnitude 7.7 and 7.8 earthquakes and in a Puente Hills earthquake in the Los Angeles basin. The pattern of large building responses is quite different in the four earthquakes. Considering the Puente Hills (top-left subfigure) and the TeraShake 2 (bottom-right subfigure) simulations, the responses of the twenty-story, more flexible building exceed a peak inter-story drift ratio of 0.007 on most of the Los Angeles, San Fernando, and San Gabriel basins. FEMA 356 defines this level as "immediate occupancy;" in either the distant TeraShake or close Puente Hills earthquake, twenty-story, more flexible buildings may not be safe for immediate occupancy throughout the entire Los Angeles area. The Puente Hills earthquake, however, induces collapses on a larger area than does the TeraShake earthquake.

The building responses as functions of peak ground velocity are generally con-

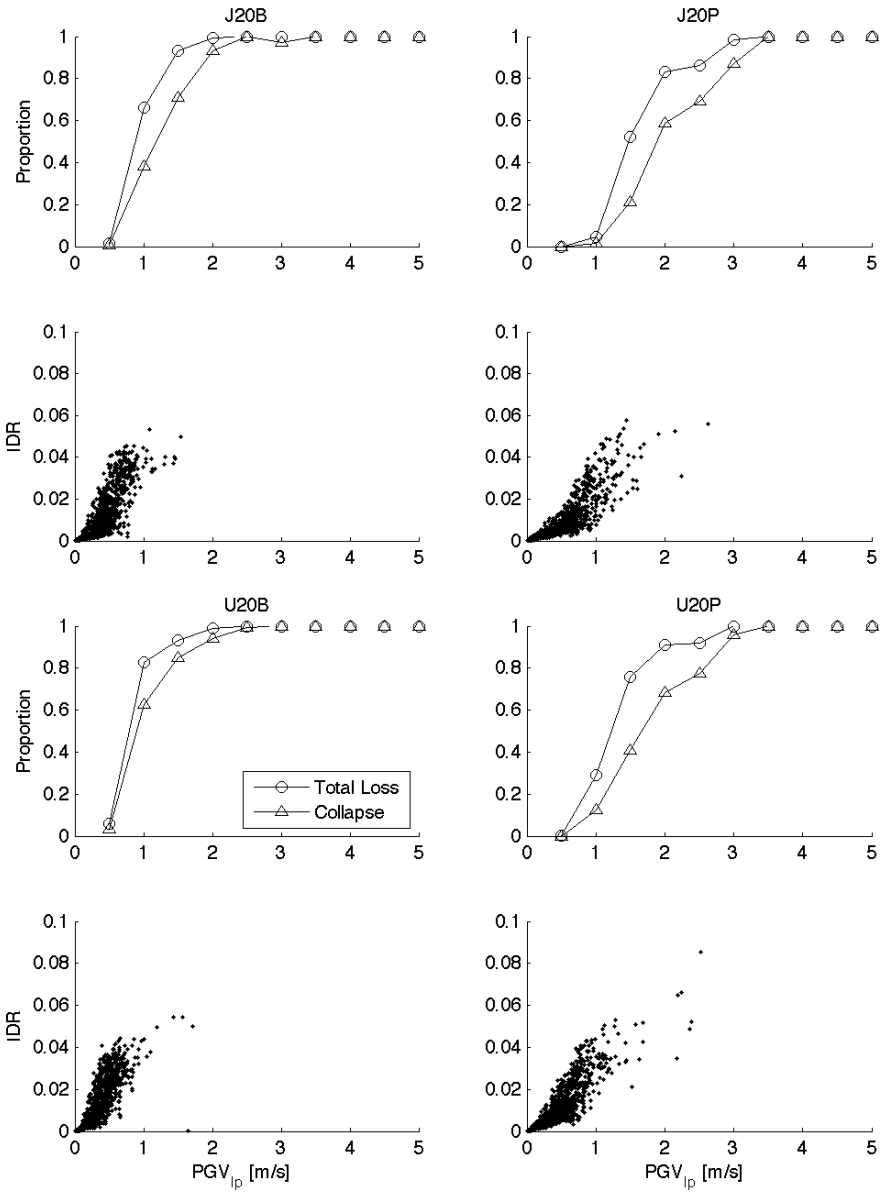

Figure 5.5: This figure shows the twenty-story building responses to magnitude 7.7 and 7.8 simulations on the southern San Andreas fault as functions of the peak ground velocity. The increase in peak ground velocity necessary to change the expected building response from total structural loss to collapse is small. For the buildings with brittle welds, this increase is especially small.

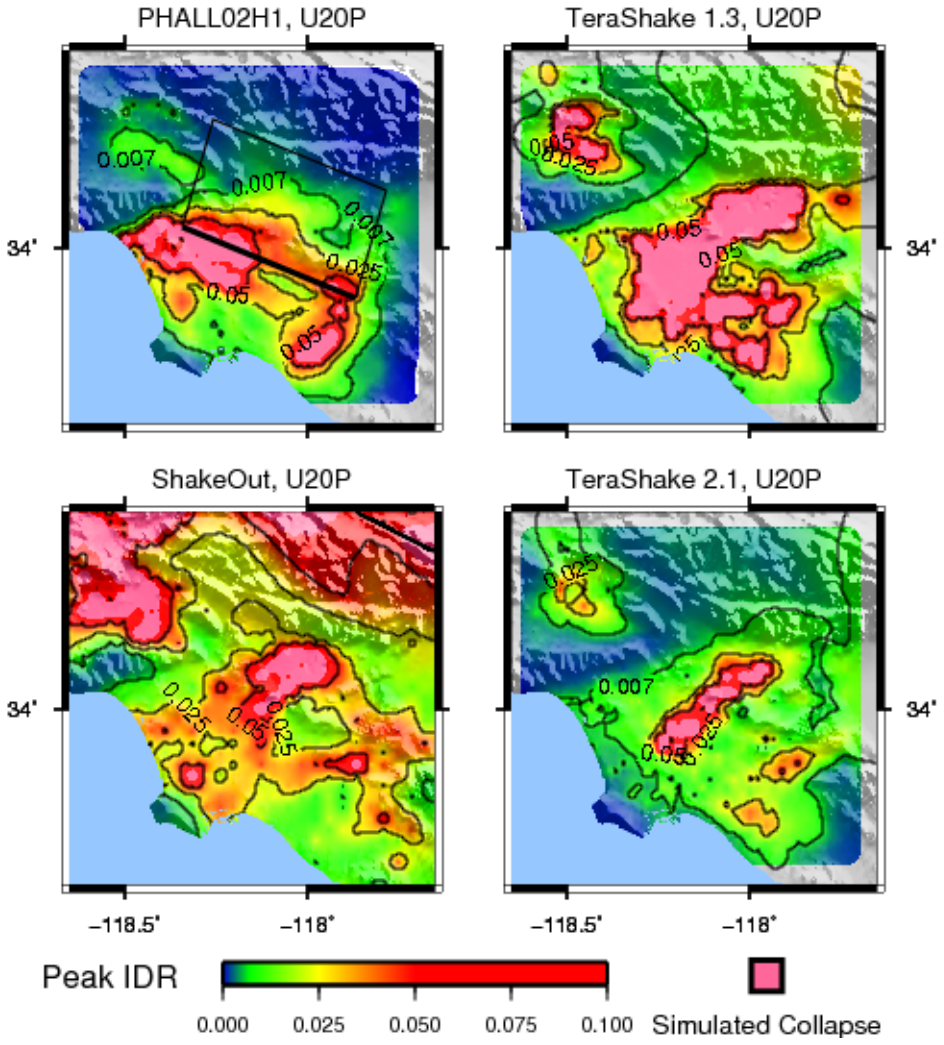

Figure 5.6: These four simulations induce large responses in the twenty-story, more flexible building with perfect welds (U20P). The Puente Hills fault is in the Los Angeles basin, and the TeraShake and ShakeOut simulations rupture the southern San Andreas fault, which is distant from the Los Angeles metropolitan area. The magnitude 7.1 Puente Hills and magnitude 7.7 TeraShake 2.1 simulations suggest that, if either earthquake happened, twenty-story, more flexible buildings throughout the Los Angeles and San Fernando basins may require inspections of the structural systems. (That is, the peak IDR exceeds 0.007, the FEMA 356 immediate occupancy level.) The Puente Hills earthquake induces collapse on a large area compared to the TeraShake 2.1 simulation.

sistent whether the earthquake rupture is distant or near. Figure 5.7 plots the proportions of collapse and total structural loss and the peak inter-story drift ratio versus the ground motion intensity measure. The proportions of collapse from the TeraShake 1 and 2 simulations are larger than those from the ShakeOut and magnitude 7.1 Puente Hills simulations. The differences between TeraShake 2, ShakeOut, and Puente Hills may be due to the normal variation seen previously (for example, Figure 4.13). However, the proportion of collapse from the TeraShake 1 simulation is unusually large. There is a similar difference between the TeraShake versus ShakeOut and Puente Hills simulations as measured by the permanent total drift. For long-period peak ground velocities greater than 1 m/s, the U20P model is always a total structural loss in the TeraShake simulations, but may be repairable in the ShakeOut and Puente Hills simulations. These different building responses may be due to the duration of long-period ground motions in the Los Angeles basin. Considering the building response solely as a function of peak ground velocity neglects this important aspect of ground motion from a distant rupture. Note, though, the consistency in proportion of total structural loss for the four simulations.

The mechanisms of building response are different in near-source ground motions compared to basin-amplified ground motions. In pulse-like, near-source ground motions, the building yields and accumulates damage soon after the transient pulse in ground motion. In the far-source ground motions considered here, sedimentary basins amplify the long-period content and prolong the duration of large ground motion. Thus, the buildings may achieve steady-state resonance, and cyclic excitation may eventually degrade the lateral force-resisting capacity of the buildings. (Section 2.3.1 discusses the different building responses in more detail.) Although the mechanism of building response is different for the two types of ground motions, the end results—measured as collapse, total structural loss, and peak inter-story drift—seem similar for the same peak ground velocity. This observation provides evidence to support using both types of ground motions to develop models to predict building response. In the next chapter, I disregard what simulation produced the ground motions and building responses and consider only the building response as a function of intensity

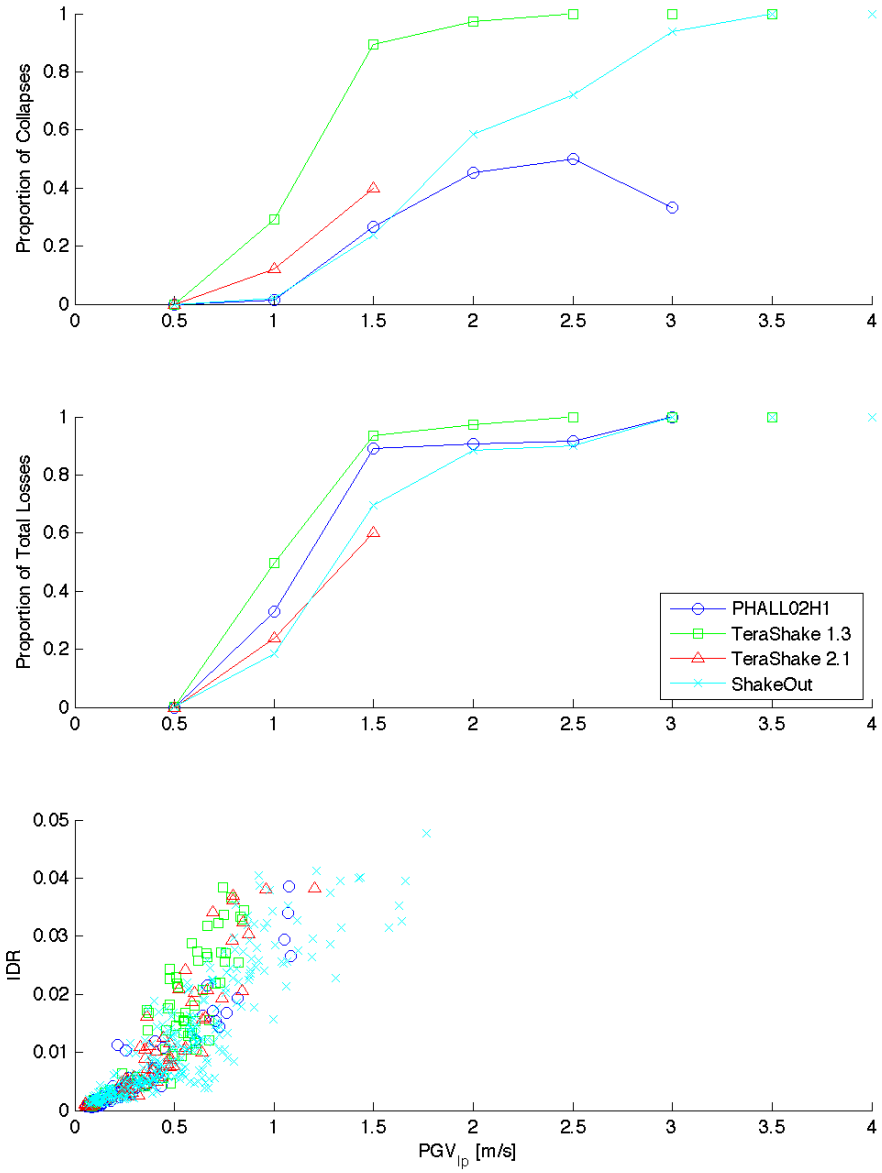

Figure 5.7: The responses of twenty-story, more flexible buildings with perfect welds (U20P) are similar for near-source and basin-amplified ground motions. The TeraShake 1 simulation predicts an unusually large number of collapses for the same peak ground velocity compared to the other simulations. For PGV_{lp} greater than 1 m/s, ground motions from both TeraShake simulations cause the U20P model to be a total structural loss. The differences between building response in the TeraShake versus ShakeOut and Puente Hills simulations may be due to longer duration shaking in TeraShake, which is not characterized by peak ground velocity. Also, the proportion of collapse curve for the Puente Hills simulation (PHALL02H1) is flat and curves down for PGV_{lp} greater than 2 m/s because there is insufficient data from this simulation to characterize collapse at these large values. (Consider Section 4.3.)

measure.

Chapter 6

Building Response Prediction

This chapter interprets the simulated building responses by developing relationships to predict collapse, the permanent total drift ratio, and peak inter-story drift ratio (IDR) from ground motion intensity measures. Previous chapters consider the simulation results for each ground motion study individually. In that light, the results describe regional patterns of building response. The building response prediction models developed in this chapter disregard which study produced the ground motions and consider only the building response as a function of intensity measure. Since these prediction models include a measure of the uncertainty due to nonlinearities in building response, it is reasonable to forgo the full nonlinear time history analysis for some purposes. These relationships can be used as general structural analyses to approximate the lifetime costs of a proposed steel moment-resisting frame (MRF) design, or to compare at an initial stage several designs, or for other general analyses.

6.1 Simulated Ground Motions and Ground Motion Prediction Equations

Simulated earthquakes of magnitudes 6.3–7.8 produced the ground motions used in this thesis. The sites of the ground motions range from 1 to 200 km distant to the generating fault. Figure 6.1 compares the magnitudes of the simulated earthquakes to the measure of distance between the faults and ground motion sites for all simulation do-

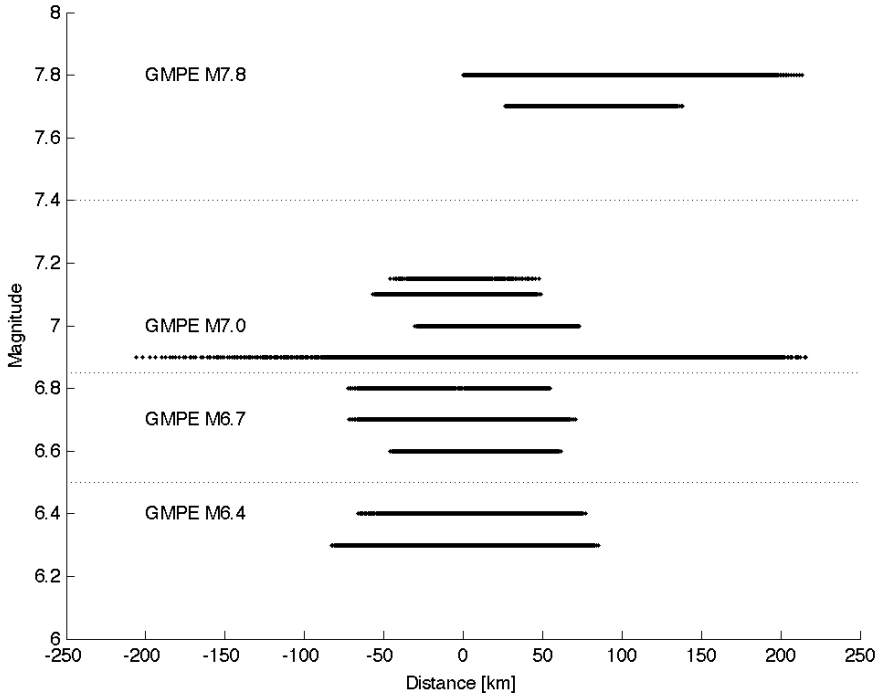

Figure 6.1: The simulated ground motions in this thesis cover a range of magnitudes and distances between the fault and ground motion site. Negative distances are sites on the hanging wall of a thrust fault. This figure shows the magnitude grouping of the simulations for comparison with ground motion prediction equations.

mains. This distance is the shortest path between each site and the surface projection of the rupture on a strike-slip fault or the projection of the top edge of a thrust fault. Figure 6.2 shows the peak ground displacements (PGD_{lp}s) and peak ground velocities (PGV_{lp}s) of the simulated ground motions as functions of the distance between the fault and the site. Since there are not many recorded ground motions within 10 km of a large magnitude earthquake, these simulated ground motions suggest what the peak ground displacements and velocities may be for near-source records of strong ground motions.

Figure 6.3 compares the simulated ground motions to the extended magnitude ground motion prediction equations (GMPEs) by Cua and Heaton (2008). For the smallest simulations (magnitudes 6.3 and 6.4), the GMPEs and the simulated ground motions do not agree. At rock and soil sites within 5 km of the fault, the median

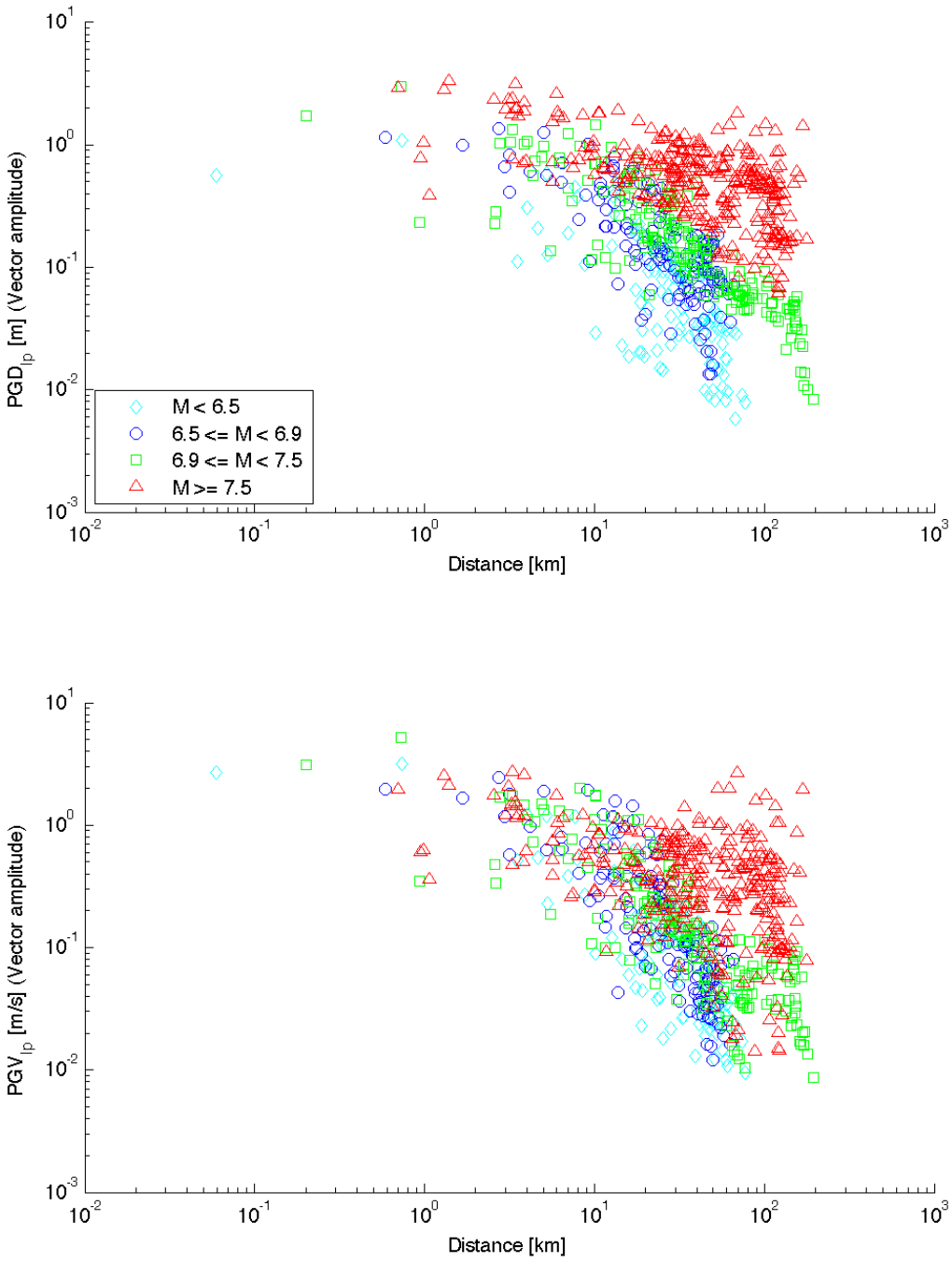

Figure 6.2: There are few recorded ground motions from near-source sites in strong ground motions. The simulated ground motions in this thesis suggest what the long-period peak ground displacements and velocities may be for near-source sites.

PGV_{lp} of the simulated ground motions is more than one log-standard deviation from the GMPE median PGV. The GMPE median PGV saturates at small distances whereas the median PGV_{lp} of the simulated ground motions continues to increase linearly on the log-scale. For the large simulations (magnitudes 6.6 to 7.2), the GMPE and simulated ground motions generally agree for rock sites but not for soil sites. At soil sites within 10 km of the fault, the median PGV_{lp} of the simulated ground motion is more than one log-standard deviation from the GMPE median PGV. For the largest magnitudes (7.7 and 7.8), the median PGV_{lp} of the simulated ground motions is generally within one log-standard deviation of the predicted median. However, the median PGV_{lp} of the simulated ground motions at sites within 10 km are consistently larger than what is predicted.

For sites 30 to 200 km distant from the rupture of the largest magnitude earthquakes, the log-standard deviation of the simulated ground motions can be twice that of the GMPEs. Figure 6.4 shows the data that produced these large log-standard deviations. The large spread is consistent for the three sets of southern San Andreas simulations. (Although, TeraShake 1 has some unusually small peak ground velocities.) The spread in the peak ground velocity from the simulations based on the 1906 San Francisco earthquake on the northern San Andreas fault is smaller than the spread from the southern San Andreas events. Thus the southern San Andreas ground motions are the source of the unexpectedly large uncertainty in peak ground velocity for distant sites in the largest magnitude earthquakes.

For the building response prediction models developed in the following sections to be widely applicable, they must be based on plausible ground motions. The simulated ground motions used to calculate the steel MRF responses should be reasonably consistent with the patterns of recorded ground motions. The simulations and empirical relations need not match exactly because there are gaps in the recorded data and the building response prediction models disregard the magnitude and distance information associated with each ground motion. Each study that produced the simulated ground motions used in this thesis was satisfied that the ground motions were plausible. (The TeraShake 2 simulations are now considered more likely than TeraShake 1

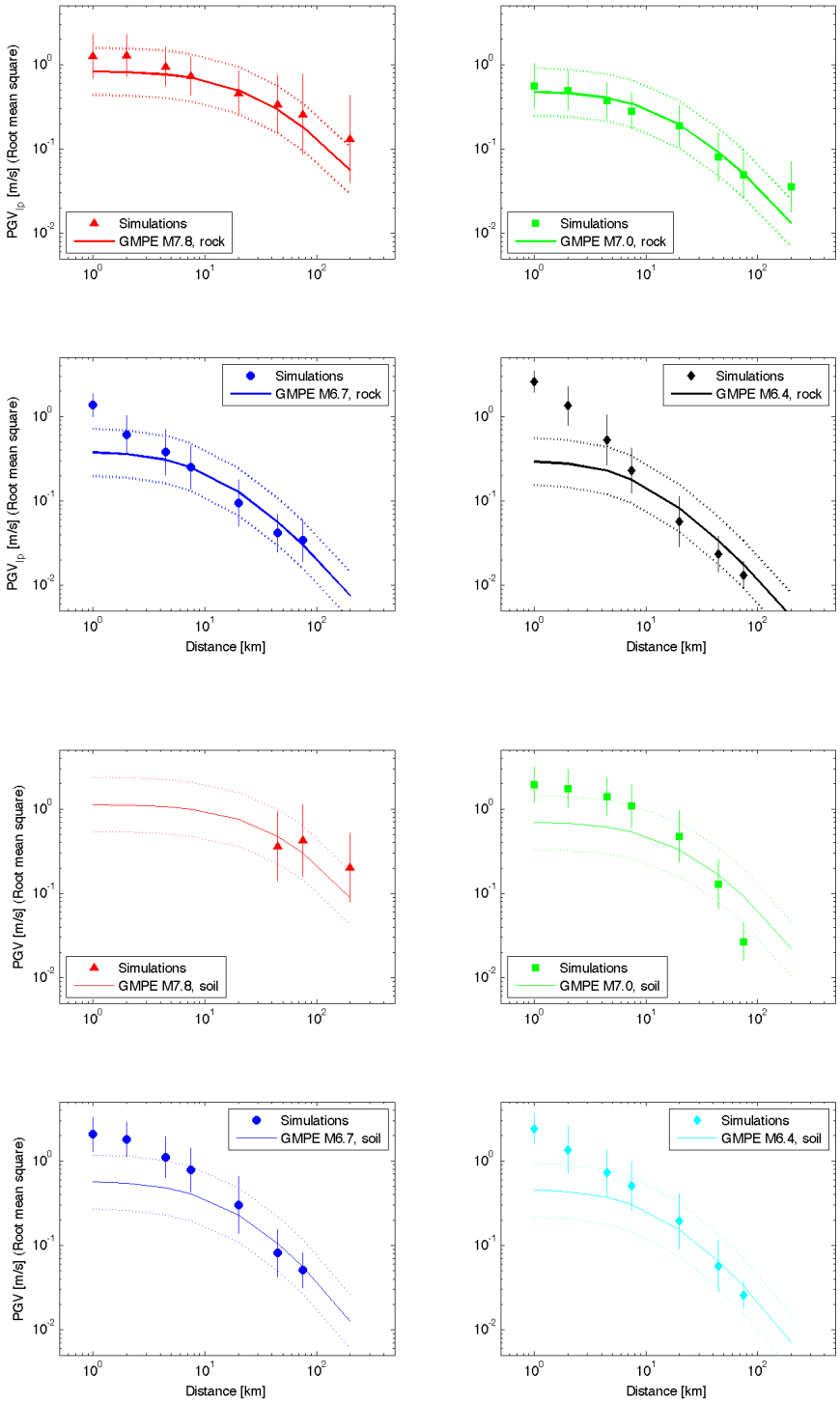

Figure 6.3: This figure compares the peak ground velocity medians and log-standard deviations of the simulated ground motions to those of GMPEs by Cua and Heaton (2008). The top four plots compare rock sites (shear wave speeds greater than 464 m/s), and the bottom four plots compare soil sites (shear wave speeds less than or equal to 464 m/s). Each plot compares PGVs from similar magnitudes; Figure 6.1 defines the magnitude groups. Note that the long-period PGVs have been converted to the root mean square velocity: $\mathrm{PGV_{rms}} = \mathrm{PGV_{lp}}/1.18$ (Cua and Heaton, 2008). Converting long-period, vector amplitude PGV to broadband, vector amplitude PGV does not significantly affect this comparison.

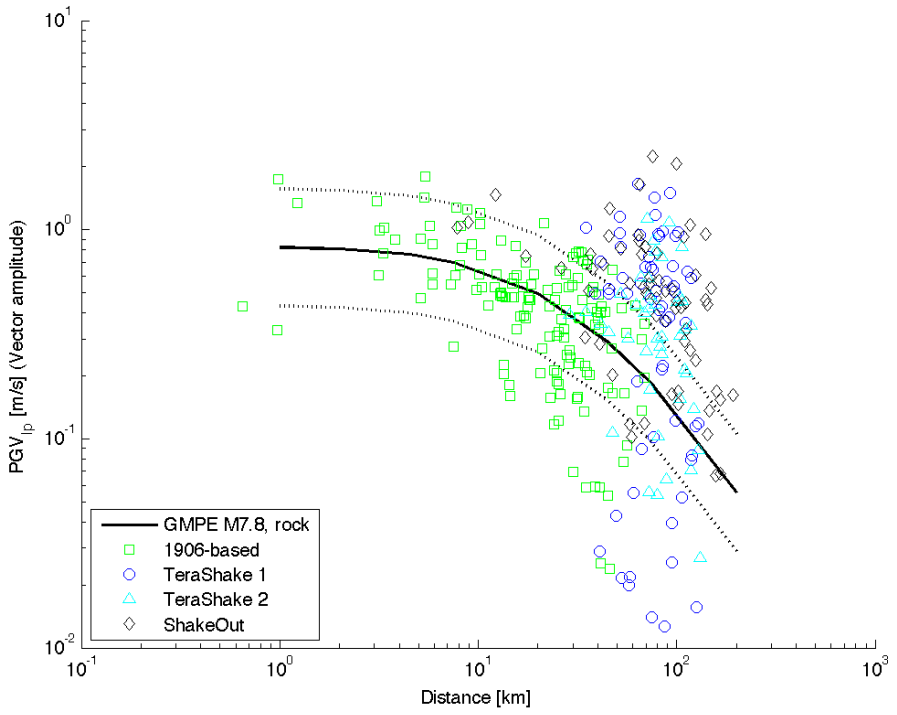

Figure 6.4: This figure shows the long-period peak ground velocities for the largest magnitude simulations at rock and soil sites. The data for sites over 30 km from the fault have a large spread. The simulations on the southern San Andreas (TeraShake and ShakeOut) contribute exclusively to the large range of peak ground velocities at distant sites.

because its less coherent source model generated ground motions more consistent with past experience and current expectations.) With further investigation, seismologists may reconcile the differences between the simulated ground motions and the GMPEs. The simulated ground motions are sufficiently consistent with the expectations developed from recorded ground motions to justify their use in developing building response prediction models.

6.2 Bayesian Model Class Selection

This section develops models to predict the state of a steel MRF building from intensity measures of ground motions. The states of building response are: collapsed or standing; total structural loss or repairable; and if repairable, the peak IDR. I propose several possible prediction models and apply Bayesian model class selection to determine the most likely prediction model based on the simulated building responses, the structure of the proposed model, and prior information about the parameters of the models.

6.2.1 Data

The intent of this thesis is to model steel moment frame building response in strong ground motions. Building responses in small ground motions can be adequately modeled by modal analysis because the buildings remain elastic. Approximately one-third of the simulated ground motions in this thesis can be considered too small to induce inelastic building behavior. These small ground motions would dominate the fit of the building response prediction models. Thus, I remove data for PGD_{lp} less than 0.15 m and PGV_{lp} less than 0.3 m/s. Removing these ground motions from the data set results in prediction models that better describe building response in strong ground motions. Figure 6.5 locates the remaining data in the PGD_{lp}-PGV_{lp} plane and indicates the amount of data at each location. The preponderance of the data is from ground motions with PGD_{lp} less than 1.5 m and PGV_{lp} less than 1.5 m/s.

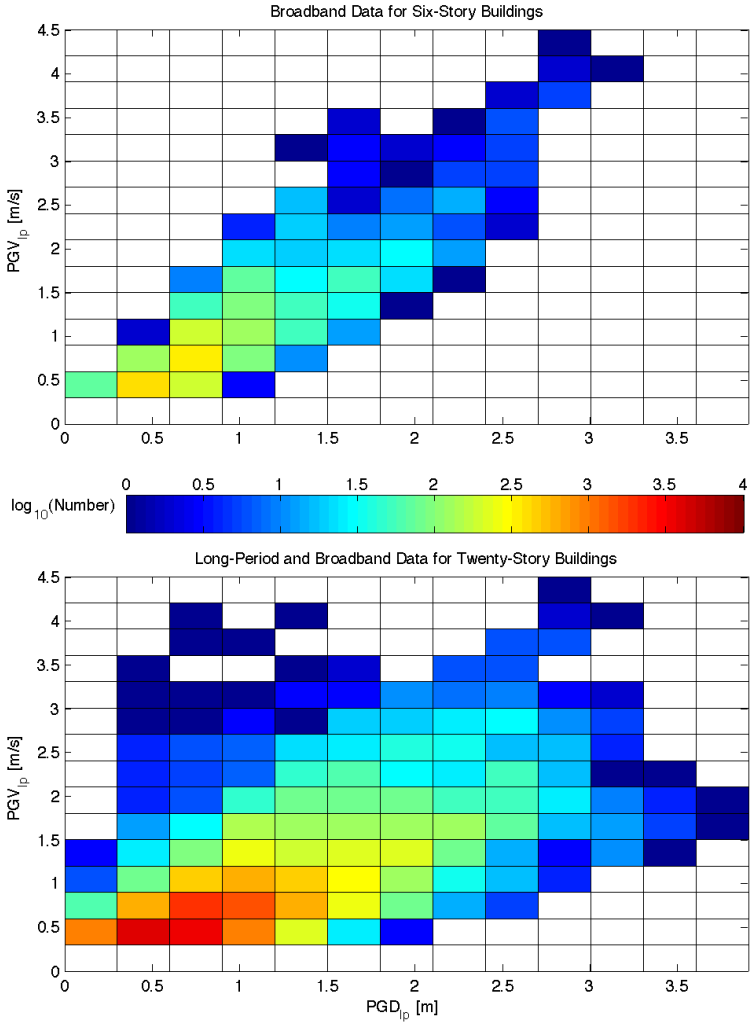

Figure 6.5: This figure shows the location of data in the PGD_{lp}-PGV_{lp} plane. Ground motions with PGD_{lp} less than 0.15 m and PGV_{lp} less than 0.3 m/s have been removed. The remaining data comes primarily from ground motions with PGD_{lp} less than 1.5 m and PGV_{lp} less than 1.5 m/s.

The data set for the six-story buildings is different than that for the twenty-story buildings. Approximately 10% of the ground motions are broadband, which can be applied to both six- and twenty-story building models. Most simulated ground motions in this thesis are long-period, which can only be applied to the twenty-story buildings. Furthermore, the peak ground measures of broadband ground motions are almost always larger than those of long-period ground motions. I apply a low-pass Butterworth filter with a corner period of 2 s to the broadband ground motions in order to make the peak ground measures consistent. I filter the broadband ground motions only to produce consistent PGD and PGV measures; the nonlinear time history analyses use the unfiltered simulated ground motions. Thus, the PGD and PGV in this chapter are calculated from long-period ground motions.

The peak ground displacements and velocities of the data set for the six-story buildings are highly correlated, whereas the data set for the twenty-story buildings does not show a strong correlation. The prediction models for the six-story buildings should only be applied to ground motions with a PGD approximately equal to the PGV. The prediction models for the twenty-story buildings can be applied to ground motions in a larger area of the PGD-PGV plane.

The building responses as a function of PGD and PGV are consistent with intuition: larger PGDs and PGVs induce larger building responses (Figures 6.6–6.8). Generally speaking, the six- and twenty-story models with perfect welds collapse in ground motions with PGD_{lp} greater than 1 m and PGV_{lp} greater than 2 m/s (Figure 6.6). Models with brittle welds collapse in smaller ground motions than do models with perfect welds. For ground motions with PGD_{lp} greater than 0.6 m and PGV_{lp} greater than 0.6 m/s, the building may remain standing but be deemed a total structural loss (defined in this thesis as a permanent total drift ratio greater than 0.0091; Figure 6.7). In many simulations with large ground motions, the buildings experience large dynamic inter-story drifts but are not total structural losses (Figure 6.8).

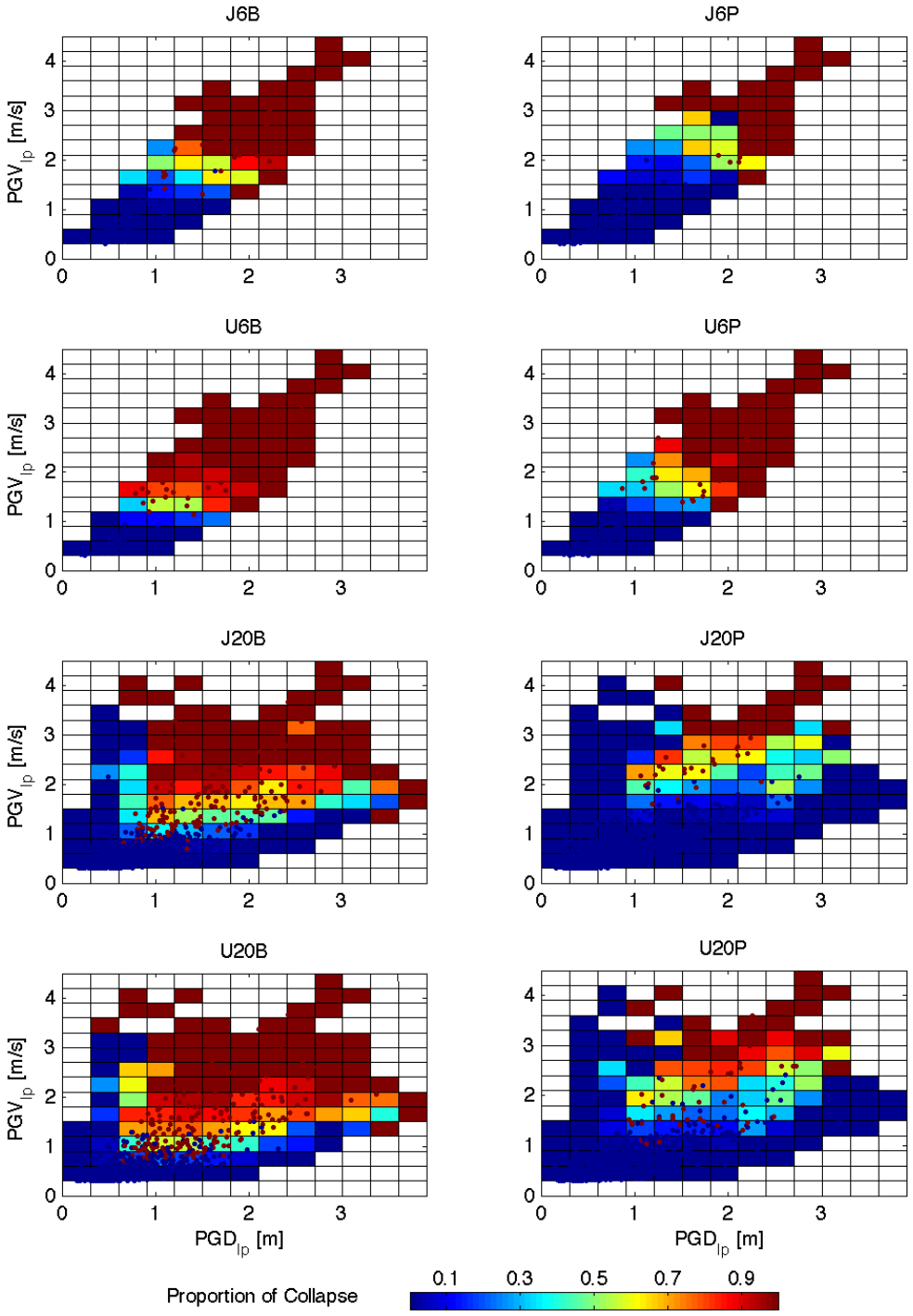

Figure 6.6: This figure shows the location of collapse data in the PGD_{lp}-PGV_{lp} plane. The coloring of a box represents the proportion of buildings that collapse in that range of PGD_{lp} and PGV_{lp}. Blue and red dots locate some data points for buildings that remain standing or collapse, respectively.

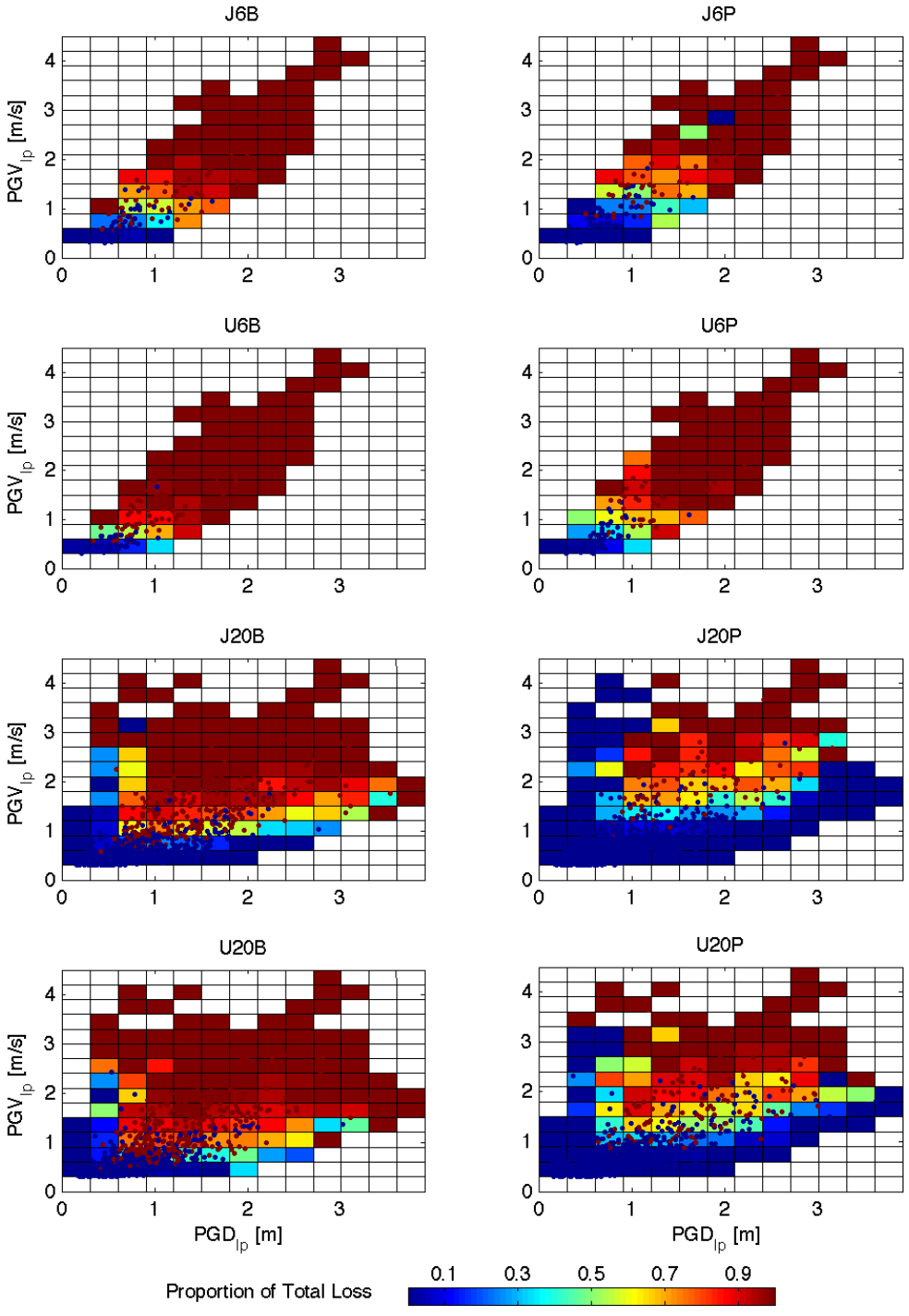

Figure 6.7: This figure locates the total structural loss data in the PGD_{lp}-PGV_{lp} plane. Similar to the plot of collapse data, the box color represents the proportion of buildings that are a total structural loss, and blue and red dots locate some data points for buildings that are repairable or a total structural loss, respectively.

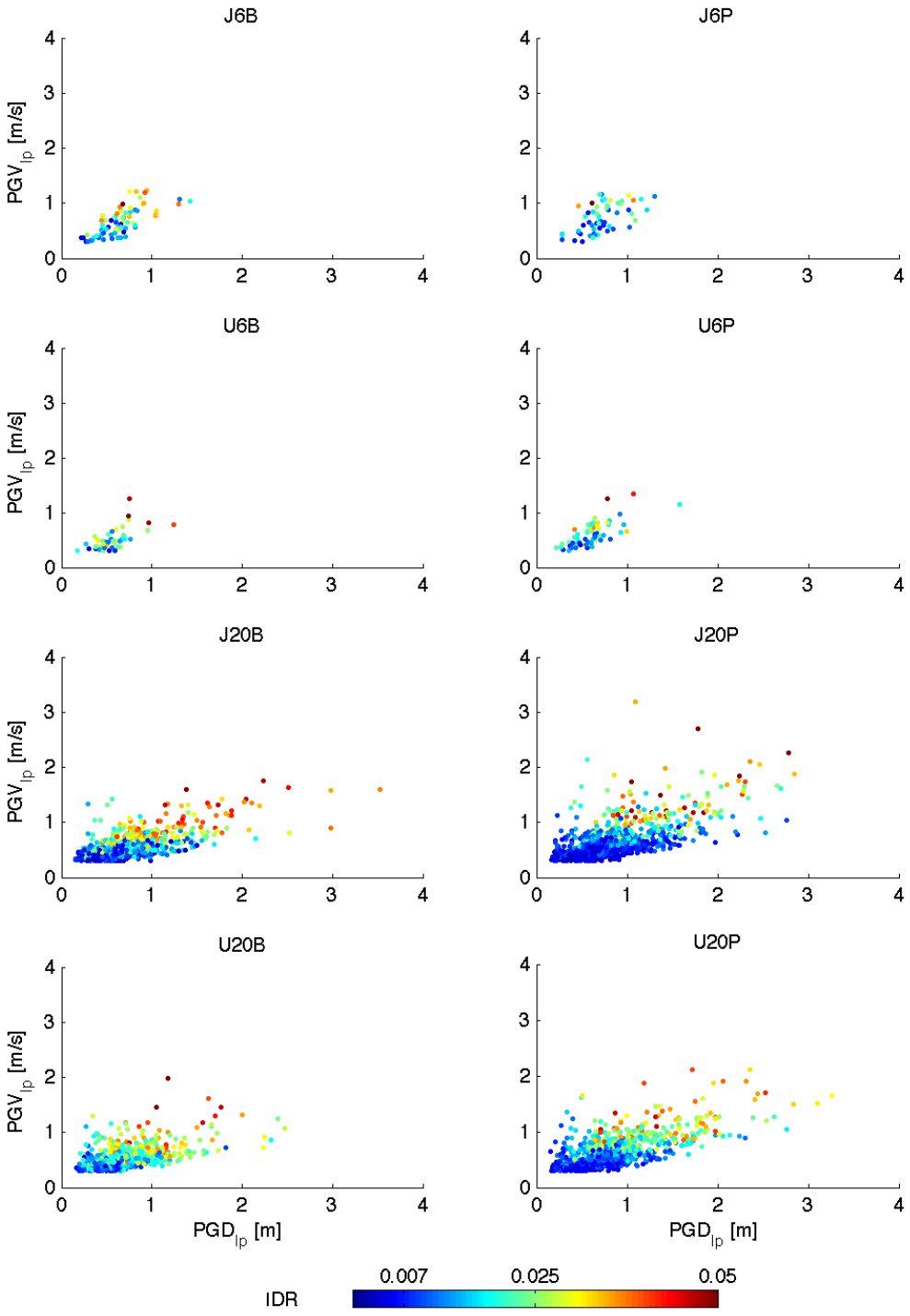

Figure 6.8: This figure locates some of the peak IDR data in the PGD_{lp}-PGV_{lp} plane. The color of the data indicate the peak IDR. The peak IDR data assumes that the building is not a total structural loss.

6.2.2 Theory

Bayesian model class selection is a technique to compare proposed models based on the Bayesian interpretation of probability and statistics. The fundamental distinction between the traditional, or frequentist, and Bayesian approaches is the understanding of probabilistic statements. (See, for example, Gill (2002) or Muto (2006).) A frequentist understands probability as the long-term outcome of repeated trials; a Bayesian understands probability as a degree of belief, or degree of plausibility, which may be different for different observers. For this thesis, an important consequence of the Bayesian approach is the treatment of uncertain model parameters. Traditional model fitting determines values for uncertain model parameters by minimizing the least squares error, and an ad hoc information criterion can be used to compare proposed models. Bayesian model fitting uses a probability density function (PDF) of the uncertain model parameters to represent the plausibility of different parameter value combinations. Analysis of this PDF (that is, its maximum and average values) determines the most probable model among the proposed models based on prior information, or judgement, and available data.

There are two levels of analysis in Bayesian model class selection: (1) determine the most probable values of the uncertain parameters for each proposed model class; and then (2) determine the most probable model class from the proposed model classes. A model class refers to the general structure of a proposed model with N_B uncertain parameters. The uncertain parameters form a N_B-dimensional space (also known as the parameter space). A particular combination of the parameter values defines a particular model in the model class. A PDF in the parameter space quantifies the relative likelihood of each combination of parameter values based on available information. For example, previous studies may suggest a model class, and there is data which can revise, or update, the parameter values. In this case, the PDF quantifies both the prior information and the new data. If there were no previous studies, then the PDF would only quantify the information in the new data. The PDF is used to determine the most probable values of the uncertain parameters, as

well as the most probable model class.

The posterior PDF updates prior information about the uncertain parameter values with information from collected data using Bayes' Theorem. Mathematically, the posterior PDF is proportional to the product of the prior PDF and the likelihood function (Equation 6.1, lines 1 and 2). The prior PDF is a weighting function over the parameter space based on judgement from prior information. For example, a model with negative parameter values may be undefined, and therefore the prior PDF would be zero where the parameter values are negative. In another application, previous studies may recommend certain combinations of parameter values (here the prior PDF may be assigned a higher value), and thus significantly different combinations of parameter values are not expected (here the prior PDF may be assigned a lower value). The likelihood function quantifies the probability of observing the available data set from the model defined by a particular combination of the parameter values (line 3 of Equation 6.1). In other words, assuming only a model defined by a particular combination of parameter values (for example, β_1 for model class $\mathcal{M}_1$), the likelihood function at β_1 is the probability of getting all the available data according to that model. The likelihood function at another combination of parameter values (say, β_2) is the probability of getting the same available data according to this second model in model class $\mathcal{M}_1$. In this way, each model class has an associated posterior PDF constructed from prior information and the available data, through Bayes' Theorem as follows:

$$
\begin{aligned}
\text{Posterior PDF} &\propto \text{(prior PDF)(likelihood function)} \\
p(\beta \,|\, \mathcal{D}, \mathcal{M}) &\propto p(\beta \,|\, \mathcal{M})\, p(\mathcal{D} \,|\, \beta, \mathcal{M}) \\
&\propto p(\beta \,|\, \mathcal{M}) \prod_{i=1}^{N} p(y_i \,|\, x_i, \beta, \mathcal{M}) \qquad (6.1) \\
&\quad \text{(assuming the data are independent and identically distributed)} \\
&\quad \text{where } \beta \text{ is a vector of the uncertain parameters with } N_B \text{ elements,} \\
&\quad \mathcal{D} \text{ is the set of } x_i, y_i \text{ data with } N \text{ elements,}
\end{aligned}
$$

and $\mathcal{M}$ is a proposed model class.

Each posterior PDF is a function over the parameter space, so it can be imagined as a surface over this space. A peak in the posterior PDF at β is caused by a large amount of data well modeled by the proposed model with parameter values of β. This surface can have multiple peaks, and each peak can be narrow or broad depending on the uncertainty in the parameter value. A narrow peak has less uncertainty in the parameter value, whereas a broad peak has more. The parameter values that correspond to the global maximum value of this surface are the most probable combination of parameter values for the proposed model class (Equation 6.2). Thus the most probable values of each proposed model's uncertain parameters can be found by maximizing each posterior PDF with respect to the parameters.

$$\hat{\beta} = \arg \max_{\beta \in B} p(\beta \,|\, \mathcal{D}, \mathcal{M}) \tag{6.2}$$

where $\hat{\beta}$ is the most probable combination of parameter values and B is the parameter space.

Take the linear model class $y(x) = \alpha x + \gamma$, with uncertain parameters α and γ, as an example. The set of all possible values of α and γ form a two-dimensional parameter space for this model class. A previous study suggested $\alpha \approx 6$ and $\gamma \approx 0.1$, and so the prior PDF could be quantified such that α and γ are normally distributed with means of 6 and 0.1, respectively, and variances such that the coefficient of variation is 0.5. Suppose new data is available to update this previous study via Bayes' Theorem. If maximizing the posterior PDF finds $\hat{\alpha} = 7.2$ and $\hat{\gamma} = 0.19$, then $\hat{y}(x) = 7.2x + 0.19$ is the most probable model in the linear model class.

The second level of analysis in Bayesian model class selection is finding the most probable model class among a set of proposed model classes (Beck and Yuen, 2004). Each model class has an associated evidence, which is the integral over the parameter space of the likelihood function weighted by the prior PDF (Equation 6.3). Thus

the evidence can be understood as the weighted average likelihood for the entire model class. It is also the normalizing constant in the definition of the posterior PDF (Equation 6.4; compare to Equation 6.1). Beck and Yuen (2004), Ching et al. (2005), and Muto (2006, Section 2.2) showed that the evidence can be decomposed into two terms that quantify how well the model class fits the data and the information gained from the data. The first term promotes models that predict the data well, whereas the second term promotes models with a simpler structure. The model class should provide a structure consistent with observations, but that structure should not be unnecessarily complex. Using Bayes' Theorem at the model class level, the probability of a model class can be quantified as the model class's evidence divided by the sum of the evidences for all proposed model classes (Equation 6.5), assuming all model classes are equally probable (Beck and Yuen, 2004). Bayesian model class selection compares multiple proposed model classes and selects the simplest model class (that is, extracts the least information from the data) that accounts for the available data.

$$EV_i = \int_B p(\beta_i \,|\, \mathcal{M}_i)\, p(\mathcal{D} \,|\, \beta_i, \mathcal{M}_i)\, d\beta_i \tag{6.3}$$

where $\mathcal{M}_i$ is the i$^{\text{th}}$ proposed model class,

EV_i is the evidence for $\mathcal{M}_i$,

and β_i is the most probable parameter values for $\mathcal{M}_i$.

$$\begin{aligned} \text{Posterior PDF} &= \frac{(\text{prior PDF})(\text{likelihood function})}{\text{evidence}} \\ p(\beta_i \,|\, \mathcal{D}, \mathcal{M}_i) &= \frac{p(\beta_i \,|\, \mathcal{M}_i)\, p(\mathcal{D} \,|\, \beta_i, \mathcal{M}_i)}{\int_B p(\beta_i \,|\, \mathcal{M}_i)\, p(\mathcal{D} \,|\, \beta_i, \mathcal{M}_i)\, d\beta}. \end{aligned} \tag{6.4}$$

$$p(\mathcal{M}_i \,|\, \mathcal{D}) = \frac{EV_i}{\sum_i EV_i}. \tag{6.5}$$

Returning to the previous example of the linear model class, now consider a second model class $y(x) = \delta x^2 + \zeta x + \eta$. Each of these two proposed model classes has an evidence based on prior information and the available data. If the data has a clear curvature in the x-y-plane, then the quadratic model class should be preferred. The evidence of the quadratic model class would be much larger than the evidence of the linear model because a quadratic model fits curved data much better than a linear model. However, if the output data is predominantly linear, the quadratic model class may fit the data slightly better, but the linear model class should be preferred because it extracts less information from the data (one fewer parameter). The evidence for each proposed model class quantifies this trade-off.

There are two practical considerations that apply to this procedure. For computational ease, I minimize the negative of the logarithm of the posterior PDF, which is an equivalent optimization to maximizing the posterior PDF. Also, I apply a Laplace approximation to evaluate the evidence (Equation 6.6). The Laplace approximation idealizes the posterior PDF as a multidimensional Gaussian, which has an integral with a closed form (Beck and Yuen, 2004). Thus, this approximation is best for surfaces with a single peak; the model class is said to be globally identifiable.

$$\begin{aligned} EV &= \int_B p(\beta \,|\, \mathcal{M})\, p(\mathcal{D} \,|\, \beta, \mathcal{M})\, d\beta \\ &\approx (2\pi)^{(N_B+1)/2} p(\mathcal{D} \,|\, \hat{\beta}, \mathcal{M}) \left|\hat{H}\right|^{-1/2} \end{aligned} \tag{6.6}$$

where $\hat{H}$ is the Hessian of the negative of the logarithm of the product of the prior PDF and the likelihood function, evaluated at $\hat{\beta}$.

6.2.3 Application

I apply Bayesian model class selection to two sets of proposed building response models. I select one model to predict collapse given a value of intensity measure; I select a second model to predict whether the building is a total structural loss (including collapse) in a ground motion with a given intensity measurement; and I select a third

model to predict the peak IDR, assuming the building is not a total structural loss in a ground motion with a given intensity measurement. The intensity measure may be a vector quantity. I distinguish between these three building response measures (that is, collapse, total structural loss, and peak IDR) because they categorize or quantify three distinct building responses.

The data suggest forms for the prediction models. Figures 6.9–6.11 plot the building responses as functions of three intensity measures: pseudo-spectral acceleration (PSA), peak ground displacement, and peak ground velocity. PSA may predict building response well because it is commonly used to characterize seismic hazard and building response. Peak ground measures, however, are independent of a particular building and are more broadband measures of strong ground motions. The data suggest that collapse and total structural loss can be modeled with a sigmoidal function of the intensity measures. The peak IDR seems to be a linear function of the considered intensity measures with a log-normal distribution about the expected peak IDR. Figure 6.12 shows the distribution of peak IDR about a line through the data as functions of $\mathrm{PGD}_{\mathrm{lp}}$ and $\mathrm{PGV}_{\mathrm{lp}}$. These distributions appear log-normal in shape.

Equations 6.7 define the four proposed model classes to predict collapse and total structural loss from the ground motion intensity measures. These equations have the functional form of a sigmoid, which is approximately zero for small values of intensity measures and approximately one for large values. The four models consider polynomials of the three intensity measures as well as polynomials of their logarithms. Equations 6.8 define the four model classes to predict peak IDR from the intensity measures. The form of the argument of the exponentials in Equation 6.7 is similar to the form of the models to predict peak IDR.

$$
\begin{aligned}
\mathcal{M}_1\text{: } p(\text{state}) &= \left[1 + \exp\left(-\alpha_0 - \alpha_1 \ln PSA\right)\right]^{-1} \\
\mathcal{M}_2\text{: } p(\text{state}) &= \left[1 + \exp\left(-\alpha_0 - \alpha_1 PGD_{\mathrm{lp}} - \alpha_2 PGV_{\mathrm{lp}} - \alpha_3 PGD_{\mathrm{lp}} PGV_{\mathrm{lp}}\right)\right]^{-1} \\
\mathcal{M}_3\text{: } p(\text{state}) &= \left[1 + \exp\left(-\alpha_0 - \alpha_1 \ln PGD_{\mathrm{lp}} - \alpha_2 \ln PGV_{\mathrm{lp}} - \alpha_3 \ln PGD_{\mathrm{lp}} \ln PGV_{\mathrm{lp}}\right)\right]^{-1}
\end{aligned}
$$

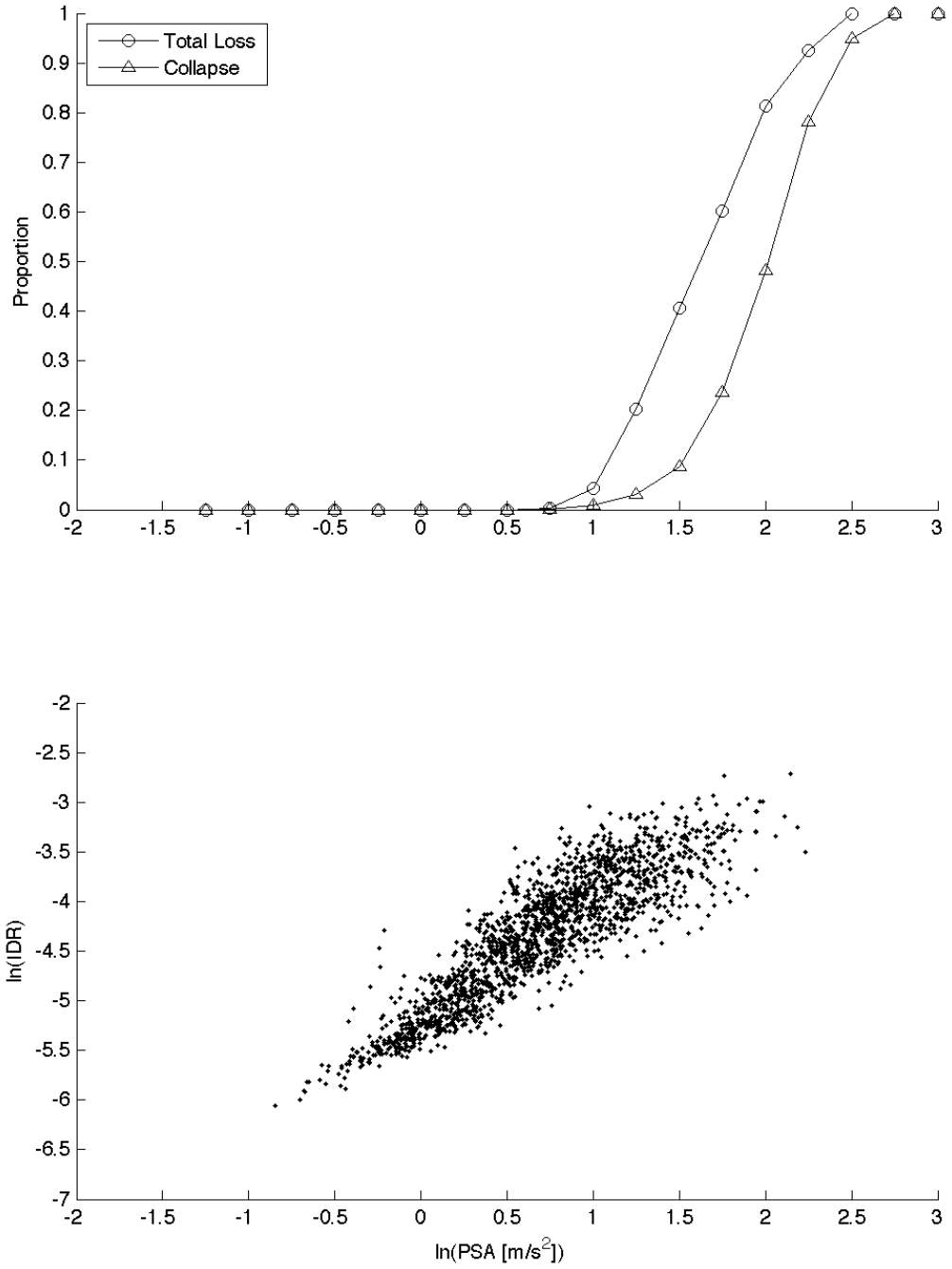

Figure 6.9: The simulation data suggest that PSA may predict building response well. The proportions of total structural loss and collapse appear to smoothly vary from zero to one as a function of log-PSA. The log-peak IDR varies linearly with log-PSA, but the variance about that line generally increases with log-PSA.

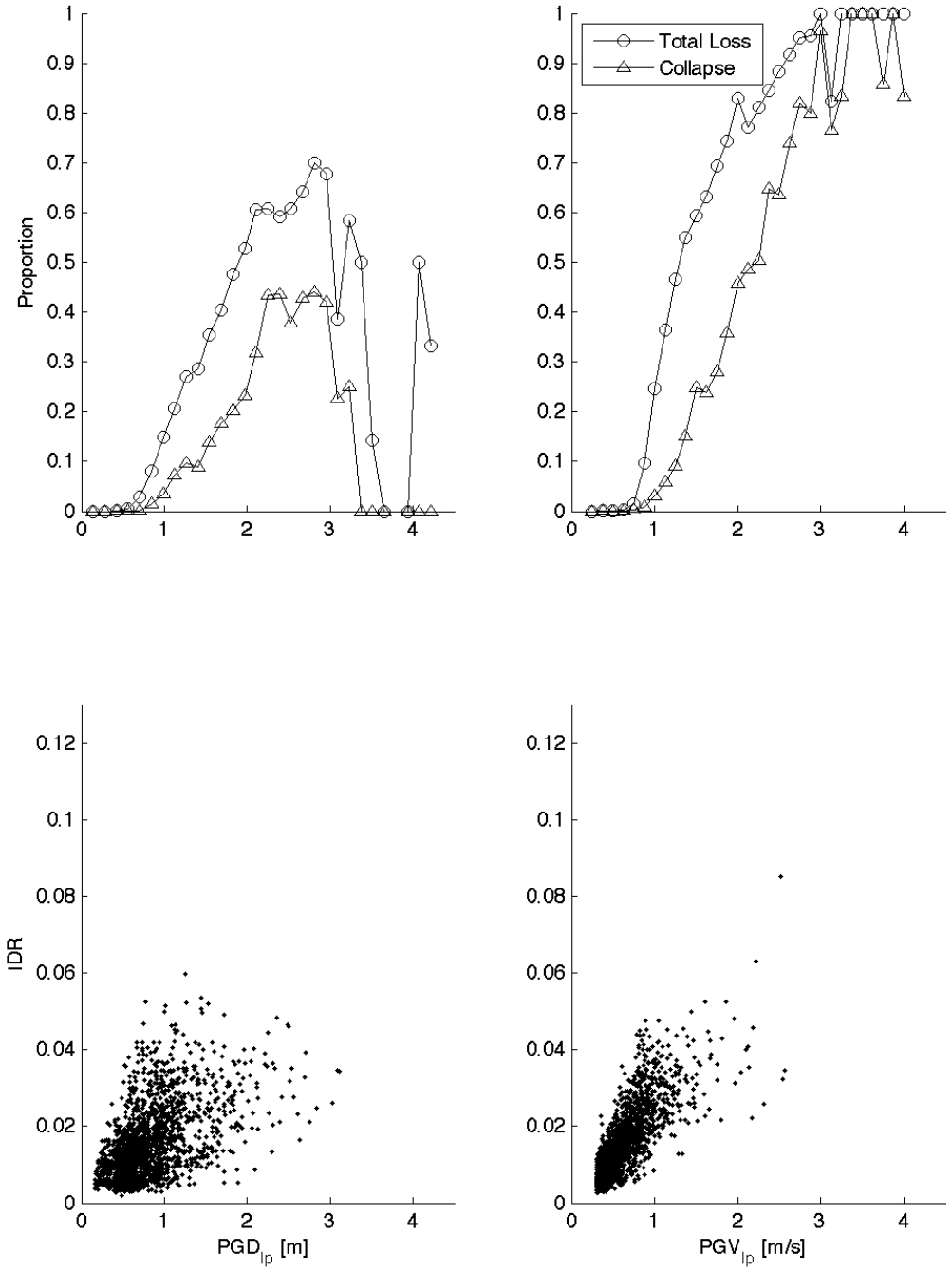

Figure 6.10: This figure projects some of the building response data onto the PGD_{lp}-response and PGV_{lp}-response planes. The proportions of total structural loss and collapse do not vary smoothly for PGD_{lp} greater than 3 m and PGV_{lp} greater than 3 m/s. The data are sparse for such strong ground motions. Peak IDR apparently increases linearly with PGD and PGV, but the variances are large.

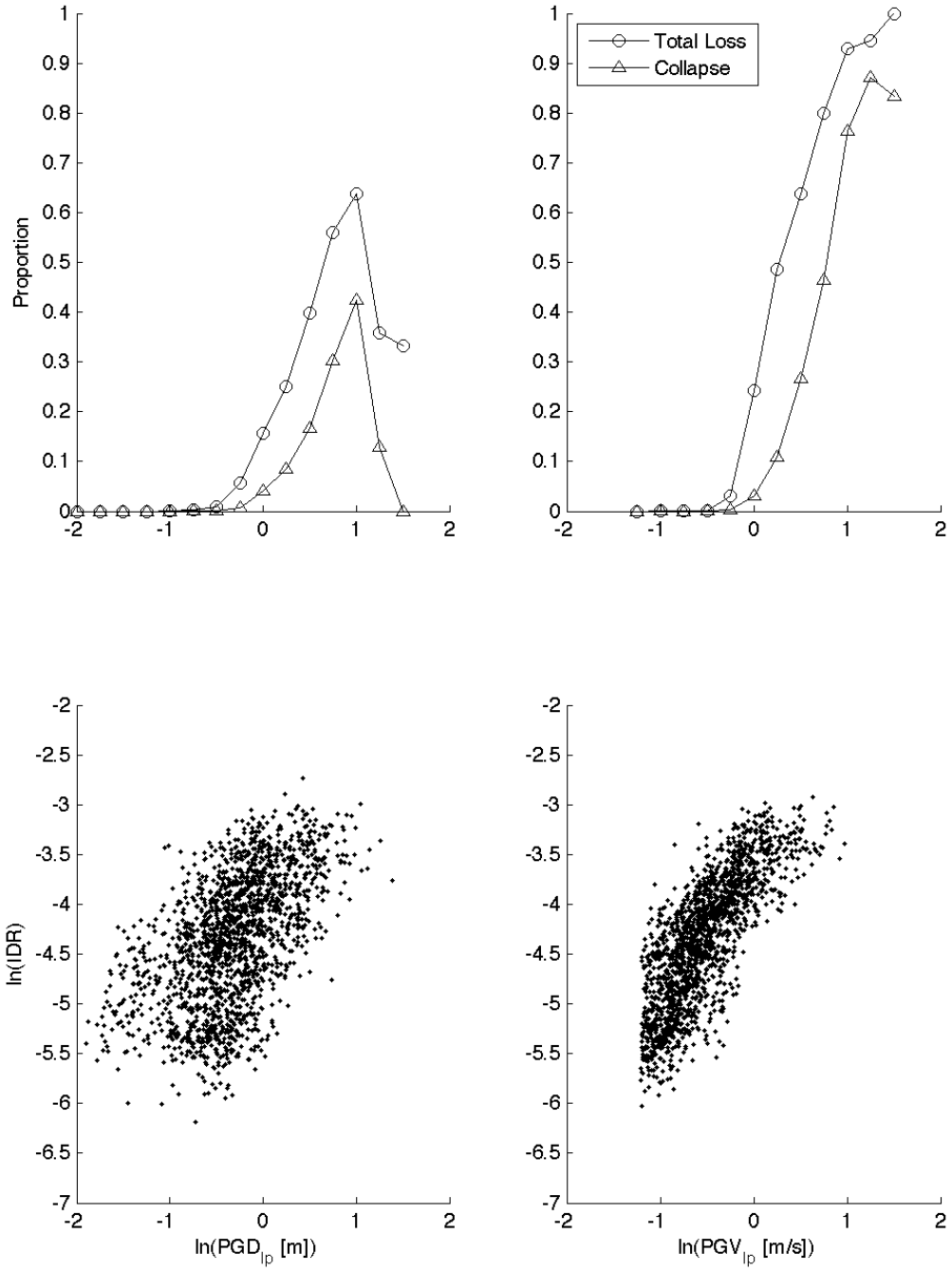

Figure 6.11: This figure shows the building responses as functions of log-PGD_{lp} and log-PGV_{lp}. The proportions of total structural loss and collapse generally increase with log-PGD_{lp} and log-PGV_{lp}. The log-peak IDR varies linearly as a function of log-PGD_{lp} and log-PGV_{lp} with approximately constant variances.

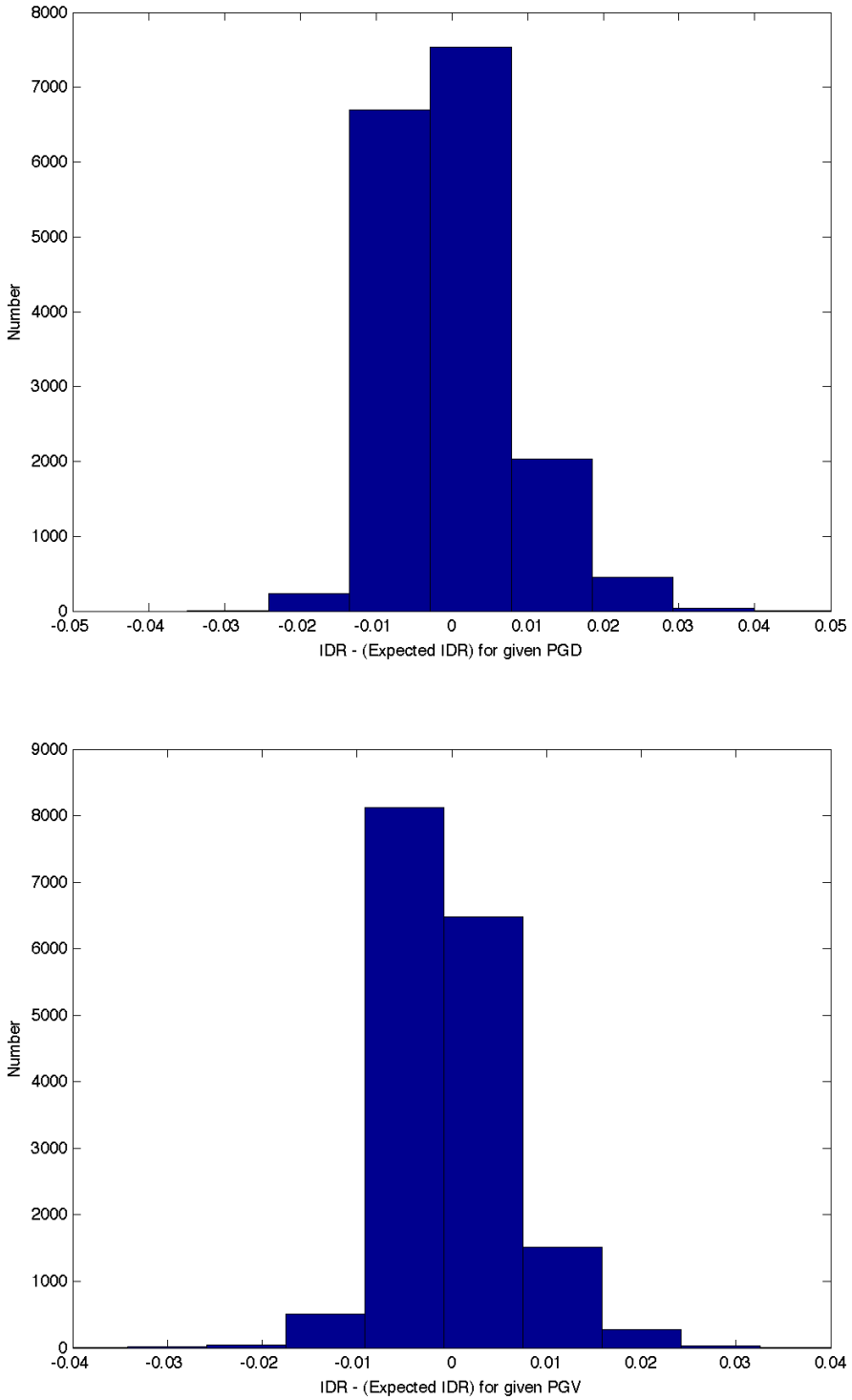

Figure 6.12: The peak IDR prediction models in this thesis predict the median peak IDR as well as a measure of the uncertainty. The data suggest that the distribution of peak IDR about a line through the data (that is, the expected peak IDR) is log-normal for given values of peak ground displacement and velocity.

$$\begin{aligned} \mathcal{M}_4\text{: } p(\text{state}) &= [1 + \exp(-\alpha_0 - \alpha_1 \ln PGV_{\text{lp}})]^{-1} \\ &\quad \text{where state is either collapse or total structural loss} \\ &\quad \text{given a value of intensity measure.} \end{aligned} \tag{6.7}$$

$$\begin{aligned} \mathcal{M}_1\text{: } \ln PeakIDR &= \beta_0 + \beta_1 \ln PSA + \epsilon_1 \\ \mathcal{M}_2\text{: } \ln PeakIDR &= \ln(\beta_1 PGD_{\text{lp}} + \beta_2 PGV_{\text{lp}} + \beta_3 PGD_{\text{lp}} PGV_{\text{lp}}) + \epsilon_2 \\ \mathcal{M}_3\text{: } \ln PeakIDR &= \beta_0 + \beta_1 \ln PGD_{\text{lp}} + \beta_2 \ln PGV_{\text{lp}} + \beta_3 \ln PGD_{\text{lp}} \ln PGV_{\text{lp}} + \epsilon_3 \\ \mathcal{M}_4\text{: } \ln PeakIDR &= \beta_0 + \beta_1 \ln PGV_{\text{lp}} + \epsilon_4 \\ &\quad \text{where the peak IDR assumes the building is repairable} \\ &\quad \text{and } \epsilon_i \sim \mathcal{N}(0, \sigma_i^2). \end{aligned} \tag{6.8}$$

Prior information about the parameter values completes the specification of each model class for Bayesian model class selection. I assume the parameters are independent, and each is normally distributed. I choose a value for the prior mean of each parameter based on the character of the data in Figures 6.9–6.11. I choose a fairly wide, Gaussian distribution about the mean, defined as a coefficient of variation equal to one-third. This definition of prior information does not significantly affect the Bayesian model class selection in this application. The amount of data used in the model class selection contributes significantly more evidence to the model than does the prior definition.

For each of the four building designs with fracture-prone or sound welds, I maximize the posterior PDF for each proposed model in Equations 6.7 and 6.8. Figures 6.13–6.17 show the proposed models with the most likely parameter values plotted with the data. Figures 6.13 and 6.14 show the models based on PSA for collapse, total structural loss, and peak IDR. Note that these figures show the complete models as functions of PSA (unlike the next figures which show contours of the prediction models). Figures 6.15–6.17 present the three models based on PGD_{lp} and PGV_{lp}

for collapse, total structural loss, and peak IDR, respectively. Models 2 and 3 are functions of both PGD_{lp} and PGV_{lp}, making the predicted building response a three-dimensional surface. Model 4 is a function of PGV_{lp} alone. To compare the prediction models, I show the contour where the probability of collapse or total structural loss is 0.3.

Figures 6.15 and 6.16 show that the separating contours (here defined as a 30% probability of collapse or total structural loss) for Models 2–4 are similar where there is available data. Consider the separating contours for the responses of the six-story buildings. Where there is no available data, the separating contours diverge. Model 2 curves toward the origin; the separating contour intersects the abscissa and ordinate. Model 3 curves away from the origin; the separating contour appears to approach the PGD and PGV axes for values of PGD and PGV greater than those considered here. Model 4 is only a function of PGV. For the twenty-story models, the separating contours for Models 2–4 appear similar and almost independent of PGD, suggesting that PGD is not needed in the building response prediction models.

Table 6.1 reports the probabilities for the collapse prediction models. For all building models, collapse prediction Model 1 is the least likely structure for the data. For two building models (J6B and J6P) Model 2 is the most likely collapse prediction model. For two other building models (U6P and U20B) Model 3 is the most likely collapse prediction model. For the remaining four building models (J20B, J20P, U6B, and U20P) Model 4 is the most likely collapse prediction model. No proposed model is consistently most likely to predict collapse.

Table 6.2 reports the probabilities for the total structural loss prediction models. Again, no proposed prediction model is consistently the most likely to predict total structural loss. Model 1 is most likely to predict total structural loss for three buildings: J6P, J20P, and U6P. Model 2 is never the most likely to predict total structural loss. Model 3 is most likely to predict total structural loss in two buildings: U20B and U20P. Model 4 is most likely for three buildings: J6B, J20B, and U6B. The Bayesian model class selection criterion does not consistently select the same functional form for all four building designs and for both weld states.

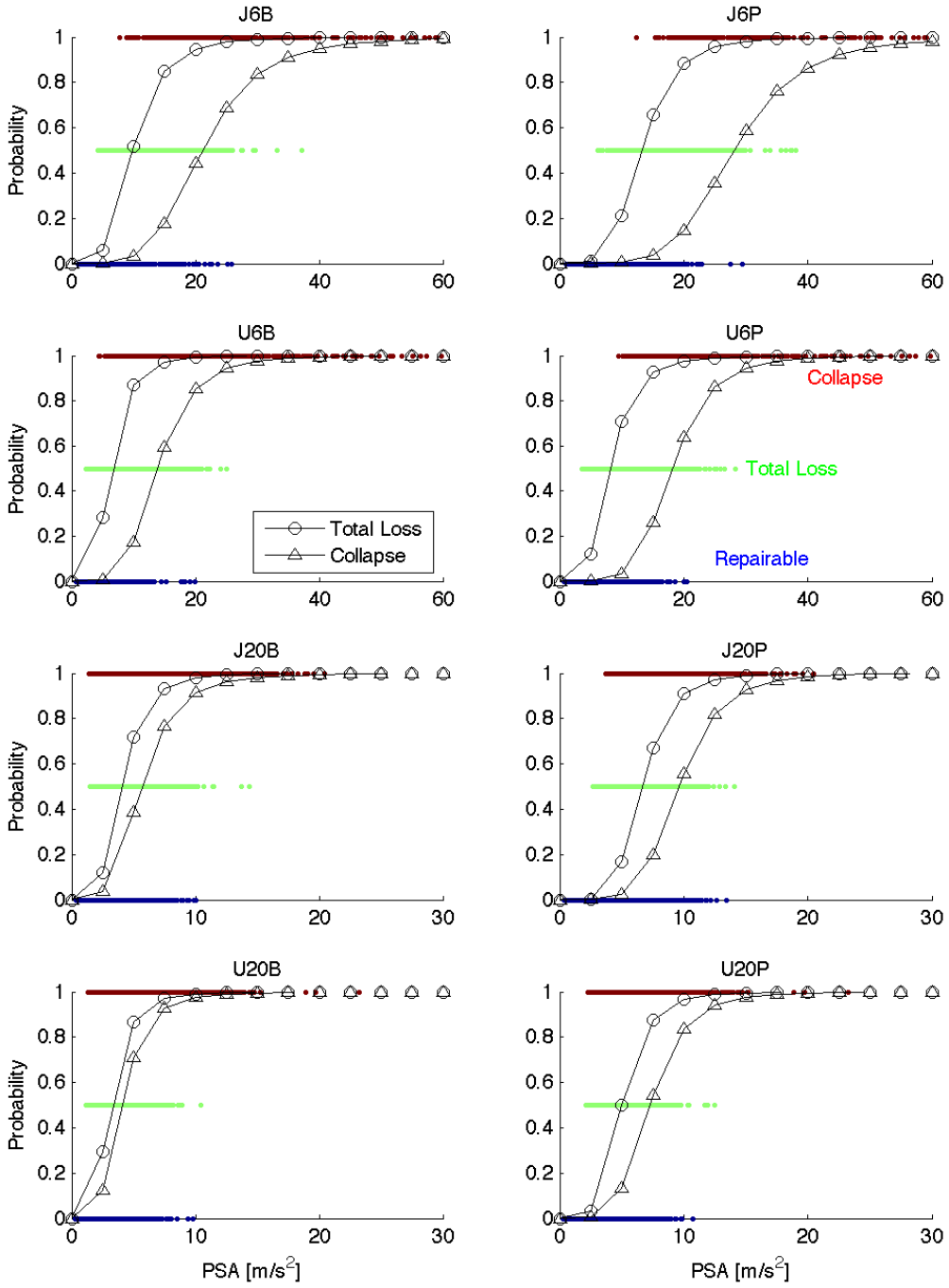

Figure 6.13: This figure locates the collapse, total structural loss, and repairable building response data as functions of PSA. I locate the data at probabilities of 1, 0.5, and 0, respectively, to distinguish what PSAs result in each response and to suggest how well the collapse and total structural loss models distinguish the building states. The black lines with symbols show Model 1 with the most probable parameter values for collapse and total structural loss. For the twenty-story buildings with brittle welds (J20B and U20B), the total structural loss and collapse models are almost the same.

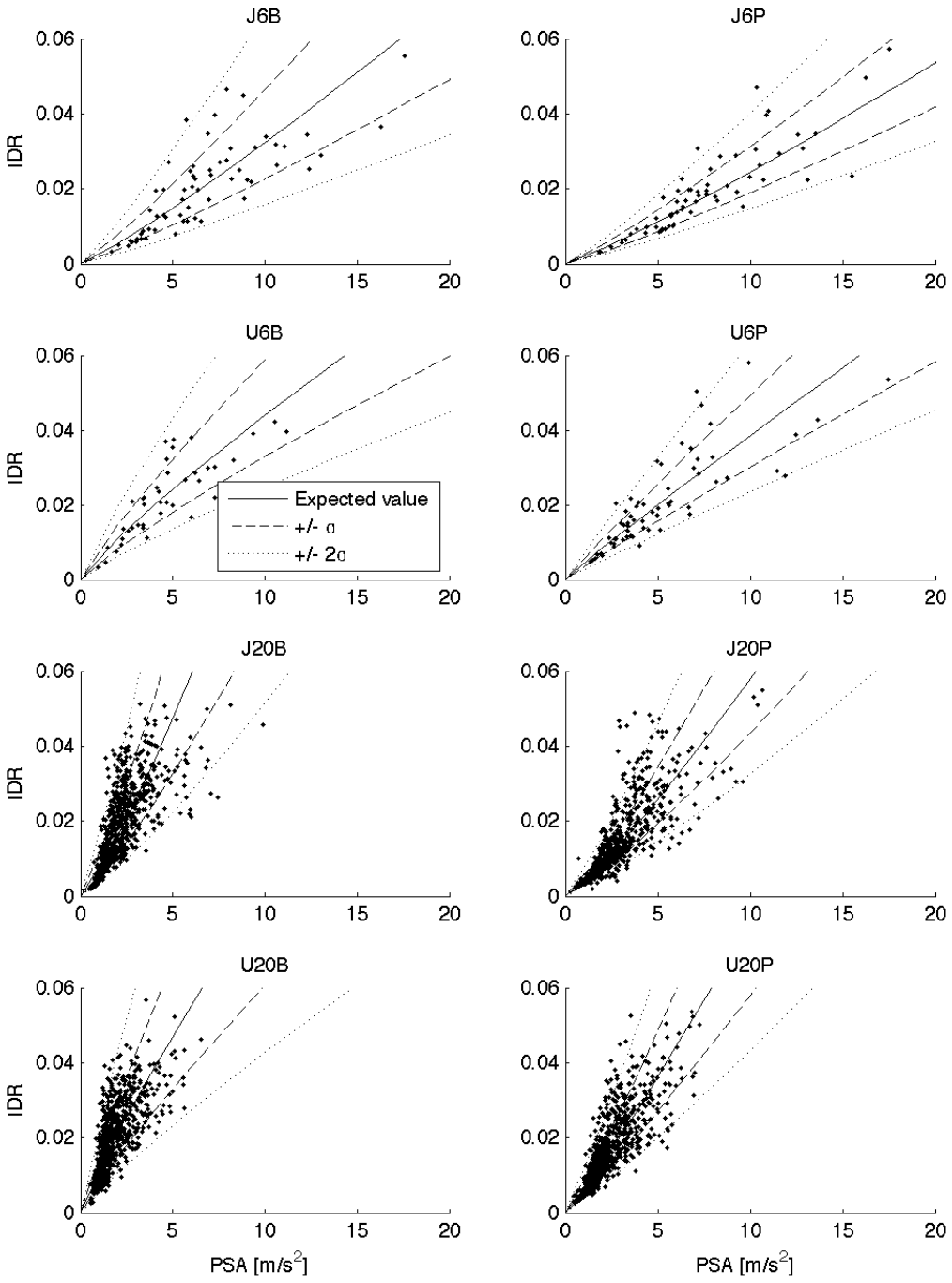

Figure 6.14: This figure shows the peak IDR data as a function of PSA. The lines indicate the prediction models with the most likely parameter values from the maximum posterior PDF analysis.

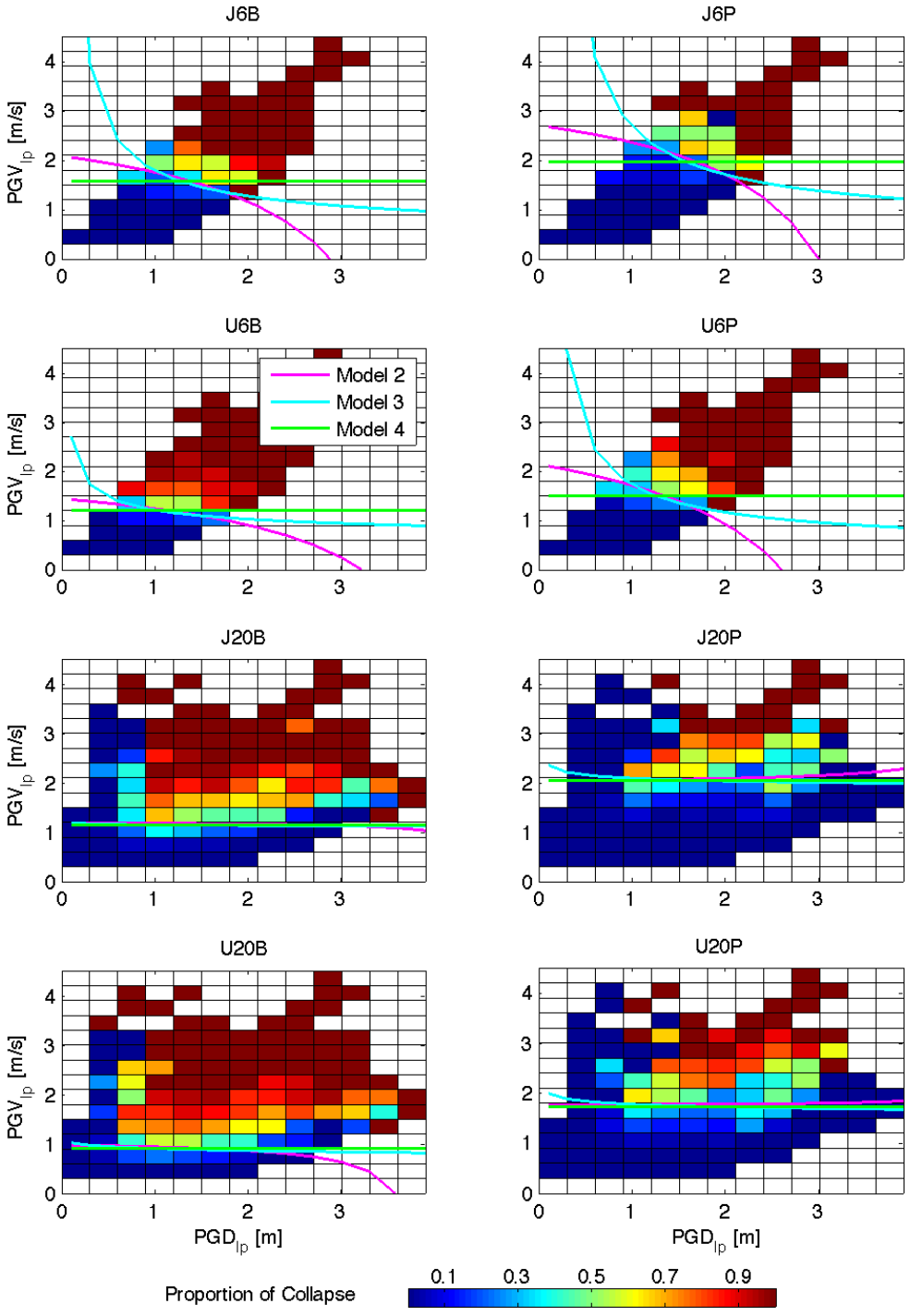

Figure 6.15: This figure compares the collapse prediction models with the most likely parameter values to the data. The contours represent a predicted collapse probability of 0.3 for Models 2–4. Note how similar the predictions of these models are where there is available data.

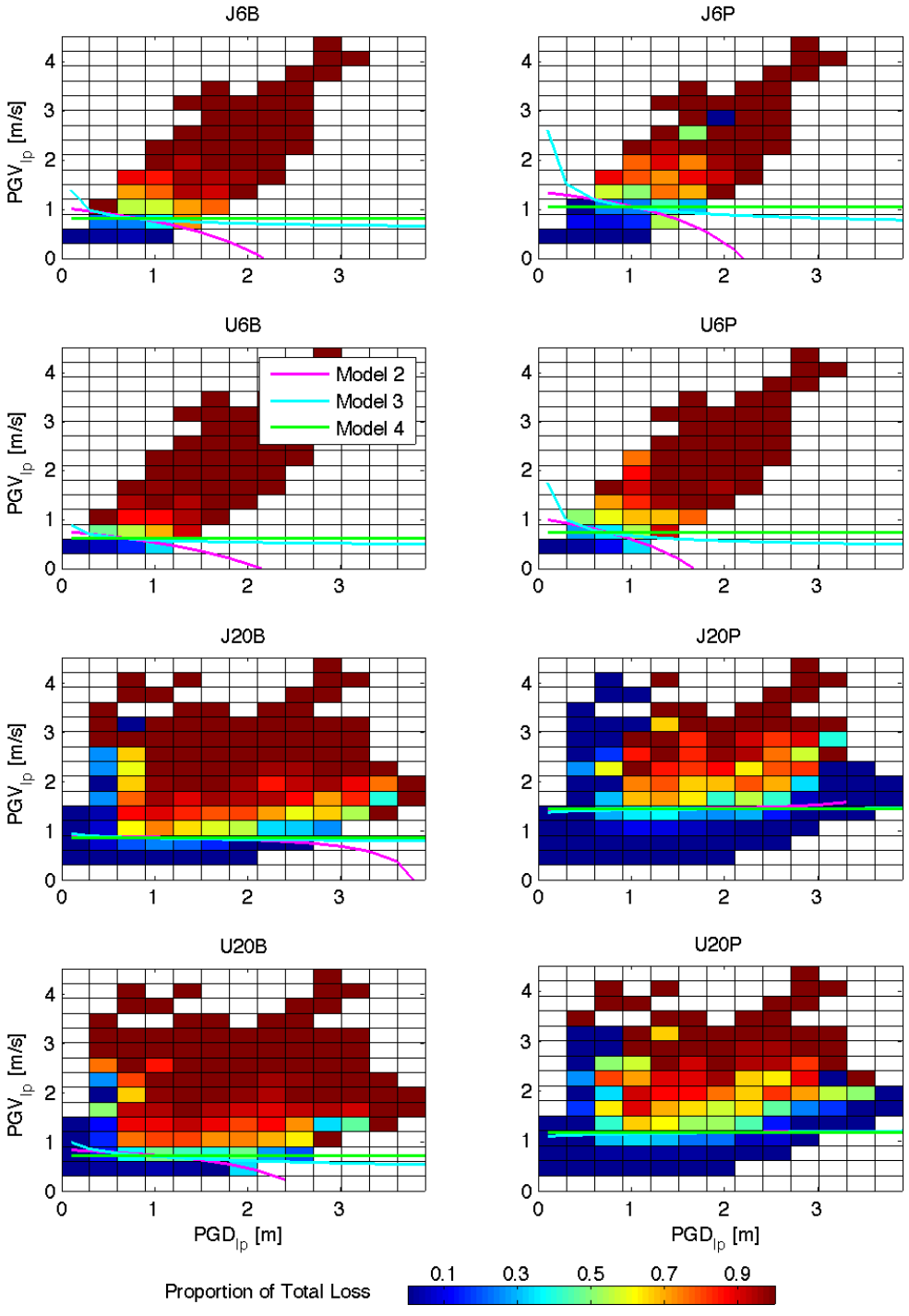

Figure 6.16: This figure compares the total structural loss prediction models with the most likely parameter values to the data. The contours represent a probability of total structural loss of 0.3 for Models 2–4.

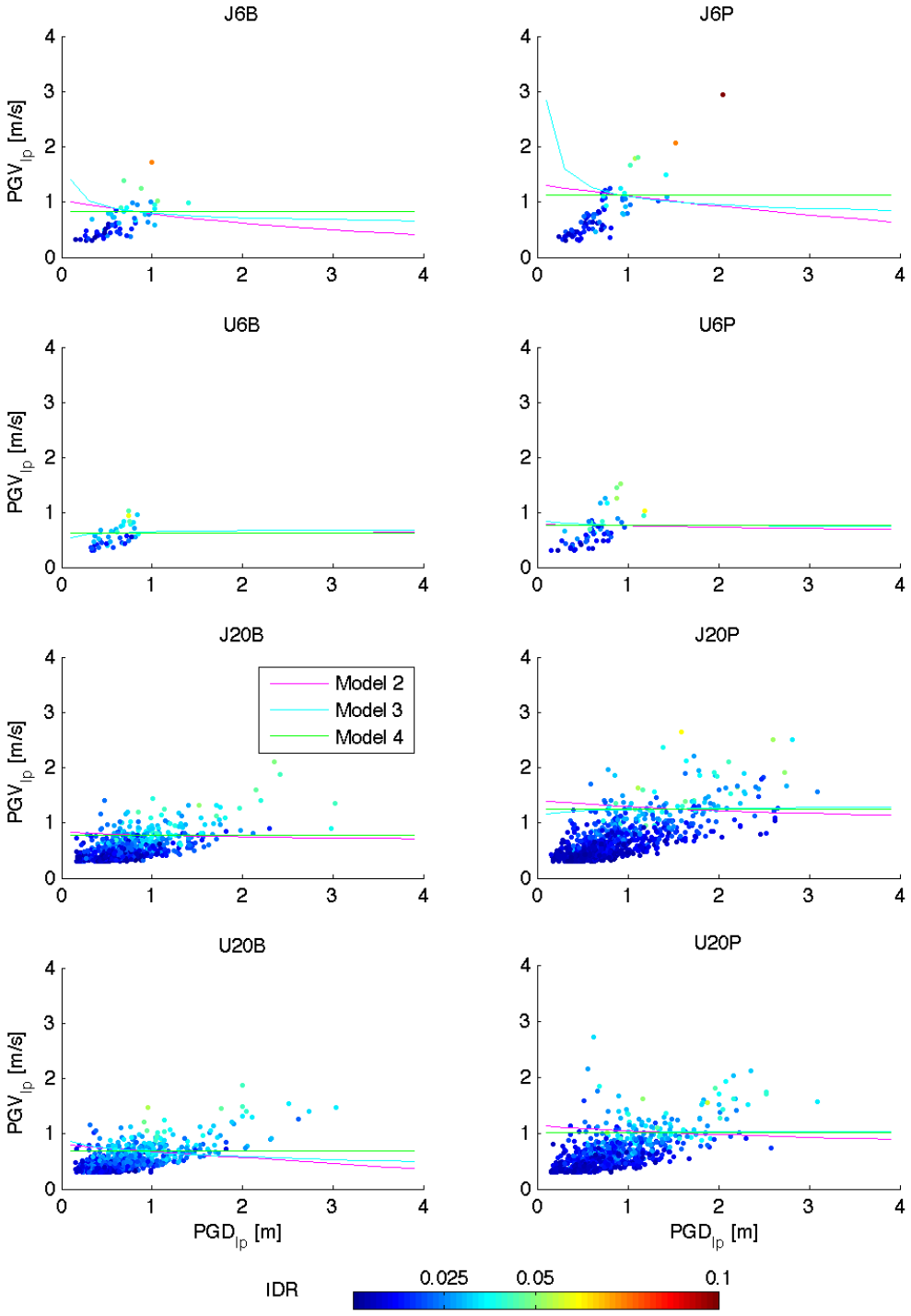

Figure 6.17: This figure compares the peak IDR prediction models with the most likely parameter values to the data. The contours represent a predicted peak IDR of 0.025, the FEMA 356 level for life safety. Again, note the similar predictions where there is available data.

Model	*J6B*	*J6P*	*J20B*	*J20P*
1	0.0	0.0	0.0	0.033
2	**0.92**	**1.0**	0.0	0.0
3	0.077	0.0	0.0	0.0
4	0.0	0.0	**1.0**	**0.97**
Model	*U6B*	*U6P*	*U20B*	*U20P*
1	0.0	0.0	0.0	0.0
2	0.013	0.0027	0.0	0.0
3	0.14	**1.0**	**0.95**	0.0
4	**0.84**	0.0	0.048	**1.0**

Table 6.1: This table reports the probabilities of each proposed collapse prediction model. None of the four proposed models is consistently most likely for all building designs and weld states.

Model	*J6B*	*J6P*	*J20B*	*J20P*
1	0.0	**1.0**	0.0	**1.0**
2	0.0	0.0	0.0	0.0
3	0.25	0.0	0.00051	0.0
4	**0.75**	0.0	**1.0**	0.0
Model	*U6B*	*U6P*	*U20B*	*U20P*
1	0.0	**1.0**	0.0	0.0
2	0.040	0.0	0.0	0.0
3	0.00017	0.0	**1.0**	**1.0**
4	**0.96**	0.0	0.0	0.0

Table 6.2: This table reports the probabilities of the proposed total structural loss models. As with the collapse prediction models, no proposed total structural loss model is consistently best for all building models.

Model	*J6B*	*J6P*	*J20B*	*J20P*
1	1.0	1.0	1.0	1.0
2	0.0	0.0	0.0	0.0
3	0.0	0.0	0.0	0.0
4	0.0	0.0	0.0	0.0
Model	*U6B*	*U6P*	*U20B*	*U20P*
1	1.0	1.0	1.0	1.0
2	0.0	0.0	0.0	0.0
3	0.0	0.0	0.0	0.0
4	0.0	0.0	0.0	0.0

Table 6.3: This table reports the probabilities of the proposed peak inter-story drift ratio prediction models. The prediction model based on pseudo-spectral acceleration is the most likely building response prediction model for all considered buildings.

Table 6.3 reports the model probabilities for the prediction of peak IDR given that the building is not a total structural loss. For all building models, the model based on PSA is most likely to predict peak IDR. This result should not be surprising because PSA filters the ground motion at the fundamental period of each building. Thus PSA is a good characterization of ground motion for mildly to moderately inelastic building responses.

6.2.4 Interpretation

The building response prediction models for a categorical state (that is, collapse or standing and total structural loss or repairable) define a probability that the building assumes a particular state. Ideally a separating curve could be drawn at a value of intensity measure to properly categorize the building states, keeping in mind that the intensity measure could be a vector quantity. For intensity measures below the curve, the buildings do not collapse or are not a total structural loss, and for intensity measures above the curve, the buildings collapse or are a total structural loss. The models in this thesis quantify the probability of the state, rather than drawing a distinct demarcation between the states. Considering the data, a curve is not justified: for a relatively large range of intensity measures, both states are possible simultaneously. Drawing a single line to separate the states would result in a large number of

misclassifications. A better characterization of the states is to provide a probability of the state for a given value of intensity measure.

The most successful categorical model will have the steepest slope separating the states. The ideal model has an infinite slope, corresponding to the clear demarcation between the states. As the slope decreases, the distinction between the states becomes less clear. In the extreme, a large change in the intensity measure causes a small change in the probability of the state. The data in this thesis do not support this characterization: by visual inspection of Figures 6.6, 6.7, and 6.13, there is a narrow band of intensity measure values on which different simulations predict both states. That is, for the same value of intensity measure, the building may collapse or stand or may be a total structural loss or repairable. The Bayesian model class selection procedure implicitly accounts for this consideration, since a model with a slope that is too small will not accurately predict the building state.

Even though a probabilistic statement about the categorical state of a building is more informative, there are times when a line must be drawn, figuratively and literally. The choice of the curve that separates the two states of building response reflects a value judgement. One person may be willing to accept a probability of 0.5 that the building will collapse. A second person may be more cautious and judge a probability of 0.1 as sufficiently risky. For this thesis, I consider a probability of 0.3 to be the separating curve, or separating contour, between collapse and standing and between total structural loss and repairable. I use this separating contour to compare the predictions of the proposed models and to compare the performance of the building models. The choice of a specific probability would not significantly affect the location of the separating contour for models with a steep slope, but it would affect that location for models with shallow slopes.

The most direct way to use the building response prediction models in this thesis is to employ the most likely model according to the metric of Bayesian model class selection. The selection procedure quantifies the probability of each proposed model, and for the proposed models in this thesis, one prediction model is obviously most likely for each building model. To predict the response of a building similar to one of

Collapse Model 3 Parameter Estimates				
Building	α_0	α_1	α_2	α_3
J6B	-4.1	2.6	5.7	0.88
J6P	-5.3	2.4	4.5	0.96
U6B	-2.2	1.6	7.0	0.80
U6P	-3.7	2.8	5.3	0.90
J20B	-1.5	0.092	4.9	-0.076
J20P	-5.0	-0.12	5.6	0.48
U20B	-0.41	0.24	4.4	-0.45
U20P	-3.6	0.11	4.7	0.18

Table 6.4: This table provides the most likely values for the parameters in collapse prediction Model 3.

Total Structural Loss Model 3 Parameter Estimates				
Building	α_0	α_1	α_2	α_3
J6B	0.26	0.86	4.4	0.76
J6P	-0.99	1.0	4.1	0.66
U6B	2.0	1.0	5.2	0.65
U6P	0.72	1.3	3.9	0.61
J20B	0.088	0.23	5.5	-0.16
J20P	-2.9	0.0021	5.8	-0.29
U20B	0.83	0.69	4.7	-0.42
U20P	-1.6	-0.013	5.3	-0.98

Table 6.5: This table lists the most likely values for the parameters in Model 3 to predict whether a building is a total structural loss.

those considered, consult Tables 6.1–6.3 to find the most likely proposed model, and then find the values of the parameters from the tables in Appendix B. This approach ensures that the employed prediction model is more probable than the other four proposed models for the building under consideration.

A single functional form for steel moment frame response prediction is simpler and more intuitive than choosing the most likely model according to a metric. The Bayesian model class selection criterion should inform the decision of which functional form to choose to predict the building response, but there are other considerations as well. The prediction model should be consistent with a physical understanding of the underlying problem. The recommended model may be extrapolated beyond the currently available data, and thus a model consistent with the underlying physical

Peak IDR Model 1 Parameter Values			
Building	β_0	β_1	σ^2
J6B	-6.0	1.1	0.13
J6P	-6.3	1.1	0.062
U6B	-5.1	0.86	0.084
U6P	-5.4	0.95	0.061
J20B	-5.0	1.2	0.14
J20P	-5.5	1.2	0.083
U20B	-4.5	0.87	0.12
U20P	-5.1	1.1	0.087

Table 6.6: This table presents the most likely values of the parameters for the most likely prediction model for peak inter-story drift ratio.

behavior should be preferred. (This is not, however, an endorsement of extrapolation.) The preferred model class should also have a low rate of misclassification.

Model 1 provides some physical insight into the patterns of building response as a function of pseudo-spectral acceleration. Figure 6.13 compares the predictions of Model 1 for total structural loss and collapse. Note the relative locations of the total structural loss and collapse curves for the eight building models. For the six-story buildings, the two curves are relatively far apart: the pseudo-spectral acceleration must increase by 10–15 m/s^2 for a building with perfect welds to go from total structural loss to collapse or increase by 5–10 m/s^2 for a building with brittle welds. The increase in pseudo-spectral acceleration required for a building to go from a total structural loss to collapse is smaller for the twenty-story buildings. For buildings with brittle welds, this increase in pseudo-spectral acceleration is smaller than for buildings with perfect welds. Twenty-story buildings with brittle welds need only a small change in pseudo-spectral acceleration for a total structural loss to become a collapse. Similar statements about the relative performance of the buildings can be made for the peak ground measures, too.

Model 1 is consistently less likely to accurately predict collapse or total structural loss than Models 2–4. Pseudo-spectral acceleration filters the ground motion at the fundamental period of the building. For small ground motions, the building remains elastic, and a spectral characterization of the ground motion accurately predicts build-

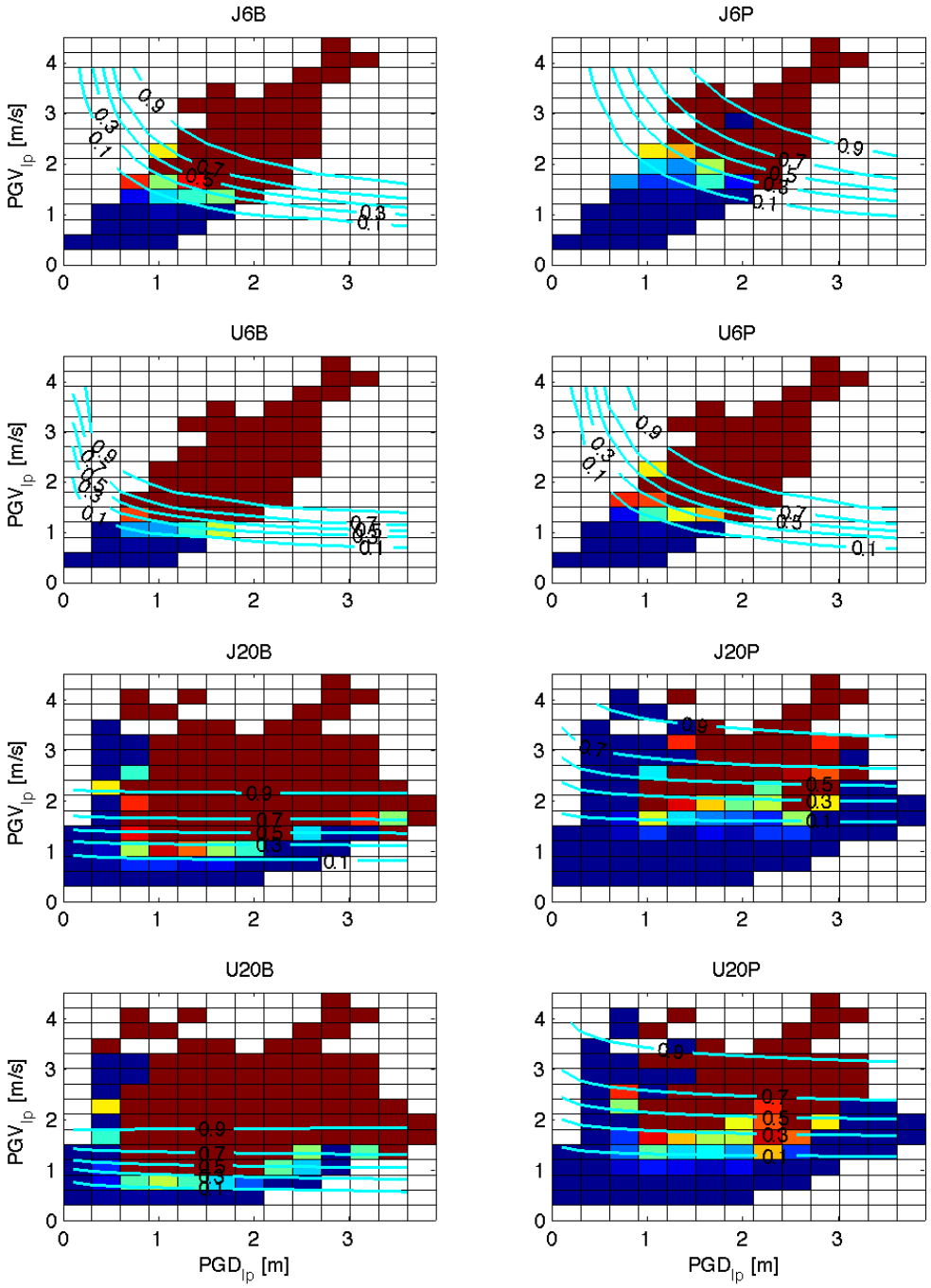

Figure 6.18: This figure compares the contours of Model 3 at 10, 30, 50, 70, and 90% probabilities of collapse to the data. For the six-story buildings (top four subfigures), the contours are close, indicating that the model classifies collapse or standing well. For the twenty-story buildings (bottom four subfigures), the contours are more widely spaced. Also, these contours do not distinguish the twenty-story buildings that do not collapse in peak ground displacements less than 0.6 m.

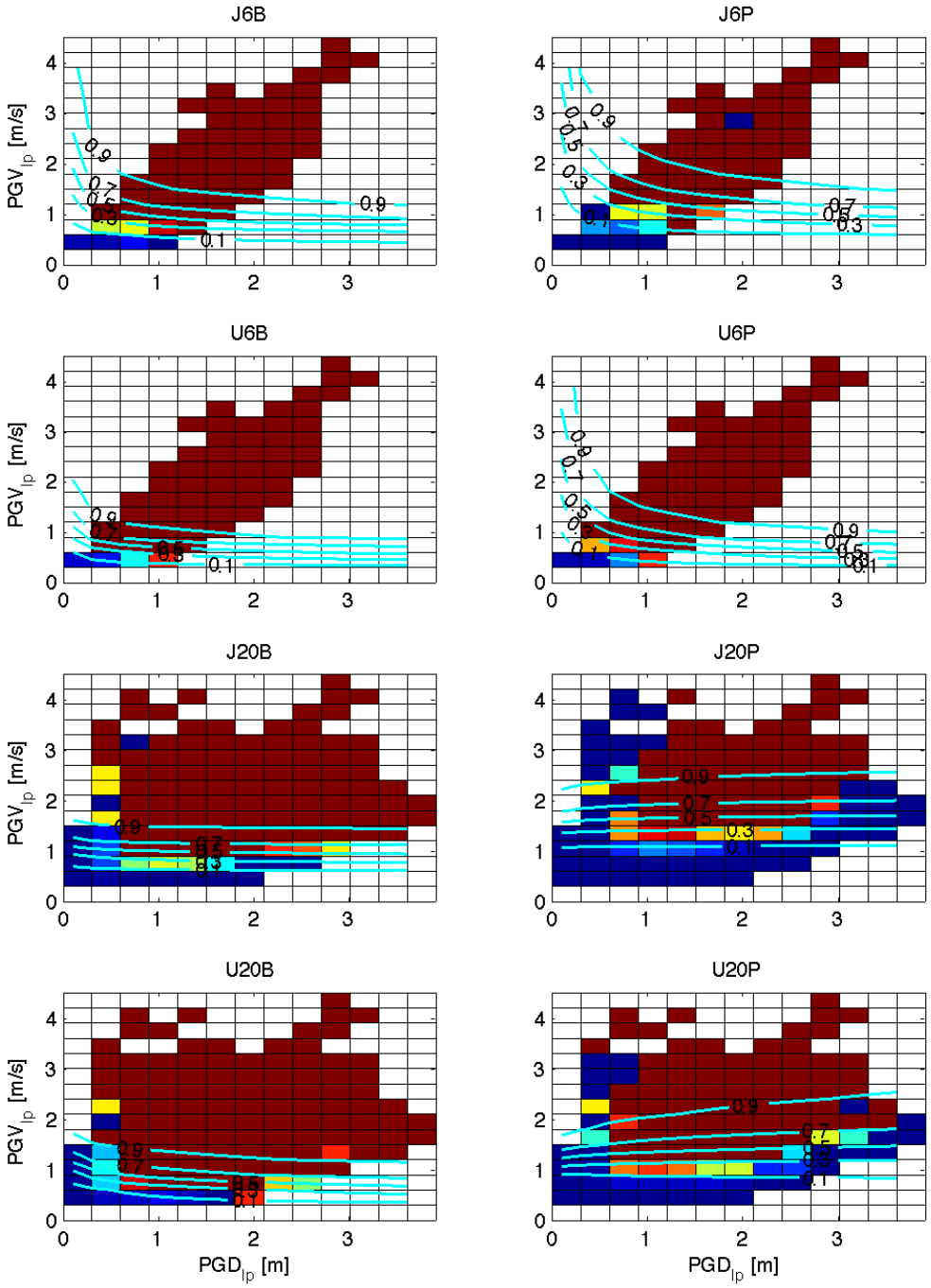

Figure 6.19: Similar to Figure 6.18, this figure compares the contours of Model 3 at 10, 30, 50, 70, and 90% probabilities of total structural loss to the data. This model seems to characterize the data well, even though Bayesian model class selection does not consistently rank it most probable. For some building models, the building response prediction models based on pseudo-spectral acceleration or peak ground velocity alone are more probable than this model, which is a function of both peak ground displacement and velocity.

ing response. In strong ground motions, the building exceeds its yield strength and accumulates damage. The fundamental period of a building accumulating damage lengthens as the building softens. The characterization of the ground motion at the elastic fundamental period does not accurately predict inelastic building response. For severely inelastic building responses, such as total structural loss and collapse, an intensity measure based on a filter with a narrow band of periods does not predict building response as well as a more broadband measure such as the peak ground motion measures.

Models 2–4 tend to be the most likely prediction models for collapse and total structural loss. Section 6.2.3 discusses the curvature of these models in the PGD-PGV plane. Physically, Model 3 better describes steel moment frame response in strong ground motions because it curves away from the origin. Ground motions with a large PGD and a small PGV imply that the ground is slowly moving a large distance. In this type of ground motion, the building would follow the ground motion as an approximately rigid body with only small deformations. High frequencies tend to dominate ground motions with a small PGD and a large PGV. Tall steel moment frames are not significantly affected by short-period ground motions, so the building responses in this type of ground motion would be small. Model 3 describes these physical building responses because it allows low probabilities of collapse or total structural loss for both types of ground motions, unlike Models 2 and 4. This consideration is more important for the six-story building response prediction models since there is less available data to constrain the model, compared to the data for the twenty-story models.

The misclassification of the available data using the prediction models also indicates the predictive power of the categorical models. I use the separating contour where the collapse probability is 0.3 to categorize the available data as collapsed or standing and as total structural loss or repairable. Tables 6.7 and 6.8 list the percentage of the data misclassified by the four models. The model using pseudo-spectral acceleration to predict building response (Model 1) has a higher rate of misclassification compared to the other four models. Among Models 2–4 there are similar rates

Misclassification of Collapse Data [% of Available Data]				
Building	*Model 1*	*Model 2*	*Model 3*	*Model 4*
J6B	9.4	6.3	6.5	7.4
J6P	4.6	3.7	3.9	4.4
U6B	13	8.1	8.3	8.5
U6P	8.8	7.0	7.5	7.8
J20B	10.	9.2	9.5	9.5
J20P	2.9	2.7	2.8	2.9
U20B	14	13	13	13
U20P	4.8	4.7	4.9	4.9

Table 6.7: I use the proposed prediction models to classify the available data as collapsed or standing. Model 1 misclassifies collapse data more often than Models 2–4.

Misclassification of Total Structural Loss Data [% of Available Data]				
Building	*Model 1*	*Model 2*	*Model 3*	*Model 4*
J6B	18	18	19	19
J6P	14	16	16	17
U6B	16	15	15	15
U6P	17	19	19	19
J20B	15	11	11	11
J20P	6.0	5.8	6.0	6.0
U20B	19	15	15	15
U20P	9.9	8.8	8.9	8.8

Table 6.8: Similar to Table 6.7, I use the proposed models to categorize the available data as total structural loss or repairable. The rate of misclassification is much larger for the total structural loss models than for the collapse models.

of misclassification.

Of the four proposed building response prediction models of the categorical states, I prefer Model 3. Bayesian model class selection recommends it for several building types. The functional form of the model is consistent with a physical understanding of the response of tall steel moment frames in strong ground motions, and there is a low rate of misclassification. However, depending on the specific application, Model 2 or 4 may be useful to predict collapse or total structural loss responses.

Model 1 should be preferred to predict the peak inter-story drift ratio, assuming that the building is not a total structural loss in a given ground motion. The probability of this model is consistently 1 using the Bayesian model class selection criterion.

Pseudo-spectral acceleration is also widely used in the earthquake engineering community to characterize seismic risk and building response. The interpretation of building response as a function of spectral quantities has a sound physical explanation.

The building response prediction models developed in this chapter predict the same relative building performance as seen in the data. Figure 6.20 compares the collapse separating contours for the four building designs with perfect or brittle welds. The stiffer, higher-strength designs have separating contours that vary with both PGD and PGV. The more flexible, lower-strength designs, however, are almost independent of PGD. According to these prediction models, a ground motion with large PGV but small PGD would collapse the more flexible, and not the stiffer, design. A ground motion with large PGD but small PGV tends to collapse the buildings with stiffer designs and not those with more flexible designs. The six-story buildings require larger ground motions than the twenty-story buildings to collapse. The presence of brittle welds shifts the separating contours to smaller combinations of peak ground motion responses. The effect of brittle welds on the stiffer designs is less distinct for large PGD.

Figure 6.21 shows the total structural loss separating contours for the four building designs with perfect and brittle welds. The prediction models show that the probability of total structural loss depends on PGD only for ground motions with PGD_{lp} less than 1 m. The six- and twenty-story, more flexible designs with perfect welds would be deemed total structural losses in ground motions with PGV_{lp} greater than approximately 1.5 m/s and 1.2 m/s, respectively. The other considered building models would likely be total structural losses in ground motions with PGV_{lp} greater than 0.5–1 m/s.

Figure 6.22 compares the relative performance of the steel moment frame buildings assuming they are repairable following an earthquake. As expected, the stiffer, higher-strength designs have lower peak IDR compared to the more flexible, lower-strength designs for the same PSA. The six-story designs have lower peak IDR compared to the equivalent twenty-story designs, and the presence of brittle welds increases the expected peak IDR.

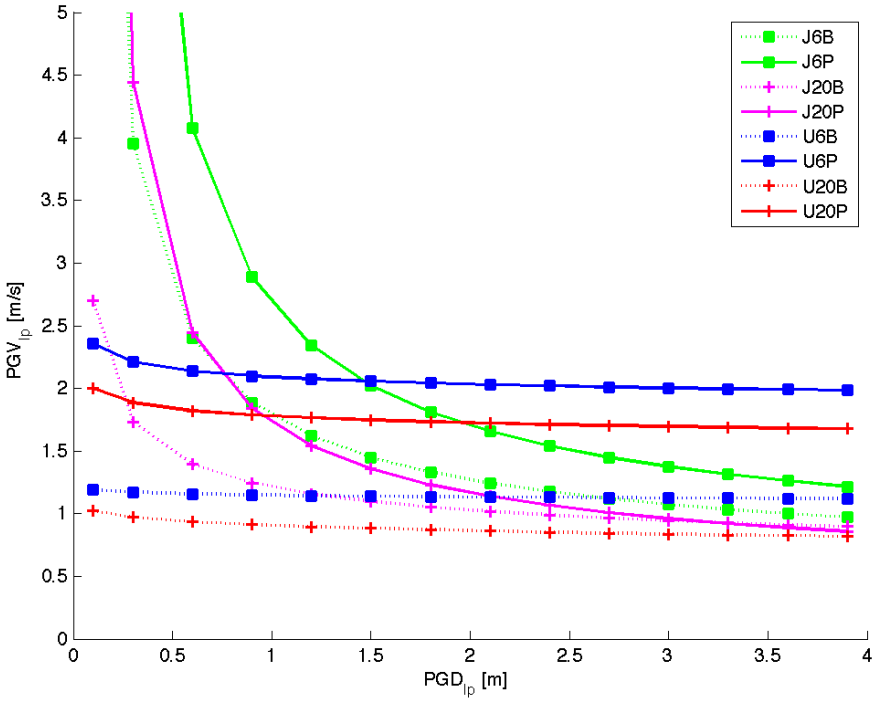

Figure 6.20: This figure shows the collapse separating contours (30% probability of collapse) as functions of peak ground displacement and velocity for the four building designs with brittle or perfect welds. The presence of brittle welds significantly increases the probability of collapse. The stiffness and strength of the building design changes the shape of the separating contour. A six-story building is less likely to collapse in a given ground motion than a twenty-story building.

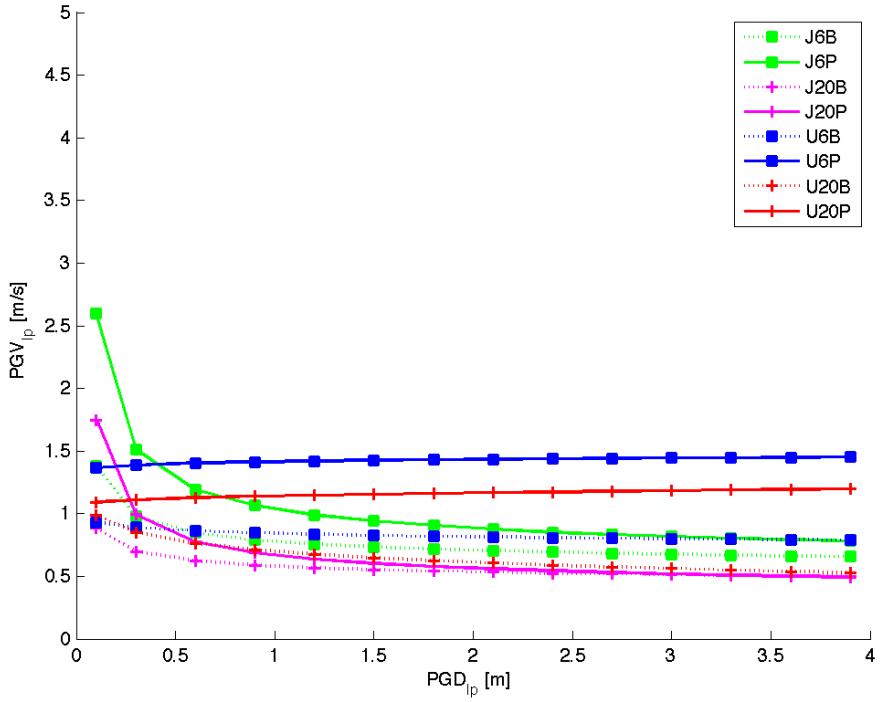

Figure 6.21: This figure shows the total structural loss separating contours (30% probability of total structural loss) as functions of peak ground displacement and velocity. The probability of total structural loss is mostly independent of PGD, and only somewhat dependent on PGV for small PGD. The separating contours of the more flexible, lower-strength designs of twenty and six stories are at approximately 1 and 1.5 m/s, respectively. The separating contours for the other considered designs and for buildings with brittle welds are mostly between 0.5 and 1 m/s.

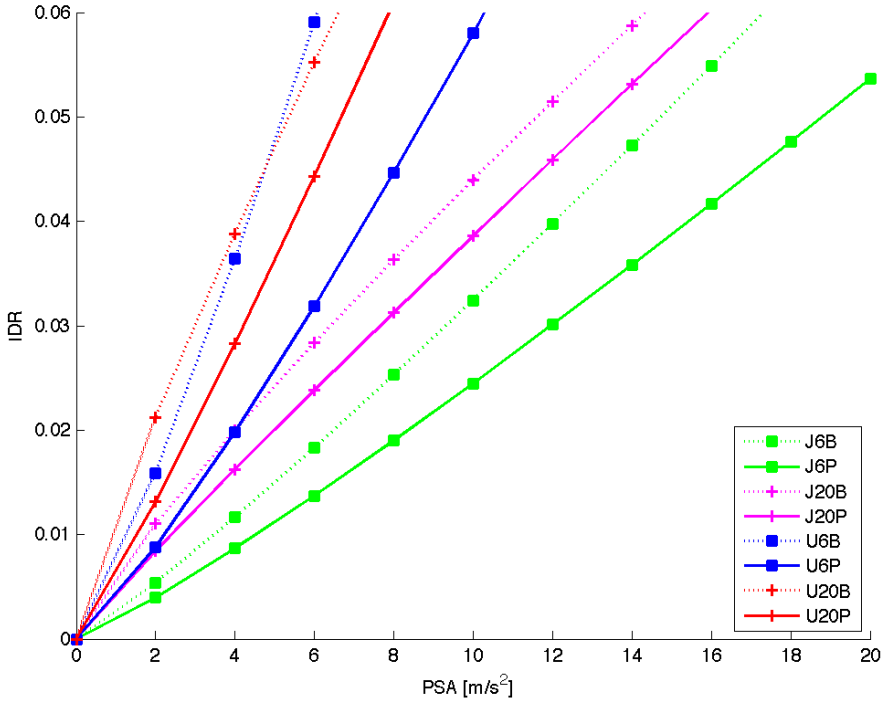

Figure 6.22: Pseudo-spectral acceleration best predicts the peak inter-story drift ratio, assuming that the building is not a total structural loss. The expected peak inter-story drift ratio in buildings with stiffer designs is smaller than the expectation for more flexible designs. Six-story buildings have smaller peak inter-story drifts than the similarly designed twenty-story buildings. The presence of brittle welds increases the expected peak inter-story drift ratio.

Recall that the building response prediction models developed in this chapter are based on simulated data. These prediction models have not been validated against the experiences of steel moment frames in historic earthquakes. Validating these models would require knowing the ground motion—or at least the intensity measure—at each steel moment frame that was subjected to strong ground motions. One result of this thesis is to anticipate the building response in ground motions not previously experienced in modern urban areas. Thus it may not be possible to validate these prediction models with available data from historic earthquakes.

Chapter 7

Discussion and Conclusions

7.1 Discussion

Experience from historic earthquakes provides evidence for seismic building response. Some classes of buildings are known to be unsafe because they have performed poorly in the past. Unreinforced masonry buildings crumbled in the 1906 San Francisco earthquake. The 1971 San Fernando earthquake exposed the problem of non-ductile concrete frames. Long-period resonance in the sedimentary basin under Mexico City significantly damaged many, and collapsed some, mid-rise buildings in 1985. The 1994 Northridge earthquake demonstrated the widespread problem of steel moment-resisting frames with brittle welds. These and other experiences motivated immediate study and eventual changes to the building code.

Computational and experimental models allow engineers to study building behavior from a physical understanding. Models are an efficient way to study various building systems in the absence of documented real-world behavior. An engineer can propose several designs and test each to provide a client with the best of all considered designs. Researchers generate new models to explain observed building behavior or predict future building response to seismic ground motions. Structural modeling provides an explanation for observed building behavior and helps to anticipate future problems.

7.1.1 Simulations as Proxies for Experience

This thesis anticipates what might be learned about steel moment frames in the next large earthquake near a major urban center. Simulations provide this next large earthquake in the form of ground motions on regional simulation domains. By applying these tens of thousands of ground motions to models of steel moment frames, this thesis predicts what may happen to this class of buildings in future earthquakes. This study can only account for known building behavior; it cannot anticipate unknown problems. However, based on the current best understanding of steel moment frame physics and ground motions from large earthquakes, this study provides important lessons before the next devastating earthquake.

To make accurate predictions of future building behavior, simulated ground motions should be consistent with recorded ground motions. The simulated ground motions used in this thesis have time histories consistent with recorded ones. However, there are some inconsistencies between the peak ground velocities (PGVs) of these simulated ground motions and the PGVs of ground motion prediction equations (GMPEs). For near-source sites in earthquakes of magnitudes between 6.3 and 6.8, the PGV of the simulated ground motions does not saturate as predicted by GMPEs. Also, for distant sites in earthquakes of magnitudes 7.7 and 7.8, the variance of PGV from simulated ground motions is larger than that defined in GMPEs. These inconsistencies do not affect the building response prediction equations developed in this thesis because I disregard magnitude and distance information for the simulated ground motions in the building response prediction models. Resolving these differences in PGV as a function of magnitude and distance between simulated and recorded ground motions may be of interest to the seismological community.

7.1.2 "Lessons Learned"

Fracture-prone welds significantly degrade a building's lateral force-resisting capacity. In the same ground motion, a steel MRF with brittle welds is 2–8 times more likely to collapse than the same building with sound welds. If the buildings remain standing,

the peak inter-story drift ratio (IDR) of the building with brittle welds is likely 1.7 times the peak IDR of the perfect weld building. The design considerations of building height and the combination of strength and stiffness do not affect building response as significantly as the state of the welded connections. The results and predictive models in this thesis quantify the problem of brittle welds. A building owner contemplating a retrofit can better estimate the benefits of improved building performance due to fixing brittle welds.

This thesis also considers the seismic responses of shorter and taller steel moment frames. Properly designed and constructed short (as represented by six stories) and tall (as represented by twenty stories) buildings are approximately equally likely to collapse in the same strong ground motion. If both buildings with sound welds remain standing, the six-story building develops a peak IDR 1.3–1.6 times the peak IDR in a twenty-story building, depending on the stiffness and strength of the design. However, twenty-story buildings with brittle welds are up to five times more likely to collapse than six-story buildings with brittle welds, depending on the ground motion. If both buildings with brittle welds remain standing, the peak IDR of the six-story building is 1.2–1.4 times that of the twenty-story building, depending on the stiffness and strength of the design.

Taking a more philosophical point of view, consider brittle welds not as a known problem but rather as exemplary of an unknown problem. The problem of brittle welds was not widely known before the 1994 Northridge earthquake. If this study had been performed in 1994, there would have been no consideration of the brittle weld problem. The conclusion at the time would have been unqualified: shorter and taller buildings are approximately equally likely to collapse, and if they remain standing, six-story buildings develop larger peak IDRs. Today there is almost certainly an unknown problem with tall buildings. Considering the experience of historic earthquakes, it is inevitable that there are presently unknown problems. Newer systems are more likely to have unknown problems simply because previously unknown problems of older systems became known problems through experience. Taller buildings are less robust against these unknown problems; they are inherently more unstable than shorter

buildings, so a design or construction flaw is more likely to catastrophically weaken a taller building compared to a shorter building. A taller building is riskier than a shorter building in an uncertain world.

The stiffness and strength of a building design affects building response, albeit less significantly than do weld state or building height. A more flexible, lower-strength design is 1–4 times more likely to collapse in strong ground motions than a stiffer, higher-strength design, depending on the ground motion. If both designs remain standing in a ground motions, the stiffer, higher-strength design develops a smaller peak IDR than does the more flexible, lower-strength design, as expected.

A great earthquake is literally and figuratively an order of magnitude larger than a large earthquake. The areal extent of large building responses to the simulated earthquakes in this thesis is qualitatively different for large and great earthquakes. Compare the building responses in the 1989 Loma Prieta (Figure 3.4) and 1906 San Francisco (Figure 3.6) earthquakes, for example. Inelastic building responses dominate the simulation domain in the three magnitude 7.8 simulations, whereas the area of inelastic building response in the magnitude 6.9 simulations is much smaller. Specifics of the assumed slip model and rupture propagation alter the ground motions, and thus the building responses, at a particular site. However, the regional extent of large building responses remains similar for similar magnitude simulations.

7.1.3 Building Response Prediction Models

The building response prediction models developed in this thesis succinctly characterize the simulated steel moment frame response data. The prediction models quantify in a probabilistic sense the seismic response as collapse, total structural loss, and if repairable, the peak inter-story drift ratio. As observed in the simulation data, the presence of brittle welds increases the probability of collapse; buildings with brittle welds tend to collapse in smaller ground motions. Applying the prediction models where there is little available data, the shape of the collapse separating contours are different for the stiffer, higher-strength designs versus the more flexible, lower-strength

designs. For ground motions with small peak ground displacement (PGD) and large peak ground velocity (PGV), the stiffer designs are less likely to collapse, whereas for ground motions with large PGD and small PGV, the more flexible designs are less likely to collapse. At a given intensity measure, a six-story building is less likely to collapse than a twenty-story building. Also, for most ground motions, the more flexible designs with either building height and perfect welds are less likely to be a total structural loss than the other considered buildings.

Different intensity measures are more appropriate for predicting different building responses. Pseudo-spectral acceleration (PSA) unquestionably best predicts the peak inter-story drift ratio if the building is not a total structural loss in a particular ground motion. Not surprisingly, for elastic and mildly inelastic building response, PSA accurately characterizes the response. To predict total structural loss, however, PGD and PGV do as well as PSA, and to predict collapse, PGD and PGV are superior to PSA. As the building deformations become more severe, the character of the building changes, and the information from a spectral quantity no longer applies to a damaged building. More broadband intensity measures, such as PGD and PGV, better characterize the ground motion for steel moment frame collapse and total structural loss.

The intended use of the collapse, total structural loss, and peak inter-story drift prediction models is in series: for a given ground motion, predict the probability of collapse and total structural loss; and then, assuming that the building is repairable, predict the peak inter-story drift ratio. In this way, these models predict the state of a steel moment frame building, explicitly acknowledging the possible collapse and total structural loss responses which are often overlooked. These prediction models have not been validated with the experience of steel moment frames in historic earthquakes. Data from 2,000 (six-story buildings) and 20,000 (twenty-story buildings) simulations of steel frame building response support these prediction models.

These building response predicition models can be used in conjunction with seismic hazard, damage, and loss analyses to probabilistically characterize the full performance of steel moment frames in seismically active areas. For example, they could be

used for a simplified structural analysis in the modular procedure for performance-based earthquake engineering presented in Goulet et al. (2007). Also, a building owner contemplating the replacement of fracture-prone welds with sound welds can quantify the reduced probability of collapse or total structural loss of the building. At an initial design stage, engineers can compare the relative performance of different building heights and designs with different strength and stiffness combinations for the seismic hazard at the proposed site. These building response prediction models should not replace full nonlinear time history analyses of buildings when such detailed analyses are warranted.

7.2 Conclusions

- The presence of fracture-prone welds in a steel moment frame significantly degrades the seismic response. Steel moment frames with brittle welds collapse in weaker ground motions than do moment frames with sound welds. For the same ground motion, fixing brittle welds reduces the probability of collapse by a factor of 2–6 and reduces the median peak inter-story drift ratio by a factor of 0.59.

- In general, properly designed and constructed shorter steel moment frames are slightly less likely to collapse than taller buildings in a given strong ground motion. If the buildings remain standing, then the six-story building develops larger peak inter-story drifts. Taller buildings are less robust to flaws such as brittle welds: a taller building with brittle welds is 2–4 times more likely to collapse compared to a shorter building with brittle welds.

- The stiffness and strength of a steel moment frame design affect seismic response less than welds state and building height do. A more flexible, lower-strength design is 1–4 times more likely to collapse compared to a stiffer, higher-strength design. As expected, if the designs remain standing, the median peak inter-story drift ratio in the stiffer design is 0.75 times that of the more flexible design.

- The experience of a large earthquake (magnitude between 7.0 and 7.5) does not predict the experience of a great earthquake (magnitude greater than 7.5).

- Building response prediction models can estimate probabilistically the likelihood of collapse and total structural loss, as well as peak inter-story drift ratio (assuming the building is repairable) of steel moment frames. I recommend Model 3 in Equation 6.7 to predict the collapse and total structural loss states. Model 1 in Equation 6.8 should be used to predict the peak inter-story drift ratio, assuming the building is repairable. These prediction models can be incorporated into broader studies of damage and loss for this class of buildings in seismically active areas.

- For steel moment frames, a combination of peak ground displacement and peak ground velocity predicts the likelihood of collapse better than pseudo-spectral acceleration. PSA predicts total structural loss equally well as PGD and PGV. Assuming the building is not a total structural loss, however, PSA predicts the peak inter-story drift ratio better than a combination of PGD and PGV.

- Future engineering studies would benefit from a resolution of the differences between simulated ground motions and ground motion prediction equations. For magnitudes between 6.3 and 6.8, this thesis shows that the long-period peak ground velocities of the simulated ground motions considered here are larger than those expected by ground motion prediction equations.

Appendix A

Beam and Column Schedules

Columns

C3	W14X99	C6	W24X84	C9	W14X74
C2	W14X132	C5	W27X114	C8	W14X74
C1	W14X159	C4	W27X161	C7	W14X132

Girders		Beams		Foundations		Slabs	
G3	W24X55	B1	W24X55	F1	150-2.5	S1	1160-7.6
G2	W24X76			F2	153-2.5	S2	2090-7.6
G1	W24X94			F3	161-2.5		
		Walls		F4	247-2.5		
		W1	61 cm thk				

| foundations: K_H-D_{YH} where K_H = horizontal stiffness (tons/cm) and D_{YH} = yield displacement for horizontal (cm). For vertical: $K_V = K_H$, $D_{YD} = D_{YH}$ (down) and $D_{YU} = D_{YH}/2$ (up).
| slabs: A_{10}-h_{10} where A_{10} = effective area (cm^2) and h_{10} = distance from top of girder/beam to centroid of slab (cm).

Figure A.1: U6 Beam and Column Schedule. Reproduced from Hall (1997)

Columns

C3	W14X120	C6	W24X104
C2	W14X176	C5	W27X178
C1	W14X211	C4	W30X211

Girders		Beams		Foundations		Slabs	
G3	W24X84	B1	W24X55	F1	199-2.5	S1	1160-7.6
G2	W27X102			F2	199-2.5	S2	2090-7.6
G1	W30X124			F3	199-2.5		
		Walls		F4	247-2.5		
				F5	199-2.5		
		W1	61 cm thk	F6	247-2.5		

| foundations: K_H-D_{YH} where K_H = horizontal stiffness (tons/cm) and D_{YH} = yield displacement for horizontal (cm). For vertical: $K_V = K_H$, $D_{YD} = D_{YH}$ (down) and $D_{YU} = D_{YH}/2$ (up).
| slabs: A_{10}-h_{10} where A_{10} = effective area (cm^2) and h_{10} = distance from top of girder/beam to centroid of slab (cm).

Figure A.2: J6 Beam and Column Schedule. Reproduced from Hall (1997)

Columns

C10	W14X109	C20	W21X122	C30	W14X74
C9	W14X132	C19	W24X146	C29	W14X74
C8	W14X159	C18	W24X146	C28	W14X82
C7	W14X176	C17	W24X162	C27	W14X109
C6	W14X211	C16	W24X176	C26	W14X132
C5	W14X257	C15	W24X176	C25	W14X159
C4	W14X283	C14	W27X178	C24	W14X193
C3	W14X311	C13	W27X178	C23	W14X211
C2	W14X342	C12	W27X178	C22	W14X233
C1	W14X370	C11	W30X191	C21	W14X283

Girders		Beams		Foundations		Slabs	
G10	W27X84	B1	W21X50	F1	468-2.5	S1	1160-7.6
G9	W27X94			F2	336-2.5	S2	2090-7.6
G8	W30X99			F3	353-2.5		
G7	W30X108		Walls	F4	534-2.5		
G6	W30X116						
G5	W30X116	W1	61 cm thk				
G4	W30X116						
G3	W30X116						
G2	W30X116						
G1	W30X116						

foundations: K_H-D_{YH} where K_H = horizontal stiffness (tons/cm) and D_{YH} = yield displacement for horizontal (cm). For vertical: $K_V = K_H$, $D_{YD} = D_{YH}$ (down) and $D_{YU} = D_{YH}/2$ (up).

slabs: A_{10}-h_{10} where A_{10} = effective area (cm^2) and h_{10} = distance from top of girder/beam to centroid of slab (cm).

Figure A.3: U20 Beam and Column Schedule. Reproduced from Hall (1997)

Columns

C10	W14X109	C20	W21X122	C30	W21X122
C9	W14X132	C19	W24X146	C29	W24X146
C8	W14X159	C18	W24X162	C28	W24X162
C7	W14X176	C17	W24X176	C27	W27X178
C6	W14X211	C16	W27X178	C26	W30X191
C5	W14X257	C15	W27X178	C25	W30X211
C4	W14X283	C14	W30X191	C24	W30X235
C3	W14X311	C13	W30X191	C23	W30X261
C2	W14X342	C12	W30X211	C22	W30X292
C1	W14X370	C11	W30X235	C21	W30X292

Girders		Beams		Foundations		Slabs	
G10	W27X84	B1	W21X50	F1	468-2.5	S1	1160-7.6
G9	W27X102			F2	336-2.5	S2	2090-7.6
G8	W30X108			F3	353-2.5		
G7	W30X116	Walls		F4	534-2.5		
G6	W30X124						
G5	W30X132	W1	61 cm thk				
G4	W30X132						
G3	W30X132						
G2	W30X132						
G1	W30X132						

foundations: K_H-D_{YH} where K_H = horizontal stiffness (tons/cm) and D_{YH} = yield displacement for horizontal (cm). For vertical: $K_V = K_H$, $D_{YD} = D_{YH}$ (down) and $D_{YU} = D_{YH}/2$ (up).
slabs: A_{10}-h_{10} where A_{10} = effective area (cm^2) and h_{10} = distance from top of girder/beam to centroid of slab (cm).

Figure A.4: J20 Beam and Column Schedule. Reproduced from Hall (1997)

Appendix B

Parameter Values for Building Response Prediction Models

Building	α_0	α_1
J6B	-13.8981	4.5647
J6P	-17.3565	5.2063
U6B	-12.6149	4.8026
U6P	-16.2975	5.6305
J20B	-7.0129	4.0649
J20P	-12.9018	5.7055
U20B	-5.7308	4.1158
U20P	-9.9853	5.0448

Table B.1: Collapse Prediction Model 1 Parameter Values

Building	α_0	α_1	α_2	α_3
J6B	-14.1268	4.5944	6.3764	-1.4251
J6P	-15.8686	5.0122	5.567	-1.3208
U6B	-12.2557	3.5358	7.9055	-1.5656
U6P	-13.0851	4.6856	5.7154	-1.3132
J20B	-7.9504	1.5484	5.9786	-1.269
J20P	-10.9504	1.8709	4.9608	-0.95595
U20B	-7.3563	1.8157	6.642	-1.6564
U20P	-9.1289	1.7062	4.676	-0.97268

Table B.2: Collapse Prediction Model 2 Parameter Values

Building	α_0	α_1	α_2	α_3
J6B	-4.1347	2.5639	5.6936	0.87725
J6P	-5.3053	2.4328	4.5461	0.95854
U6B	-2.2026	1.647	7.0295	0.80455
U6P	-3.7288	2.8481	5.3092	0.89557
J20B	-1.5128	0.09216	4.8507	-0.075789
J20P	-4.9742	-0.11738	5.5992	0.47816
U20B	-0.4146	0.24178	4.4301	-0.45459
U20P	-3.5582	0.11023	4.7065	0.18378

Table B.3: Collapse Prediction Model 3 Parameter Values

Building	α_0	α_1
J6B	-4.6156	8.3926
J6P	-5.9971	7.5651
U6B	-2.4834	8.7822
U6P	-4.0757	7.8837
J20B	-1.5119	4.9178
J20P	-5.1287	6.0111
U20B	-0.42514	4.6164
U20P	-3.5577	4.9053

Table B.4: Collapse Prediction Model 4 Parameter Values

Building	α_0	α_1
J6B	-9.3457	4.0855
J6P	-12.5107	4.8573
U6B	-7.5787	4.1261
U6P	-8.6433	4.1359
J20B	-5.8643	4.2238
J20P	-10.7328	5.676
U20B	-4.4971	3.9596
U20P	-7.7667	4.828

Table B.5: Total Structural Loss Prediction Model 1 Parameter Values

Building	α_0	α_1	α_2	α_3
J6B	-6.7548	2.7145	5.7626	-1.5201
J6P	-7.8295	3.1617	5.1603	-1.5469
U6B	-6.9945	2.8625	8.0309	-1.8572
U6P	-6.467	3.3422	5.4862	-1.6938
J20B	-8.4202	1.9819	8.5133	-2.0369
J20P	-10.2929	2.2802	6.6464	-1.6433
U20B	-7.8503	2.6738	8.3734	-2.3943
U20P	-9.1823	2.2497	7.1271	-1.9313

Table B.6: Total Structural Loss Prediction Model 2 Parameter Values

Building	α_0	α_1	α_2	α_3
J6B	0.26232	0.85857	4.4082	0.75626
J6P	-0.99461	1.0247	4.1312	0.6551
U6B	1.9577	1.0225	5.1668	0.6486
U6P	0.72386	1.2857	3.8893	0.6063
J20B	0.088395	0.22919	5.4783	-0.15528
J20P	-2.86	0.0021268	5.7967	-0.29115
U20B	0.83382	0.69224	4.6958	-0.42055
U20P	-1.5508	-0.013309	5.3367	-0.97901

Table B.7: Total Structural Loss Prediction Model 3 Parameter Values

Building	α_0	α_1
J6B	0.21926	4.8912
J6P	-1.0657	4.9242
U6B	1.8839	5.6889
U6P	0.61411	4.6249
J20B	0.10757	5.6793
J20P	-2.8891	5.7171
U20B	0.89319	5.2686
U20P	-1.63	5.0824

Table B.8: Total Structural Loss Prediction Model 4 Parameter Values

Building	β_0	β_1	σ_1^2
J6B	-6.0027	1.1181	0.12821
J6P	-6.3171	1.1324	0.062353
U6B	-5.1041	0.86007	0.083564
U6P	-5.4306	0.94544	0.060581
J20B	-4.9716	1.1962	0.14049
J20P	-5.5475	1.1729	0.0828
U20B	-4.4545	0.86974	0.12281
U20P	-5.1004	1.1072	0.086538

Table B.9: IDR Prediction Model 1 Parameter Values

Building	β_1	β_2	β_3	σ_2^2
J6B	0.0014688	0.024175	0.0056618	0.25576
J6P	0.002293	0.018916	0.0015644	0.21324
U6B	-0.0022285	0.040543	0.0032437	0.15208
U6P	-0.00066393	0.032036	0.0020584	0.14791
J20B	-0.0076289	0.029818	0.011979	0.26426
J20P	-0.0042281	0.017802	0.0047692	0.16918
U20B	0.0032245	0.031332	0.00059847	0.17011
U20P	-0.0031545	0.022054	0.0050911	0.15753

Table B.10: IDR Prediction Model 2 Parameter Values

Building	β_0	β_1	β_2	β_3	σ_3^2
J6B	-3.4522	0.20738	1.0567	0.15098	0.256
J6P	-3.7841	0.20922	0.95957	0.1761	0.21313
U6B	-3.1691	0.034795	1.1951	0.20948	0.15083
U6P	-3.3927	0.079362	1.1248	0.20223	0.14711
J20B	-3.3758	-0.016413	1.2768	-0.06432	0.26507
J20P	-3.9761	-0.037192	1.3317	0.014034	0.16927
U20B	-3.3533	0.076216	0.82062	-0.14245	0.16672
U20P	-3.7075	-0.00071213	1.1407	-0.11191	0.15523

Table B.11: IDR Prediction Model 3 Parameter Values

Building	β_0	β_1	σ_4^2
J6B	-3.4987	1.0595	0.25605
J6P	-3.8089	0.98168	0.2142
U6B	-3.2275	0.98107	0.15226
U6P	-3.4234	0.99531	0.14779
J20B	-3.371	1.31	0.26537
J20P	-3.9802	1.2935	0.16959
U20B	-3.3262	0.99188	0.1722
U20P	-3.7083	1.2042	0.1566

Table B.12: IDR Prediction Model 4 Parameter Values

Bibliography

Aagaard, B. T., T. M. Brocher, D. Dolenc, D. Dreger, R. W. Graves, S. Harmsen, S. Hartzell, S. Larsen, K. McCandless, S. Nilsson, N. A. Petersson, A. Rodgers, B. Sjögreen, and M. L. Zoback (2008b, April). Ground-motion modeling of the 1906 San Francisco earthquake, part II: Ground-motion estimates for the 1906 earthquake and scenario events. *Bulletin of the Seismological Society of America 98*(2), 1012–1046.

Aagaard, B. T., T. M. Brocher, D. Dolenc, D. Dreger, R. W. Graves, S. Harmsen, S. Hartzell, S. Larsen, and M. L. Zoback (2008a, April). Ground-motion modeling of the 1906 San Francisco earthquake, part I: Validation using the 1989 Loma Prieta earthquake. *Bulletin of the Seismological Society of America 98*(2), 989–1011.

Aagaard, B. T., J. F. Hall, and T. H. Heaton (2004, February). Effects of fault dip and slip rake angles on near-source ground motions: Why rupture directivity was minimal in the 1999 Chi-Chi, Taiwan earthquake. *Bulletin of the Seismological Society of America 94*(1), 155–170.

Albert C. Martin & Associates (1972, January). Post earthquake analysis: San Fernando earthquake of February 9, 1971: The Department of Water and Power Headquarters Building, Los Angeles, California. *Technical Report*, Structural Engineers Association of Southern California.

American Society of Civil Engineers (2000, November). Prestandard and commentary for the seismic rehabilitation of buildings. *Technical Report FEMA 356*, Federal Emergency Management Agency, Washington, D.C.

Anderson, J. C. and V. V. Bertero (1987, August). Uncertainties in establishing design earthquakes. *Journal of Structural Engineering 113*(8), 1709–1724.

Applied Technology Council (2007, May). Guidelines for seismic performance assessment of buildings: ATC-58 35% draft. *Technical Report*, Applied Technology Council.

Baker, J. W. and C. A. Cornell (2005). A vector-valued ground motion intensity measure consisting of spectral acceleration and epsilon. *Earthquake Engineering and Structural Dynamics 34*, 1193–1217.

Beck, J. L. and K.-V. Yuen (2004, February). Model selection using response measurements: Bayseian probabilistic approach. *Journal of Engineering Mechanics 130*(2), 192–203.

Beroza, G. C. (1991, October). Near-source modeling of the Loma Prieta earthquake: Evidence for heterogeneous slip and implications for earthquake hazard. *Bulletin of the Seismological Society of America 81*(5), 1603–1621.

Bertero, V. V., S. A. Mahin, and R. A. Herrera (1978). Aseismic design implications of near-fault San Fernando earthquake records. *Earthquake Engineering and Structural Dynamics 6*, 31–42.

Building Research Institute (1996, March). A survey report for building damages due to the 1995 Hyogo-Ken Nanbu earthquake. *Technical Report*, Building Research Institute, Japanese Ministry of Construction.

Carlson, A. E. (1999). *Three-Dimensional Nonlinear Inelastic Analysis of Steel Moment-Frame Buildings Damaged by Earthquake Excitations*. Ph.D. thesis, California Institute of Technology, Pasadena, California.

Challa, V. R. M. and J. F. Hall (1994). Earthquake collapse analysis of steel frames. *Earthquake Engineering and Structural Dynamics 23*, 1199–1218.

Chi, W.-M., S. El-Tawil, G. G. Deierlein, and J. F. Abel (1998). Inelastic analyses of a 17-story steel framed building damaged during Northridge. *Engineering Structures 20*, 418–495.

Ching, J., M. Muto, and J. L. Beck (2005, June). Bayesian linear structural model updating using Gibbs sampler with modal data. In *Proceedings of the 9th International Conference on Structural Safety and Reliability*, Rome, Italy.

Chopra, A. K. and C. Chintanapakdee (2001). Comparing response of SDF systems to near-fault and far-fault earthquake motions in the context of spectral regions. *Earthquake Engineering and Structural Dynamics 30*, 1769–1789.

Cua, G. and T. H. Heaton (2008, February). Characterizing average properties of southern California ground motion amplitudes and envelopes. *Bulletin of the Seismological Society of America (Submitted).*

Day, S. M., J. Bielak, D. Dreger, S. Larsen, R. Graves, A. Pitarka, and K. B. Olsen (2001, September). Lifelines program task 1A01: Tests of 3D elastodynamic codes. *Technical Report*, Pacific Earthquake Engineering Research Center.

Day, S. M., J. Bielak, D. Dreger, S. Larsen, R. Graves, A. Pitarka, and K. B. Olsen (2003, October). Lifelines program task 1A02: Tests of 3D elastodynamic codes. *Technical Report*, Pacific Earthquake Engineering Research Center.

Day, S. M., J. Bielak, D. Dreger, S. Larsen, R. Graves, A. Pitarka, and K. B. Olsen (2005, June). Lifelines program task 1A03: 3D ground motion simulation in basins. *Technical Report*, Pacific Earthquake Engineering Research Center.

Derleth, Jr., C. (1907). *The Destructive Extent of the California Earthquake: Its Effect Upon Structures and Structural Materials within the Earthquake Belt.* San Francisco: A. M. Robertson.

Frazier, G. A., J. H. Wood, and G. W. Housner (1971, June). Earthquake damage to buildings. In P. C. Jennings (Ed.), *Engineering Features of the San Fernando*

Earthquake of February 9, 1971. Pasadena, California: California Institute of Technology. EERL 71-02.

Gill, J. (2002). *Bayesian Methods: A Social and Behavioral Sciences Approach*. New York: Chapman & Hall/CRC.

Goulet, C. A., C. B. Haselton, J. Mitrani-Reiser, J. L. Beck, G. G. Deierlein, K. A. Porter, and J. P. Stewart (2007). Evaluation of the seismic performance of a code-conforming reinforced-concrete frame building - from seismic hazard to collapse safety and economic losses. *Earthquake Engineering and Structural Dynamics 36*, 1973–1997.

Graves, R., B. Aagaard, K. Hudnut, L. Star, J. Stewart, and T. Jordan (2008, May). Broadband ground motion simulations for a M_w 7.8 southern San Andreas earthquake. (*Manuscript in preparation*).

Graves, R. and A. Pitarka (2004, August). Broadband time history simulation using a hybrid approach. In *Thirteenth World Conference on Earthquake Engineering Conference Proceedings*, Vancouver, BC. Paper 1098.

Gupta, A. and H. Krawinkler (2000a, January). Behavior of ductile SMRFs at various seismic hazard levels. *Journal of Structural Engineering 126*(1), 98–107.

Gupta, A. and H. Krawinkler (2000b, January). Dynamic P-Δ effects for flexible inelastic steel structures. *Journal of Structural Engineering 126*(1), 145–154.

Gupta, A. and H. Krawinkler (2000c). Estimation of seismic drift demands for frame structures. *Earthquake Engineering and Structural Dynamics 29*, 1287–1305.

Hall, J. F. (1997). Seismic response of steel frame buildings to near-source ground motions. *Technical Report EERL 97-05*, California Institute of Technology, Pasadena, California.

Hall, J. F. (1998). Seismic response of steel frame buildings to near-source ground motions. *Earthquake Engineering and Structural Dynamics 27*, 1445–1464.

Hall, J. F. and V. R. M. Challa (1995, December). Beam-column modeling. *Journal of Engineering Mechanics 121*(12), 1284–1291.

Hall, J. F., T. H. Heaton, M. W. Halling, and D. J. Wald (1995, November). Near-source ground motion and its effects on flexible buildings. *Earthquake Spectra 11*(4), 569–605.

Himmelwright, A. L. A. (1906). *The San Francisco Earthquake and Fire: A Brief History of the Disaster: A Presentation of Facts and Resulting Phenomena, with Special Reference to the Efficiency of Building Materials: Lessons of the Disaster*. New York: The Roebling Construction Company.

Huang, C.-T. (2003, April). Considerations of multimode structural response for near-filed earthquakes. *Journal of Engineering Mechanics 129*(4), 458–467.

Hudnut, K. W., L. M. Jones, and B. T. Aagaard (2007, April). The southern California ShakeOut scenario, part I: Earth science specification of a big one. In *Seismological Society of America Annual Meeting Abstracts*, Waikoloa, HI.

Iwata, Y., H. Sugimoto, and H. Kuwamura (2006). Repairability limit of steel structural buildings based on the actual data of the Hyogoken-Nanbu earthquake. *Technical Memorandum of Public Works Research Institute* (4022), 86–95.

Jennings, P. C. and J. Bielak (1973, February). Dynamics of building-soil interaction. *Bulletin of the Seismological Society of America 63*(1), 9–48.

Krishnan, S., J. Chen, D. Kmoatitsch, and J. Tromp (2006, August). Case studies of damage to tall steel moment-frame buildings in southern California during large San Andreas earthquakes. *Bulletin of the Seismological Society of America 96*(4A), 1523–1537.

Krishnan, S. and M. Muto (2008). ShakeOut 2008: Tall steel moment frame building response. *Unpublished report to the United States Geological Survey*.

Lee, K. and D. A. Foutch (2006, September). Seismic evaluation of steel moment frame buildings designed using different R-values. *Journal of Structural Engineering 132*(9), 1461–1472.

Liao, K.-W., Y.-K. Wen, and D. A. Foutch (2007a, March). Evaluation of 3D steel moment frames under earthquake excitations. I: Modeling. *Journal of Structural Engineering 133*(3), 462–470.

Liao, K.-W., Y.-K. Wen, and D. A. Foutch (2007b, March). Evaluation of 3D steel moment frames under earthquake excitations. II: Reliability and redundancy. *Journal of Structural Engineering 133*(3), 471–480.

Luco, N. and C. A. Cornell (2000, January). Effects of connection fractures on SMRF seismic drift demands. *Journal of Structural Engineering 126*(1), 127–136.

MacRae, G. A. and J. Mattheis (2000, January). Three-dimensional steel building response to near-fault motions. *Journal of Structural Engineering 126*(1), 117–126.

MacRae, G. A., D. V. Morrow, and C. W. Roeder (2001, September). Near-fault ground motion effects on simple structures. *Journal of Structural Engineering 127*(9), 996–1004.

Mahin, S. A., J. O. Malley, R. O. Hamburger, and M. Mahoney (2003, May). Overview of the U.S. program for reduction of earthquake hazards in steel moment-frame structures. *Earthquake Spectra 19*(2), 237–254.

Makris, N. and C. J. Black (2004, September). Evaluation of peak ground velocity as a *Good* intensity measure for near-source ground motions. *Journal of Engineering Mechanics 130*(9), 1032–1044.

Mavroeidis, G. P., G. Dong, and A. S. Papageorgiou (2004). Near-fault ground motions, and the response of elastic and inelastic single-degree-of-freedom (SDOF) systems. *Earthquake Engineering and Structural Dynamics 33*, 1023–1049.

Mitrani-Reiser, J. (2007). *An Ounce of Prevention: Probabilistic Loss Estimation for Performance-Based Earthquake Engineering*. Ph.D. thesis, California Institute of Technology, Pasadena, California.

Muto, M. M. (2006). *Application of Stochastic Simulation Methods to System Identification*. Ph.D. thesis, California Institute of Technology, Pasadena, California.

Mylonakis, G. and A. M. Reinhorn (2001). Yielding oscillator under triangular ground acceleration pulse. *Journal of Earthquake Engineering 5*(2), 225–251.

Naeim, F. and R. W. Graves (2006). The case for seismic superiority of well-engineered tall buildings. *The Structural Design of Tall and Special Buildings 14*(5), 401–416.

Nakashima, M. (2000, September). Overview of damage to steel building structures observed in the 1995 Kobe earthquake. In *State of the Art Report on Past Performance of Steel Moment-Frame Buildings in Earthquakes*, Number FEMA 355E, Appendix C. SAC Joint Venture.

Olsen, A. H., B. T. Aagaard, and T. H. Heaton (2008, April). Long-period building response to earthquakes in the San Francisco Bay area. *Bulletin of the Seismological Society of America 98*(2), 1047–1065.

Olsen, K. B., S. M. Day, J. B. Minster, Y. Cui, A. Chourasia, M. Faerman, R. Moore, P. Maechling, and T. Jordan (2006, April). Strong shaking in Los Angeles expected from southern San Andreas earthquake. *Geophysical Research Letters 33*, L07305.

Olsen, K. B., S. M. Day, J. B. Minster, Y. Cui, A. Chourasia, D. Okaya, P. Maechling, and T. Jordan (2007, June). TeraShake2: Simulation of M_w7.7 earthquakes on the southern San Andreas fault with spontaneous rupture description. *Bulletin of the Seismological Society of America (To be submitted).*

Poland, C., J. Hill, and R. Sharpe (1995). Vision 2000: Performance based seismic engineering of buildings. *Technical Report*, Structural Engineers Association of California, Sacramento, California.

Porter, K., R. Graves, E. Reis, and P. Somerville (2007, November). Index woodframe houses and their response to Puente Hills scenario earthquakes. *Technical Report USC-SCEC/CEA Technical Report #9*, Southern California Earthquake Center, Los Angeles, California.

Reis, E. and D. Bonowitz (2000, September). State of the art report on past performance of steel moment-frame buildings in earthquakes. *Technical Report FEMA 355E*, SAC Joint Venture.

Rodgers, J. E. and S. A. Mahin (2006, January). Effects of connection fractures on global behavior of steel moment frames subjected to earthquakes. *Journal of Structural Engineering 132*(1), 78–88.

Safak, E. (1999, April). Wave-propagation formulation of seismic response of multistory buildings. *Journal of Structural Engineering 125*(4), 426–437.

Somerville, P., R. Graves, and C. Saikia (1995, December). Characterization of ground motions during the Northridge earthquake of January 17, 1994. *Technical Report SAC 95-03*, SAC Joint Venture.

Song, S. G., G. C. Beroza, and P. Segall (2008, April). A unified source model for the 1906 San Francisco earthquake. *Bulletin of the Seismological Society of America 98*(2), 823–831.

Soulé, F. (1907). The earthquake and fire and their effects on structural steel and steel-frame buildings. In *The San Francisco Earthquake and Fire of April 18, 1906 and Their Effects on Structures and Structural Materials*, Volume Bulletin No. 324 of *R, Structural Materials, 1.* Washington: Government Printing Office.

Steinbrugge, K. V., E. E. Schader, H. C. Bigglestone, and C. A. Weers (1971?). San Fernando earthquake, February 9, 1971. *Technical Report*, Pacific Fire Rating Bureau, San Francisco, California.

Steinbrugge, K. V., E. E. Schader, and D. F. Moran (1975). Building damage in San Fernando valley. In G. B. Oakeshott (Ed.), *San Fernando, California, Earthquake*

of 9 February 1971, Chapter 25. Sacramento, California: California Division of Mines & Geology. Bulletin 196.

Stewart, J. P., S. Kim, J. Bielak, R. Dobry, and M. S. Power (2003, August). Revisions to soil-structure interaction procedures in NEHRP design provisions. *Earthquake Spectra 19*(3), 677–696.

Süss, M. P. and J. H. Shaw (2003). *P* wave seismic velocity structure derived from sonic logs and industry reflection data in the Los Angeles basin, California. *Journal of Geophysical Research 108*(B3), 13–1–13–18.

Todorovska, M. I. and M. D. Trifunac (1989, December). Antiplane earthquake waves in long structures. *Journal of Engineering Mechanics 115*(12), 2687–2708.

Villaverde, R. (2007, January). Methods to assess the seismic collapse capacity of building structures: State of the art. *Journal of Structural Engineering 133*(1), 57–66.

Wald, D. J., D. V. Helmberger, and T. H. Heaton (1991, October). Rupture model of the 1989 Loma Prieta earthquake from the inversion of strong-motion and broadband teleseismic data. *Bulletin of the Seismological Society of America 81*(5), 1540–1572.

Whitman, R. V., S.-T. Hong, and J. W. Reed (1973, April). Optimum seismic protection and building damage statistics. Report number 7. Damage statistics for high-rise buildings in the vicinity of the San Fernando earthquake. *Technical Report R73-24 Structures Publication Number 363*, Massachusetts Institute of Technology, Department of Civil Engineering.

Wong, H. L. (1975, May). Dynamic soil-structure interaction. *Technical Report EERL 75-01*, California Institute of Technology, Pasadena, California.